

INCREMENTAL SHEET FORMING APPLIED TO THE MANUFACTURING OF BIOCOMPATIBLE POLYMER PROSTHESES

Isabel Bagudanch Frigolé

Per citar o enllaçar aquest document:
Para citar o enlazar este documento:
Use this url to cite or link to this publication:
<http://hdl.handle.net/10803/461838>



<http://creativecommons.org/licenses/by-nc-sa/4.0/deed.ca>

Aquesta obra està subjecta a una llicència Creative Commons Reconeixement-NoComercial-CompartirIgual

Esta obra está bajo una licencia Creative Commons Reconocimiento-NoComercial-CompartirIgual

This work is licensed under a Creative Commons Attribution-NonCommercial-ShareAlike licence



DOCTORAL THESIS

**Incremental sheet forming
applied to the manufacturing of
biocompatible polymer prostheses**

Isabel Bagudanch Frigolé

2017



DOCTORAL THESIS

**Incremental sheet forming
applied to the manufacturing of
biocompatible polymer prostheses**

Isabel Bagudanch Frigolé

2017

Doctoral Programme in Technology

Supervisors: Maria Luisa Garcia-Romeu and Gabriel Centeno Báez

Tutor: Joaquim de Ciurana Gay

**Thesis submitted in partial fulfillment of the requirements for the degree of Doctor
from the University of Girona**



La Dra. Maria Luisa Garcia-Romeu de Luna, professora titular del Departament d'Enginyeria Mecànica i de la Construcció Industrial de la Universitat de Girona, el Dr. Gabriel Centeno Báez, professor del Departament d'Enginyeria Mecànica i Fabricació de la Universitat de Sevilla, i el Dr. Joaquim de Ciurana Gay, catedràtic del Departament d'Enginyeria Mecànica i de la Construcció Industrial de la Universitat de Girona,

DECLAREM:

Que el treball titulat "Incremental Sheet Forming applied to the manufacturing of biocompatible polymer prostheses", que presenta Isabel Bagudanch Frigolé per a l'obtenció del títol de doctora, ha estat realitzat sota la nostra direcció.

I, perquè així consti i tingui els efectes oportuns, signem aquest document.

Signatures

Handwritten signature of Maria Luisa Garcia-Romeu de Luna in blue ink.

Handwritten signature of Gabriel Centeno Báez in blue ink.

Handwritten signature of Joaquim de Ciurana Gay in blue ink.

Girona, 8 de setembre de 2017

*“Now I’ve had the time of my life
No I never felt like this before
Yes I swear it’s the truth
And I owe it all to you”*

*(I’ve had) The Time of My Life
Dirty Dancing*

Acknowledgements

I would like to acknowledge in the first place my supervisors, Maria Luisa Garcia-Romeu and Gabriel Centeno, for their valuable contributions, dedication, guidance, encouragement and expertise. I really appreciate the enthusiasm and initiative that both of you always demonstrate, which have significantly contributed to increase the value of this thesis. Maria Luisa, ja fa més de vuit anys que vaig començar al GREP i des del principi m'he sentit molt còmode treballant al teu costat, moltíssimes gràcies per la confiança que sempre has tingut en mi i per tots els consells rebuts, tant els relacionats amb la recerca com a nivell personal, per mi ets molt més que la meva “jefa”. Gabi, nosotros nos conocimos en Aachen en 2011 y desde entonces no hemos dejado de colaborar y crecer dentro del mundo del ISF, estableciendo además una bonita amistad. Gracias por todo, pero sobre todo por tratarnos como reinas todas las veces que hemos venido a Sevilla y llevarnos siempre a restaurantes buenísimos!

I gratefully acknowledge the financial support provided by grant FPU12/05402 from the Spanish Ministry of Education, as well as the funding received under several research projects from the Spanish Ministry of Innovation, Science and Technology (DPI2012-36042, DPI2009-098052), the European Commission (FP7-PEOPLE-2009-IRSES-247476) and the University of Girona (MPCUdG2016/036).

Many thanks to Rogelio Pérez-Santiago, from Universidad de las Américas Puebla (UDLAP), Mexico, because it all started with the “Chiquito pero picoso” setup, you were the precursor of ISF in Girona. We owe you many of our achievements. Gracias de todo corazón!

Thanks to Instituto Tecnológico y de Estudios Superiores de Monterrey (ITESM), Mexico, mainly to Álex Elías for his support and advices which have enriched this work, and special thanks for your kindness during my stay in Monterrey. Also thanks to Marcelo Lozano for sharing experimental tasks, some of them were a bit hard but they kept us fit! Elisa Vázquez, thanks for our friendship and for always being there, even though an ocean separates us, I miss you so much!

I wish to acknowledge the collaboration and support provided by Centro de Investigación en Química Aplicada (CIQA), in Saltillo (Mexico), especially to Luis Ernesto Elizalde and Jorge Espinosa.

Thanks also to Jorge V. L. Silva and Daniel T. Kemmoku from Three-dimensional Technologies Division of the Renato Archer Information Technology Center, Brazil, for providing one of the cases of study of the thesis.

I am very grateful to the colleagues of University of Seville, Carpóforo Vallengano, Javier García-Lomas, Domingo Morales, Andrés Martínez, Marcos Borrego and Jaime Domínguez. Mil gracias por vuestra hospitalidad y colaboración.

I really acknowledge the collaboration of AMADE research group from University of Girona during the characterization of the polymers mechanical behavior.

Thanks to Marina Vives for her statistical support, your expertise has added a lot of value to this research.

I would also like to thank Laura Puigpinós, from EURECAT, for sharing your knowledge on ISF with us and for your great assistance.

Many thanks to the EURECAT-Girona team and ex-GREP members: Guillem Quintana, Dani Teixidor, Jordi Grabalosa and Arcadi Castanyer. Gràcies pels bons moments, pels pastissos i pels cafès compartits els últims anys!

Of course, I am very thankful to my research group, GREP, and my workmates. I have learnt many things from all of you, I only have good words to describe this amazing experience. Thanks to Quim de Ciurana, for giving me the opportunity of joining GREP several years ago, Inés Ferrer, Marc Sabater, Antonio Guerra and also to the ones who have been part of GREP in some moment during my stay here: Sílvia Míguez, Anna Ymbert, Jéssica Gomar, Lídia Serenó, Jordi Delgado, Xevi Gómez and Francesc Tauler. M'enduc bons records i bones amistats! Also thanks to the students that have collaborate in some experimental tasks of the thesis: Aleix Lleget, Albert Segade, Martí Puig, Marc López, Jordi Canal, Adrià Garcia, Gerard Gutiérrez and Pol Andaluz.

My sincere gratitude to the reviewers who helped me improving this thesis with their valuable comments and suggestions.

Moltíssimes gràcies als meus grans amics, Jordi, Dolors, Esther, David, Glòria, Xevi, Miki i als petitons de la colla, en Martí, l'Adrià i l'Aina. Hem tingut la sort de crear un vincle molt especial i gaudir dels millors moments de les nostres vides junts, i tot i que també hi ha hagut moments no tan bons, entre tots fem que siguin més fàcils de portar. Sou els millors amics que podria desitjar!

Vull donar les gràcies als meus pares i als meus sogres per recolzar-me sempre i ajudar-me en tantes coses, sobretot els últims temps, i a la resta de la meva família, en David, la Berta i les meves precioses nebodes, la Joana i la Neus.

Per acabar, només em falta agrair a les dues persones més especials de la meva vida. A l'Ivan, perquè sense tu no hauria aconseguit arribar fins aquí, sempre has cregut en mi i m'has animat a seguir endavant, no tinc prou paraules per agrair-te tot el que has fet per mi en la casi mitja vida que portem junts. I a la meva petita i dolça Júlia, perquè tu has nascut amb aquesta tesi sota el braç, i gràcies perquè amb les teves mirades i rialles estàs omplint la nostra vida de moments inigualables, gaudim cada dia veient com creixes a passos de gegant i com descobreixes el món que t'envolta. Us estimo molt!

List of publications

This doctoral dissertation is presented as a compendium of publications. The following list contains the publications presented as chapters of this PhD thesis.

CHAPTER 3: Bagudanch, I., Garcia-Romeu, M.L., Centeno, G., Elías-Zúñiga, A., Ciurana, J., 2015. Forming force and temperature effects on single point incremental forming of polyvinylchloride. *Journal of Materials Processing Technology* 219, 221–229.

In 2015, the JOURNAL OF MATERIALS PROCESSING TECHNOLOGY had an Impact Factor of 2.539.

This table shows the ranking of this journal in its subject categories based on Impact Factor.

Category Name	Total Journals in Category	Journal Rank in Category	Quartile in Category
ENGINEERING, INDUSTRIAL	44	5	Q1
ENGINEERING, MANUFACTURING	42	7	Q1

CHAPTER 4: Bagudanch, I., Garcia-Romeu, M.L., Sabater, M., 2016. Incremental forming of polymers: Process parameters selection from the perspective of electric energy consumption and cost. *Journal of Cleaner Production* 112, 1013–1024.

In 2016, the JOURNAL OF CLEANER PRODUCTION had an Impact Factor of 5.715.

This table shows the ranking of this journal in its subject categories based on Impact Factor.

Category Name	Total Journals in Category	Journal Rank in Category	Quartile in Category
GREEN&SUSTAINABLE SCIENCE&TECHNOLOGY	31	5	Q1
ENGINEERING, ENVIRONMENTAL	49	6	Q1
ENVIRONMENTAL SCIENCES	229	17	Q1

CHAPTER 5: Bagudanch, I., Vives-Mestres, M., Sabater, M., Garcia-Romeu, M.L., 2017.

Polymer incremental sheet forming process: Temperature analysis using response surface methodology. *Materials and Manufacturing Processes* 32, 44–53.

In 2016, the journal of MATERIALS AND MANUFACTURING PROCESSES had an Impact Factor of 2.274.

This table shows the ranking of this journal in its subject categories based on Impact Factor.

Category Name	Total Journals in Category	Journal Rank in Category	Quartile in Category
ENGINEERING, MANUFACTURING	44	18	Q2
MATERIALS SCIENCE, MULTIDISCIPLINARY	275	107	Q2

CHAPTER 6: Bagudanch, I., Centeno, G., Vallellano, C., Garcia-Romeu, M.L., 2017.

Revisiting formability and failure of polymeric sheets deformed by single point incremental forming. *Polymer Degradation and Stability* 144, 366-377.

In 2016, the journal of POLYMER DEGRADATION AND STABILITY had an Impact Factor of 3.386.

This table shows the ranking of this journal in its subject categories based on Impact Factor.

Category Name	Total Journals in Category	Journal Rank in Category	Quartile in Category
POLYMER SCIENCE	86	15	Q1

CHAPTER 7: Centeno, G., Morales-Palma, D., Gonzalez-Perez-Somarrriba, B., Bagudanch, I., Egea-Guerrero, J.J., Gonzalez-Perez, L.M., Garcia-Romeu, M.L., Vallellano, C., 2017. A functional methodology on the manufacturing of customized polymeric cranial prostheses from CAT using SPIF. *Rapid Prototyping Journal* 23(4), 771-780.

In 2016, the RAPID PROTOTYPING JOURNAL had an Impact Factor of 2.400.

This table shows the ranking of this journal in its subject categories based on Impact Factor.

Category Name	Total Journals in Category	Journal Rank in Category	Quartile in Category
ENGINEERING, MECHANICAL	130	30	Q1

CHAPTER 8: Bagudanch, I., Garcia-Romeu, M.L., Ferrer, I., Ciurana, J., 2018. Customized cranial implant manufactured by Incremental Sheet Forming using a biocompatible polymer. *Rapid Prototyping Journal* 24(5). doi:10.1108/RPJ-06-2016-0089.

In 2016, the RAPID PROTOTYPING JOURNAL had an Impact Factor of 2.400.

This table shows the ranking of this journal in its subject categories based on Impact Factor.

Category Name	Total Journals in Category	Journal Rank in Category	Quartile in Category
ENGINEERING, MECHANICAL	130	30	Q1

List of symbols

65Cr2	Steel alloy
AA1050	Aluminum alloy, series 1XXX
AA1050-O	Aluminum alloy, series 1XXX, annealed
AA3003	Aluminum alloy, series 3XXX
AA3003-O	Aluminum alloy, series 3XXX, annealed
AA5754	Aluminum alloy, series 5XXX
AISI304	Stainless steel alloy
AZ31	Magnesium alloy
AZ31-O	Magnesium alloy, annealed
CaCO₃	Calcium carbonate
CO₂	Carbon dioxide
CP Ti	Commercially pure titanium
DC01	Steel alloy
DC04	Steel alloy
d_t	Tool diameter (mm)
FeP04	Deep drawing steel
F_x	In-plane force component (N)
F_y	In-plane force component (N)
F_z	Axial force component (N)
MoS₂	Solid graphite
mp	Melting point (°C)
Ni-MoS₂	Nickel disulfide metal matrix composite

R_a	Average surface roughness (μm)
R_m	Tensile strength of the formed material aligned with the wall direction (MPa)
t₀	Initial sheet thickness (mm)
t₀/R	Initial sheet thickness to tool radius ratio
T_g	Glass transition temperature (°C)
Ti6Al4V	Titanium alloy
TiO₂	Titanium dioxide
T_m	Melting temperature (°C)
X6Cr17	Ferritic stainless steel
α	Initial wall angle (°)
Δh	Scallop height (mm)
ΔT	Rise in temperature (°C)
ΔT/mp	Softening index
Δz	Depth step / Step down (mm)
Δθ	Angular increment (°)

List of acronyms

ADIFAP	Avances en la Deformación Incremental para su aplicación en la Fabricación de Prótesis Poliméricas Biocompatibles
AM	Additive Manufacturing
ANOVA	Analysis of Variance
ASEBIO	Asociación Española de Bioempresas
BUT	Bending-under-tension
CAD	Computer Aided Design
CAGR	Compound Annual Growth Rate
CAT	Computerized Axial Tomography
CCD	Central Composite Design
CMM	Coordinate Measuring Machine
CNC	Computer Numerical Control
CT	Computerized tomographies
DC	Direct current
DDQ	Deep Drawing Quality
DMLS	Direct Metal Laser Sintering
DOE	Design of Experiments
DSC	Differential Scanning Calorimetry
EDM	Electrical Discharge Machining
FEM	Finite Element Method
FFL	Fracture Forming Limit
FFLD	Fracture Forming Limit Diagrams
FLC	Forming Limit Curve
FLD	Forming Limit Diagrams
GDP	Gross Domestic Product

GREP	Research Group on Product, Process and Production Engineering
hcp	Hexagonal-closed-packed
HDPE	High density polyethylene
HSS	High-speed steel
IREBID	International Research Exchange for Biomedical Devices Design and prototyping
ISF	Incremental Sheet Forming
ISMF	Incremental Sheet Metal Forming
LM	Laser Milling
MR	Magnetic Resonance
MWCNTs	Multi-wall carbon nanotubes
PA	Polyamide
PC	Polycarbonate
PCL	Polycaprolactone
PE	Polyethylene
PESTEL	Political, Economic, Social, Technological, Environmental and Legal factors to assess the macro-environment in business management
PET	Polyethylene terephthalate
PLA	Polylactic acid
PMMA	Polymethylmethacrylate
POM	Polyoxymethylene
PP	Polypropylene
PVC	Polyvinylchloride
R&D	Research & Development
RISF	Rotational Incremental Sheet Forming
RSM	Response Surface Methodology
SEM	Scanning Electron Microscope
SFFL	Shear fracture forming limit line
SPIF	Single Point Incremental Forming
SWAXS	Small and wide angle X-ray scattering
TECNIPLAD	Caracterització de tecnologies innovadores per a la planificació detallada dels processos
TGA	Thermogravimetric analysis
TPIF	Two Point Incremental Forming
UHMWPE	Ultra-high molecular weight polyethylene
UWA	Uniform wall angle

List of figures

Figure 1.1. Graphical representation of the unitary cost as a function of the batch production size for the forming processes deep drawing and ISF (adapted from Tuomi and Lamminen (2004)).	4
Figure 1.2. Evolution of the number of papers published in indexed journals from 1970 to 2015 (information retrieved from Scopus data base).	4
Figure 1.3. World map publication number distribution concerning Incremental Sheet Forming from 1970 to 2015 (information retrieved from Scopus data base).	5
Figure 1.4. Thesis road map	10
Figure 2.1. 3D schematic representation of the process.	12
Figure 2.2. SPIF variant (Allwood et al., 2010).	13
Figure 2.3. TPIF process variants: a) negative full die, b) positive full die and c) positive partial die (Allwood et al., 2010).	14
Figure 2.4. a) Rotational ISF (Park et al., 2009). b) Hot clamping system (Ambrogio et al., 2008). c) Hot chamber (Zhang et al., 2009). d) Electric resistance (Fan et al., 2008). e) Laser assisted ISF (Dufloy et al., 2008).	15
Figure 2.5. Magnesium strains at failure at different temperatures (Ambrogio et al., 2008).	16
Figure 2.6. AZ31 forming limits at different temperatures (Ji and Park, 2008).	17
Figure 2.7. RISF results using AZ31: a) grain size, b) FLD, c) thickness distribution (Park et al., 2009).	18
Figure 2.8. Schematic representation of the SPIF system with dynamic local heating by laser irradiation (Hino et al., 2014).	18

Figure 2.9. a) Experimental system for warm ISF. b) Geometric accuracy (Sy and Nam, 2015).....	19
Figure 2.10. Variation of the forming force with the tool diameter in electric hot incremental forming (Honarpisheh et al., 2015).	20
Figure 2.11. High-speed SPIF in a CNC lathe (Ambrogio et al., 2013).....	20
Figure 2.12. Operation principle of the hybrid process (a) experimental setup, (b) first stage: stretch forming, (c) second stage: ISF (Araghi et al., 2009).	21
Figure 2.13. Robot cell for incremental forming of aluminum metal sheet (Schafer and Schraft, 2005).....	22
Figure 2.14. Experimental set-up of Roboforming (Meier et al., 2009).....	22
Figure 2.15. An example of microincremental forming, miniature dots 0.1 mm in diameter in aluminum AL-2 with 12 μ m sheet thickness (Obikawa et al., 2009).	23
Figure 2.16. a) Torsion appeared due to unidirectional or spiral tool path. b) Part manufactured using bidirectional toolpath to avoid torsion.	24
Figure 2.17. a) Spiral toolpath with good surface finishing. b) Unidirectional or bidirectional toolpath, with tool indentation.....	24
Figure 2.18. Measured forces during SPIF process of a truncated pyramid (Jeswiet and Szekeres, 2005).	27
Figure 2.19. Axial force evolution for different: a) sheet thicknesses, b) step down, c) tool diameter and d) wall angle (Filice et al., 2006).	27
Figure 2.20. Classification of the forming force trends: a) steady state. b) polynomial. c) monotonically decreasing (Filice et al., 2006).	28
Figure 2.21. a) Three force components. b) Detailed view of the force evolution (Duflou et al., 2007b).	29
Figure 2.22. Acquisition system for force measurements in SPIF (Petek et al., 2009).	29
Figure 2.23. Evolution of the maximum axial force depending on the t_0/R (initial sheet thickness to tool radius ratio) (Centeno et al., 2014).	30
Figure 2.24. Fishbone diagram with the parameters that affect the forming force in ISF. ...	31
Figure 2.25. Representation of the principal strain space (Isik et al., 2014).	32
Figure 2.26. Definitions of ISF undeformed part (A), through-thickness shear (B) and out-of-plane shear (C) (Emmens and van den Boogaard, 2009).	32

Figure 2.27. Sine law (Jeswiet et al., 2005b).....	33
Figure 2.28. Fractography at the fracture initiation zone for SPIF tests using 20 mm tool diameter (a) and 10 mm tool diameter (b) (Centeno et al., 2014).....	34
Figure 2.29. Schematic representation of strain loading conditions for a variable wall angle truncated pyramid formed by SPIF.	35
Figure 2.30. Fracture loci (FFL and SFFL) (Isik et al., 2014).	35
Figure 2.31. Variable wall angle truncated lobe conical geometry proposed to determine SFFL (Soeiro et al., 2015).....	36
Figure 2.32. Schematic representation of the FLD determination method proposed by Isik et al. (2014) (a) and the method proposed by Soeiro et al. (2015) (b).....	36
Figure 2.33. Geometrical error topologies observed during the SPIF of UWA parts (Micari et al., 2007).	37
Figure 2.34. Summary of accuracy improvement approaches for ISF.....	38
Figure 2.35. Schematic representation of the effect of the step down on surface roughness (Hagan and Jeswiet, 2004).	38
Figure 2.36. Main effects plot for surface roughness vs. the considered process parameters in aluminum alloy (AA1050) (Radu and Cristea, 2013)	39
Figure 2.37. Modes of failure in SPIF of thermoplastic sheets (adapted from Franzen et al. 2009).....	41
Figure 2.38. Macro-environment (Guerras and Navas, 2015).....	49
Figure 2.39. Evolution of the evaluation of the government support (facilitating factor) versus low sensitivity of government towards the sector (inhibiting factor) from 2000 to 2014 (ASEBIO, 2014).....	49
Figure 2.40. Global market for bio-implants (left) and percentage of share of the different types of bio-implants (right) (Deshmukh, 2014).....	50
Figure 2.41. Global medical polymer market (NanoMarkets, 2013).	51
Figure 2.42. Global biomaterials market for implantable devices (TMR, 2014).....	52
Figure 2.43. European classification of medical devices (MDD 93/42/EEC).	53
Figure 2.44. a) Process cycle for a customized medical device. b) Ankle final part (Ambrogio et al., 2005).	55

Figure 2.45. Pure titanium denture plate formed by SPIF and trimmed using wire-EDM (Tanaka et al., 2007).	55
Figure 2.46. a) Complete cast-metal denture base and b) SPIF manufactured denture base in DC04 (left) and X6Cr17 (right) (Milutinovic et al., 2014).	56
Figure 2.47. Condylar implant components: articular resurfacing component and fastening screw (Oleksik et al., 2010).	56
Figure 2.48. a) Cranial prosthesis design. b) Cranial prosthesis manufactured by SPIF before trimming (Duflou et al., 2005).	56
Figure 2.49. a) Cranial prosthesis design, b) positive die, c) produced part (Han et al., 2010).	57
Figure 2.50. Cranial model (a, b), positive full die design (c, d), die area covered by the implant (e) and manufactured implant (f) (Göttmann et al., 2013).	57
Figure 2.51. Cranial implants produced from expanded metal sheets and from solid metal sheets (the holes were drilled after forming) (Göttmann et al., 2013).	57
Figure 2.52. Skull model (a) and finished part (b) (Lu et al., 2016).	58
Figure 2.53. a) Severe cranial injury. b) Assembly of the implant manufactured by TPIF in the biomodel (Castelan et al., 2014).	58
Figure 2.54. Comparison between the CAD model and the ISF manufactured cranial implant after trimming (Ambrogio et al., 2015).	59
Figure 2.55. a) Generation of the CAD model of a frontal orbit implant and b) accuracy of the implant manufactured by SPIF (Duflou et al., 2013).	59
Figure 2.56. Model of the facial implant manufactured by SPIF (Araujo et al., 2014).	59
Figure 9.1. Procedure for determining the safe forming zone in SPIF.....	148

List of tables

Table 1.1. Benefits and drawbacks.....	7
Table 2.1. Summary of the most important process parameters.	26
Table 2.2. Summary of the experimental research works related with the manufacturing of polymer parts using ISF.....	44
Table 2.3. Duration of contact and degree of invasiveness criteria for medical devices in Europe (MDD 93/42/EEC).....	53
Table 2.4. Strategic profile of the environment	54
Table 9.1. Summary of the polymeric materials properties provided in the polymer ISF literature. Legend: ● Information explicitly provided in the paper; ○ Information obtainable from figures provided in the paper; ◇ Information provided at various testing speeds and/or temperatures; - Information not available.	149
Table 9.2. Summary of the normalized mechanical requirements for a UHMWPE surgical part and the material data sheet and characterization results	152

Contents

Summary	<i>Resum</i>	Resumen	1
Chapter 1. Introduction.....			3
1.1 Incremental Sheet Forming: general overview			3
1.2 Interest.....			5
1.3 Motivation.....			6
1.4 Objectives.....			7
1.5 Thesis structure			8
Chapter 2. State of the art			11
2.1 Introduction			11
2.2 ISF variants			13
2.2.1 Single Point Incremental Forming (SPIF)			13
2.2.2 Two Point Incremental Forming (TPIF)			14
2.2.3 Hot ISF.....			14
2.2.4 Stretch Forming with ISF			21
2.2.5 Roboforming			21
2.3 Process parameters			22
2.3.1 Design			23

2.3.2 Tool.....	23
2.3.3 Process	25
2.4 Process outputs.....	26
2.4.1 Forming forces	26
2.4.2 Formability.....	31
2.4.3 Geometric accuracy	36
2.4.4 Surface roughness	38
2.5 Polymeric materials	40
2.6 Application of ISF in the biomedical field	47
2.6.1 Political factors	49
2.6.2 Economic factors	50
2.6.3 Social factors	51
2.6.4 Technological factors	51
2.6.5 Environmental factors.....	52
2.6.6 Legal factors.....	52
2.6.7 Strategic profile of the environment.....	53
2.6.8 Examples of biomedical devices manufactured using ISF.....	54
2.7 Summary and thesis framework	60
Chapter 3. Forming force and temperature effects on single point incremental forming of polyvinylchloride	61
Chapter 4. Incremental forming of polymers: process parameters selection from the perspective of electric energy consumption and cost	73
Chapter 5. Polymer incremental sheet forming process: temperature analysis using response surface methodology	87
Chapter 6. Revisiting formability and failure of polymeric sheets deformed by single point incremental forming.....	99

Chapter 7. A functional methodology on the manufacturing of customized polymeric cranial prostheses from CAT using SPIF	113
Chapter 8. Customized cranial implant manufactured by Incremental Sheet Forming using a biocompatible polymer.....	125
Chapter 9. Discussion	145
9.1 Study of the influence of process parameters on basic geometries manufactured by SPIF	145
9.2 Cases of study: approaching ISF to the manufacturing of custom cranial implants .	150
9.3 List of additional publications.....	153
Chapter 10. Conclusions.	157
10.1 General conclusions	157
10.2 Main contributions	159
10.3 Further work.....	160
Chapter 11. References	161

Summary

Resum

Resumen

Incremental Sheet Forming (ISF) is a technology that has been mainly applied on metallic sheets during the last two decades. Nevertheless, its use on polymeric materials is more recent. Without distinguishing the raw material employed, ISF is used due to its flexibility, low machine and tooling costs, low batch production, the possibility of producing complex geometries and high degree of customization. For this reason ISF seems to be the ideal process for prosthesis production. There are several research works on ISF technology for producing biocompatible devices with titanium sheet metal parts, while there is scarce work regarding its use with polymeric materials.

For this reason, the main objective of the thesis is to study the applicability of the ISF technology, considering Single Point Incremental Forming (SPIF) and Two Point Incremental Forming (TPIF) variants, on biocompatible polymers to obtain a real customized cranial implant, which is the case study of the thesis. To achieve this goal, a methodology based on the following steps is proposed: a) Experimental work in SPIF to produce basic geometries using non-biocompatible and biocompatible polymers, b) Study of the influence of the process parameters in the SPIF process of polymers, as well as its influence in formability, c) Case study: customized cranial implant. Achieving the objectives established in these stages will permit to improve the knowledge about ISF process in order to successfully manufacture customized implants at a low cost and reduced time-to-market.

La tecnologia de deformació incremental de xapa (ISF) és una tecnologia que s'ha aplicat majoritàriament a la xapa metàl·lica durant les últimes dues dècades. Malgrat tot, el seu ús en materials polímers és molt més recent. Independentment del material de partida, les aplicacions típiques d'aquest tipus de tècnica es caracteritzen per la flexibilitat del procés amb costos baixos, possibilitat de produir en lots petits, la possibilitat d'obtenir geometries complexes i en la personalització del producte final. Aquestes característiques del procés fan que un dels camps d'aplicació de la tecnologia sigui la fabricació de pròtesis. En aquest sector existeixen ja treballs en els que s'ha aplicat la tecnologia ISF en xapes de titani, per ser un material biocompatible. Mentre que la seva aplicació en polímers biocompatibles es pràcticament inexistent a la literatura.

Per aquest motiu, l'objectiu principal de la tesis és el d'estudiar l'aplicabilitat de la tecnologia ISF, en les seves variants de Single Point Incremental Forming (SPIF) i Two Point Incremental Forming (TPIF), sobre materials polímers biocompatibles sota la geometria que proporciona el cas real d'una pròtesi de crani personalitzada. Per poder aconseguir-ho es proposa una metodologia basada en els següents passos: a) Experimentació en SPIF de geometries bàsiques utilitzant polímers no biocompatibles i biocompatibles, b) Determinació de la influència dels paràmetres de procés en SPIF de polímers, així com la seva influència en l'augment dels límits de formabilitat, c) Cas d'estudi: pròtesi de crani personalitzada. L'assoliment d'aquestes etapes permetrà obtenir de forma satisfactòria pròtesis personalitzades de crani amb un baix cost i un temps de fabricació reduït.

La tecnología de deformación incremental de chapa (ISF) es una tecnología que se ha aplicado mayoritariamente a la chapa metálica durante las últimas dos décadas. Sin embargo, su uso sobre materiales polímeros es mucho más reciente. Independientemente del material de partida, las aplicaciones típicas de este tipo de técnica se caracterizan por la flexibilidad del proceso con costes bajos, posibilidad de producción en lotes pequeños, la posibilidad de obtener geometrías complejas y en la personalización del producto final. Estas características del proceso hacen que uno de los campos de aplicación de la tecnología sea la fabricación de prótesis. En este sector existen ya trabajos en los que se ha aplicado la tecnología ISF en chapas de titanio, por ser un material biocompatible. Mientras que su aplicación sobre polímeros biocompatibles es prácticamente inexistente en la literatura.

Por este motivo, el objetivo principal de la tesis es el de estudiar la aplicabilidad de la tecnología ISF, en sus variantes de Single Point Incremental Forming (SPIF) y Two Point Incremental Forming (TPIF), sobre materiales polímeros biocompatibles bajo la geometría que proporciona el caso real de una prótesis craneal personalizada. Para poder lograrlo se propone una metodología basada en los siguientes pasos: a) Experimentación en SPIF de geometrías básicas utilizando polímeros no biocompatibles y biocompatibles, b) Determinación de la influencia de los parámetros de proceso en SPIF de polímeros, así como su influencia en el aumento de los límites de conformado, c) Caso de estudio: prótesis de cráneo personalizada. La cumplimentación de estas etapas permitirá obtener de forma satisfactoria prótesis personalizadas de cráneo con un bajo coste y un tiempo de fabricación reducido.

Chapter 1. Introduction

Chapter 1 presents a general introduction of the incremental sheet forming technology and gives the justification and the motivation for this thesis.

1.1 Incremental Sheet Forming: general overview

Deep drawing is one of the most common forming processes used in industrial applications due to its low cycle time and process maturity. In order to carry out this process it is necessary to manufacture a tooling system (die, punch, binder, etc.) specific for each product. The tooling system has to be manufactured using high resistant materials able to withstand the high forces generated in the process. Furthermore, high accuracy must be guaranteed to avoid collisions between parts of the tooling system and ensure the final part's dimensional accuracy. To reach these requirements the materials used for the tooling system and the manufacturing processes utilized to obtain it are very expensive. The cost of the process is only justified for high volume production. This effect can be observed in Figure 1.1.

In order to be able to produce highly customized products at a reasonable manufacturing cost, several innovative forming processes have been developed. Incremental Sheet Forming (ISF) is one of these new technologies and it has gained importance in the last years, becoming the focus of interest for many researchers and institutions.

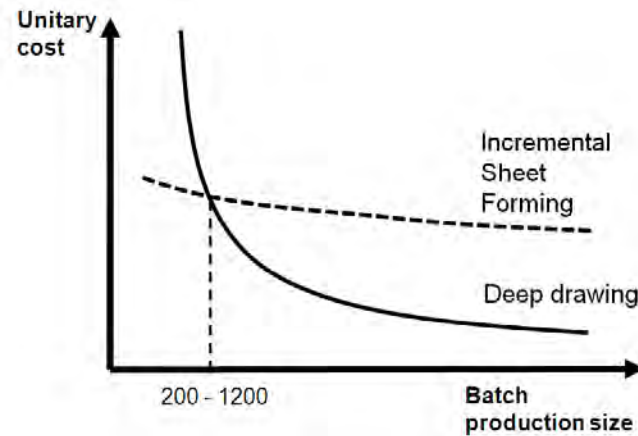


Figure 1.1. Graphical representation of the unitary cost as a function of the batch production size for the forming processes deep drawing and ISF (adapted from Tuomi and Lamminen (2004)).

The first research work related with the ISF process was done by Mason, in 1978, as it has been reported in the historical review of Emmens et al. (2010).

Although the first reference of the technology is dated more than three decades ago, is not until 2004 that ISF process research attracted the attention of research groups of different universities around the world (Figure 1.2). The increasing effort in the development of the technology is aligned with the changing trends in manufacturing like the more frequent use of small production batches or one-of-a-kind products in order to meet the customer's requirements and obtain customized product features.

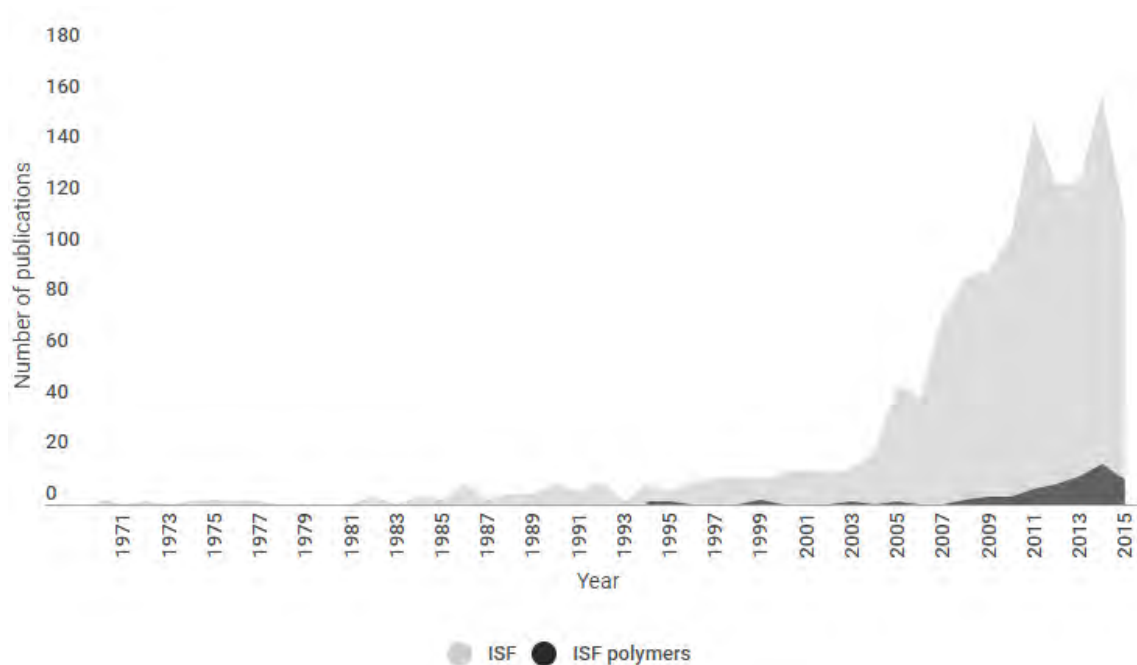


Figure 1.2. Evolution of the number of papers published in indexed journals from 1970 to 2015 (information retrieved from Scopus data base).

Among the ISF research topics, the use of polymers, has increasingly gained importance from 2009 to the present, as represented in Figure 1.2, becoming a niche field and the main focus of the present dissertation.

Analyzing the world map distribution of the number of publications related to the Incremental Sheet Forming topic (Figure 1.3) it can be observed that China is the country that has paid more attention to this process and it can be considered the pioneer of ISF in terms not only of number of publications but also on number of patents, followed by Germany and United States.

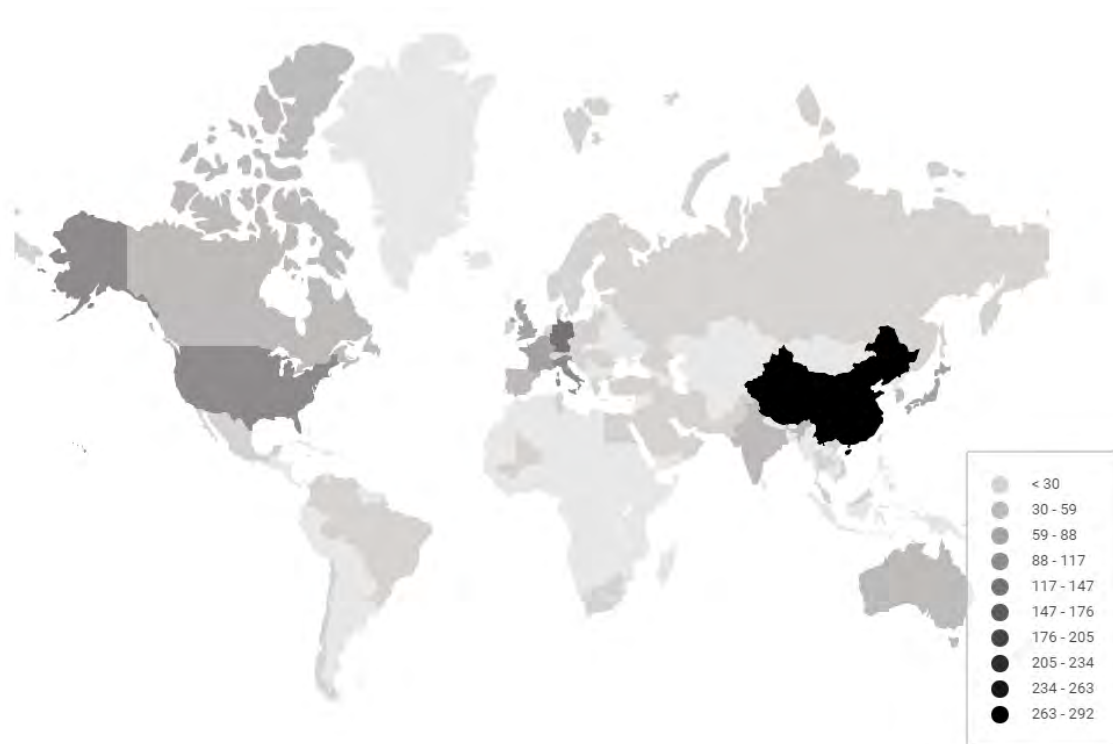


Figure 1.3. World map publication number distribution concerning Incremental Sheet Forming from 1970 to 2015 (information retrieved from Scopus data base).

1.2 Interest

This thesis is developed within the framework of the Research Group on Product, Process and Production Engineering (GREP) in the University of Girona, as a contribution to the development of one of its main research lines, in collaboration with the University of Seville.

The expertise of the research group regarding ISF technology has its origins in 2009, promoted by a grant from the Spanish Ministry of Innovation, Science and Technology (DPI2009-098052, TECNIPLAD). The objectives of that research project were twofold: (i) to deepen the knowledge of innovative manufacturing processes such as Electrochemical

Discharge Machining (EDM), Laser Milling (LM), Direct Metal Laser Sintering (DMLS) and Incremental Sheet Forming (ISF); (ii) to develop assisting systems for the selection of process parameters in order to be useful, helpful and applicable for all types of companies, working off-line and in-line. From the results of this project it was possible to participate in several international conferences (Bagudanch et al., 2011a, 2011b; Garcia-Romeu et al., 2012; Pérez-Santiago et al., 2012a, 2012b, 2011; Puigpinós et al., 2012), and a doctoral thesis was developed (Pérez-Santiago, 2012).

Driven by the growing demand for more effective, appropriate, and affordable health products, new customized medical devices are being developed opening a new market opportunity for the technological and industrial sectors. Nevertheless, there is a marked lack of knowledge exchange among stakeholders (doctors, patients, engineers) when it comes to medical product design and development. Doctors and patients need to transmit their necessities and requirements to the engineers in order to generate more efficient devices. This was the start point of a European project lead by GREP research group: International Research Exchange for Biomedical Devices Design and prototyping (IREBID), a Marie Curie funded project (FP7-PEOPLE-2009-IRSES-247476).

From the join of the ISF background and the new opportunities offered by the research developed in the biomedical field, in 2012 started a new research project funded by the Spanish Ministry of Science and Innovation (DPI2012-3604, ADIFAP), aiming to study and characterize the ISF process using biocompatible polymers in order to produce customized cranial implants. This is how this thesis arises, using the joint-venture in the knowledge already had in the research group and the need to increase it to try to answer the growing demand for customized implants.

Besides the aforementioned projects, which constitute the basis of this thesis, there are other research projects that are related with the ISF technology and have also contributed to enhance the background and expertise of the research group and its research partners: DPI2012-32913, DPI2015-64047-R and DPI2016-77156-R.

1.3 Motivation

In the traditional processing techniques of plastic materials it must be applied heat and/or pressure to give the desired shape to the material (injection molding, thermoforming, etc.). In fact, temperature has a very important role in the behavior of plastic materials, specially referred to the phase transition, fluency characteristics, morphology and degradation. These processing techniques require high production batches to recover the costs derived of machinery, tools and energy. With this aim, it is necessary to develop new technologies that allow the production of smaller batches with shorter life cycles and a very low time to market. Using ISF the production costs can be reduced as far as it is possible to work with polymers at room temperature and the experimental set-up necessary to carry out the

process is quite simple. In this sense, it is an economically viable manufacturing process to produce small batches and customized plastic products.

The following lists of benefits and drawbacks can serve as a summary of the different aspects related to ISF (Table 1.1).

Table 1.1. Benefits and drawbacks.

Benefits
<ul style="list-style-type: none"> • Changes in part's design can be quickly and easily performed, being a flexible technology. • Significantly improvement of material formability compared to the traditional forming processes. • Easily implemented in a CNC milling machine. • Due to the process nature, the forming forces are low. • Good surface finishing can be achieved.
Drawbacks
<ul style="list-style-type: none"> • High forming time. • Limited to low batch production or unique products. • Significant springback effect, reducing the geometric accuracy.

This thesis is based on the following initial hypothesis:

By increasing the knowledge regarding the use of polymeric materials for manufacturing basic geometries with Incremental Sheet Forming it will be feasible to produce complex customized biomedical implants at a low cost and reduced time-to-market.

To achieve it, it is necessary to work on the issues established in the next section.

1.4 Objectives

The main objective of this thesis is to increase the existing knowledge in ISF process, specifically for obtaining polymer parts, evaluating and defining the parameters involved to improve the process based on the analysis of quantitative outputs. This should help to provide process guidelines useful for manufacturing complex and customized products.

This thesis aims to develop studies and experiments needed to reach a high level of knowledge of the process and to provide significant contributions to this field.

More specifically, the objectives of the thesis are:

- Study of the influence of the process parameters on the results obtained for the testing basic geometries manufactured by Single Point Incremental Forming (SPIF) for non-biocompatible and biocompatible polymers.

- Characterization of the polymeric materials from the mechanical and thermal point of view and establish the failure mechanisms.
- Evaluation of the feasibility of using polymeric materials for two of the most common ISF process variants: SPIF and TPIF (Two Point Incremental Forming).
- Validation of the process for biomedical applications, more in detail, for manufacturing customized cranial implants.

Achieving the objectives established will permit to improve the knowledge about ISF process in order to successfully manufacture customized implants.

1.5 Thesis structure

The Thesis is organized as follows:

Chapter 1 presents the general domain of the thesis, brief introduction of the ISF technology and exposes the interest, motivation and objectives persecuted in this work.

Chapter 2 reviews the state of the art of ISF. First, presents the ISF process variants and process parameters. Afterwards, presents an extensive review about the use of polymers in ISF and the outputs commonly studied.

Chapter 3 presents an experimental study of the Single Point Incremental Forming (SPIF) process parameters influence on the maximum forming force, the maximum achieved depth and the surface roughness for a non-biocompatible polymer, polyvinylchloride (PVC).

Chapter 4 presents an experimental work to: (i) analyze the time share, power and energy consumption in SPIF; (ii) to select the most suitable process parameters to achieve an appropriate compromise between final depth, surface roughness and energy consumption and (iii) calculate the cost of the experiments. In this work two non-biocompatible polymers are used, PVC and polycarbonate (PC).

Chapter 5 deeply studies the effect of the main process parameters (tool diameter, spindle speed, feed rate and step down) on the maximum forming temperature for three non-biocompatible polymers (PVC, PC and polypropylene or PP) and two biocompatible polymers (ultra-high molecular weight polyethylene or UHMWPE, and polycaprolactone or PCL).

Chapter 6 revisits the formability and failure modes of polymers sheets deformed by SPIF and studies the effect of the spindle speed on the forming limits.

Chapter 7 proposes a functional methodology to produce cranial prosthesis in non-biocompatible polymeric sheet (PC), analyzing the spifability of a series of polymeric sheets

and carrying out a case study with the aim of determining the potential of this process to obtain partial cranial prostheses with complex geometries.

Chapter 8 demonstrates the feasibility of Two Point Incremental Forming (TPIF) to produce a customized cranial implant using a biocompatible polymer (UHMWPE), ensuring an appropriate geometric accuracy at a relative low cost.

Chapter 9 provides a general discussion of the results presented in the thesis.

Finally, Chapter 10 presents the conclusions and main contributions of the dissertation.

Figure 1.4 summarizes the relationships between the different chapters of the thesis.

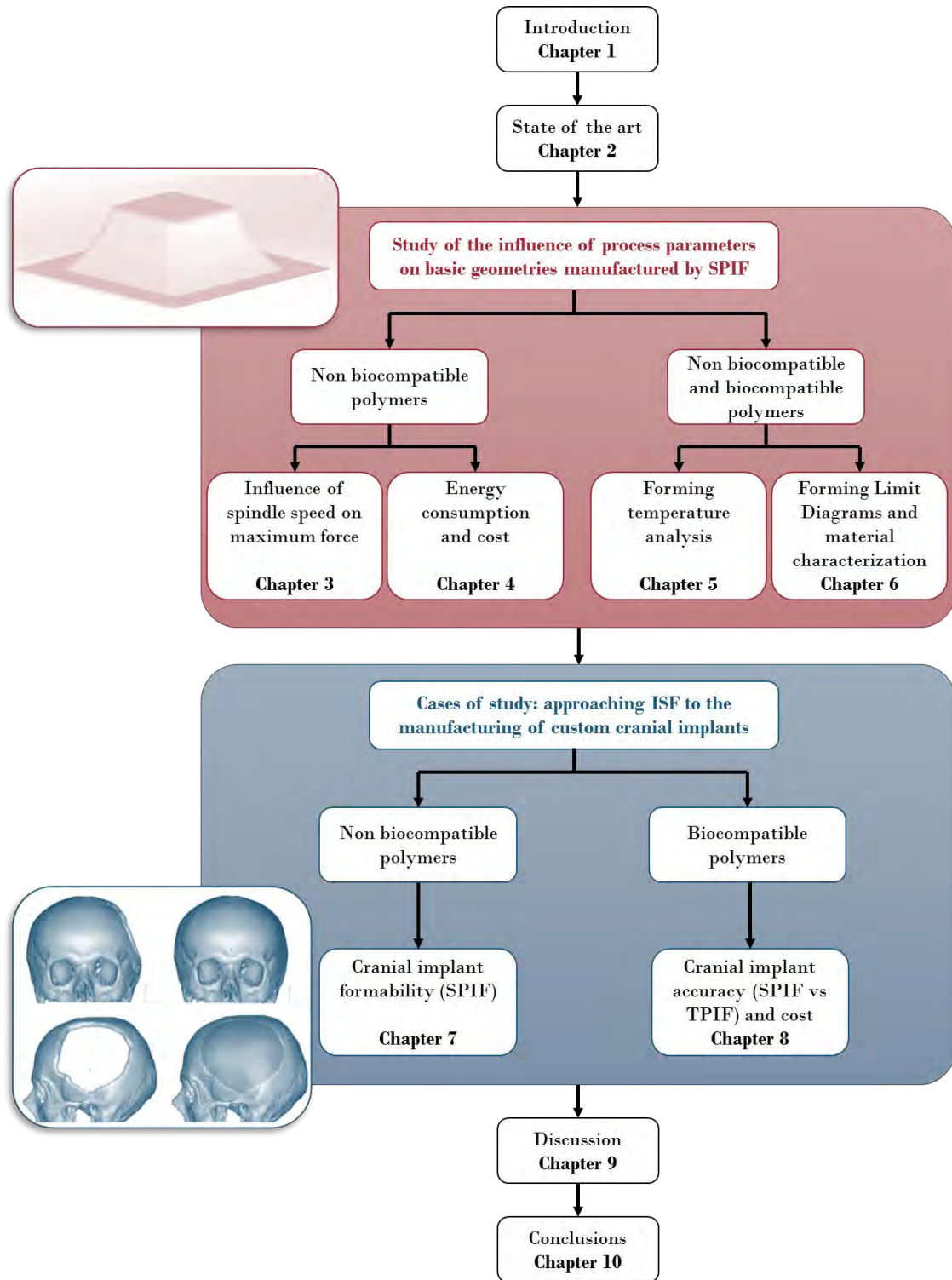


Figure 1.4. Thesis road map

Chapter 2. State of the art

Chapter 2 reviews the state of the art of Incremental Sheet Forming (ISF). First, presents an introduction to the technology, based on the functioning principles, variants of the technology, process parameters and process outputs commonly studied. Afterwards, the literature review is focused on the use of polymeric materials in ISF and the constitutive equations useful for modelling polymer behavior. Then, the potential application fields of polymer incremental forming are analyzed using a business tool to track the influencing external factors. Finally, the last subsection summarizes the gap of knowledge identified from this review, which will establish the basis of the research carried out in the present dissertation.

2.1 Introduction

The functioning principle of ISF is simple: based on the geometry of the target component, a tool path planning software generates the trajectory to be followed by a CNC controlled machine. A forming tool attached to the driving machine deforms incrementally the sheet blank, which is clamped at its boundaries. Deformation occurs at successive layers below the initial sheet surface until the geometry of the part is generated (Figure 2.1). The incremental movement implies that the processing time is long (usually within hours, depending on the part size) compared with deep drawing which can produce a part in a few seconds.

The forming tool used in ISF process is not dedicated for a specific product but can be used in a wide range of parts with different geometries and characteristics. This feature becomes one major advantage of the process: its high flexibility. Another advantage can be derived from the fact that the cost related with the manufacturing of the punch is low, making the ISF technology economically viable for low batch production (Jeswiet et al., 2015).

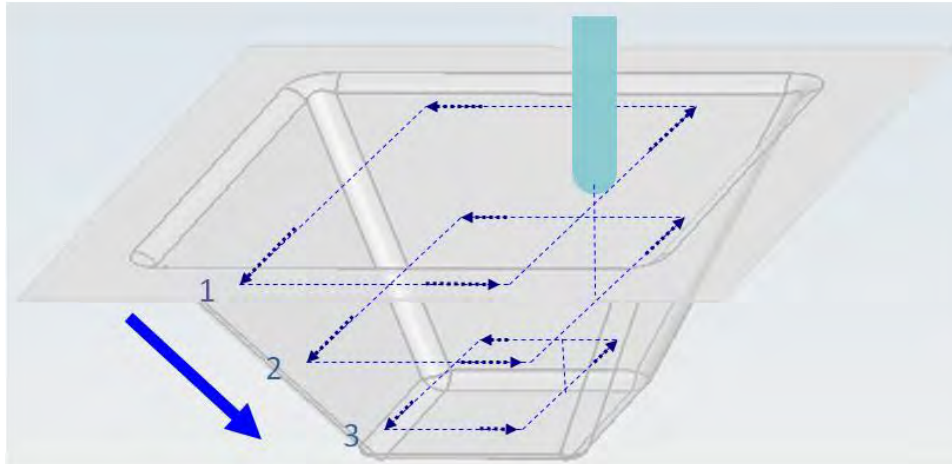


Figure 2.1. 3D schematic representation of the process.

In the early days of the technology, only metallic materials were experimentally tested, therefore, the technology was also known as Incremental Sheet Metal Forming (ISMF). Nowadays, this nomenclature is not used due to the diversification of materials that can be employed in the process.

Commonly, the metallic materials used in ISF are soft aluminum alloys (AA1050) (Ambrogio et al., 2004; Araghi et al., 2009; Fratini et al., 2004) or some steels: DC04 (Bambach et al., 2009), AISI304 (Aerens et al., 2010; Ceretti, 2004), etc. The main reason of using these materials is that they are relatively easy to deform at room temperature. They have been used very frequently and therefore their behavior and properties under ISF conditions are widely known. More recently, researchers are focused on other metal materials such as magnesium alloys or titanium, as it will be deeply reviewed in Section 2.2.3.

Afterwards, the process has also been applied to polymers. The combination of polymers and incremental deformation has as main advantage that can be done at room temperature, thereby reducing heat generation costs required in most processing techniques of plastics. The present thesis is basically focused on forming polymeric material using ISF, therefore, an extensive part of the state of the art will be dedicated to this research topic (Sections 2.5 and 2.6).

2.2 ISF variants

The ISF process can be conducted in any numerically controlled 3-axis machine as they allow high feed rates, significant work volume and stiffness. Indeed, one of the most frequent resources used for ISF is a non-dedicated CNC milling machine because it is available in most workshops, meaning that it is not necessary to make a large investment in machinery. Besides the forming tool, a forming setup including a clamping system is required to convert a milling machine into an ISF system, therefore it is a relatively economic solution (Jeswiet et al., 2005b).

There is also machinery especially dedicated to the ISF technology, such as the one developed by AMINO. These machines are equipped with a movable clamping system, allowing the realization of different process variants (Ingarao et al., 2014).

A third type of equipment that can be used to realize ISF is an industrial robot. The main limitations are the low stiffness and maximum force that it can withstand. The die can be substituted by another robot acting as a support tool (Ingarao et al., 2014).

2.2.1 Single Point Incremental Forming (SPIF)

In terms of set-up, this is the simplest variant of the technology and the most deeply and, as it will be seen throughout this section, it is also the most widely studied in the academic field due to its high flexibility and low cost. There is only one point in which force is applied: the contact zone between the forming tool and the blank sheet (Figure 2.2). In this case neither partial nor total die is utilized; hence, the blank is only supported at the edges by the clamping system. Precisely due to the lack of a die, the main drawback of this variant is the low accuracy, mainly as a consequence of the global springback that occurs once the final part is unclamped. In order to compensate the geometrical deviation, one of the commonly used solutions is the modification of the toolpath to impose larger deformation on the sheet. Then, when the springback effect occurs, the sheet will be located in the desired point.



Figure 2.2. SPIF variant (Allwood et al., 2010).

2.2.2 Two Point Incremental Forming (TPIF)

In this case there are two points in which the force is applied, hence the name of this process variant. The first point, as in SPIF, is in the contact zone between the forming tool and the blank. The second point is at the blank-die interface. The die can be total (Figure 2.3a,b) or partial (Figure 2.3c) and the die, and consequently the forming process, can be negative (Figure 2.3a) or positive (Figure 2.3b,c). In the negative case, the tool is in contact with the inner side of the part, while the outer side of the part is contacted in the positive case. In the later situation, the complexity of the set-up increases because there is need to move the fixing device in perfect synchrony with the axial feed of the tool.

The die can be manufactured using materials that are cheap and easy to machine (wood, resins, etc.). Therefore, the costs associated with the die production are still not comparable with the ones related to the production of dies used in deep drawing processes. Consequently, the TPIF technology is also viable to manufacture small batch products.

Although the complexity of the set-up is higher in TPIF than in SPIF the dimensional accuracy obtained in the former variant can be significantly improved (Attanasio et al., 2008).

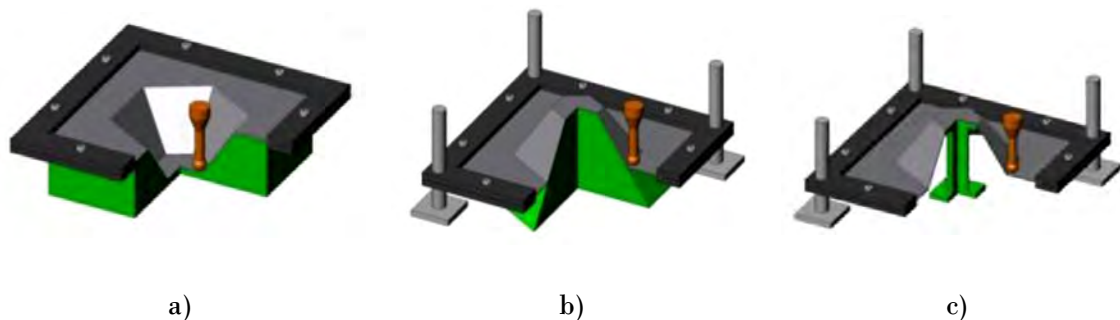


Figure 2.3. TPIF process variants: a) negative full die, b) positive full die and c) positive partial die (Allwood et al., 2010).

2.2.3 Hot ISF

This variant is the combination of the ISF technology (either in SPIF or TPIF variant) with a heating system. The most important advantage of using the heating system is that the formability of the sheet can be significantly increased. There are few research papers that have been focused on the performance of warm ISF, mainly applying this variant in materials that are very difficult to deform at room temperature like magnesium (e.g. AZ31) or titanium alloys (e.g. Ti6Al4V). Therefore, this section provides a review of these works according to the kind of material and the heating system employed.

Several heating systems have been used (Figure 2.4): (a) local heating produced due to the friction between the tool rotating at a high spindle speed and the material (Park et al., 2009); (b) heating device attached to the clamping system (Ambrogio et al., 2008); (c) heating chamber covering the entire ISF process (forming tool, clamping system and blank) in order to obtain a global warming (Zhang et al., 2009); (d) localized heating system

generated from electrical circuit (Fan et al., 2008) and (e) laser beam used as a heating source to locally heat the sheet (Dufloy et al., 2008).

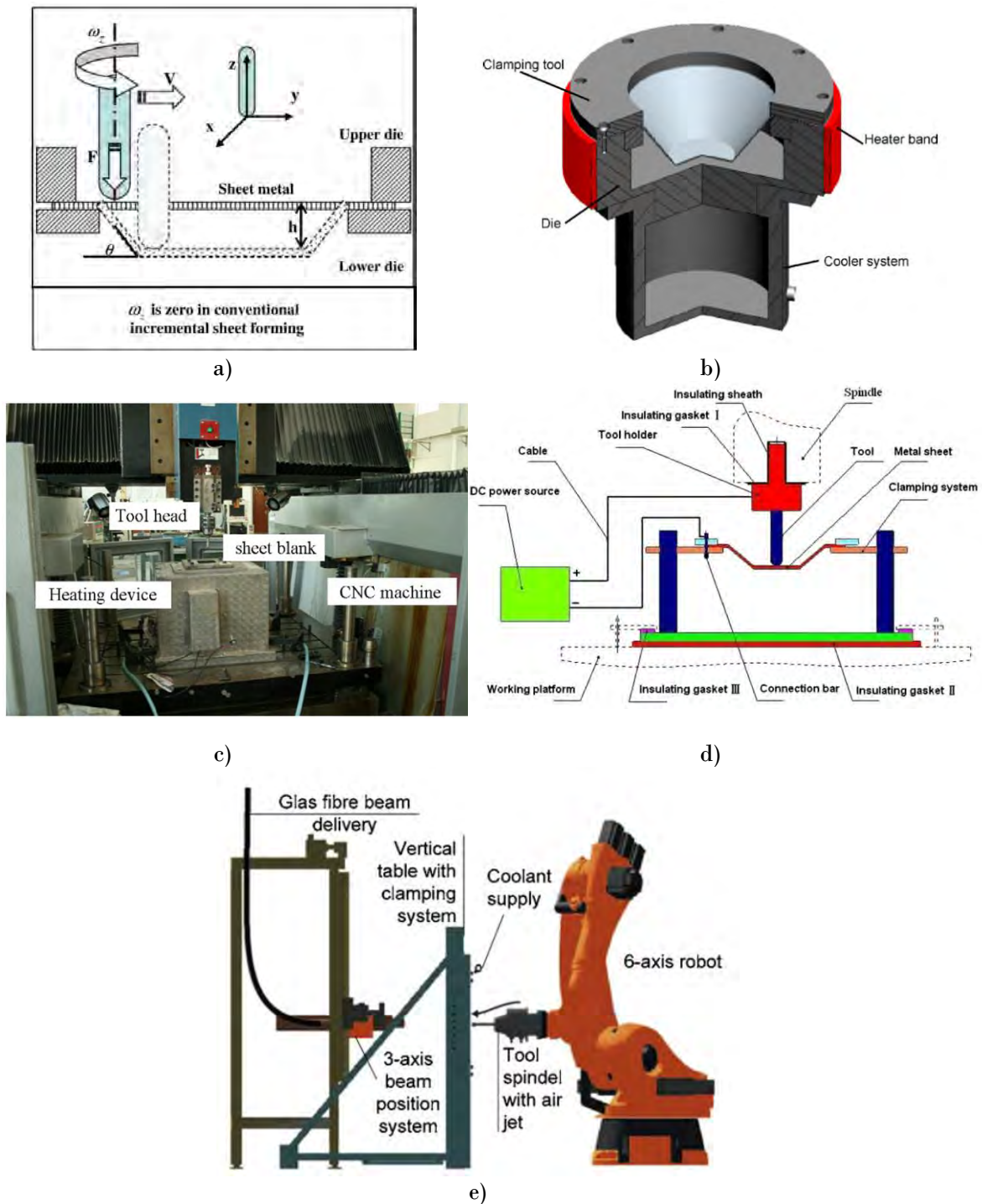


Figure 2.4. a) Rotational ISF (Park et al., 2009). b) Hot clamping system (Ambrogio et al., 2008). c) Hot chamber (Zhang et al., 2009). d) Electric resistance (Fan et al., 2008). e) Laser assisted ISF (Dufloy et al., 2008).

Magnesium alloys

Taking advantage of magnesium lightweight property, its use in automotive, aeronautic and electronic applications is considerably increasing in recent years. However, because of its

hexagonal-closed-packed (hcp) crystal structure it has very low ductility and so formability at room temperature.

Nowadays, magnesium is used basically in die casting processes being able to obtain complex parts, however, the mechanical properties (strength and ductility) of these parts are not good enough. Forming processes arise as an alternative for processing magnesium alloys since a fine grained structure, without porosity and with better mechanical properties can be achieved (Park et al., 2009) if the forming process is carried out at elevated temperatures to improve material formability.

Several researchers have used warm ISF, developing different heating devices, to manufacture parts using magnesium alloys.

In one of the pioneers works in this field (Ambrogio et al., 2008), it was shown that the formability of magnesium AZ31-O at room temperature was very low whereas at 250°C there was a significant increase of the strains at fracture (Figure 2.5). They developed a new heating equipment consisting on a heating band around the clamping device to increase the global temperature of the sheet. The setup was also designed to avoid heat transmittance to the machine using a cooling system on the lower part. With this equipment it was possible to clamp circular blanks with the aim of forming truncated cones having the following dimensions: 100 mm major diameter and 40 mm depth.

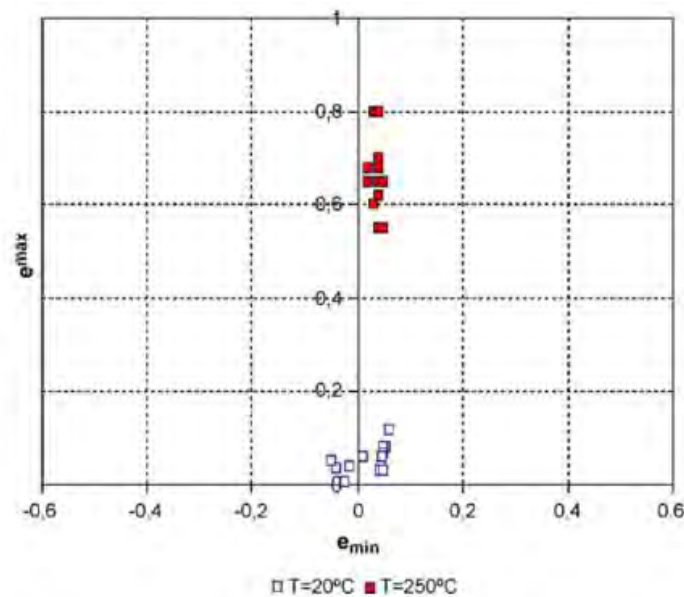


Figure 2.5. Magnesium strains at failure at different temperatures (Ambrogio et al., 2008).

They conducted a CCD (Central Composite Design) experimental campaign with the following process parameters: tool diameter (12, 15, 18 mm), tool depth step (0.3, 0.65, 1 mm), sheet temperature (200, 250, 300°C) and wall angle (45, 50, 55, 60, 65°). The sheet thickness was 1 mm for all the tests. When magnesium alloys are used it is very important to correctly choose the lubricant, being able to withstand the local deformation and the elevated temperatures, avoiding material peeling off (Zhang et al., 2010). One of the most appropriate lubricants is solid graphite (MoS_2), being the chosen one in Ambrogio's work.

Forming Limit Diagrams (FLD) and forming forces were analyzed (Ambrogio et al., 2008), showing that the maximum formability occurred at 250°C and that the forming force decreased with the increase of the temperature. Similar results regarding the improvement of the formability with the temperature were found by Ji and Park (2008), as shown in the forming limit curves obtained from plane-strain stretching and axisymmetric stretching tests (Figure 2.6).

It is also possible to locally increase the sheet temperature without an external device, simply using high tool rotations in order to accelerate plastic deformation (Park et al., 2009). This process is called RISF (Rotational Incremental Sheet Forming).

In RISF the sheet is clamped on the framework while the tool rotates to its own axis at high speed, penetrating step by step along the established tool path. This generates an important amount of heat in the contact zone due to the friction between the tool and the sheet and also due to the energy of plastic deformation. This localized heat accelerates the plastic deformation and increases formability.

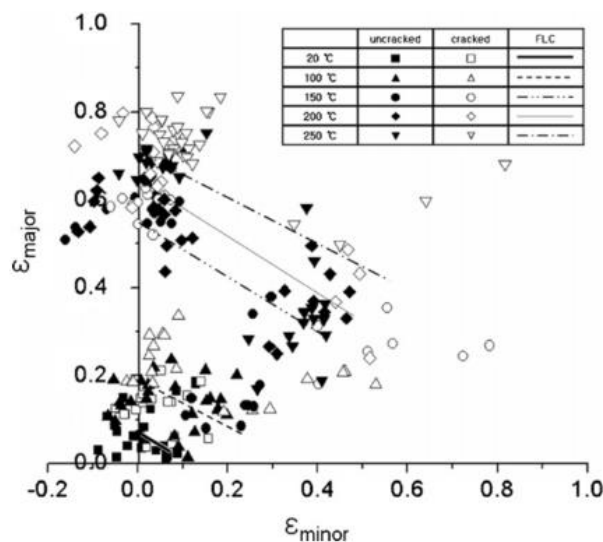


Figure 2.6. AZ31 forming limits at different temperatures (Ji and Park, 2008).

Park et al. (2009) determined the formability of AZ31 magnesium sheets (150x150x1 mm) forming square cups (80x80x25 mm with wall angles of 45, 60 and 70°). Tool radius was 6 mm, feed rate was 400 mm/min and tool speed rotation was 4000 rpm (counterclockwise). An infrared thermometer measured the achieved temperatures. Rotation speed was decreased once the temperature reached 100°C (when chips appeared) ensuring that the material surface was not deteriorated. They analyzed the variation of the grain size (the grain size is in inverse proportion of strain rate), the FLD (showing plane strain at the walls and biaxial stress at the corners, represented in blue and red circles respectively) and thickness distribution (Figure 2.7 a, b and c respectively).

The influence of anisotropy of AZ31 magnesium alloy sheets has also been studied depending on the sheet's fabrication method (Zhang et al., 2009). These sheets were used in single point incremental forming process and the formability and surface quality of the parts

was determined. In this work, a heating chamber was used for increasing the sheet temperature.

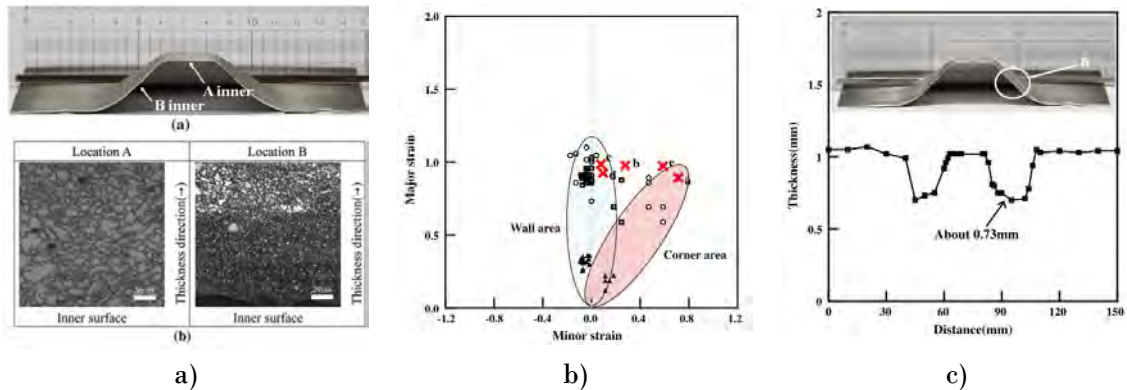


Figure 2.7. RISF results using AZ31: a) grain size, b) FLD, c) thickness distribution (Park et al., 2009).

Recently, dynamic local heating assisted by laser irradiation (Figure 2.8) has also been employed for improving magnesium formability in SPIF (Hino et al., 2014). The local heating temperature was measured using thermocouples and infrared thermography at various laser powers, laser spot speed and defocus. It was observed that the temperature increased when laser beam spot speed is slow, the defocusing distance is short and laser power is high. It was also confirmed the improvement of the formability and the reduction of residual stresses.

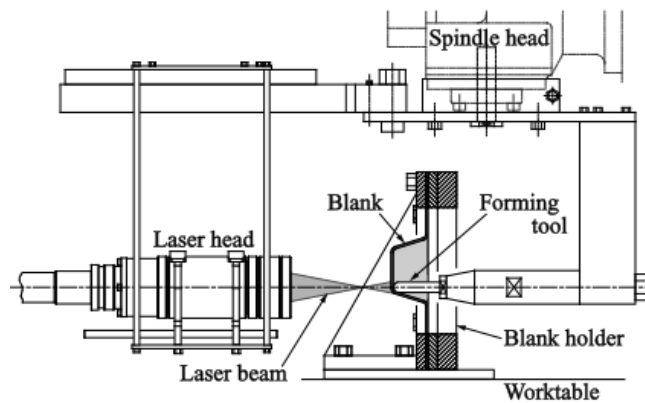


Figure 2.8. Schematic representation of the SPIF system with dynamic local heating by laser irradiation (Hino et al., 2014).

The effect of depth step and feed rate on formability and geometric accuracy on AZ31 warm ISF has been recently studied in the work of Sy and Nam (2015). They used a heating system based on Joule effect, adjusting the forming temperature using a feedback control system with thermocouples (Figure 2.9a). As previously revealed in other research works (Ambrogio et al., 2008; Ji and Park, 2008), the optimum forming temperature was around 250°C. Regarding geometric accuracy, at 250°C a maximum error between the CAD profile and the manufactured one was 0.7 mm (Figure 2.9b), while for higher temperatures (300°C) the part was twisted, decreasing significantly the accuracy.

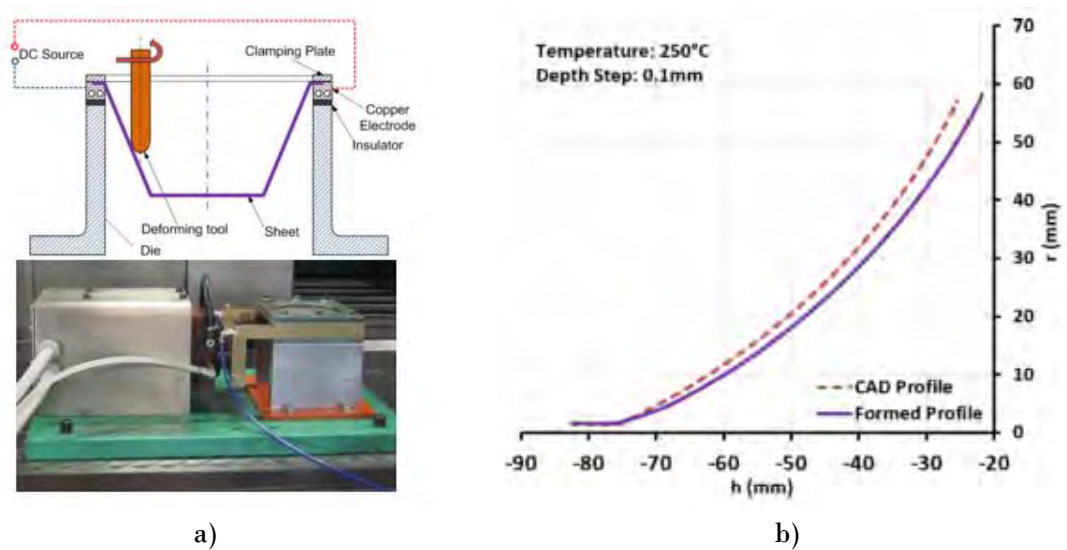


Figure 2.9. a) Experimental system for warm ISF. b) Geometric accuracy (Sy and Nam, 2015).

Titanium alloys

Titanium is a widely used material in aerospace and biomedical sectors, due to its high corrosion resistance, lightweight and good mechanical properties.

Commercially pure titanium (CP Ti) sheets were deformed using ISF at room temperature (Hussain et al., 2008b) in order to evaluate the effect of several process parameters (step down, tool diameter, feed rate and friction between the sheet and the tool) on the formability. The test geometry was a conical frustum with a variable wall angle. The best process conditions to enhance material formability were: low step down, low feed rate, low tool diameter and low friction. In another work of the authors (Hussain et al., 2008a), different tool materials were used to deform incrementally CP Ti sheets at room temperature to determine the effect on the tool wear and material adherence in the tool tip. High-speed steel (HSS) surface-hardened was the most suitable tool material. Furthermore, they experimented with several lubricants and it was shown that organic lubricants are not appropriate whereas the best lubricant was a dispersion of MoS_2 powder in white petroleum jelly with a 4:1 ratio.

Ti6Al4V is the most commonly used alpha/beta titanium alloy. It has high strength, corrosion resistance, low density and good biocompatible properties. However, the formability at room temperature is very poor, thus, a heating system is required to be able to form this alloy. Fan et al. (2008) developed a novel technique, electric hot incremental forming, consisting of obtaining an electric closed circuit with DC power supply, cables, the tool and the sheet. Due to Joule's law, when current passes from the tool to the sheet, heat is obtained, so local temperature increases. This variation of temperature increases the ductility of the material in the contact zone. In a subsequent work, Fan et al. (2009) used this principle to form Ti6Al4V sheets. Their investigations were mainly focused on determining the best kind of lubricant and the optimum forming temperature. Regarding the lubricant, it must withstand the elevated temperatures required for forming the

titanium alloy (more than 500°C), therefore, liquid lubricants cannot be used. The best results were obtained when self-lubricating nickel disulfide metal matrix composite (Ni-MoS₂) was used. The optimum forming temperature ranges from 500 to 600°C, over 600°C severe oxidation on the titanium sheet appears and the formability is not enhanced. Honarpisheh et al. (2015) have used the electric hot incremental forming setup to determine the influence of the process parameters on the evolution of the forming forces during the manufacturing of Ti6Al4V sheets truncated cones. Increasing the tool diameter it is possible to decrease the forming force due to the increased contact area between the sheet and the tool (Figure 2.10).

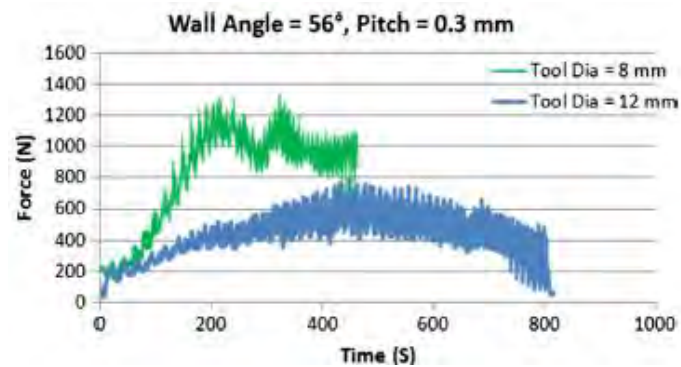


Figure 2.10. Variation of the forming force with the tool diameter in electric hot incremental forming (Honarpisheh et al., 2015).

Other heating techniques can be used to increase the temperature of titanium sheets in the ISF process, such as a high-speed tool rotation (Ambrogio et al., 2013). In this work a CNC lathe (Figure 2.11) is used instead of a CNC milling machine in order to increase the process speed, however, only axisymmetric parts can be formed. Experimental tests using two titanium alloys (CP Ti and Ti6Al4V, grade 2 and grade 5 respectively) were performed. Their results demonstrated that it is possible to successfully form titanium alloys in few minutes without modifying the material microstructure and micro-hardness. In a recent work, Ambrogio and Gagliardi (2014) analyzed statistically the variation of the temperature during the incremental forming of two lightweight alloys, Ti6Al4V and AA5754. They varied the step down and feed rate in order to increase the temperature allowing an improvement of the formability for these materials. Later, this work was extended in order to provide a model for predicting the temperature during the forming process (Ambrogio et al., 2016).



Figure 2.11. High-speed SPiF in a CNC lathe (Ambrogio et al., 2013).

2.2.4 Stretch Forming with ISF

In order to solve the principal drawbacks of the ISF technology (sheet thinning, accuracy and process time), a new hybrid process that combines ISF with Stretch Forming has been proposed by Araghi et al. (2009).

The first stage of the hybrid variant consists on obtaining a pre-form using Stretch Forming. In this first stage an approximation to the final geometry can be reached. The slots, cavities or deep corrugations are achieved in a subsequent ISF manufacturing stage (Figure 2.12). This hybrid process allows a reduction of the process time and more uniform thickness distribution.

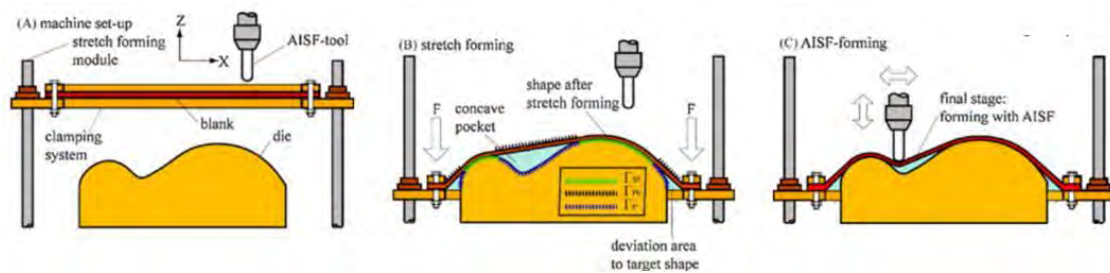


Figure 2.12. Operation principle of the hybrid process (a) experimental setup, (b) first stage: stretch forming, (c) second stage: ISF (Araghi et al., 2009).

2.2.5 Roboforming

Many manufacturing industries have in their installations industrial robots, therefore several researchers have interest in the performance of the ISF technology using industrial robots, a variant known as Roboforming. The main features of the robots are: fast movements, low stiffness and low capacity of withstanding high forces. The last two features might limit its use for the manufacturing of incremental formed parts.

Schafer and Schraft (2005) published one of the first works in which the use of industrial robots in incremental sheet forming was studied. They developed the process using hammering tools and without any die plate (Figure 2.13), being able to form several complex geometries with an acceptable geometric accuracy.

With the use of robots it is possible to replace the partial or full die by another robot (Meier et al., 2009), which acts as a support tool of the sheet, as it can be seen in Figure 2.14.

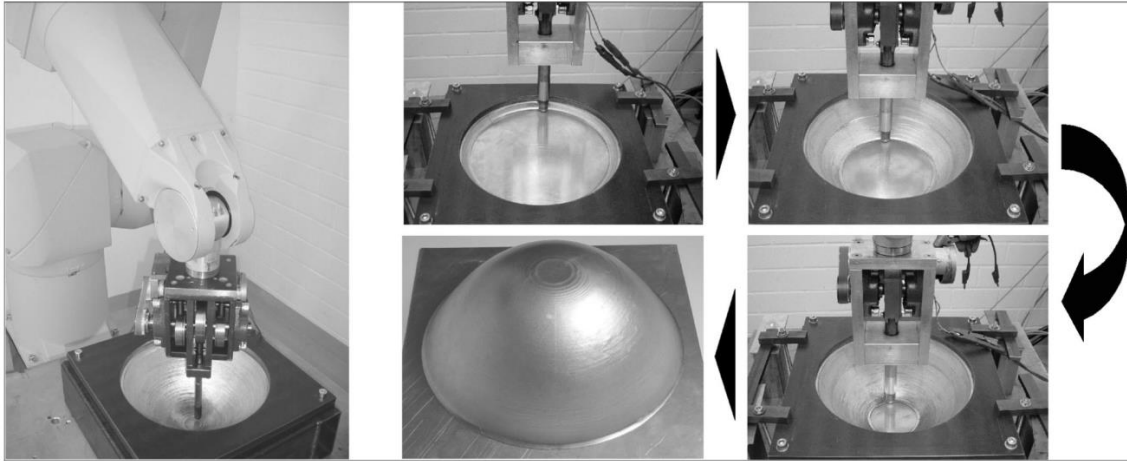


Figure 2.13. Robot cell for incremental forming of aluminum metal sheet (Schafer and Schraft, 2005).



Figure 2.14. Experimental set-up of Roboforming (Meier et al., 2009).

2.3 Process parameters

The most important process parameters involved in the ISF technology can be classified into three main groups: (i) the factors related to the design of the part to be manufactured; (ii) the tool features and (iii) the process factors. As it has already been mentioned, the most widely used metallic materials in ISF are some aluminium and steel alloys, due to their high formability at room temperature, justifying why almost all of the papers cited in sections 2.3 and 2.4 will be based on these materials.

2.3.1 Design

According to the feature's complexity of the part that has to be manufactured using ISF, the geometry can be classified as follows:

- *Simple*: basic geometries, mainly used in basic research to determine the effect that the process parameters have on several outputs, such as forming forces, accuracy, etc. Generally are truncated cones or pyramids with a constant wall angle.
- *Intermediate*: this type of geometries are also used in research works, which usually are not applicable in the industrial field, but have interesting geometric features (variable wall angle, a combination of concave and convex parts...).
- *Complex*: this group includes the industrial components, such as prototypes, dies, automotive parts or prostheses.

Once the geometry is decided, the material has to be chosen. As already mentioned, up to now, it is possible to form incrementally aluminium alloys, steel, magnesium, titanium and polymers. The initial sheet thickness is usually in the range of 0.5-5 mm, although it is also possible to perform microincremental forming (Figure 2.15) with sheet thicknesses below 0.1 mm (Obikawa et al., 2009; Puigpinós et al., 2012; Santo et al., 2010).

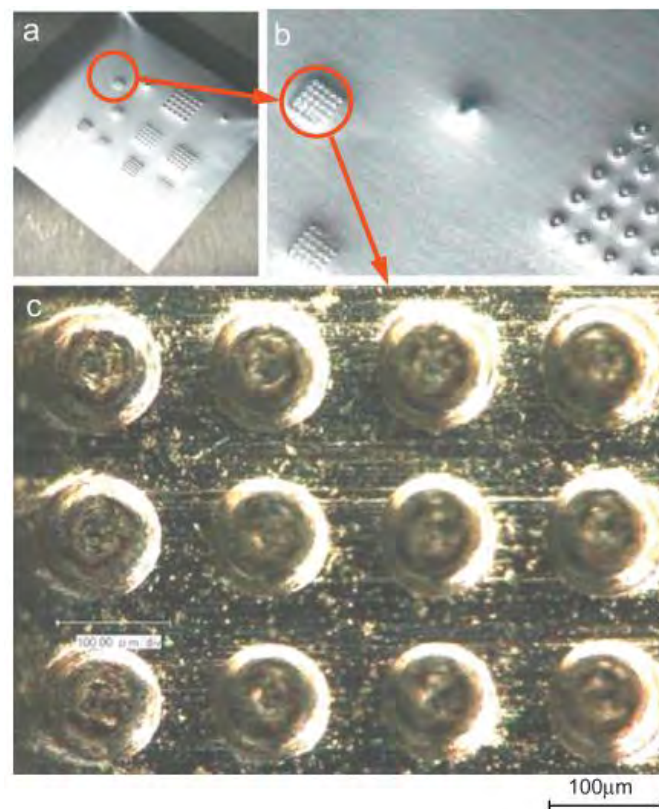


Figure 2.15. An example of microincremental forming, miniature dots 0.1 mm in diameter in aluminum AL-2 with 12 μm sheet thickness (Obikawa et al., 2009).

2.3.2 Tool

Regarding to the toolpath, the most common strategies are (Jeswiet et al., 2005b):

- *Unidirectional*: the tool is moved in the same direction (clockwise or counterclockwise) along a plane. Torsion and tool indentation appear in the final part. The profile of the geometry is followed in a discrete way.
- *Bidirectional*: in this case the tool movement changes its direction in each plane, avoiding the appearance of torsion but tool indentation appears. The profile of the geometry is followed in a discrete way.
- *Spiral*: it is basically used in order to improve the surface finishing, because the profile of the geometry is followed in a continuous way and there is no tool indentation in the surface of the sheet. Torsion appears to the final part.

From the experimental work, some examples of the abovementioned effects of torsion and tool indentation are shown in Figure 2.16 and Figure 2.17, respectively.

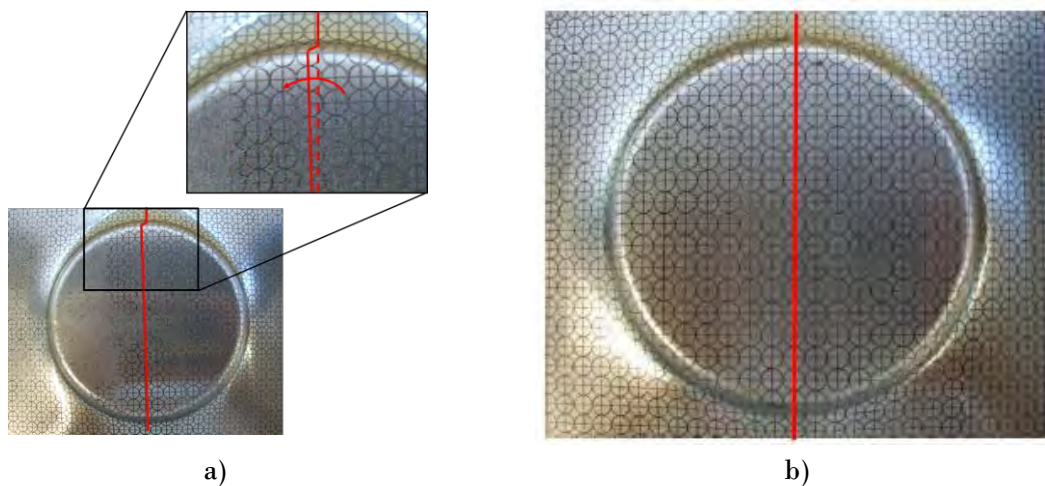


Figure 2.16. a) Torsion appeared due to unidirectional or spiral tool path. b) Part manufactured using bidirectional toolpath to avoid torsion.

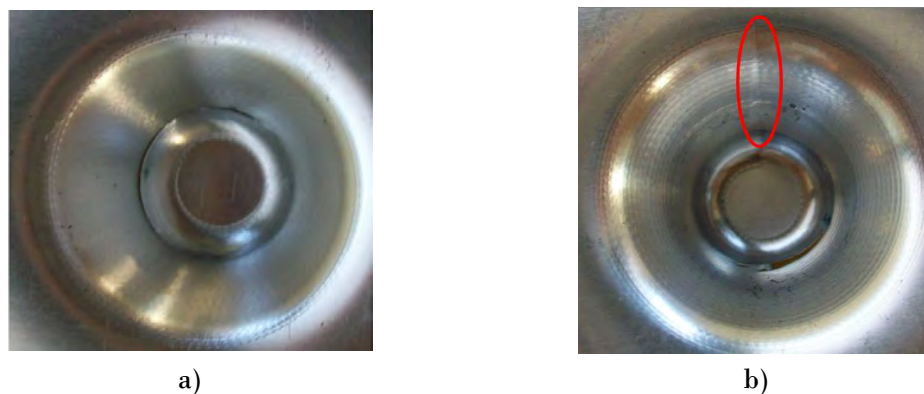


Figure 2.17. a) Spiral toolpath with good surface finishing. b) Unidirectional or bidirectional toolpath, with tool indentation.

There are three different types of tools: *flat* (the less used in the literature) (Ziran et al., 2009), *ball end* (the ball has free rotation in order to have the minimum friction) (Kim and Park, 2002; Li et al., 2014) and *hemispherical*, being the last one the most commonly used.

The tool diameter is usually in the range of 4-20 mm, but in order to perform microincremental forming smaller tools are required (below 1 mm).

2.3.3 Process

A process parameter with strong influence in the accuracy, surface finishing, forming forces and operational time is the *step down*. This parameter determines the tool displacement along the different forming layers. Higher step downs will provide worst surface finishing, higher forming forces and forming time. Usually, a forming process is considered as *incremental* if the step down is below 1 mm, for higher values the deformation mechanism will be more similar to a deep drawing process rather than an incremental forming process. The step down can be defined according to three strategies:

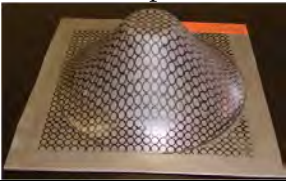
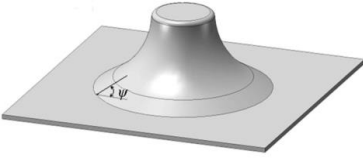

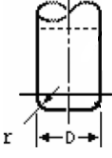
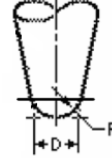
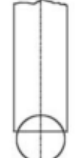
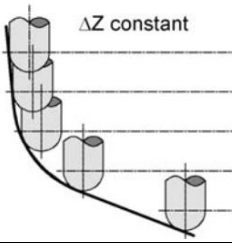
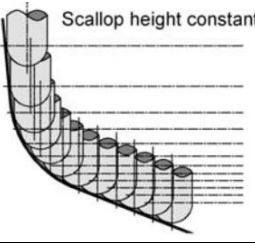
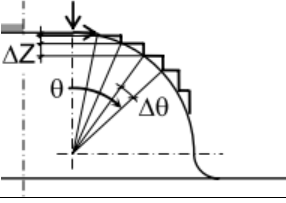
- *Constant step down (Δz)*: the axial movement of the tool is defined with a constant value. The surface finishing is better in steep walls (Attanasio et al., 2008, 2006).
- *Constant scallop height (Δh)*: the separation of the different layers varies with the wall angle, allowing better surface finishing than in the previous case (Callegari et al., 2006).
- *Constant angular increment ($\Delta\theta$)*: the angular increment between two successive layers has to be constant. The main disadvantage is that for very steep walls the surface finishing is not acceptable (Fiorentino et al., 2009).

The feed rate should be as higher as possible in order to reduce the forming time and energy consumption (Ingarao et al., 2014). The spindle speed or tool rotation can be set “free” meaning that it will rotate depending on the friction conditions between the tool and the blank, or can be set at a fixed value. As mentioned in section 2.2.3 it can be used as a local heating solution for increasing material formability.

Finally, it is important to adequately select the forming lubricant depending on the sheet material. Grease (Duflou et al., 2007b; Jackson and Allwood, 2009; Kopac and Kampus, 2005) and oil (Bambach et al., 2009; Li et al., 2015; Park and Kim, 2003; Takano et al., 2008; Verbert et al., 2008) are the most widely used lubricants. Several researchers use a water-soap emulsion for lubricating the tool-sheet interface in polymer ISF (Franzen et al., 2009; Marques et al., 2012; Silva et al., 2010). In order to withstand the elevated temperatures required for forming magnesium and titanium alloys, solid lubricants, for instance, graphite powder and MoS₂ should be employed (Fan et al., 2009; Husmann and Magnus, 2016; Zhang et al., 2010).

Table 2.1 summarizes the classification of the ISF process parameters.

Table 2.1. Summary of the most important process parameters.

Design	Geometry					
	Material	Aluminum	Steel	Magnesium	Titanium	Polymers
	Sheet thickness	Microforming (<0.1 mm)			Macroforming (0.5 – 5 mm)	
Tool	Tool path	Unidirectional (clockwise or counterclockwise)		Bidirectional		Spiral
	Type					
	Dimensions	Microforming (<1 mm)			Macroforming (4 – 20 mm)	
Process	Step down					
	Feed rate	400 – 3000 mm/min				
	Spindle speed	Free – 4000 rpm				
	Lubricant	Grease	Oil	Water-soap emulsion	Solid	

2.4 Process outputs

2.4.1 Forming forces

The determination of the forming force magnitude in ISF is especially important in the case of using machinery adapted for the process like milling centers and robots, in order to verify if the equipment will be capable of carry out the process. The first research works dealing with the experimental measurement of the ISF forces, appeared in 2005. Jeswiet et al. (2005a) and Jeswiet and Szekeres (2005) used a force sensor consisting on a spindle mounted cantilever beam with strain gauge Wheatstone bridges to measure the three orthogonal forces of AA3003-O truncated cones and pyramids manufactured using SPIF and TPIF. It

was demonstrated that the predominant force in ISF is developed in the axial direction of the tool (Figure 2.18) while this, in general, is not the case in milling.

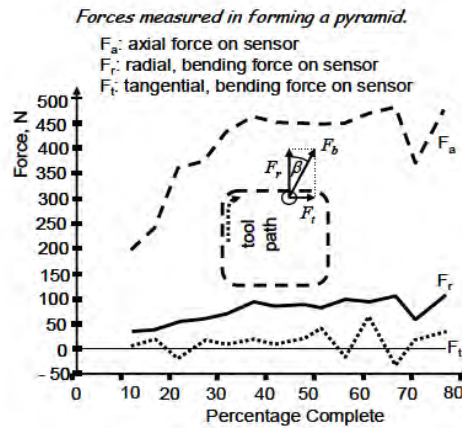


Figure 2.18. Measured forces during SPIF process of a truncated pyramid (Jeswiet and Szekeres, 2005).

The axial forming force was used as a monitoring and control approach to determine when the material is close to failure due to excessive thinning (Filice et al., 2006). The clamping system was fixed on a Kistler piezoelectric dynamometer. They presented how the forming force trend varied with the sheet thickness, step down, tool diameter and wall angle during the SPIF manufacturing of a truncated cone in AA1050-O aluminum alloy (Figure 2.19).

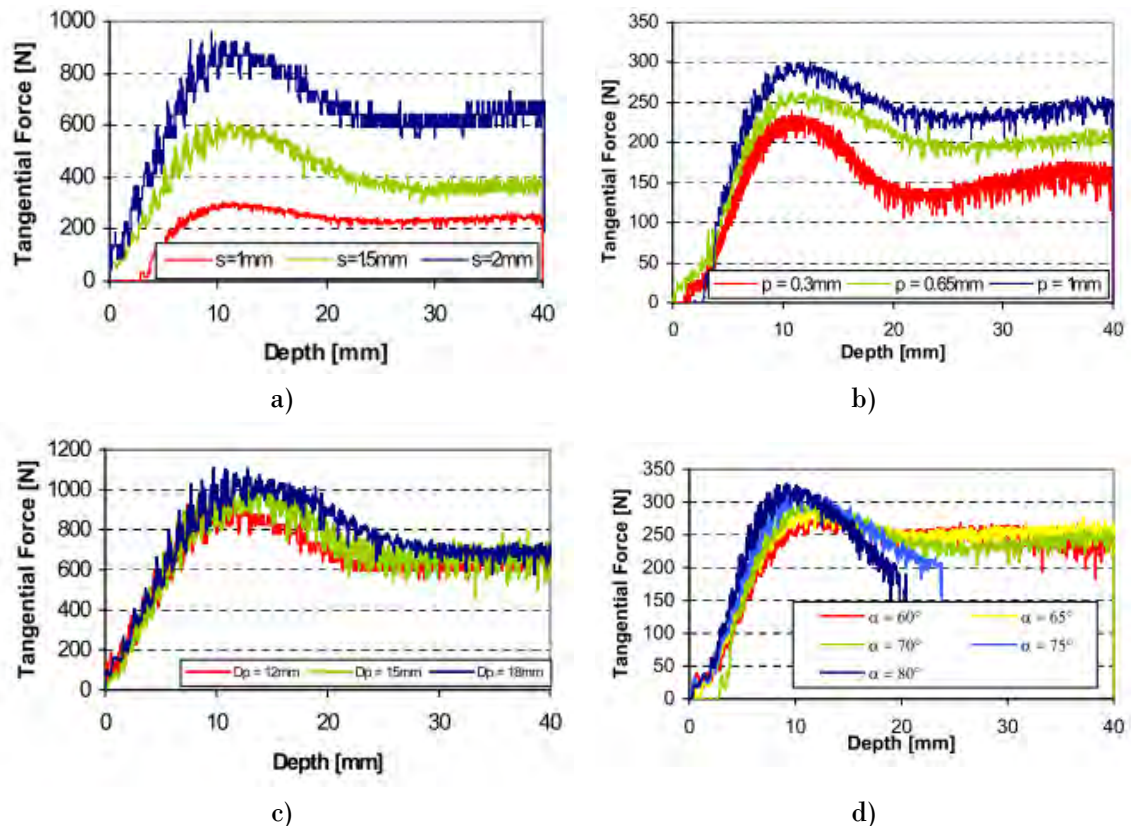


Figure 2.19. Axial force evolution for different: a) sheet thicknesses, b) step down, c) tool diameter and d) wall angle (Filice et al., 2006).

The forming force trends were classified as follows:

- *Steady state*: appears for low wall angle values, after reaching the maximum value, the forming force remains constant due to the equilibrium between the sheet thinning and strain hardening effect (Figure 2.20a).
- *Polynomial*: this trend occurs when parts with higher wall angle are formed, after reaching the peak, the force is reduced because of the important thickness reduction. Then, the force becomes stationary again since the process conditions do not lead to material failure (Figure 2.20b).
- *Monotonically decreasing*: in this case, the forming force decreases after the peak until material failure, because the strain hardening is not able to compensate the material thinning and reach an equilibrium (Figure 2.20c).

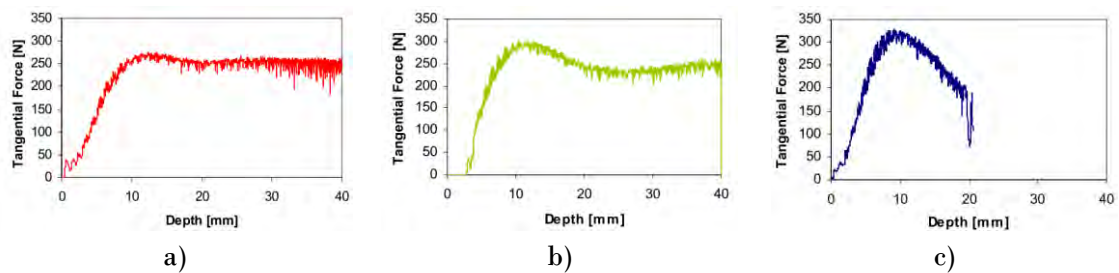


Figure 2.20. Classification of the forming force trends: a) steady state. b) polynomial. c) monotonically decreasing (Filice et al., 2006).

These trends were used to verify the effectiveness of the on-line force monitoring system to avoid failure by automatically modifying some process parameters (tool diameter and step down). This strategy could be used in industrial applications to automatically update the initially defined process parameters in order to avoid material collapse.

Later, Duflou et al., (2007b) published a similar work for AA3003-O truncated cones obtained by SPIF. Forces were measured with a Kistler 9265B dynamometric table connected to an amplifier. A filter was applied to reduce the noise from the force signal. Again, it was demonstrated that the axial component was the predominant one (Figure 2.21a). It was also observed that when one contour of the tool path was completed, the axial component of the force (F_z) drop to zero, then reaches a peak at the step down and finally reached a stable value, while F_x and F_y followed a sinusoidal trend (Figure 2.21b). The increase of step down, tool diameter, wall angle and sheet thickness increase the forming force, as previously found in Filice et al. (2006).

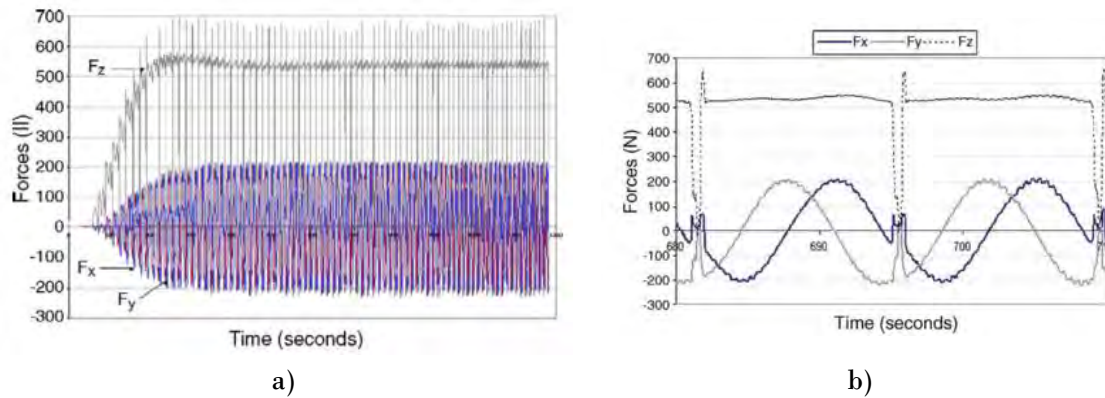


Figure 2.21. a) Three force components. b) Detailed view of the force evolution (Duflou et al., 2007b).

Almost in parallel, another experimental work showing the effect of the process parameters on the forming force evolution in SPIF forming of a steel DC01 truncated cone was done (Petek et al., 2009). A force acquisition system (Figure 2.22) similar to the one presented by Duflou et al., (2007b) was used, obtaining similar results.

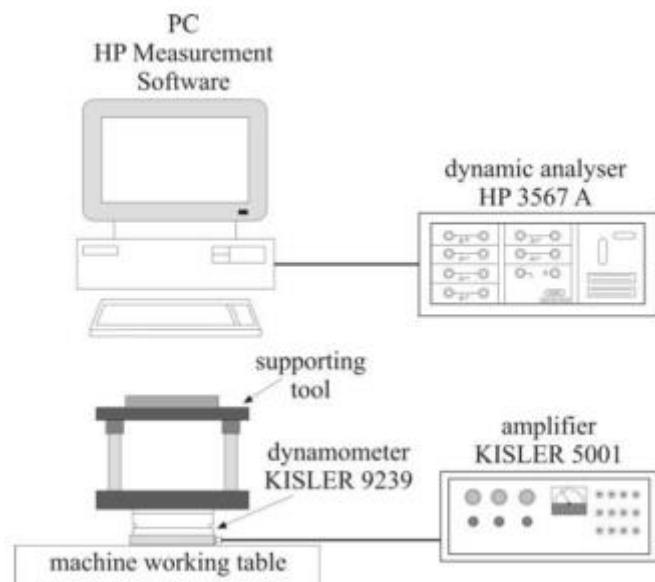


Figure 2.22. Acquisition system for force measurements in SPIF (Petek et al., 2009).

A comparison of the forming forces for variable wall angle geometries manufactured in deep drawing steel (FeP04) using SPIF, TPIF negative and TPIF positive revealed an increase of the forming force with the presence of a die (Fiorentino et al., 2009). In the case of the TPIF variant, less forming force was required to obtain the final part when a positive die was used.

Several research works have focused on providing an accurate estimation of the maximum axial force developed during the forming process in order to ensure the safe utilization of the hardware and guarantee the structural integrity of the work piece.

Aiming for quick estimations of the maximum force, several analytical models intended for uniform wall angle (UWA) geometries formed with different materials have been proposed.

The first ISF force analytical model was proposed by Iseki (2001), who assumed plane-strain conditions, uniform sheet deformation and neglected friction for its derivation. When designing and manufacturing a dedicated ISF equipment, Allwood et al. (2005a) proposed a second analytical model to estimate the vertical force limits of its equipment. However, recent research (Pérez-Santiago, 2012) has confirmed that the model developed by Aereus et al. (2010) provides accurate estimations of the steady state axial forming force (F_{Zs}) of truncated Uniform Wall Angle (UWA) cones formed with the metallic alloys, for instance aluminum or stainless steel, generally utilized in ISF works. This analytical model, Equation 1, is a phenomenological correlation originated from the results of an experimental campaign conducted on two aluminum alloys, AA3003 and AA5754, and three steel alloys DC01, AISI304 and 65Cr2.

$$F_{Zs} = 0.0716 R_m t_0^{1.57} d_t^{0.41} \Delta h^{0.09} \alpha \cos \alpha \quad (1)$$

R_m (MPa) is the tensile strength of the formed material aligned with the wall direction; t_0 (mm), initial sheet thickness; d_t (mm), tool diameter; Δh (mm) the scallop height; and α (°) initial wall angle.

Recent research works have shown that the spindle speed, in addition to the abovementioned process parameters, has an important effect on the maximum axial forming force variation (Centeno et al., 2014) as shown in Figure 2.23 for tests performed using AISI 304, mainly due to the heat originated due to the increase of the friction with the spindle speed.

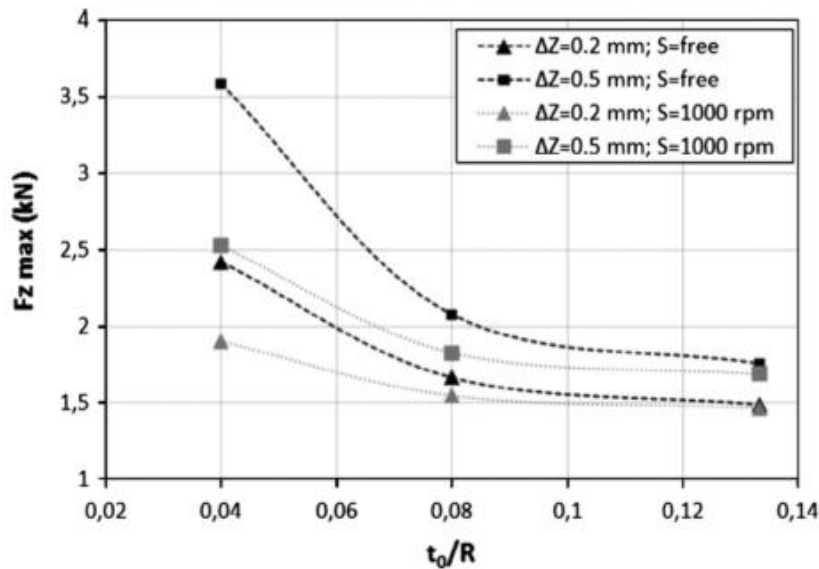


Figure 2.23. Evolution of the maximum axial force depending on the t_0/R (initial sheet thickness to tool radius ratio) (Centeno et al., 2014).

A fishbone diagram is presented in Figure 2.24 as a summary of the parameters that have been mostly investigated in the literature and that have shown to have an effect on the variation of the forming force.

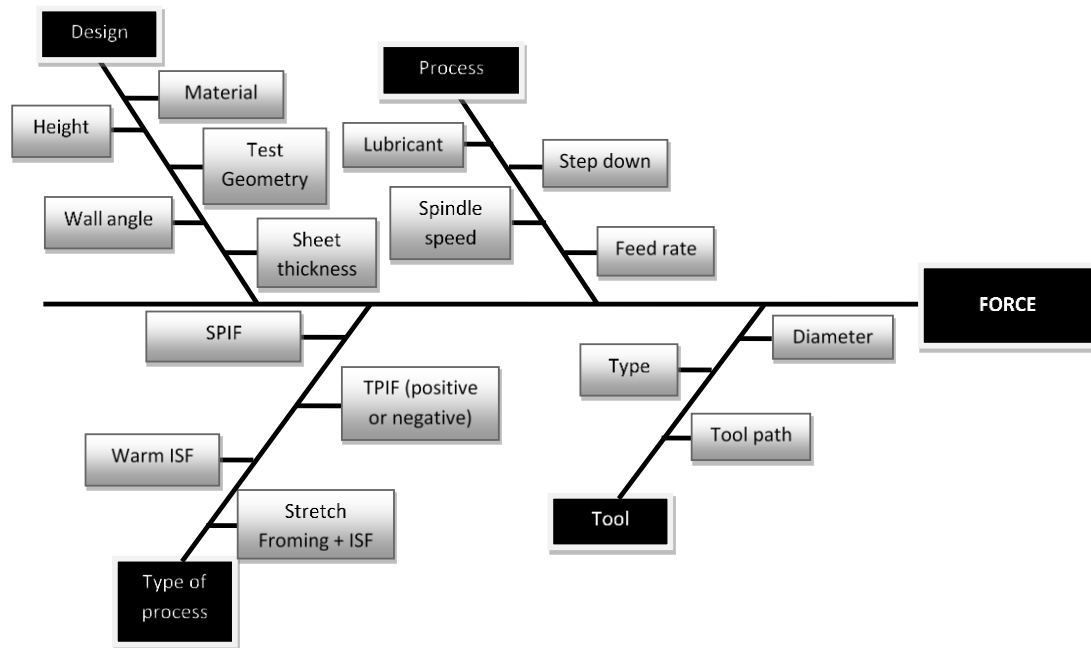


Figure 2.24. Fishbone diagram with the parameters that affect the forming force in ISF.

2.4.2 Formability

In sheet metal forming processes, each zone of the sheet might be subjected to a different combination of strain depending on the process conditions.

In order to determine formability, which is the ability of a certain material to undergo plastic deformation without damage, several researchers used the maximum wall angle achievable as an indicator of the material forming limits (Hussain et al., 2009, 2007). However, it is preferable to use the methods based on FLD (Forming Limit Diagrams) which graphically locate the strain state of different points of a part in a (Y-positive) Cartesian plane bounded by the in-plane major and minor principal strains axes, in combination with curves indicating the limit strains (for necking and/or fracture) of the sheet material. The minor strain on the sheet surface is represented in the horizontal axis and the major strain on the sheet surface in the vertical one. The FLD is also called the Keeler-Goodwin diagram (Keeler, 1986; Goodwin, 1968).

For compressive states (like rolling) it is possible to obtain large levels of strain without damage, whereas for tensile states (deep drawing) failure is usually controlled by necking followed by an instable process leading to fracture. In this case, the deformation is concentrated into a small region (neck) and the material will fail. In Incremental Sheet Forming, the forming limit has a radically different trend in comparison of the typical forming limit obtained for deep drawing and ISF presents an enhanced formability than the one allowed under deep drawing conditions. This is because during ISF there is the suppression of necking and fracture appears without the formation of instabilities. The stabilization mechanisms that can avoid necking are widely discussed in the comprehensive review done by Emmens and van den Boogaard (2009).

In a FLD, the Forming Limit Curve (FLC) shows the combinations of in-plane strains at the onset of local necking, whereas the Fracture Forming Limit line (FFL) shows the combinations of in-plane strains at the beginning of ductile fracture. According to this, Figure 2.25 depicts the presumed FLD including both the FLC and the FFL for ductile metal sheets. In most of these ductile materials, the FFL is sensibly above the FLC, as it has been recently reported in a series of research works (Centeno et al., 2014; Emmens and van den Boogaard, 2009; Isik et al., 2014). The current characterization of the necking and fracture curves within FLDs has been also widely discussed in the sheet metal forming community, which is providing continuously novel experimental techniques for the determination of this forming limit (Centeno et al., 2015).

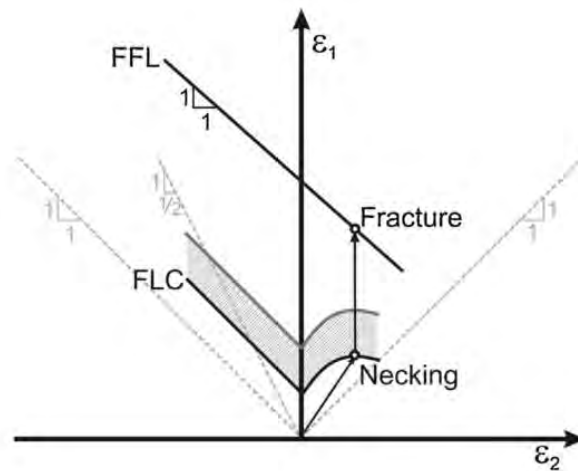


Figure 2.25. Representation of the principal strain space (Isik et al., 2014).

It has to be said that although extensive research in ISF over the last decade has been carried out, the deformation mechanism under the ISF process is not fully understood. Usually, the enhanced formability is attributed to the localization of plastic deformation (Hussain et al., 2007) without providing a deep explanation.

One of the deformation mechanism assumed in the literature (as well in SPIF as in TPIF) has been a mechanism of out-of-plane shear as reviewed in Emmens and van den Boogaard (2009), see Figure 2.26c. According to Jackson and Allwood (2009), this mechanism has become associated to ISF process over the last 7-10 years but it has not been experimentally verified. The mechanism is based on shear spinning rotary forming process.

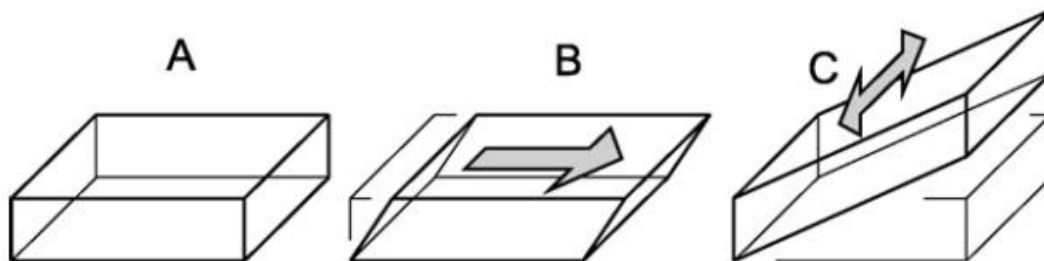


Figure 2.26. Definitions of ISF undeformed part (A), through-thickness shear (B) and out-of-plane shear (C) (Emmens and van den Boogaard, 2009).

In shear spinning the part is formed over the mandrel by a shear deformation process in which the outside diameter remains constant and the wall thickness is therefore reduced. This shear straining and consequent thinning of the metal distinguish this process from the bending action in conventional spinning. The resulting thickness of the spun wall can readily be determined by the sine law (Figure 2.27), which is only valid for the first stage, when performing multi-stage operations this relationship is not valid.

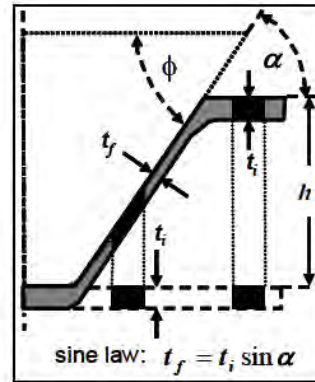


Figure 2.27. Sine law (Jeswiet et al., 2005b).

As it was pointed out by Jackson and Allwood (2009) “a real understanding of the deformation mechanism is important to allow accurate numerical models of the process to be developed for tool path design and process control and, to develop an understanding of the increased forming limits observed in ISF in comparison to pressing”. In that sense the findings of their work based on an annealed copper (C101) plate formed to a truncated cone of wall angle of 30° are noteworthy: firstly, the deformation mechanisms of both SPIF and TPIF are significantly different to the idealized mechanism of shear spinning. In both SPIF and TPIF the deformation is a combination of stretching and shear that increases on successive tool laps, with the greatest strain component being shear in the tool direction, therefore, there is the presence of through-thickness shear (Figure 2.26b). Shear occurs perpendicular to the tool direction in both SPIF and TPIF, which is more significant in SPIF resulting in a piling up of the material at the center of the plate. Other researchers have found evidences of through-thickness shear in their works (Bambach et al., 2003; Jackson et al., 2008).

Furthermore, based on experimental results, Jackson and Allwood (2009) concluded that the deformation mechanism is intrinsically different for SPIF and TPIF. Therefore the two processes should be distinguished in future discussions of their deformation mechanics.

On the contrary, the other main supposition of the deformation mechanisms that take place in ISF is that the localized bending of the sheet around the punch causes a contact compressive stress normal to the surface of the sheet. This additional contact stress is able to reduce the yield stress in tension and increase the material formability (Emmens and van den Boogaard, 2009; Martins et al., 2008; Silva et al., 2008). Formability and contact stress increase with increasing sheet thickness and decreasing tool diameter.

Several recent and relevant publications have supported experimentally and analytically this behavior, considering that formability is limited by fracture without previous necking, being this absence of necking the key factor for the increased formability in ISF. Silva et al. (2011) carried out tests that revealed the possible existence of both deformation mechanisms, either fracture with a previous necking or failure by direct ductile fracture, depending on the ratio between the initial thickness of the sheet and the radius of the tool (t_0/R). More recent studies (Madeira et al., 2015; Soeiro et al., 2015) demonstrated that in both of the abovementioned cases, i.e. failure controlled either by necking or by ductile fracture, fracture strains are always within a scatter band of the FFL. It was again observed that for high tool diameters, the failure mode was due to necking followed by ductile fracture. However, for the lowest tool diameters considered, failure occurred by fracture in the absence of necking. To sum up, although failure by necking could still occur in incremental forming, for small tool diameters fracture in the absence of necking would usually be promoted, and formability should then be represented by the FFL. Furthermore, in the paper of Madeira et al. (2015) it was proved that failure by fracture in SPIF occurs by in-plane tension (corresponding to mode I of fracture mechanics), whereas the alternatively proposed deformation mechanisms and associated crack opening modes based on in-plane (mode II) or out-of-plane (mode III) shear stresses should not be considered because they do not ensure consistency between plastic deformation and fracture mechanics.

The effect of the localized bending induced by the forming tool through the t_0/R ratio in the stabilization of plastic deformation above the FLC in SPIF was studied in Centeno et al. (2014). It was observed that for higher tool diameters the failure mode was due to necking followed by ductile fracture (Figure 2.28a). However, for the analyzed material (AISI 304), for low tool diameters the failure by fracture without the appearance of necking was not found (Figure 2.28b).

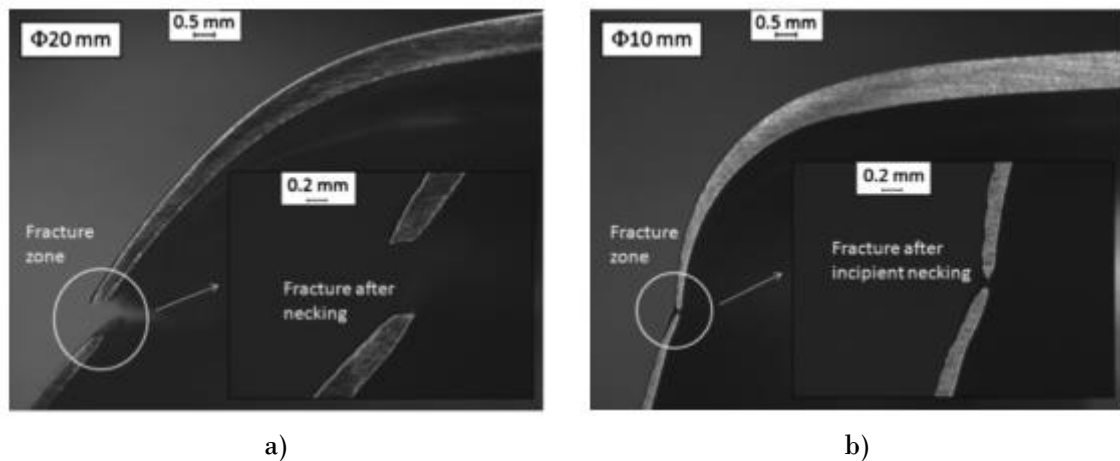


Figure 2.28. Fractography at the fracture initiation zone for SPIF tests using 20 mm tool diameter (a) and 10 mm tool diameter (b) (Centeno et al., 2014).

Considering that in SPIF for low tool diameters failure will occur without previous necking, Isik et al. (2014) proposed a new methodology to determine the maximum strains at fracture directly from the in-plane strain measurements without evaluating the gauge length strains, which simplifies the procedure for obtaining the FFL. SPIF tests of variable wall angle truncated conical parts (plane strain conditions) and truncated pyramidal parts (plane

strain conditions in the walls of the pyramid and biaxial stretching at the corners, as schematically represented in Figure 2.29) are required. The authors also introduced the concept of Shear Fracture Forming Limit line (SFFL). In-plane torsion tests and plane shear tests are required for representing this new forming limit (Figure 2.30).

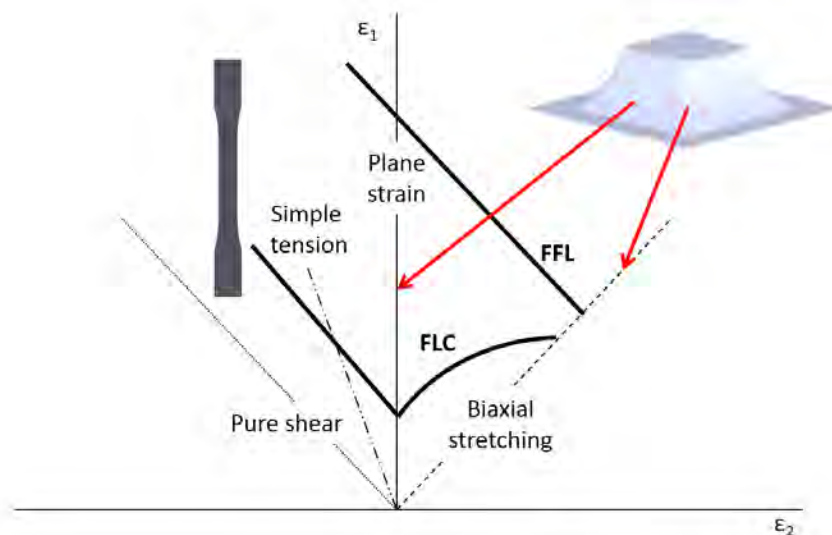


Figure 2.29. Schematic representation of strain loading conditions for a variable wall angle truncated pyramid formed by SPIF.

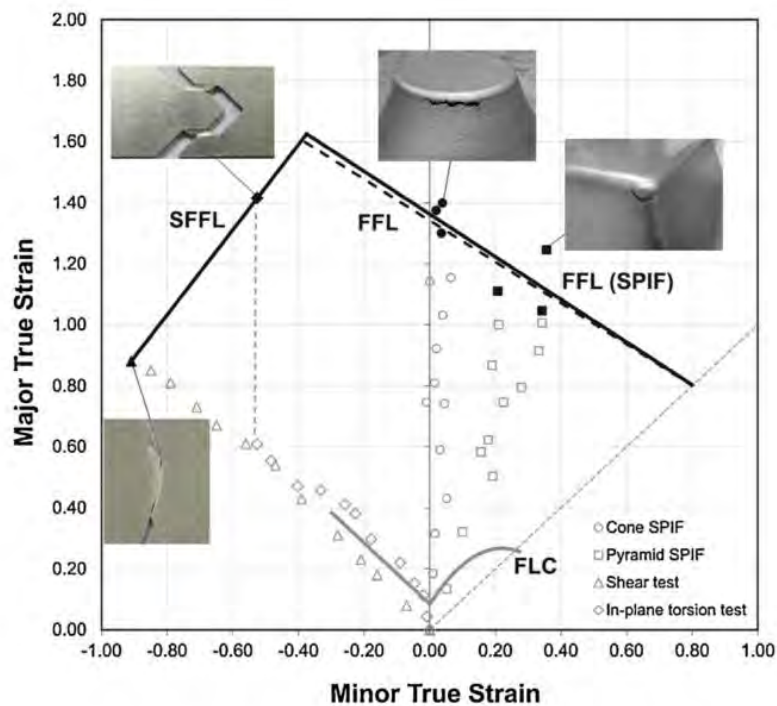


Figure 2.30. Fracture loci (FFL and SFFL) (Isik et al., 2014).

In order to simplify and facilitate the determination of SFFL, a new geometry manufactured by SPIF has been recently proposed (Soeiro et al., 2015). They proposed to use a truncated lobe conical shape with varying wall angles (Figure 2.31) and measure the

in-plane strains at fracture, avoiding the need of measuring gauge length strains, which is required if the typical tests specimens (in-plane torsion and plane shear tests) are used. Figure 2.32 shows the schematic representation of the two different methods for obtaining the shear fracture forming limit line (SFFL).



Figure 2.31. Variable wall angle truncated lobe conical geometry proposed to determine SFFL (Soeiro et al., 2015).

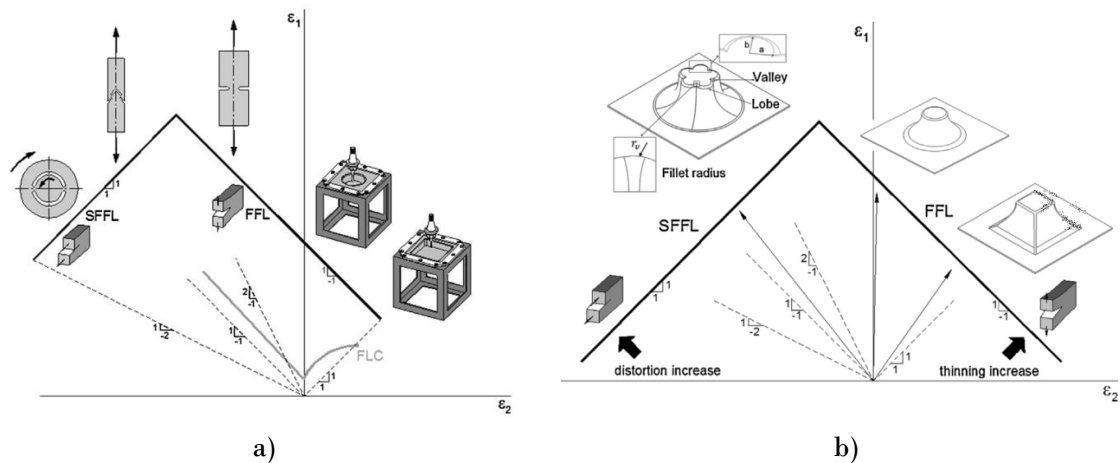


Figure 2.32. Schematic representation of the FLD determination method proposed by Isik et al. (2014) (a) and the method proposed by Soeiro et al. (2015) (b).

2.4.3 Geometric accuracy

One of the most important drawbacks of the ISF process is its poor dimensional accuracy compared with the requirements of the industrial applications. Allwood et al. (2005b) based on data provided by developers, showed that most of the industrial applications where ISF could fit-in require geometric tolerances below 1 mm, which are unfeasible with the normal ISF process chain (they estimated that, in general terms and without considering the material used, the tightest tolerance process window for ISF was 2 mm.).

Specifically for the SPIF variant, the main geometric error typologies were classified by Micari et al. (2007) (Figure 2.33) as:

- Sheet bending close to the blank's clamping region. The deviation in the outermost zone of the part is considerable. This deviation takes place in the first stages of the process, because sheet is prone to bending rather than being locally deformed. In order to reduce this deviation, it is necessary to use a backing plate. However, this support is not able to eliminate the low accuracy in the central zones.
- Deviations in the wall caused by the elastic recovery (springback) of the sheet when the load is removed.
- The pillow effect in the bottom of the part, which is originated by the spread of elastic stresses of zones where the tool has not exerted plastic deformation to other parts of the piece.

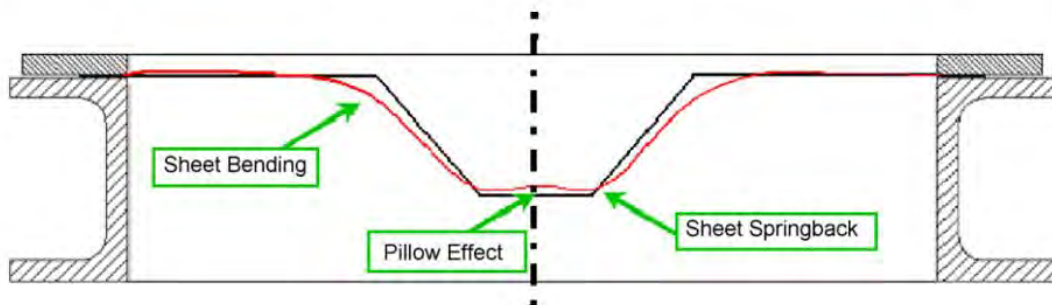


Figure 2.33. Geometrical error topologies observed during the SPIF of UWA parts (Micari et al., 2007).

Poor accuracy is one of the main barriers for the implementation of ISF in the industry, explaining the large amount of research works aimed to soften the inaccuracy issue. The precision improvement approaches can be classified into three main types: hardware dependent, software dependent and stiffness modification (Figure 2.34).

In order to better control the material deformation, the hardware dependent approaches consist on the addition of components to the ideal “dieless” process. Examples of this strategies are the addition of backing plates, partial or complete dies (Attanasio et al., 2008, 2006; Fiorentino et al., 2009), mechanisms to stretch the material (Araghi et al., 2009) and counter-tools driven by a rotating table (Franzen et al., 2008) or robots (Meier et al., 2009).

The second type of approach is related to the modification of the basic tool-path generated from the CAD model of the candidate part. In turn, the tool-path correction strategies can be classified as single-stage or multiple-stage depending on the number of trajectory phases required to obtain the desired part. Ambrogio and co-workers (Ambrogio et al., 2007, 2004; Micari et al., 2007), Tekkaya et al. (2007) and Rauch et al. (2009) have worked in single-stage strategies, whereas the research groups of Duflou (Duflou et al., 2007a; Verbert et al., 2009, 2008) and Hirt (Bambach et al., 2009; Hirt et al., 2004) have tried both single-stage and multiple-stage strategies.

Finally, some research works have been focused on the modification of the blank stiffness using heating devices (Duflou et al., 2008; Fan et al., 2008), tailored rolled blanks (Hirt et al., 2004) or partially cut-out blanks (Allwood et al., 2010).

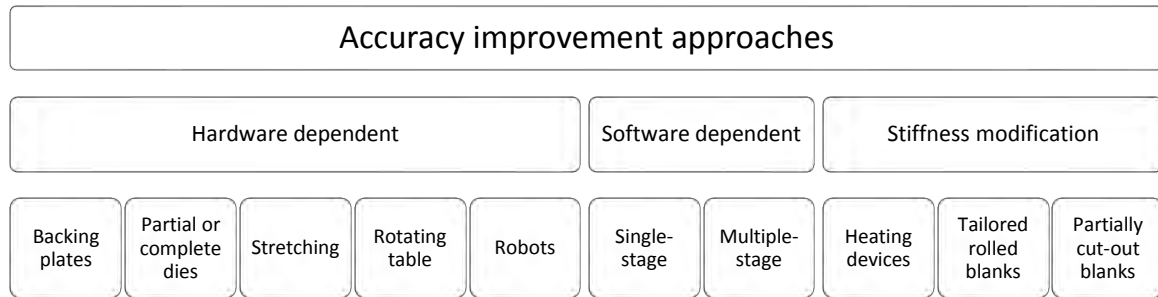


Figure 2.34. Summary of accuracy improvement approaches for ISF.

The measurement of the geometrical accuracy is usually done using 3D scanning systems (Ham and Jeswiet, 2008; Li et al., 2015) or coordinate measuring machines (CMM) (Lu et al., 2016; Silva and Martins, 2013).

2.4.4 Surface roughness

In ISF, surface roughness is one of the concerns related to the quality of the final product. As it was demonstrated in the early research works (Hagan and Jeswiet, 2004), the step down is one of the process parameters that will directly influence the surface roughness value (Figure 2.35). Increasing the step down the productivity will be increased, however the surface quality will be worst.

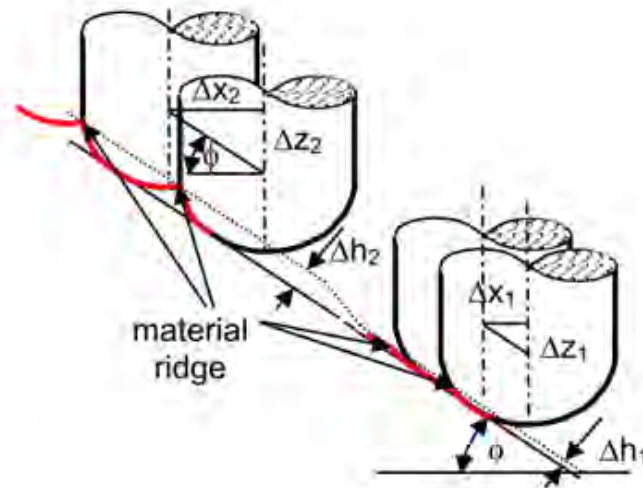


Figure 2.35. Schematic representation of the effect of the step down on surface roughness (Hagan and Jeswiet, 2004).

Durante et al. (2010) proposed an analytical model to predict the average surface roughness (R_a) based on three process parameters: tool radius, step down and wall angle. They obtained good agreement (error below 10%) between the predicted values and the measured ones.

Hamilton and Jeswiet (2010) analyzed the effect of using high feed rates and rotational speeds in SPIF on the non-contact surface roughness, in order to determine the orange peel effect (appearance of a rough surface on the non-contact side of the formed part). The aim of

the work was to demonstrate the feasibility of using high feed rates to decrease the forming time without compromising the part's quality. They proposed a model to predict the orange peel effect depending on the step down, spindle speed and wall angle.

The effect of tool diameter, step down, spindle speed and feed rate on the surface roughness on parts manufactured by SPIF in three different metallic materials (DC01, AA1050, and AISI304) have been recently investigated (Radu and Cristea, 2013). They analyzed statistically the results using ANOVA and the main effects plots, obtaining that it was possible to improve the surface roughness using the highest tool diameters considered, spindle speed and feed rate and low step down (Figure 2.36).

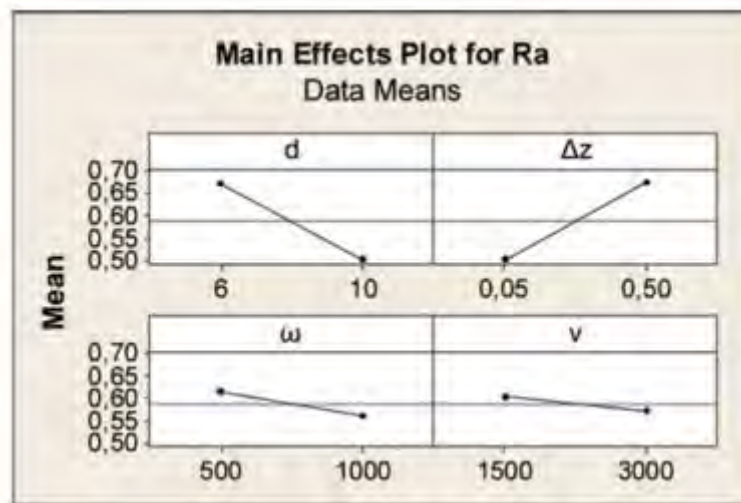


Figure 2.36. Main effects plot for surface roughness vs. the considered process parameters in aluminum alloy (AA1050) (Radu and Cristea, 2013)

A recent work has used a Box-Behnken Design of Experiments (DOE) and Response Surface Methodology (RSM) to evaluate the importance of step down, feed rate, sheet thickness and tool diameter on the overall surface in ISF (Liu et al., 2014). Then, a multi-objective function is used to minimize the surface roughness and provide the optimal forming conditions.

A similar research was carried out almost in parallel with the same aim: providing a predictive model and the optimal process parameters (feed rate, step down, tool diameter and spindle speed) to minimize the surface roughness (Echrif and Hrairi, 2014). Their DOE was based on the Taguchi method and the results were statistically analyzed using ANOVA and main effects plots. A smoother surface is obtained if high tool diameters and small step down are used (which according to their research the best parameters were 30 mm tool diameter and 0.25 mm step down).

2.5 Polymeric materials

As already reviewed in the previous subsections of Chapter 2, the materials commonly used in ISF are metallic materials, such as soft aluminum alloys (AA1050) or some steels (DC04, AISI304, etc.). However, some recent publications have revealed an increasing interest in forming polymeric materials, more specifically thermoplastic materials.

In the traditional processing techniques of plastic materials it must be applied heat and pressure to give the desired shape to the material. Temperature has a very important role in the behavior of plastic materials, specially referred to the phase transition, fluency characteristics, morphology and degradation.

These processing techniques require high production batches to recover the costs derived of machinery, tools and energy. Therefore it is necessary to develop new technologies that allow the production of smaller batches with shorter life cycles and a very low time to market. With ISF it is possible to reduce costs due to the tools and work at room temperature. Thus, it would be economically viable to produce small batches and customized products.

One of the first research works in which the feasibility of using ISF to produce parts with thermoplastic materials was demonstrated was done by Franzen et al. (2009). The paper was focused on the evaluation of the performance of PVC (polyvinylchloride) in SPIF applications. The formability limits and accuracy were characterized and evaluated by varying some process parameters (sheet thickness and tool diameter). The test geometry used was a hyperbolic frustum cone.

The results demonstrated that new deformation mechanisms and modes of failure appeared, which some of them were absent when working with metallic sheets. The following modes of failure were identified (Figure 2.37):

- **Mode 1: Cracking.** This defect appears in the transition zone of the inclined wall and the corner radius and is due to stretching mechanisms (tensile stresses). The morphology and the propagation of this cracks is similar to those found on producing metallic parts with ISF.
- **Mode 2: Wrinkling.** Wrinkles appear in the inclined wall and occur earlier than the cracks of mode 1. They start in the corner radius where thinning is more significant. This phenomenon is due to the rotation of the tool. When the sheet is thinner it is easier to find this mode of failure.
- **Mode 3: Oblique cracking.** The cracks are propagated through the inclined wall because the sheet cannot withstand the straining by shearing at the early stages of deformation. This mode of failure has never been found in metals.

In another work, Le et al. (2008) published the results of a preliminary set of experiments for the SPIF of PP (polypropylene). The experimental campaign consisted on a 2^{4+1} factorial design with three replications for each experiment. The analyzed factors were step size, tool

size, feed rate and spindle speed. The response was the maximum wall angle achieved when a truncated cone with a generatrix radius was manufactured. The influence of the forming parameters and their interaction on the formability was analyzed. The results corroborate two of the aforementioned modes of failure found by Franzen et al. (2009) (mode 1 and 2).

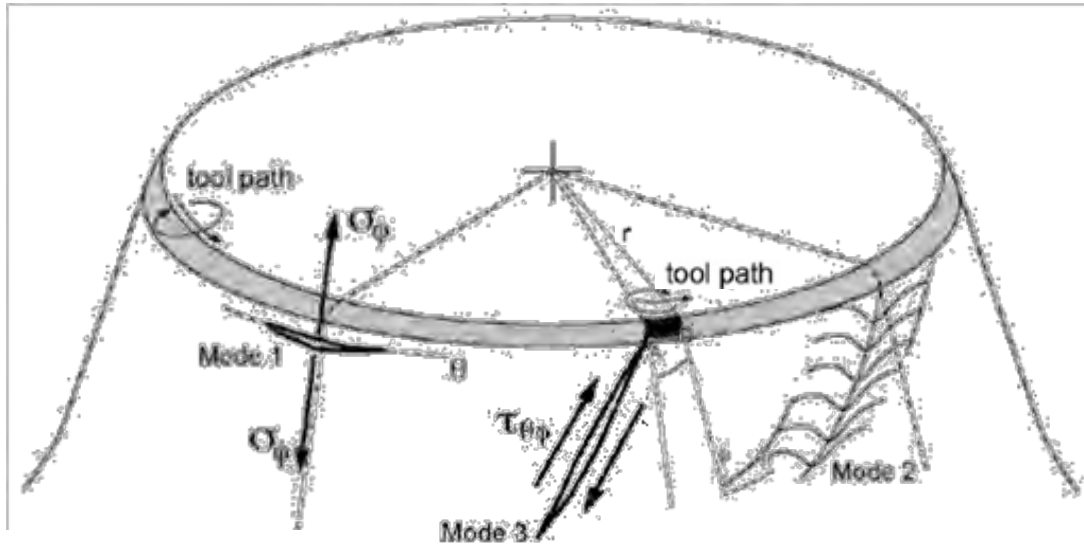


Figure 2.37. Modes of failure in SPIF of thermoplastic sheets (adapted from Franzen et al. 2009).

The work of Martins et al. (2009) has also been focused on the evaluation of the applicability of different polymers in the process of SPIF. Five polymers were studied: POM (polyoxymethylene, which has a high-crystalline structure), HDPE (high density polyethylene), PA (polyamide), PVC, PC (polycarbonate, amorphous structure). For each material, the FFLD (Fracture Forming Limit Diagram) was obtained. The thicknesses of the sheets were 2 and 3 mm. Modes of failure, strains at rupture, formability, accuracy of final parts and color variation during cold formation were evaluated. With this information, a selection mechanism of polymeric materials was elaborated, based on ductility, springback, color variation (aesthetic factor) and cost.

More recently, Silva et al. (2010) identified a theoretical framework for rotationally symmetric conditions that allowed studying quantitatively and qualitatively the influence of major forming parameters. The paper was based on membrane analysis and SPIF tests using PVC sheets. An analytical framework able to model the first mode of failure identified by Franzen et al. (2009) was developed. The second and third modes of failure were not modelled. The experimental results demonstrated that the formability of SPIF in polymers is mostly influenced by sheet thickness, tool radius, ductility of the material and the initial wall angle. This last parameter does not have influence in the formability when working with metallic sheets, but in the case of polymers it has a significant influence.

In a subsequent work, Marques et al. (2012) extended the analytical model previously described by Silva et al. (2010) in order to be able to model the second and third modes of failure by means of membrane analysis. The experimentation was carried out using four thermoplastic materials: PET (polyethylene terephthalate, high crystalline structure), PA,

PVC and PC. Two sheet thicknesses were used for each material: 2 and 3 mm. The experimental campaign considered the influence of the most relevant process parameters: thickness of the sheet, tool radius and initial wall angle. The geometries used were cones and pyramids with an angle increasing with the depth. They highlight the outstanding performance of PET and that PC is able to keep its transparency after being formed.

The effect of step down and spindle speed on polymer parts formed by SPIF regarding failure, forming forces, void content and crystallinity is reported in the recent paper of Davarpanah et al. (2015). They used two polymers, PVC and PLA (polylactic acid), which results to be biodegradable. The results demonstrated a surprisingly increase of the formability with an increase of the step down, which is the opposite in the case of working with metallic materials, and that the spindle speed does not significantly varies the polymer formability. Regarding the forming forces, it was shown that they increase with the step down and decrease for higher spindle speeds. It is worth mentioning that this was the first work that analyzed the enhance of the crystallinity of the formed material compared with the raw material due to the polymer chain orientation and rearrangement during the forming operation.

A response surface analysis to determine the effect of the SPIF process parameters on the formability and associated heat effects of PVC and PE has been recently done by Hussain et al. (2016). They found that the failure mode of PVC is mainly limited by fracture whereas in the case of PE is limited by wrinkling. A softening index, $\Delta T/mp$, defined as the rise in temperature (ΔT) during the SPIF process divided by the melting temperature of the polymer (mp). This softening index basically increases with the increase of the tool radius and the spindle speed, which in turn, leads to an increase of the formability.

Davarpanah et al. (2017) examined the influence of step down and spindle speed on the mechanical properties (by means of tensile and stress relaxation tests) and the chain orientation (using DSC and X-ray diffraction) on PVC and PA parts manufactured by SPIF. It was found that after the forming process, the toughness and ductility are increased, whereas the yield stress and Young modulus are reduced. Furthermore, their results pointed out that there is a chain reorientation in the formed polymer with a minimal change in the degree of crystallinity. This chain reorientation is the principal cause of the modification of the mechanical properties. However, the effect that the step down and the spindle speed have on these changes did not present a clear trend.

Very recently, Lozano-Sánchez et al. (2017) used polymer composites sheet consisting of multi-wall carbon nanotubes (MWCNTs) and polypropylene (PP) to carry out the SPIF process with the aim of studying the effect of the nanotubes. They reported that there was a chain reorientation of both, PP chains and MWCNTs during SPIF of the composite sheets. Moreover, it was observed a whitening on the outside of cone-shaped manufactured parts as a consequence of the SPIF processing, which was associated to the presence of crazing due to disentanglement of polymer chains. The difference on coloration between the inner and outer surfaces of the manufactured parts was related to compressive and tensile stresses on each side, respectively.

Hole-flanging is a forming process consisting on forming a sheet with a pre-cut hole in order to obtain a smooth cylindrical or conical hole-flange. Hole-flanging by SPIF is an emerging processes useful for rapid prototyping and small batch production. The use of polymers in hole-flanging by SPIF is very recent (Silva et al., 2013). In this novel work, the overall formability of the process using fracture forming limit diagrams (FFL) is analyzed. Two polymers were studied (PET and PC). In the first part of the work, the strain loading paths of truncated conical parts manufactured by SPIF were measured. Then, the hole-flanging by multi-stage SPIF was carried out. A multi-stage strategy, with an increase of 5° wall angle at each step, was employed until reaching the desired angle or fracture. A new mode of deformation, which is a combination of in-plane stretching and bending, was found.

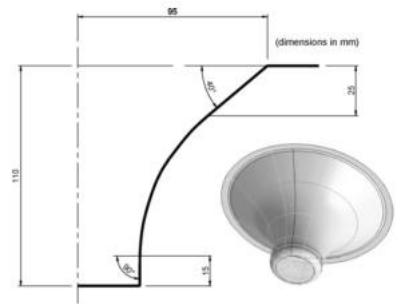
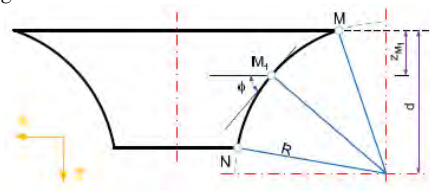
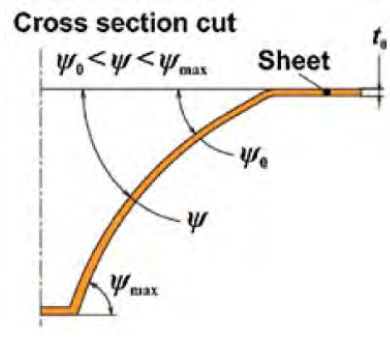
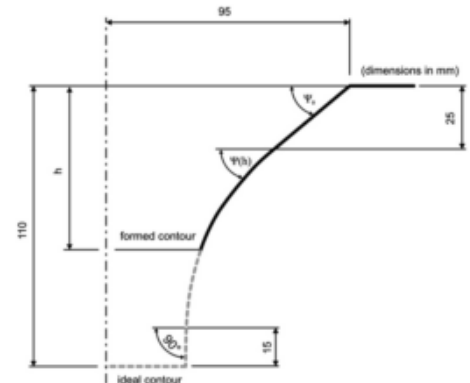
All of the papers reviewed until this point are basically experimental works. The first attempt to model the incremental forming process of a polymeric material was done by Alkas Yonan et al. (2013), who implemented a finite strain extension of a non-linear viscoplastic material model in ABAQUS in order to use it for the simulation of the incremental forming of PVC. These material model parameters were identified by fitting the constitutive equations to the experimental tensile curves. The simulations were run using implicit time integration and solid elements, the results are then compared in terms of geometric accuracy, thickness distribution and forming force with the experimental tests. Although the discrepancies, mainly in the accuracy and thickness distribution, the model seems to be a promising approximation to the polymer behavior for small deformations.

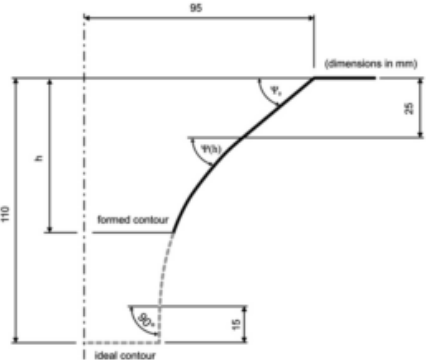
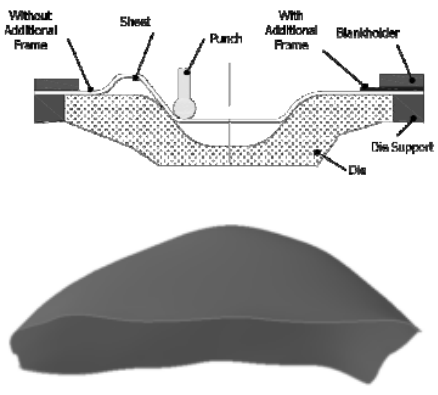
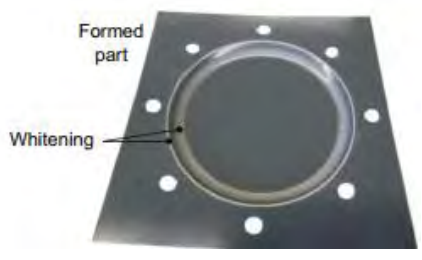
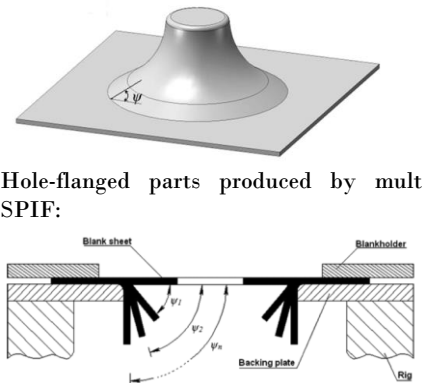
As a result of the collaboration between Alkas Yonan and co-workers (Alkas Yonan et al., 2013) and Silva and co-workers (Silva et al., 2013), an alternative methodology to characterize plastic flow and failure of polymers in SPIF and in hole-flanging by SPIF was proposed (Alkas Yonan et al., 2014). With this methodology it was possible to determine the in-plane stresses and the accumulated damage at various positions over the surface of the obtained parts directly from the experimental strain measurements and FFL, avoiding the need to use inverse procedures based on numerical simulations.

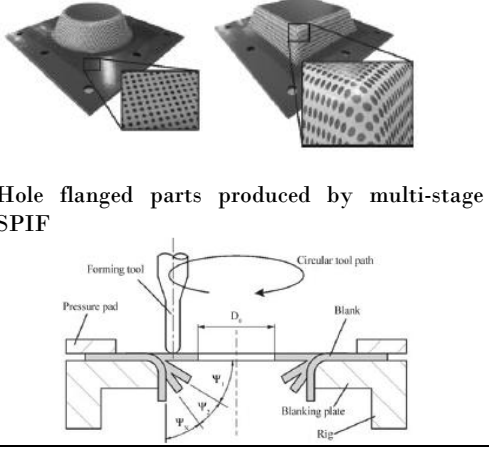
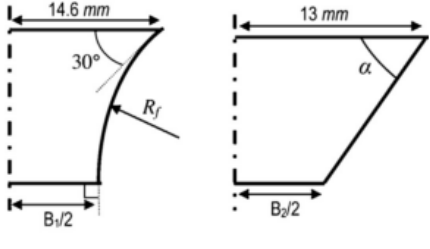
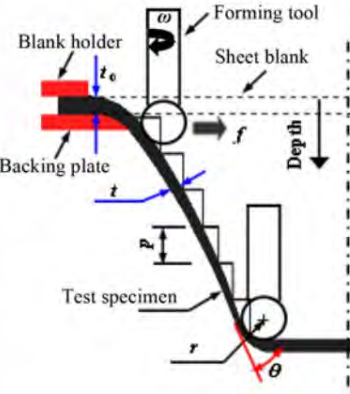
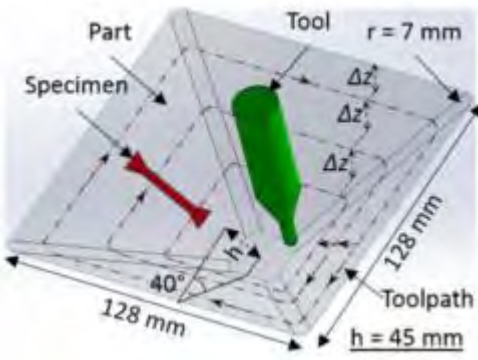
Finally, it is worth mentioning that the first publication dealing with the production of any biomedical device or prosthesis manufactured with Incremental Sheet Forming using biocompatible polymers was authored by Fiorentino et al. (2012). They manufactured a palate prosthesis using a titanium alloy and PCL (polycaprolactone). Although their results were promising, an optimization of the process parameters should be done in order to increase the geometric accuracy of the part.

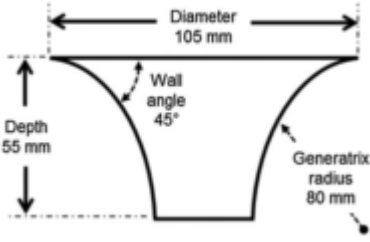
A summary of the aforementioned works, in terms of material used, geometry, constant and variable parameters, analyzed outputs and material characterization is provided in Table 2.2.

Table 2.2. Summary of the experimental research works related with the manufacturing of polymer parts using ISF.

Ref.	Mat.	Geometry	Constant parameters	Variable parameters	Outputs	Material characterization
(Franzen et al., 2009)	PVC	<ul style="list-style-type: none"> Truncated hyperbolic shape 	<ul style="list-style-type: none"> Tool depth step 0.5 mm, spiral tool path Feed rate 1500 mm/min Lubricant (water-soap emulsion) 	<ul style="list-style-type: none"> Tool diameter (10 and 15 mm) Thickness (2 and 3 mm) 	<ul style="list-style-type: none"> Failure modes Formability Surface finish Thickness evolution Accuracy 	Commercial PVC (no tests): <ul style="list-style-type: none"> Nearly amorphous Room temperature elongation 40% Tg > 75°C
(Le et al., 2008)	PP	<ul style="list-style-type: none"> Cone-shaped part with a circular arc as generatrix 	<ul style="list-style-type: none"> Sheet thickness (3 mm) 	<ul style="list-style-type: none"> Step down (0.2 and 1 mm) Tool diameter (6 and 12 mm) Feed rate (1000 and 3000 mm/min) Spindle speed (200 and 700 rpm) 	<ul style="list-style-type: none"> Formability (maximum wall angle reached) 	The authors did not provide any material characterization
(Martins et al., 2009)	POM, HDPE, PA, PVC, PC	<p>Cross section cut</p> 	<ul style="list-style-type: none"> Tool depth step 0.5 mm Feed rate 1500 mm/min 	<ul style="list-style-type: none"> Thickness (2 and 3 mm) Tool diameter (10 and 15 mm) Initial drawing angle (40 and 60°) 	<ul style="list-style-type: none"> Modes of failure Strains at failure Influences on the formability Accuracy of the colour Selection criterion 	<ul style="list-style-type: none"> Structure Yield stress Elasticity modulus Density (pycnometer) Fracture toughness (R) from tensile tests performed on double-edge notched specimens FFL
(Silva et al., 2010)	PVC		<ul style="list-style-type: none"> Step down 0.5 mm Feed rate 1000 mm/min Free spindle speed Lubricant (water-soap emulsion) 	<ul style="list-style-type: none"> Thickness (2 and 3 mm) Tool diameter (10 and 15 mm) Initial drawing angle (40 and 60°) 	<ul style="list-style-type: none"> Drawing angle at failure Adjustment of sine law Spifability Variation in colour 	<ul style="list-style-type: none"> Structure Glass transition temperature Density (Archimedes) Elasticity modulus Yield stress (tension and compression) FFL

Ref.	Mat.	Geometry	Constant parameters	Variable parameters	Outputs	Material characterization
(Marques et al., 2012)	PET, PA, PVC, PC	<p>Conical and pyramidal shape:</p> 	<ul style="list-style-type: none"> · Tool depth step 0.1 mm · Free spindle speed · Feed rate 1000 mm/min · Lubricant (water-soap emulsion) 	<ul style="list-style-type: none"> · Sheet thickness (2 and 3 mm) · Tool diameter (8, 10, 12 mm) · Initial drawing angle (30, 45, 60°) · Geometry (Conical and pyramidal) 	<ul style="list-style-type: none"> · Failure modes · Strain loading paths · Influence of tool radius, sheet thickness and initial drawing angle on the formability · Variation in color 	<ul style="list-style-type: none"> · Structure · Yield stress (tension and compression) · Elasticity modulus · Density (Archimedes) · FFL
(Fiorentino et al., 2012)	PCL		<ul style="list-style-type: none"> · Step down (0.1 mm) · Tool diameter (6 mm) · No lubricant · Sheet thickness (1 mm) 	<ul style="list-style-type: none"> · Spindle speed (0, 600 and 1000 rpm) · Feed rate (200-800 mm/min) 	<ul style="list-style-type: none"> · Final profile measured along 2 axis using CMM 	<p>Obtained from literature:</p> <ul style="list-style-type: none"> · Melting point · Glass transition temperature · Crystallinity · Young modulus · Elongation at break · Tensile stress · Biodegradation · Water permeability
(Alkas Yonan et al., 2013)	PVC		<ul style="list-style-type: none"> · Tool diameter (15 mm) · Feed rate (500 mm/min) 	<ul style="list-style-type: none"> · Step down (1, 2, 4 mm) · Wall angle (60, 80°) · outer diameter (130, 140 mm) · Maximum depth of the part (10, 12 mm) · sheet thickness (1, 2, 3 mm) 	<ul style="list-style-type: none"> · Simulation in Abaqus · Shape deviation · Evolution of sheet thickness · Forming forces 	<ul style="list-style-type: none"> · Strain controlled monotonic tensile tests at 3 different strain-rates.
(Silva et al., 2013)	PET, PC	<p>Variable wall angle truncated cone:</p>  <p>Hole-flanged parts produced by multi-stage SPIF:</p>	<ul style="list-style-type: none"> · Sheet thickness (3 mm) · Tool radius (4 mm) · Free spindle speed · 1000 mm/min feed rate · 0.2 mm step down · Hole diameter (120 mm) 	<ul style="list-style-type: none"> · Polymeric materials (PET, PC) 	<ul style="list-style-type: none"> · Strains · Thickness distribution 	<ul style="list-style-type: none"> · Elasticity modulus · Yield stress (tension and compression) · Fracture toughness · FFL

Ref.	Mat.	Geometry	Constant parameters	Variable parameters	Outputs	Material characterization
(Alkas Yonan et al., 2014)	PVC	 <p>Hole flanged parts produced by multi-stage SPIF</p>	<ul style="list-style-type: none"> · Sheet thickness (3 mm) · Tool diameter (10 mm) · Step down 0.5 mm · Feed rate 1000 mm/min · Free spindle speed · Deep-drawing oil lubricant 	<ul style="list-style-type: none"> · Hole diameter (80 and 90 mm) 	<ul style="list-style-type: none"> · Plastic flow and failure determination from measured strains 	<ul style="list-style-type: none"> · Elasticity modulus (tension and compression) · Yield stress (tension and compression) - Hollomon model to obtained true stress-strain curves - FFL
(Davaranah et al., 2015)	PLA, PVC		<ul style="list-style-type: none"> · Tool diameter (5 mm) · Sheet thickness (1.5 mm for PVC and 0.7 mm for PLA) · Feed rate 300 mm/min 	<ul style="list-style-type: none"> · Step down (0.2, 0.4, 0.6, 0.8, 1.0, 1.4, 1.8 mm) · Spindle speed (0, 1250, 5000, 7000 rpm) · Generatrix radius (10, 12, 14, 16 mm) · Angle (55, 65, 75°) 	<ul style="list-style-type: none"> · Failure modes · Forming forces · Void structure in formed material · Thermal properties and microstructure 	<ul style="list-style-type: none"> · SEM micrographs · Crystallinity · DSC
(Hussain et al., 2016)	PVC, PE		<ul style="list-style-type: none"> · Sheet thickness (2 mm) 	<ul style="list-style-type: none"> · Step down · Tool radius · Feed rate · Spindle speed 	<ul style="list-style-type: none"> · Maximum wall angle at fracture or wrinkle · Softening index 	<ul style="list-style-type: none"> · Physical properties (structure, density and melting point) · Mechanical properties (yield stress, ultimate stress, elongation and tensile area reduction)
(Davaranah et al., 2017)	PVC, PA		<ul style="list-style-type: none"> · Sheet thickness (1.5 mm) · Tool diameter (5 mm) · Feed rate (5 mm/s) 	<ul style="list-style-type: none"> · Step down (1.4, 1.8 and 2.0 mm) · Spindle speed (0, 500, 1000 and 5000 rpm) 	<ul style="list-style-type: none"> · Uniaxial tensile tests · Stress relaxation tests · Temperature · Chain orientation and crystallinity 	<ul style="list-style-type: none"> · Yield stress · Ultimate stress · Strain at fracture · Young modulus

Ref.	Mat.	Geometry	Constant parameters	Variable parameters	Outputs	Material characterization
(Lozano-Sánchez et al., 2017)	PP-MWCNTs composite		<ul style="list-style-type: none"> · Tool diameter (10 mm) · Step down (0.5 mm) · Feed rate (3000 mm/min) 	<ul style="list-style-type: none"> · Spindle speed (0 and 2000 rpm) 	<ul style="list-style-type: none"> · Forming force 	<ul style="list-style-type: none"> · Melting point · DSC · TGA · SWAXS

2.6 Application of ISF in the biomedical field

Manufacturing processes are constantly under development. Each change is a reaction of the pressures coming from the market growth, the customer, new competitors, the evolution of the technology and new and innovative trends in product and service processes. Furthermore, the majority of commercialized products have a short life cycle in the market, therefore, it is highly recommended to develop adaptable and flexible manufacturing processes in order to satisfy in every moment the existing demand.

During the last few years, some of the traditional sectors such as the automotive and mechanical machinery are decreasing its activity. In contrast to, the medical field with the intention of improving quality of life is an emerging opportunity for manufacturing processes to take advantage of the actual capabilities and transform them, contributing to the healthcare sector.

In this section, the PESTEL instrument (the letters stand for Political, Economic, Social, Technological, Environmental and Legal), a powerful tool commonly employed to assess the macro-environment in business management, is used to determine the opportunities of ISF for biomedical applications. PESTEL can be defined as follows:

“The analysis of the general environment attempt to provide a proper diagnosis of the current and future situation in order to detect threats and opportunities that this environment offers to the performance of the company both now and in the future” (Guerras and Navas, 2015).

This tool considers six different factors:

- **Political** factors related with the degree of involvement of the government in one sector of the economy. Specifically, political factors include areas such as tax policy, labor law, environmental law, trade restrictions and political stability. Political factors may also include goods and services provided or not by the government to the society. Furthermore, governments have great influence on the health, education, and infrastructure of a nation.

- Economic factors include economic growth, interest rates, exchange rates and the inflation rate. These factors have major impacts on how businesses operate and make decisions. For example, interest rates affect a firm's capital cost and, therefore, to what extent a business grows and expands, exchange rates affect the costs of exporting goods, etc.
- Social factors include the cultural aspects and health consciousness, population growth rate, age distribution, career attitudes and emphasis on safety. Trends in social factors affect the demand for a company's products and how that company operates. For example, an aging population may imply a smaller and less-willing workforce (thus, increasing the cost of labor). Furthermore, companies may change various management strategies to adapt to these social trends (such as recruiting older workers).
- Technological factors include, among others, aspects such as R&D activity, automation, technology incentives and the rate of technological change. They can determine barriers to entry, minimum efficient production level and influence outsourcing decisions. Moreover, technological shifts can affect costs, quality, and lead to innovation.
- Environmental factors take into account ecological and environmental aspects such as weather, climate, and climate change, which may especially affect industries such as tourism, farming, and insurance. Furthermore, growing awareness of the potential impacts of climate change is affecting how companies operate and the products they offer, both creating new markets and diminishing or destroying existing ones.
- Legal factors include discrimination laws, consumer laws, antitrust laws, employment laws, and health and safety laws. These factors can affect how a company operates, its costs, and the demand for its products.

In other words, it can be said that the PESTEL analysis (Figure 2.38) provides a general perspective about the macro-environment (or general environment) and driving forces of the industry, and it allows understanding the key influences of the industry profitability. The analysis of the micro-environment (or specific environment) can be performed using the Porter's five forces tool.

From a general viewpoint, the objectives of the external analysis can be summarized in the following points:

1. To comprehend how industry structure drives *competition*. This fact will determine the level of industry profitability,
2. To assess industry *attractiveness*,
3. To use evidence on changes in industry structure to forecast *future profitability*,
4. To formulate *strategies* to change structure of the industry to improve profitability, and
5. To identify the *key success factors* in order to study the most suitable marketing strategy for the commercialization of this new forming process.

Particularly, the analysis of the macro-environment presented in this section is focused on the biomedical sector and it aims to study the influence of the external or general framework and determine the opportunities that ISF has in this field.

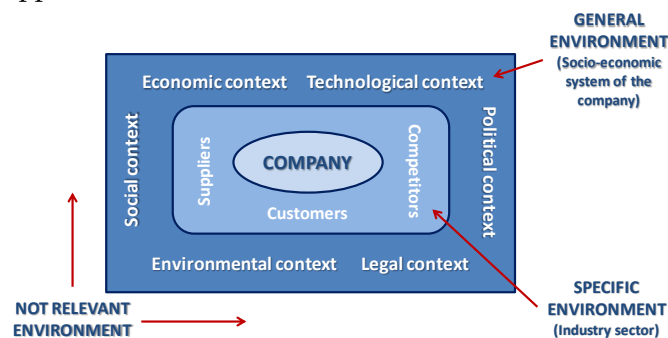


Figure 2.38. Macro-environment (Guerras and Navas, 2015).

2.6.1 Political factors

Biotechnology is a source of innovation for mature sectors (food, energy or cosmetic industries among others). For this reason, more importance is given to introduce biotechnology on the political agenda as a priority transversal technology which can be incorporated in the most competitive sectors and to obtain more flexible conditions for repayment of debts for public financial support for R & D activities.

In the last annual report published by *Asociación Española de Bioempresas* (ASEBIO, 2014), the indicators that facilitate or inhibit the development of biotechnology in Spain were evaluated using surveys. One of these indicators is related to the political scenario, the survey respondents had to evaluate whereas they feel the government support as a positive factor or whereas their perception was that the government had a low sensitivity towards the biotechnological sector. As seen in Figure 2.39, due to the economic crises the government support towards the companies and institutions of the biotechnological sector started to decrease notably between 2008 until 2013. However, in 2014 a significant increase of this indicator was detected, mainly because the government budget for R & D activities was higher.

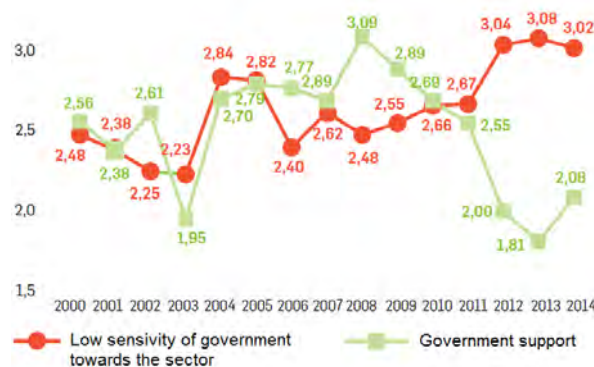


Figure 2.39. Evolution of the evaluation of the government support (facilitating factor) versus low sensitivity of government towards the sector (inhibiting factor) from 2000 to 2014 (ASEBIO, 2014)

2.6.2 Economic factors

Bio-implants have emerged as a promising solution for the variety of conditions such as cardiovascular, dental, orthopedic, ophthalmology, neurological disorders among others. The global market for bio-implants is forecast to reach \$115.8 billion by 2020, registering a CAGR (Compound Annual Growth Rate) of 10.3% from 2014 to 2020 (Figure 2.40), as explained in the report done by Allied Market Research (Deshmukh, 2014). According to American College Of Surgeons, 29% of the trauma injuries were caused by road accidents; the instances of road accidents and death due to the same are rising to about 2.2% globally.

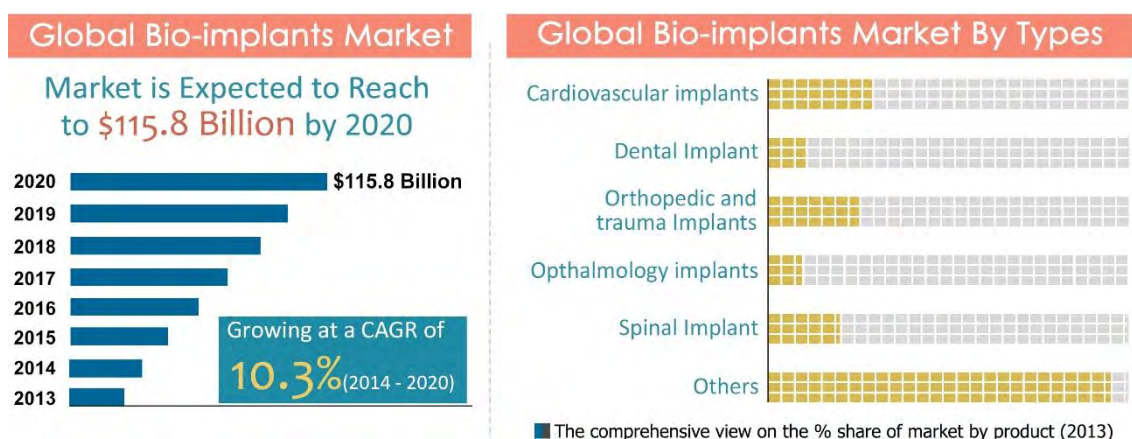


Figure 2.40. Global market for bio-implants (left) and percentage of share of the different types of bio-implants (right) (Deshmukh, 2014).

According to a new report from industry analyst firm NanoMarkets (2013), the global medical polymer market will grow from \$2.3 billion (USD) in 2013 to over \$4.2 billion in 2020 (7.82% CAGR). The report identifies the current and future opportunities in the medical polymers space and provides guidance on the technical and regulatory framework in which these opportunities are arising.

Implants currently consume about half the medical polymers produced and are expected to account for around \$1.8 billion in polymer sales by 2020 (Figure 2.41). Polymers have been penetrating the implant market because they are a cheaper and lighter weight alternatives than metals, such as titanium.

Another important issue to take into account revealed in the ASEBIO (2014) report, is that in Spain, turnovers among biotechnology user companies in 2013 have risen to 95,152 million euros (an increase of 18.48% respect to 2012). The contribution to the GDP (Gross Domestic Product) by biotechnology user companies has increased to 9.07% from 7.8% in 2012 (in 2008 this indicator was under 3%). However, internal expenditure on R&D has fallen compared to the previous year (-1.68%), which is considered to be a key element for the future competitiveness of the sector. In terms of the sources of funding, the drop in R&D expenditure must be attributed to the sharp fall (-35.7%) in investment/public procurement by national and regional administrations, while investments by other companies and through own funds have increased, up to 29.4% and 4.55% respectively.

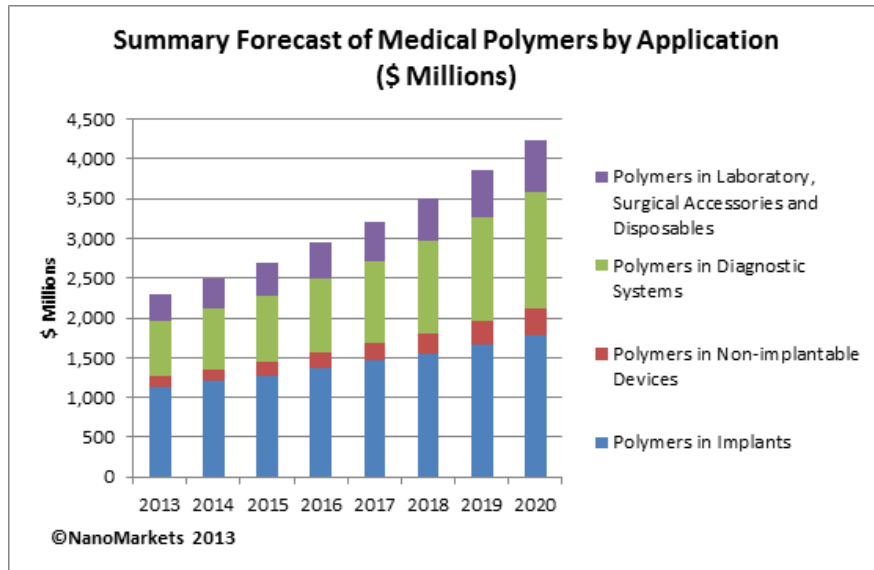


Figure 2.41. Global medical polymer market (NanoMarkets, 2013).

2.6.3 Social factors

High incidence rates of osteoporosis, osteoarthritis, obesity along with rapidly aging global population also form key drivers for the global orthopedic devices market. Increase in procedure demand and rise in people opting for minimally invasive surgeries coupled with expanded access in emerging markets are some of the other factors propelling the growth of this market. Moreover, the aged people are also more prone to accidents and injuries, which has increased the demand for graft transplant surgeries and medical implants. This in turn will drive the biomaterials market.

Orthopedic bio-implants is expected to be the second largest market segment (in terms of value) owing to rising occurrence of accidents and other such incidents that result in bone fractures, necessitating treatment via bio-implants (Deshmukh, 2014).

2.6.4 Technological factors

Technological advances introduced in the medical and healthcare industry have led to improved functionality and efficiency of medical implants and its associated procedures. These advances linked with the evolution of digital modelling techniques for tissue reconstruction has resulted in the possibility of producing customized medical implants in a relatively short time-to-market. This has contributed significantly to the growth of the biomaterials market. The research report published by Transparency Market Research (TMR, 2014) segments the biomaterials market on the basis of material types which is further divided as per applications of these biomaterials for various medical conditions. In 2012, metal type biomaterials held the largest market share in the biomaterials market, closely followed by polymeric materials (Figure 2.42).

Polymers will exhibit fastest growth in the coming years owing to its increased applications in healthcare and distinct material properties such as biocompatibility, bioinertness, flexibility, longevity, and durability.

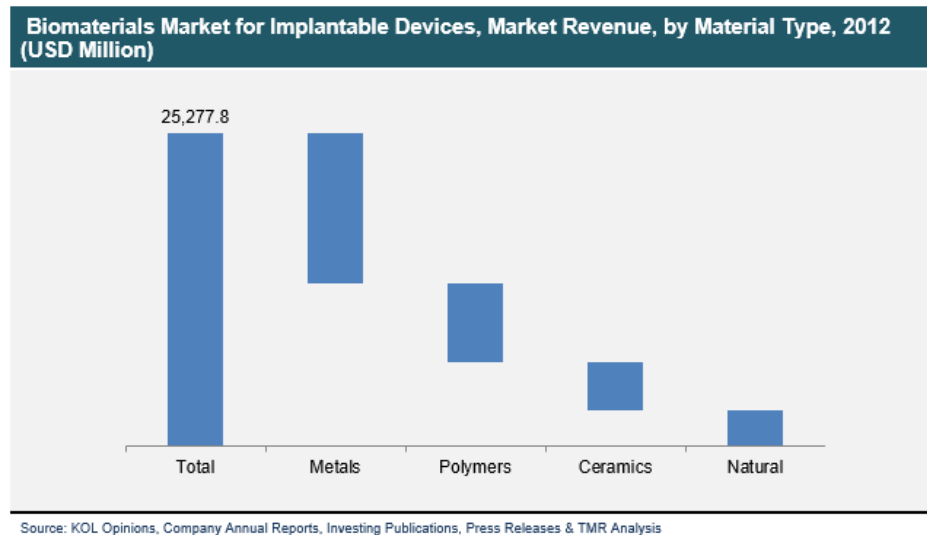


Figure 2.42. Global biomaterials market for implantable devices (TMR, 2014).

2.6.5 Environmental factors

As it was aforementioned, environmental factors are related to the environmental impact of the industrial processes carried out by a company. Overall, there have been many companies that are highly compromised in the development of clean technologies and optimized processes with the aim of reducing emissions and achieve sustainable processes.

Recent studies and government directives on energy efficiency in the manufacturing industry have revealed that cutting machine tools consume a significant amount of energy per part manufactured. Therefore, there is a great potential for saving energy by optimizing the process parameters. Anghinelli et al. (2011) carried out a functional disaggregation of the SPIF process in phases in order to quantify the inputs and outputs of raw materials, energy and lubricants, from which they calculated the CO₂ emissions. Ingarao et al. (2012) compared a traditional forming process (stamping) with ISF from the point of view of sustainability, more specifically considering waste material and energy consumption. ISF allows an important material saving compared to stamping and it is possible to reduce energy consumption by optimising the process parameters.

2.6.6 Legal factors

In Europe the medical devices are marketed following the council directive MDD 93/42/EEC, which covers the majority of the medical devices. According to this directive, the medical devices can be classified as summarized in Figure 2.43:

- Class I: low-risk, non-invasive devices (can be either sterile and measuring or non-sterile and non-measuring devices), such as wound dressings and stethoscopes.
- Class IIa: medium-risk, short-term invasive devices (tracheal tubes, lancets, etc.)
- Class IIb: high-risk, long-term surgically invasive devices, for example intra-ocular lenses or surgical lasers.
- Class III: highest-risk, including all active implantable devices (prostheses, heart valves, vascular stents...).

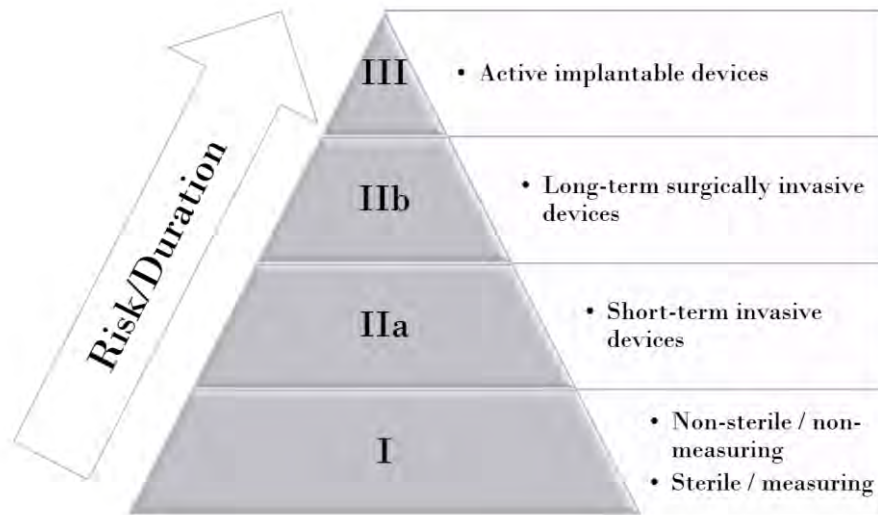


Figure 2.43. European classification of medical devices (MDD 93/42/EEC).

The directive MDD 93/42/EEC also establishes the criteria for the duration of contact and the degree of invasiveness of the medical devices (Table 2.3). A customized implant belongs to the Class III medical devices, and therefore, more strict information (including design dossiers and clinical data) has to be provided to demonstrate the compliance to the directive. This can be an impediment or a delay for the development of new manufacturing processes or materials for obtaining customized medical devices.

Table 2.3. Duration of contact and degree of invasiveness criteria for medical devices in Europe (MDD 93/42/EEC).

<p>Duration of contact criteria</p> <ul style="list-style-type: none"> • Less than 60 minutes : TRANSIENT • Less than 30 days: SHORT-TERM • More than 30 days: LONG-TERM
<p>Degree of invasiveness criteria</p> <ul style="list-style-type: none"> • Application to body surface versus and orifice • Surgically invasive or non-invasive • Implantable

2.6.7 Strategic profile of the environment

Each factor analyzed in the above sections, can be represented using the *Strategic Profile of the Environment*. The factors that compose the PESTEL analysis can be divided in the set of variables studied, and they can be graphically represented according to scale, which range from Highly Negative (HN), Negative (N), Indifferent (I), Positive (P) until Highly Positive (HP). Table 2.4 shows the result of this profile. As it can be observed, the external analysis presents a positive scenario for the development and the introduction of the ISF technology to produce customized polymer implants in the biomedical market.

Table 2.4. Strategic profile of the environment

FACTORS	BIOMEDICAL FIELD	HN	N	I	P	HP
POLITICAL	• Biotechnology is gaining importance in the political agenda					●
	• In 2014 the government Budget for R&D activities was increased					●
ECONOMIC	• Bio-implants market is forecast to increase 10.3% in 2020.					●
	• The medical polymer market will also grow (7.82%) in 2020.					●
	• About half of the medical polymers are used in implantable devices.					●
	• Internal expenditure on R & D has fallen compared to the previous year.		●			
SOCIAL	• The number of prostheses being implanted is increasing at a significant rate, due to the increased longevity of the population, the demand for increased quality of life and more active lifestyles.					●
	• Orthopedic bio-implants market is expected to be the second largest market segment (in terms of value).				●	
TECHNOLOGICAL	• Technological advances introduced in the medical and healthcare industry have led to improved functionality and efficiency of medical implants and its associated procedures.					●
	• Evolution of digital modelling techniques for tissue reconstruction has resulted in the possibility of producing customized medical implants.					●
	• Polymers will exhibit fast growth in healthcare applications.				●	
ENVIRONMENTAL	• Reduce CO ₂ emissions and material waste in the manufacturing of customized implants.				●	
LEGAL	• Demonstrate the compliance to MDD 93/42/EEC for Class III medical devices.	●				

2.6.8 Examples of biomedical devices manufactured using ISF

As it has been already stated, the biomedical field has a great potential for the application of ISF because it is a technology capable to produce unique parts in a short time and at a reasonable cost. Since the beginning of ISF, several research papers have shown a growing interest in this manufacturing process. One of the first attempts to produce a customized medical device was done by Ambrogio et al. (2005). They manufactured an ankle support using a reverse engineering approach, acquiring the patient’s shape to ensure an appropriate agreement between the manufactured part and the actual geometry (Figure 2.44a). The

ankle support was manufactured using Deep Drawing Quality steel (DDQ) and the SPIF variant (Figure 2.44b) obtaining geometric deviation below 1 mm.

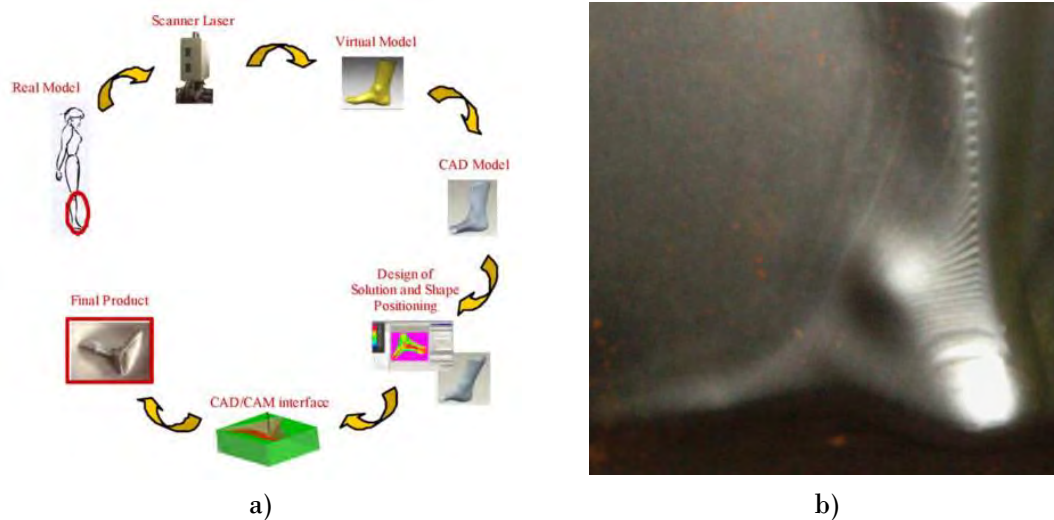


Figure 2.44. a) Process cycle for a customized medical device. b) Ankle final part (Ambrogio et al., 2005).

Tanaka et al. (2007) manufactured a pure titanium denture plate with SPIF. After trimming with wire electrodischarge machining (EDM) a severe springback recovery took place (Figure 2.45). Therefore, they analyzed the residual stresses of the sheet part using numerical simulations varying the tool diameter and feed rate.

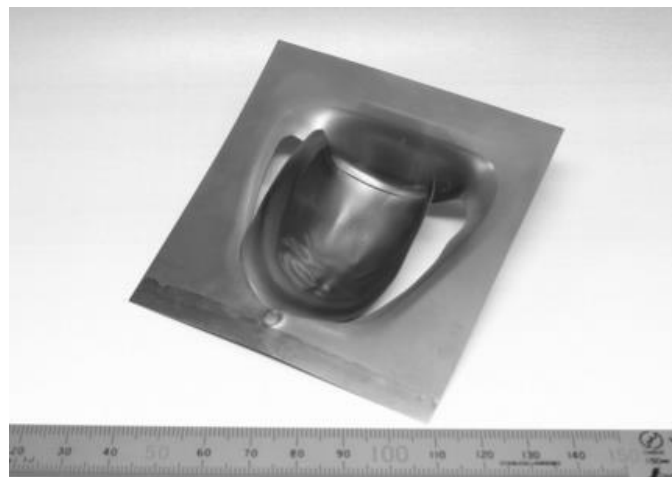


Figure 2.45. Pure titanium denture plate formed by SPIF and trimmed using wire-EDM (Tanaka et al., 2007).

A recent publication (Milutinovic et al., 2014) has also been focused on the manufacturing of a denture base by SPIF using two materials: a low carbon steel (DC04) and a ferritic stainless steel (X6Cr17) (Figure 2.46). The geometric accuracy was analyzed using a 3D scanning system, the maximum deviations (below 1 mm) were close to the edges of the denture base.



Figure 2.46. a) Complete cast-metal denture base and b) SPIF manufactured denture base in DC04 (left) and X6Cr17 (right) (Milutinovic et al., 2014).

Another biomedical application that has been manufactured using SPIF is a part for a knee implant (Oleksik et al., 2010), more specifically the articular resurfacing component of a condylar implant (Figure 2.47). The authors used numerical simulation to determine the thinning effect in the SPIF process for obtaining the knee condylar surface in pure titanium.



Figure 2.47. Condylar implant components: articular resurfacing component and fastening screw (Oleksik et al., 2010).

The most widespread medical application in ISF is the customized cranial prosthesis. The first publication that showed the possibility of manufacturing a customized cranial prosthesis was done by Duflou and coworkers (Duflou et al., 2005). They compared the steps required for manufacturing an aluminum 3003-O cranial prosthesis (Figure 2.48) using hydroforming and using SPIF. It was revealed that SPIF allowed a significant reduction of process time (16.5 days for hydroforming vs. less than 4 days for SPIF) becoming an interesting approach not only for manufacturing cranial prosthesis but also for other medical applications, such as the plates used in hip reconstructions.

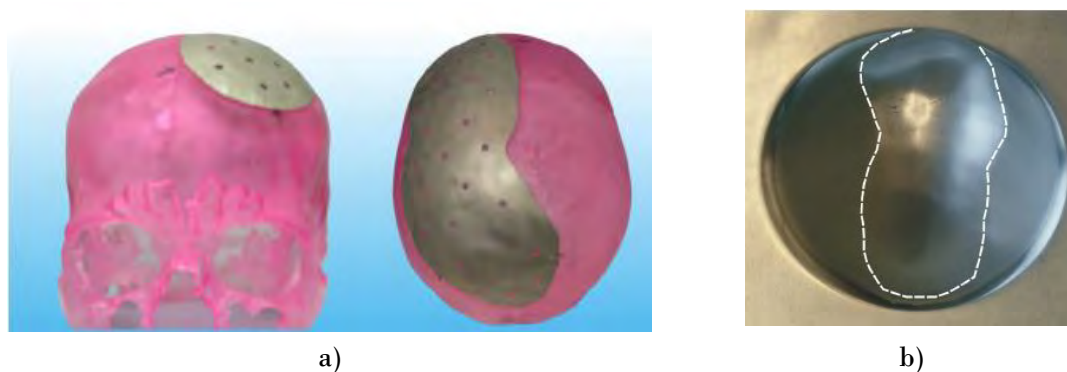


Figure 2.48. a) Cranial prosthesis design. b) Cranial prosthesis manufactured by SPIF before trimming (Duflou et al., 2005).

In the paper of Han et al. (2010) the methodology for obtaining the digital model of the customized implant from the computed tomographies (CT) of the patient was explained in detail (Figure 2.49a). The cranial prosthesis was manufactured using the TPIF positive variant (Figure 2.49b) with steel (Figure 2.49c) to show the feasibility of this ISF variant.

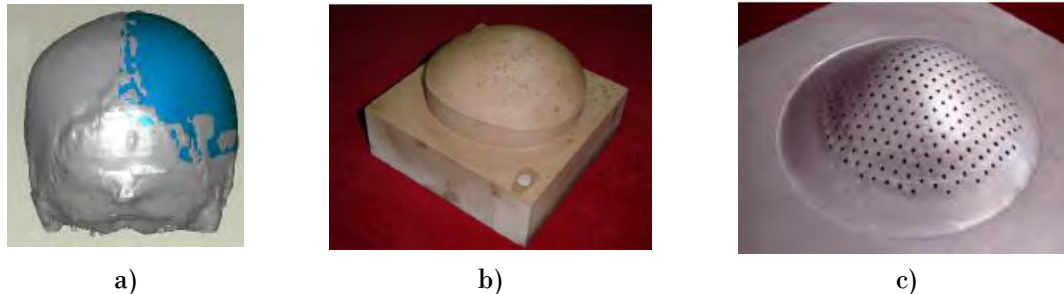


Figure 2.49. a) Cranial prosthesis design, b) positive die, c) produced part (Han et al., 2010).

In the work of Göttmann et al. (2013), customized cranial implants in titanium grade 2 sheets were manufactured using the TPIF variant with a positive full die in order to improve the accuracy of the parts (Figure 2.50). Furthermore, they evaluated the effect of different forming strategies (one-step, multi-step and previous incremental bending) and heat treatments before trimming the prostheses on the geometric deviations. They manufactured the implants using expanded metal sheets and solid sheets with holes drilled after the forming process (Figure 2.51).

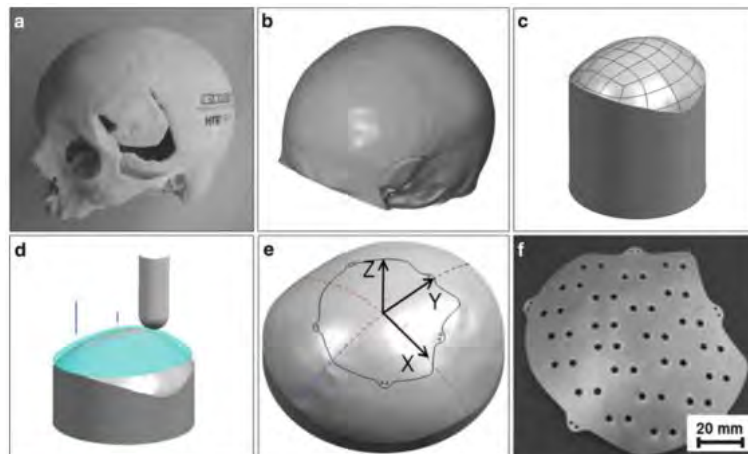


Figure 2.50. Cranial model (a, b), positive full die design (c, d), die area covered by the implant (e) and manufactured implant (f) (Göttmann et al., 2013).

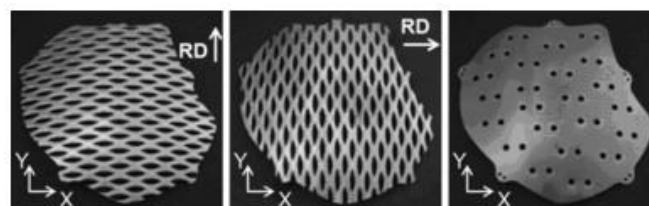


Figure 2.51. Cranial implants produced from expanded metal sheets and from solid metal sheets (the holes were drilled after forming) (Göttmann et al., 2013).

Later, Lu et al. (2014) evaluate the properties of titanium grade 1 sheets and performed finite element simulations and SPIF experimental tests to determine the feasibility for producing customized cranial implants, analyzing the force required to form the sheet, the thickness reduction, the geometric deviation and the surface finishing (Figure 2.52).



Figure 2.52. Skull model (a) and finished part (b) (Lu et al., 2016).

Castelan et al. (2014), used the negative TPIF variant in order to manufacture a customized cranial implant in titanium grade 2. The part was trimmed after performing a heat trimming for stress relief and then a dimensional analysis between the CAD model and the manufactured one was done by using a 3D scanning system. The results demonstrate that significant discrepancies were obtained (± 7 mm). However, due to the severe cranial injury of the patient (Figure 2.53a), once the implant was assembled in the biomodel obtained by 3D printing, these discrepancies were almost negligible in the visual analysis because the symmetry was nearly maintained (Figure 2.53b). They also pointed out the possibility of notably reduce the cost of the cranial implant manufactured using ISF respect to the cost of the common manufacturing processes (molding or machining), becoming an interesting approach for this kind of applications.



Figure 2.53. a) Severe cranial injury. b) Assembly of the implant manufactured by TPIF in the biomodel (Castelan et al., 2014).

Recently, Ambrogio et al. (2015) compared two alternatives for producing customized cranial implants (milling and SPIF) in terms of forming approaches and part quality. It was shown that with SPIF it is possible to reduce the raw material quantity and the material waste, as well as the production time. Higher geometric discrepancies (about 2 mm) were obtained in the lateral zones (Figure 2.54) which could be compensated using a die.

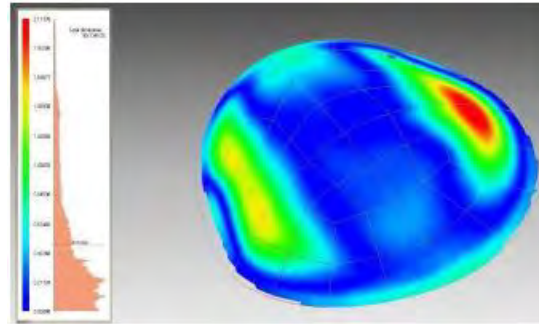


Figure 2.54. Comparison between the CAD model and the ISF manufactured cranial implant after trimming (Ambrogio et al., 2015).

ISF can be used to manufacture customized implants not only for repairing cranial injuries but also for craniomaxillofacial defects. Duflou et al. (2013) manufactured aluminum, stainless steel and titanium grade 2 frontal orbit implants (Figure 2.55a) using SPIF. A feature assisted tool path planning was used to improve the accuracy of the implants (Figure 2.55b).

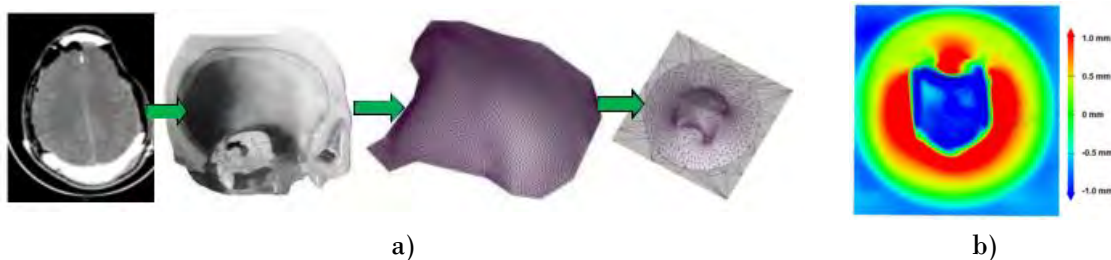


Figure 2.55. a) Generation of the CAD model of a frontal orbit implant and b) accuracy of the implant manufactured by SPIF (Duflou et al., 2013).

Araujo et al. (2014) determined the failure limits of SPIF truncated cones and pyramids manufactured in titanium grade 2 using the circle grid analysis. With this information, it was possible to obtain successfully a facial implant without failure (Figure 2.56).

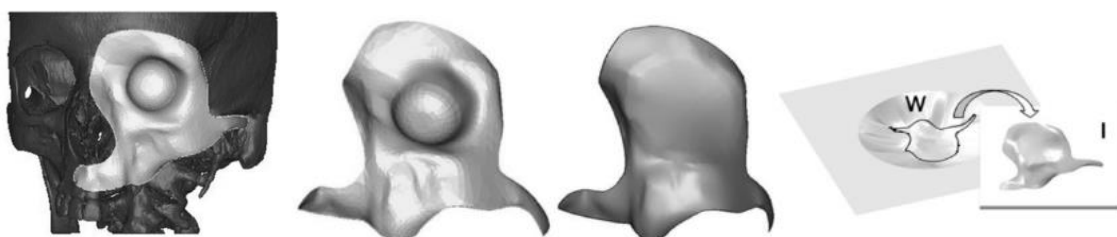


Figure 2.56. Model of the facial implant manufactured by SPIF (Araujo et al., 2014).

It is worth noting that the aforementioned research works have been carried out using metallic materials (aluminum, steel or titanium). Nowadays, there are scarce publications dealing with the production of any biomedical device or prosthesis manufactured with Incremental Sheet Forming using biocompatible polymers. Fiorentino et al. (2012) manufactured a palate prosthesis using a titanium alloy and PCL (polycaprolactone). Although their results were promising an optimization of the process parameters should be done in order to increase the accuracy of the part. Customized cranial implants

manufactured in polymeric sheet by SPIF, can be found in the literature, which are mainly focused on the evaluation of the accuracy of cranial prostheses in polycarbonate (Bagudanch et al., 2014a). However, in order to achieve better accuracy results the TPIF variant should be used. Thus, a niche market where the use of biocompatible polymers manufactured by Incremental Sheet Forming can provide remarkable advantages in terms of low cost and reduced time to market has been identified.

2.7 Summary and thesis framework

After reviewing the state of the art in ISF it has been detected an important niche of market related with the use of thermoplastic materials, which will be the main topic of this thesis. From this point of view, an initial framework (Figure 1.4) has been defined consisting in two main blocks:

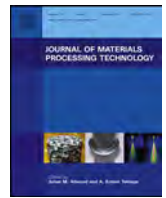
- *The study of the influence of the process parameters on basic geometries manufactured by SPIF.* This study will be carried out using non biocompatible polymers as well as some biocompatible ones. The aim of this research is to increase the knowledge regarding the behavior of polymers under the SPIF process analyzing deeply the influence of the most common process parameters on the process outputs. With this information it can be possible to obtain useful process guidelines that can be employed in the second block of the thesis framework.
- *Development of a cranial implant, the thesis cases of study, using biocompatible polymers.* In this case, the aim is to demonstrate the feasibility of producing a low cost cranial implant meeting the geometric tolerances requirements. The first attempts for obtaining a cranial implant will be done using the simplest ISF variant (SPIF) in order to reduce costs and set-up complexity. However, in order to achieve an appropriate implant with low geometric deviations the TPIF approach will be also considered.

The subsequent sections of this thesis contain the research papers already published or under review that have been developed according to the aforementioned framework and aims.

Chapter 3. Forming force and temperature effects on single point incremental forming of polyvinylchloride

Chapter 3 presents an experimental study of the process parameters in SPIF (step down, tool diameter, feed rate, spindle speed, sheet thickness) and their influence on the maximum forming force, maximum achieved depth and surface roughness for a non-biocompatible polymer, polyvinylchloride (PVC).

This study was presented in an article entitled “*Forming force and temperature effects on single point incremental forming of polyvinylchloride*”, published in *Journal of Materials Processing Technology* (Bagudanch et al., 2015a).



Forming force and temperature effects on single point incremental forming of polyvinylchloride



I. Bagudanch^a, M.L. Garcia-Romeu^{a,*}, G. Centeno^b, A. Elías-Zúñiga^c, J. Ciurana^a

^a University of Girona, Department of Mechanical Engineering and Industrial Construction, Girona, Spain

^b University of Seville, Department of Mechanical and Manufacturing Engineering, Sevilla, Spain

^c Instituto Tecnológico y de Estudios Superiores de Monterrey, Departamento de Ingeniería Mecánica, Monterrey, Mexico

ARTICLE INFO

Article history:

Received 31 October 2014

Received in revised form 3 December 2014

Accepted 5 December 2014

Available online 19 December 2014

Keywords:

Single point incremental forming

Thermoplastic polymers

Forming force

Temperature effect

ABSTRACT

Incremental Sheet Forming (ISF) is a technology that allows producing highly customized products at a reasonable manufacturing cost, and Single point incremental forming (SPIF) is one of the simplest ISF processes. In this sense, recent research works have revealed an increasing interest in forming thermoplastic materials by ISF. The present paper focuses on determining the influence of the main process parameters, i.e. the step down, spindle speed, feed rate, tool diameter and sheet thickness, on the maximum forming force. Maximum depth has been analyzed as a formability indicator and surface roughness has been also addressed. The results show a significant effect of the spindle speed in the ISF process of polymeric materials, not only on the maximum forming force but also on its formability, by means of the maximum depth reached, and on the surface roughness achieved. This is a consequent of the triggered increment of temperature obtained due to the friction between the tool and the sheet blank, as far as temperature variation is supposed to be the main factor causing the variation of the mechanical properties of thermoplastic polymers. The material used in this research work was polyvinylchloride (PVC), which becomes rubber-like with the increase of temperature as a consequence of its viscoelastic behaviour.

© 2014 Elsevier B.V. All rights reserved.

1. Introduction

In recent years, several innovative forming processes have been developed with the aim of producing highly customized products with a reasonable manufacturing cost. Incremental Sheet Forming (ISF) is one of these new technologies gaining importance in the last years and becoming the focus of interest for many researchers and institutions.

In the traditional processing techniques of plastic materials it must be applied heat and/or pressure to give the desired shape to the material. In fact, temperature has a very important role in the behaviour of plastic materials, specially referred to the phase transition, fluency characteristics, morphology and degradation. These processing techniques require high production batches to recover the costs derived of machinery, tools and energy. With this aim, it is necessary to develop new technologies that allow the production of smaller batches with shorter life cycles and a very low time to market. Using ISF the production costs can be reduced as far as

it is possible to work with polymers at room temperature and the experimental set-up necessary to carry out the process is quite simple. In this sense, it is an economically viable manufacturing process to produce small batches and customized plastic products.

The technology of ISF is mainly applied in the automotive and aeronautic sectors, either to obtain functional parts or prototypes. Moreover, there are other fields with an important potential for the technology, such as the biomedical. Several works in the literature use ISF to produce parts such as an ankle prosthesis (Ambrogio et al., 2005), a cranial implant (Duflo et al., 2005), a palate implant (Tanaka et al., 2007) and most recently a part for a knee implant (Oleksik et al., 2010). All of these applications have been manufactured using metallic materials. Some biocompatible metallic materials, such as titanium, are very difficult to deform at room temperature. Therefore an additional heating system should be used in order to increase the formability and to produce the desired part. Thus, a niche market where the use of biocompatible polymers manufactured by ISF can provide remarkable advantages in terms of low cost and reduced time to market has been identified.

The first research work in which the feasibility of using ISF to produce parts with thermoplastic materials was demonstrated was done by Franzen et al. (2008). The paper was focused on the evaluation of the performance of PVC (polyvinylchloride). Their results

* Corresponding author at: C/Maria Aurèlia Capmany, 61 (Edifici P2 Campus Montilivi), 17071 Girona, Spain. Tel.: +34 972418265; fax: +34 972418098.

E-mail address: mluisa.gromeu@udg.edu (M.L. Garcia-Romeu).

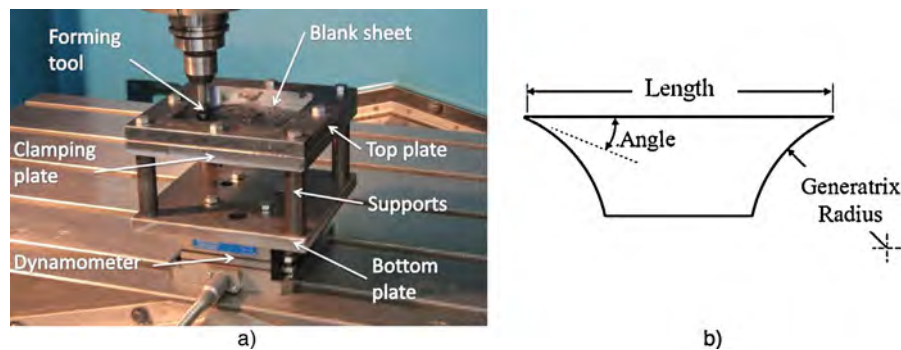


Fig. 1. (a) Experimental set-up used on a 3 axis CNC milling machine. (b) Design of the pyramidal frusta of circular generatrix.

demonstrated that new deformation mechanisms and modes of failure appeared (cracking, wrinkling and oblique cracking), which some of them were absent when working with metallic sheets (Silva et al., 2008). Le et al. (2008) published the results of a set of experiments for the SPIF of PP (polypropylene). The influence of the forming parameters and their interaction on the formability was analyzed. In the work of Martins et al. (2009) five polymers were studied. For each material FLDs (Fracture Forming Limit Diagrams) were obtained. Modes of failure, strains at rupture, formability, accuracy of final parts and colour variation during cold formation were evaluated.

Recently, Silva et al. (2010) identified a theoretical framework for rotationally symmetric conditions that allowed studying quantitatively and qualitatively the influence of major forming parameters. The paper was based on membrane analysis and SPIF tests using PVC sheets. An analytical framework able to model the first mode of failure identified in Franzen et al. (2008) was developed. In a subsequent work, Marques et al. (2012) extended the analytical model previously described in Silva et al. (2010) in order to be able to model the second and third modes of failure by means of membrane analysis.

In the paper of Alkas Yonan et al. (2014) the plastic flow and failure of PVC sheets were characterized in conventional and multi-stage SPIF. They proposed a methodology to determine the stresses and the accumulated values of ductile damage from the strains measured by means of a digital image correlation technique. The stress–strain curves were experimentally obtained by tensile and stack compression tests and they approximated the relationship of true stress and true strain by a Ludwik–Hollomon's law, typically used in metallic materials. In order to determine the damage, a pressure modified version of the von Mises yield criterion was employed.

Taking into account all the previous research work, a gap of knowledge related to the forming force involved in the SPIF process of polymer materials has been identified. The interest of studying the effect of the technological parameters in the ISF process force is relatively recent, and it has been mainly studied for metallic materials (Perez-Santiago, 2012). Forming force estimation in ISF is especially important in the case of using machinery adapted for the process like milling centres and robots. One of the first works was done by Jeswiet et al. (2005) who measured force magnitudes of TPIF and SPIF truncated cones and pyramids, using AA3003-O. Later, Duflo and Tunckol (2006) identified the differences in the force curves corresponding to successful and failed SPIF cones manufactured with AA3003-O. Durante et al. (2010a) measured the forces developed during the SPIF forming of AA7075-T0 using a more complex geometry (variable wall angle conical frusta). Aiming for quick estimations of the maximum force, several researchers have proposed analytical models intended for uniform wall angle (UWA)

geometries formed with different materials, such as the empirical equation obtained by Aereus et al. (2010).

Therefore, the present paper is mainly focused on the maximum forming force evaluation under the influence of some process parameters (step down, spindle speed, feed rate, tool diameter and sheet thickness). Maximum depth as a formability indicator and surface roughness will be studied. In addition, due to the viscoelastic behaviour of polymers, the effect of the temperature variation during the forming process will be analyzed.

2. Experimental setting

The experimental set-up used to register experimental data is widely described in a previous author's work (Bagudanch et al., 2013). The clamping system is shown in Fig. 1a.

2.1. Part geometry

The selected geometry is a pyramidal frusta with circular generatrix and variable wall angle (VWA). This part geometry has been extensively used in previous works that focus on the application of the SPIF processes of polymeric and metallic materials (Bagudanch et al., 2013). The length of the pyramidal edges is 105 mm with an initial wall angle of 45° and an 80 mm generatrix radius (Fig. 1b). The final angle was chosen to be 80° in order to capture, among others, the influence of the forming forces, temperature, feed rate, spindle speed, and workpiece thickness during its formability processes, as it will be discussed in the following sections.

2.2. PVC samples material properties

The SPIF tests were performed in several PVC (polyvinylchloride) sheet samples with two different thicknesses: 1.5 mm and 2 mm. It is well known that the PVC has an amorphous structure with polar chlorine atoms. In accordance with the supplier of the PVC material, its glass transition temperature T_g is 82°C . The mechanical properties of the PVC samples were characterized by carrying out a series of uniaxial tensile tests performed in a MTS Insight universal testing machine with 10 kN load cell. Three replications of each test were performed until the specimen failure by following the specifications of the ASTM D 638-02a norm. The tests were performed at room temperature, 40°C and 60°C in order to analyze the influence of the temperature variation in the polymeric behaviour. It was noticed that the material samples experienced a linear elastic response followed by a yielding, softened behaviour.

2.3. Experimental plan

The experiment plan was designed with the aim of learning how the forming parameters influence the formability of the PVC specimens and to quantify this influence.

Therefore, the experiments have been focused on the following five forming parameters based on the experience of the previous research works (Silva et al., 2010): step down was set to 0.2 and 0.5 mm, two tool diameter were used (6 and 10 mm), the feed rate was set to 1500 and 3000 mm/min, the spindle speed was defined as free (the tool will rotate depending on the friction due to its contact with the blank), 1000 rpm and 2000 rpm, and finally two different sheet thicknesses were used (1.5 mm and 2.0 mm).

A 2^{5-1} factorial design of experiments was defined in 16 runs. Also, three replications for each experiment were considered so that a total of 48 tests were planned.

During the recording of the experimental data, the following magnitudes were registered:

- Maximum forming force in the vertical direction ($F_{z \max}$): the forming forces were collected with a frequency of 10 values per second using the dynamometric table. Then, its magnitudes were filtered using Matlab® to obtain its maximum value. As previously demonstrated by other authors (Jeswiet et al., 2005), the predominant magnitude of the forming forces in ISF corresponds to the component aligned with the tool axis. Therefore, in the present paper the forces in the x and y directions will not be considered.
- Maximum depth (Z_{\max}): the maximum depth is obtained directly from the Computer Numerical Control (CNC) of the machine. The lecture of its value is recorded just when the failure of the sheet appears.
- Surface roughness (R_a): the measurements of the surface roughness are obtained with a Mitutoyo SurfTest SV-2000 profilometer using the following parameters: (i) measured length: 8.8 mm; (ii) profile type: R ; (iii) evaluation length: 0.8 mm; (iv) sampling length, l_m : 8.0 mm.

3. Results and discussion

Fig. 2 illustrates the PVC material response when subjected to simple uniaxial load at different testing speeds and temperatures and provides the values of the Young modulus (E) and the yield stress (σ_y). Three replicates of each test were done obtaining repeatable results. As it can be seen from Fig. 2, these experimental tests show that for increasing testing speeds, the yield stress is higher with a decreasing strain value at the material fracture and the Young modulus increases. When the testing temperature is increased the Young modulus and the yield stress diminish their value. This strain-rate and temperature dependant behaviour is very common for thermoplastic materials.

Table 1 shows a summary of the mean values (3 replicates for each test) of the collected forces, step down, and surface roughness obtained at each experimental run. Notice that in the last column of Table 1, it has been indicated if the sheet fracture (f) or it was successfully formed without wrinkles (s) or with some wrinkles defects (w).

An analysis of variance (ANOVA) has been done in order to identify the influence of the factors for maximum forming force, maximum depth and surface roughness (Table 2). This table provides information regarding the degrees of freedom (DF), the sum of squares (SS), the mean squares (MS), the F - and P -value, for each one of the main effects and the two-way interactions. The factors that have a significant effect on the analyzed responses are the ones with a P -value less than 0.05 (values in bold in Table 2).

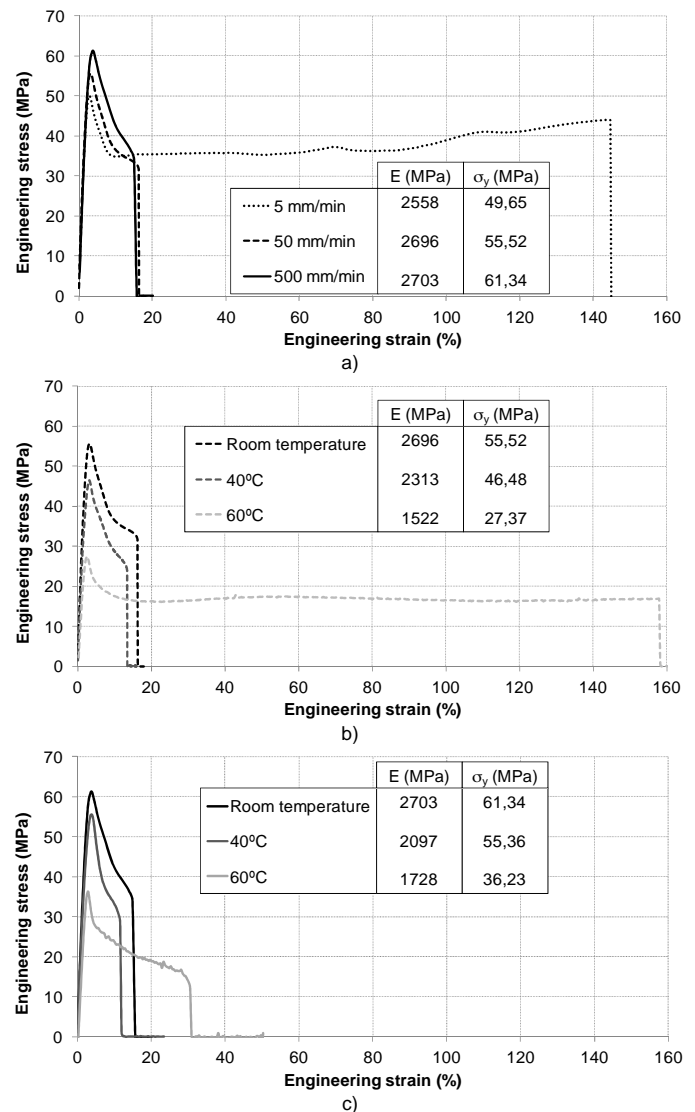


Fig. 2. Stress strain curve for PVC: (a) under different testing speeds at room temperature, (b) at 50 mm/min at various temperatures and (c) at 500 mm/min at various temperatures.

The discussion according to these results is divided in three sections: maximum force, formability and surface roughness. In order to deeply understand the behaviour of the material some additional tests and measurements have been performed as it will be explained in the subsequent sections.

3.1. Maximum forming force

Previous research works, as stated in Section 1, have reviewed the effect of technological parameters on the forming forces in Incremental Sheet Forming. From these studies it is known that the parameters that mainly influence the maximum vertical force attained during SPIF of metals are the tool diameter and the sheet thickness. Aereens et al. (2010) quantified this influence proposing an empirical formula that predicts the steady state vertical force of truncated cones as a function of the material tensile strength, the scallop height, tool geometry, and sheet thickness. This equation, obtained from the results of an experimental campaign conducted on several metallic materials, has the following structure:

$$F_{zs} = 0.0716 \cdot R_m \cdot t_0^{1.57} \cdot d_t^{0.41} \cdot \Delta h^{0.09} \cdot \alpha \cdot \cos \alpha \quad (1)$$

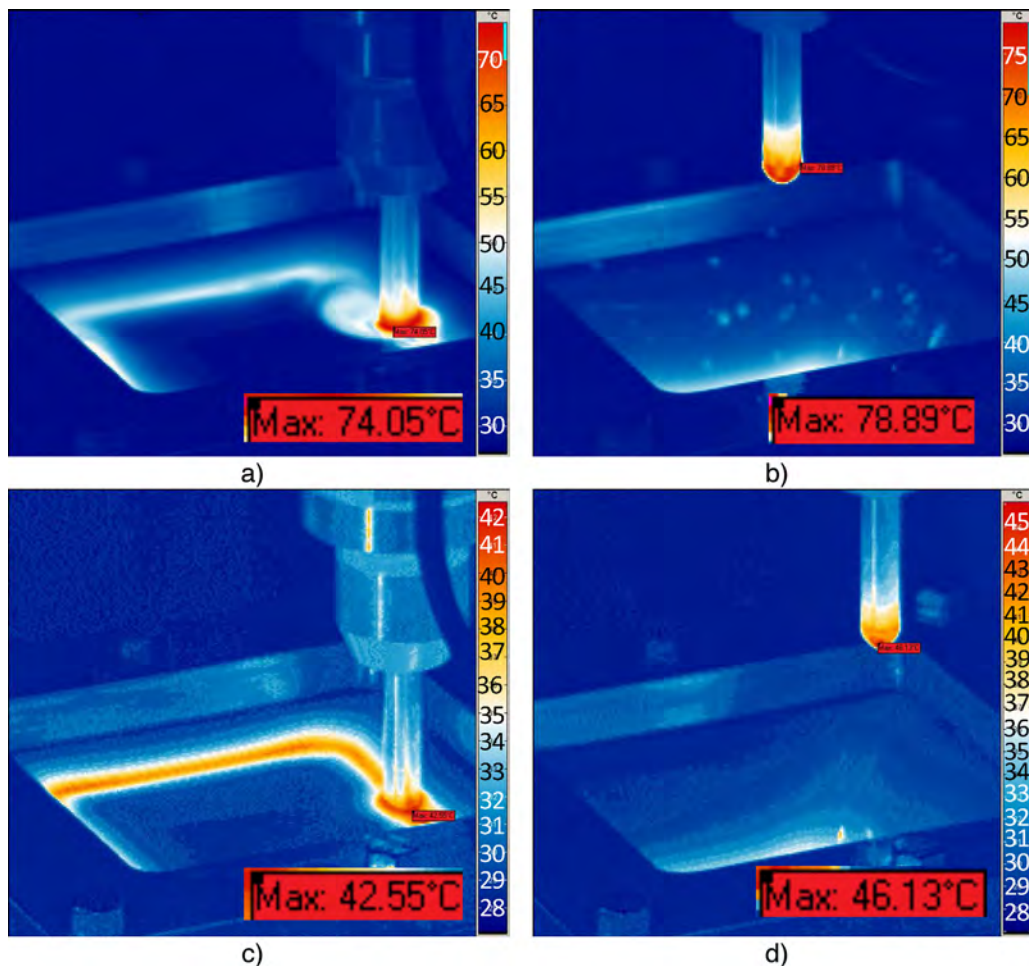


Fig. 3. Tool tip and polymeric part temperatures distribution recorded at the spindle speed of: (a) 2000 rpm during the SPIF process, (b) 2000 rpm at the end of the SPIF process, (c) “free” during the SPIF process and (d) “free” at the end of the SPIF process.

be explained with the material temperature variation during the SPIF manufacturing processes, since it is well known that the load needed to deform a polymeric-like material significantly decreases with the temperature, as discussed for instance in [Jardet and Morel \(2003\)](#). In order to validate this conclusion, a thermographic camera IRBIS ImageIR® 3300 has been used to record the material temperature values during its SPIF manufacturing processes.

Two tests were set to measure the material temperature as a function of the spindle speed: one with a spindle speed value of 2000 rpm and the other with a free tool rotation. The tests were performed by using the following values: 2 mm sheet thickness, a feed rate of 3000 mm/min, a tool diameter of 10 mm with a 0.5 mm of step down. The measurements of temperature distribution recorded for each case are shown in [Fig. 3](#). As it can be seen from this figure, the magnitude of the temperature varies on the tool tip as a function of the friction and the spindle speed ([Mens and de Gee, 1991](#)).

As shown in [Fig. 3](#), the material temperature increases slightly when the tool rotates freely. This is mainly due to small friction effects between the tool and the material specimen. In this case, an increase on the vertical force magnitude is needed to manufacture the polymeric part. However, this is not the case for which the spindle speed is 2000 rpm since it has been found that during the SPIF manufacturing processes, the specimen reached an average temperature value of 74.05 °C with a decreasing forming force magnitude F_z . In accordance with these experimental facts, it can be concluded that besides the friction between the

tool tip and the polymeric sheet, the spindle speed also influences the maximum value of the forming force that is needed to manufacture polymeric parts through the SPIF processes. Therefore, in order to increase PVC formability in SPIF, spindle speed, friction conditions and temperature effects must be taken into account.

In order to deeply analyze the effect of the spindle speed on the forming force, eight additional tests at an intermediate spindle speed (1000 rpm) have been done and added to the experimental results. With the results obtained from these tests and the results previously presented for the proposed DOE, an ANOVA analysis for the forming force is presented. The parameters used in the tests (A–H) are detailed in the table of [Fig. 4a](#) as well as the main effects plot for the forming force. The mean force values shown in [Fig. 4a](#) for free and 2000 rpm spindle speeds are obtained according to the results presented in [Table 1](#), whereas the value corresponding to 1000 rpm is obtained from the additional experiments (see experimental data in [Fig. 4a](#)). It can be observed that there is a linear decrease of the forming force with the increase of the spindle speed. Furthermore, the evolution of the vertical forming force along the part’s depth during its manufacturing process for three tests at different spindle speeds (free tool rotation, 1000 and 2000 rpm) is illustrated in [Fig. 4b](#). It is clear from this figure, that the heat generation due to the friction has an effect on the maximum forming force, as previously mentioned, but also on the force evolution during the manufacturing process. For higher spindle speeds the forming force notably decreases as well as its slope. This is a fact that

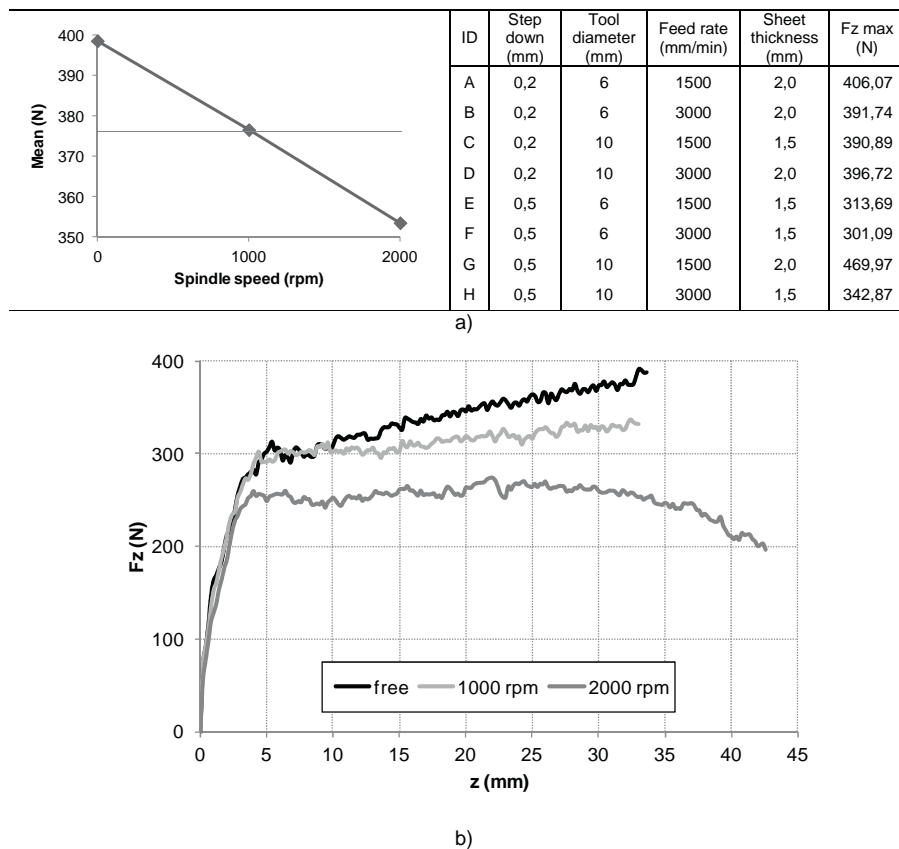


Fig. 4. (a) Main effects plot for the forming force with the variation of the spindle speed considering the tests done in the DOE and the additional tests. (b) Evolution of the vertical forming forces for different spindle speeds with the part's depth.

could be expected from the tensile tests done at different testing temperatures (Fig. 2b and c).

3.2. Formability

In this section the attention is focused on understanding how the process parameters influence the formability by means of the maximum depth achieved before tearing or wrinkling occurs in the specimen. As detailed in Table 2, every effect has a significant influence on the maximum depth. In this sense, the spindle speed has an important influence on formability evaluated by means of the maximum depth value. This effect is related to the heat generation due to the friction between the tool and the sheet since at higher material temperatures (below T_g) elongation and formability increases.

The results in Table 1 show that, for a 6 mm tool diameter, the final depth achieved is smaller than the one attained using a bigger tool. During the experimental testing, it was observed that the indentation increased with a smaller tool diameter. This can be explained by considering that the local deformation values around a small tip tool diameter are higher than those of a bigger tool. The influence of the spindle speed and the tool size on the maximum depth is similar to the experimental finding of Le et al. (2008) in the SPIF manufacturing process of a polypropylene (PP) thermoplastic material.

On the contrary to the regular behaviour of metal (Centeno et al., 2014) and polymer (Le et al., 2008) sheets deformed by SPIF, it was observed in the present case that the formability increased at larger step downs and feed rate values. For instance, this formability behaviour of PVC is the opposite from that found by Le et al. (2008) in the case of PP. An explanation for the difference in the

formability trends could be related to the rheological properties of thermoplastic materials (Shaw and MacKnight, 2005). It is well known that polymers exhibit a drastically different behaviour depending on their molecular weight (Pan et al., 2005), even to the extent to observe trends that are not in accordance to those previously found in the literature, especially if two different polymers are being compared. Furthermore, it should be mentioned that a same type of thermoplastic material (for instance, PVC) can be found with different molecular weights depending on the arrangement of polymer chains, the polymerization reaction, etc. From the literature review, it can be noticed that the polymer characterization is mainly based on the mechanical properties (Young modulus, yield stress, etc.) typically found in metallic materials. However, it is scarce regarding other inherent polymer aspects, such as the thermal or rheological characteristics. For that reason, in future work, it would be important to improve the information about the polymer properties, including, among others, the molecular weight of the materials used in SPIF in order to be able to quantify in which degree the rheological properties can influence the formability.

As it can be seen from Table 1, the final part deformed from a 2 mm thickness sheet was successfully achieved (for example, the experiment 16 shown in Fig. 5a). However, some wrinkles appeared in the final part of 1.5 mm thickness (experiment 15 in Fig. 5b). Therefore, it can be concluded that sheet thickness influences the formability and the appearance of wrinkling for PVC parts, as it occurs in sheet metal.

In order to analyze the sheet formability, a sheet of PVC has been marked using serigraphy with a circle grid of 1 mm of diameter and a distance between circle centres of 3 mm (see Fig. 5c). Principal strains on the outer sheet surface were obtained on different sections of the final part by using the 3D deformation digital

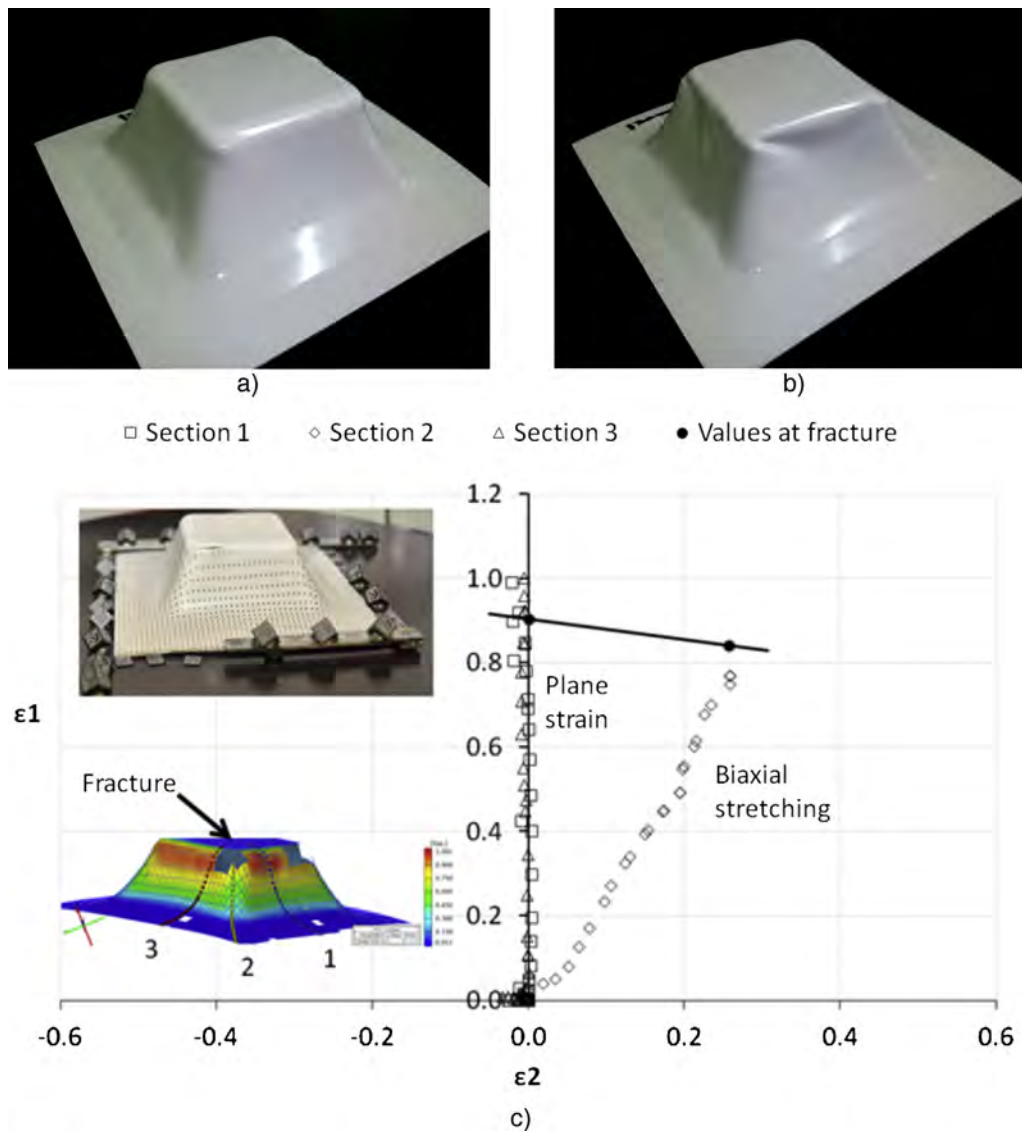


Fig. 5. Successful formed part of (a) 2 mm thick sheet (no wrinkles), (b) 1.5 mm thick sheet (wrinkles) and (c) Forming Limit Diagram (FLD) of PVC sheets.

measurement system ARGUS[®] based on circle grid analysis. The methodology used to obtain the measurements is the same as the one deeply detailed in a previous work of the authors (Centeno et al., 2014). As expected, the area of maximum major strain was located close to the crack (see Fig. 5c). The measurement system is only capable to measure the ellipses above and below the crack, so the fracture strains must be either interpolated or indirectly calculated based on volume constancy (see Centeno et al., 2014). Notice that in the walls of the pyramid the deformation mode is plane strain while in the corners is biaxial stretching.

In order to verify the material incompressibility two sections of the final part have been cut in the zone of fracture, including the biaxial stretching and the plane strain deformation modes (sections 1 and 2 in Fig. 5c). Within the FLD (Forming Limit Diagram) the major (ϵ_1) and minor (ϵ_2) strains at fracture were obtained for each section. From Fig. 5c it can be observed that the strains at fracture are close to the maximum strains obtained by ARGUS[®], meaning that the fracture mechanism is not driven by an instable process such as necking. In this regard, measuring the sheet thickness along the crack it is possible to calculate ϵ_3 from the initial sheet thickness; being its mean value in the biaxial zone -1.098 and in the plane strain zone -0.905 .

If a material is considered as incompressible the following condition of volume constancy must be satisfied:

$$\bar{\epsilon}_{3,f} = -(\bar{\epsilon}_{1,f} + \bar{\epsilon}_{2,f}) \quad (3)$$

The theoretical values of ϵ_3 (calculated using the major and minor strains at fracture) in the biaxial stretching zone and in the plane strain zone are respectively -1.099 and -0.905 , being the incompressibility error within the $\pm 10\%$. Therefore, the theoretical and the measured thickness strains at fracture are nearly identical in both strain states, i.e. plane and biaxial strains, and it is possible to conclude that the PVC specimens behave as an incompressible polymer.

3.3. Surface roughness

The study of the surface roughness in Incremental Sheet Forming compared to other responses is scarce, for both, metallic and polymeric parts. In the work of Durante et al. (2010b), an analytical model is proposed to predict the surface roughness. This model has an acceptable agreement with the experimental values. They determined that the surface roughness varied with the tool diameter, the step down and the wall angle. Recently, Liu et al. (2014) proposed

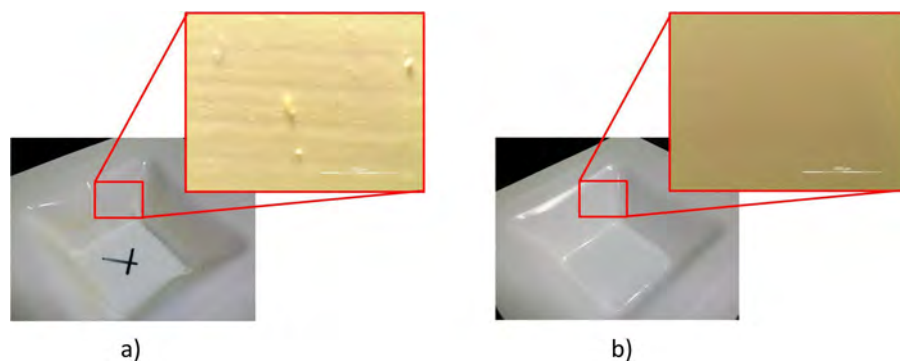


Fig. 6. (a) Worst surface roughness (experiment 14). (b) Best surface roughness (experiment 1).

a methodology to empirically describe a relationship between the overall surface roughness obtained in aluminium parts and four process parameters (tool diameter, sheet thickness, feed rate and step down). They identified by means of an ANOVA analysis that the sheet thickness and the step down were the most significant parameters.

From the results obtained in the present work (Table 2) it can be concluded that the step down and the spindle speed, as main effects, and the interactions between the step down with the feed rate, the tool diameter with the sheet thickness and the feed rate with the spindle speed are the parameters that have the most significant influence on the surface roughness values.

The influence of the step down was expected because at higher step down the generated tool path will slightly differ of the geometry profile due to the interpolation. The choice of the step down should be a compromise between the manufacturing time and the desired surface finishing.

As increasing spindle speeds, the surface roughness also increases. This effect might be mainly due to the temperature distribution during the SPIF process. In fact, when the spindle speed is 2000 rpm, the measured temperature on the polymeric part shown in Fig. 3a is about 78.89 °C. This temperature value is close to the PVC glass transition temperature ($T_g = 82$ °C). Therefore, a little rise on the sheet temperature value can cause some modifications of the polymer molecular structure (from hard to a rubber-like state) and the appearance of several blobs (Fig. 6a). As a consequence of this, alterations on the sheet surface appeared and the surface roughness increased (cases 4, 10 and 14 from Table 1, where R_a is bigger than 1 μm). On the contrary, Fig. 6b illustrates the case where the best surface roughness was achieved. These images were obtained by using a Stereoscope Discovery 11 with a magnification factor of one. Therefore, to avoid these undesirable surface roughness effects, the spindle speed must be tuned to a value for which the maximum temperature distribution is below, in some percentage, to the glass transition temperature of the polymeric part.

4. Conclusions

Two main contributions from this experimental work should be highlighted: (i) the analysis of the maximum forming force variation with respect to the most significant process parameters involved in the SPIF technology and (ii) the decisive effect of the spindle speed while forming polymeric materials by SPIF. This effect of the spindle does not only have the capability of decreasing the maximum forming force, but also increases the sheet formability, evaluated by the maximum depth achieved, and affects the surface roughness, which can be related to the increase of the temperature due to the friction between the tool and the blank. This variation of the temperature causes a change of the material properties, becoming more rubber-like at higher temperatures.

As a final remark and based on the experimental facts observed, it is clear that the material response behaviour during the SPIF manufacturing processes could be quantitatively described by using glassy polymer material models such as those proposed by Boyce et al. (1988) or Ho and Krempl (2002) on which the temperature and strain rate are taken into account. This could help to identify the spindle speed operational bandwidth to fulfil with the expected quality and cost of the finishing part and will be studied in a future research work.

Acknowledgements

The research leading to these results has received funding from the Spanish Government, DPI2012-36042. The authors would like to thank the support from the International Research Exchange for Biomedical Devices Design and Prototyping (IREBID-FP7-PEOPLE-2009-IRSES-247476). The first author gratefully acknowledges the support from the Spanish Government grant FPU12/05402. The fourth author would like to acknowledge financial support of the grant number 61061 from Consejo Nacional de Ciencia y Tecnología (Conacyt), Mexico.

References

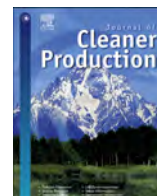
- Aerens, R., Eyckens, P., Van Bael, A., Dufloy, J.R., 2010. Force prediction for single point incremental forming deduced from experimental and FEM observations. *Int. J. Adv. Manuf. Technol.* 46 (9–12), 969–982.
- Alkas Yonan, S., Silva, M.B., Martins, P.A.F., Tekkaya, A.E., 2014. Plastic flow and failure in single point incremental forming of PVC sheets. *eXPRESS Polym. Lett.* 8 (5), 301–311.
- Ambrogio, G., Denapoli, L., Filice, L., Gagliardi, F., Muzzupappa, M., 2005. Application of Incremental Forming process for high customised medical product manufacturing. *J. Mater. Process. Technol.* 162–163, 156–162.
- ASTM D638-02a. Standard Test Method for Tensile Properties of Plastics.
- Bagudanch, I., (Master thesis) 2012. Incremental sheet forming (ISF) applied to form thermoplastic materials. Escola Politècnica Superior, University of Girona, Girona, Spain.
- Bagudanch, I., Elías-Zúñiga, A., Garcia-Romeu, M.L., 2013. Evaluating the material constitutive equations for the simulation of single point incremental forming applied to form thermoplastic materials. *Key Eng. Mater.* 554–557, 1312–1319.
- Boyce, M.C., Parks, D.M., et al., 1988. Large inelastic deformation of glassy polymers. Part I: rate dependent model. *Mech. Mater.* 7, 15–33.
- Centeno, G., Bagudanch, I., Martínez-Donaire, A.J., García-Romeu, M.L., Vallellano, C., 2014. Critical analysis of necking and fracture limit strains and forming forces in single-point incremental forming. *Mater. Des.* 63, 20–29.
- Dufloy, J., Tunckol, Y., 2006. Force modelling for single point incremental forming. In: *Esaform Conference on Material Forming*.
- Dufloy, J.R., Lauwers, B., Verbert, J., Gelaude, F., Tunckol, Y., 2005. Medical application of single point incremental forming: cranial plate manufacturing. In: *Virtual Modelling and Rapid Manufacturing – Advanced Research in Virtual and Rapid Prototyping*. Taylor & Francis Group, London, pp. 161–166, ISBN 0 415 39062 1.
- Durante, M., Formisano, A., Langella, A., Capece Minutolo, F.M., 2009. The influence of tool rotation on an incremental forming process. *J. Mater. Process. Technol.* 209 (9), 4621–4626.
- Durante, M., Formisano, A., Langella, A., 2010a. Observations on the influence of tool-sheet contact conditions on an incremental forming process. *J. Mater. Eng. Perform.* 20 (6), 941–946.

- Durante, M., Formisano, A., Langella, A., 2010b. Comparison between analytical and experimental roughness values of components created by incremental forming. *J. Mater. Process. Technol.* 210 (14), 1934–1941.
- Franzen, V., Kwiatkowski, L., Martins, P.A.F., Tekkaya, A.E., 2008. Single point incremental forming of PVC. *J. Mater. Process. Technol.* 209 (1), 462–469.
- Ho, K., Krempl, E., 2002. Extension of the viscoplasticity theory based on over-stress (VBO) to capture non-standard rate dependence in solids. *Int. J. Plast.* 18, 851–872.
- Jardet, V., Morel, P., 2003. Viscoelastic effects on the scratch resistance of polymers: relationship between mechanical properties and scratch properties at various temperatures. *Prog. Org. Coat.* 48, 322–331.
- Jeswiet, J., Duflou, J.R., Szekeres, A., 2005. Forces in single point and two point incremental forming. *Adv. Mater. Res.* 6–8, 449–456.
- Le, V.S., Ghiotti, A., Lucchetta, G., 2008. Preliminary studies on single point incremental forming for thermoplastic materials. In: *Proceedings of the 11th ESAFORM Conference on Material Forming*.
- Liu, Z., Liu, S., Li, Y., Meehan, P.A., 2014. Modeling and optimization of surface roughness in incremental sheet forming using a multi-objective function. *Mater. Manuf. Process.* 29 (7), 808–818.
- Marques, T.A., Silva, M.B., Martins, P.A.F., 2012. On the potential of single point incremental forming of sheet polymer parts. *Int. J. Adv. Manuf. Technol.* 60, 75–86.
- Martins, P.A.F., Kwiatkowski, L., Franzen, V., Tekkaya, A.E., Kleiner, M., 2009. Single point incremental forming of polymers. *CIRP Ann.: Manuf. Technol.* 58 (1), 229–232.
- Mens, J.W.M., de Gee, A.W.J., 1991. Friction and wear behaviour of 18 polymers in contact with steel in environments of air and water. *Wear* 149, 255–268.
- Oleksik, V., Pascu, A., Deac, C., Fleaca, R., Roman, M., Bologa, O., 2010. The influence of geometrical parameters on the incremental forming process for knee implants analyzed by numerical simulation. *AIP Conf. Proc.* 1252, 1208–1215.
- Pan, M., Zhang, L., Yuan, J., Shi, X., 2005. Rheological Behavior and Thermal Properties of Poly(butyl acrylate-co-2-ethylhexyl acrylate)-Grafted Vinyl Chloride Resin. *Journal of Applied Polymer Science* 95, 419–426.
- Perez-Santiago, R., (PhD thesis) 2012. Forming force estimation in single point incremental forming of uniform and variable wall angle components. Instituto Tecnológico y de Estudios Superiores de Monterrey.
- Shaw, M.T., MacKnight, W.J., 2005. *Introduction to Polymer Viscoelasticity*, third ed. John Wiley, NY.
- Silva, M.B., Skjoedt, M., Martins, P.A.F., Bay, N., 2008. Revisiting the fundamentals of single point incremental forming by means of membrane analysis. *Int. J. Mach. Tools Manuf.* 48, 73–83.
- Silva, M.B., Alves, L.M., Martins, P.A.F., 2010. Single point incremental forming of PVC: experimental findings and theoretical interpretation. *Eur. J. Mech. A: Solids* 29 (4), 557–599.
- Tanaka, S., Nakamura, T., Hayakawa, K., Nakamura, H., Motomura, K., 2007. Residual stress in sheet metal parts made by incremental forming process. *AIP Conf. Proc.* 908, 775–780.

Chapter 4. Incremental forming of polymers: process parameters selection from the perspective of electric energy consumption and cost

Chapter 4 presents an experimental work to: (i) analyze the time share, power and energy consumption in SPIF; (ii) select the most suitable process parameters (step down, tool diameter, feed rate, spindle speed, sheet thickness) to achieve an appropriate compromise between final depth, surface roughness and energy consumption and (iii) calculate the cost of the experiments and propose an empirical equation for the energy consumption. In this work two non-biocompatible polymers are used, PVC and PC.

This study was presented in an article entitled “*Incremental forming of polymers: process parameters selection from the perspective of electric energy consumption and cost*”, published in Journal of Cleaner Production (Bagudanch et al., 2016).



Incremental forming of polymers: process parameters selection from the perspective of electric energy consumption and cost



I. Bagudanch, M.L. Garcia-Romeu^{*}, M. Sabater

University of Girona, Department of Mechanical Engineering and Industrial Construction, Girona, Spain

ARTICLE INFO

Article history:

Received 26 February 2015

Received in revised form

27 May 2015

Accepted 19 August 2015

Available online 28 August 2015

Keywords:

Single point incremental forming

Energy consumption

Thermoplastic materials

Sustainable manufacturing

ABSTRACT

In recent years, environmental and sustainability concerns have attracted considerable attention in the field of mechanical engineering. A number of contributions have focused on the environmental footprint or life cycle analyses of typical manufacturing processes. However, for forming processes, this kind of analysis has just begun. To further the work in this area, this study assessed the influence of a number of process parameters on energy consumption in Single Point Incremental Forming (SPIF). Consequently, a campaign of experiments for two polymer materials (polycarbonate (PC) and polyvinylchloride (PVC)) was carried out. The results are used to identify the most suitable combination of process parameters in order to minimize energy consumption and costs.

© 2015 Elsevier Ltd. All rights reserved.

1. Introduction

Over the years, manufacturing processes have been analyzed from several points of view. One of the most widespread aims is to optimize the process parameters in order to obtain a successful part with a high degree of geometric accuracy as well as to increase productivity and to minimize costs.

When developing cost models for manufactured parts, several cost components have to be considered (Fiorentino, 2014). The traditional components are associated with the direct costs of materials, tools, equipment, processing time and labour, among others. However, in recent years, due to growing concerns about environmental and sustainability issues in manufacturing processes (Dufloy et al., 2012), the latest models also include the indirect costs from, for example, transportation, carbon emissions and energy consumption, in the pursuit of more sustainable manufacturing processes (Branker, 2011).

Recent studies and government directives on energy efficiency in the manufacturing industry have revealed that cutting machine tools consume a significant amount of energy per part manufactured. Therefore, there is a great potential for saving energy by optimizing the process parameters and many research papers have

been focussing on this line of research, the most relevant of which are as follows:

Gutowsky et al. (2006) determined the electrical energy requirements for several manufacturing processes, in an exergy framework. They demonstrated that the energy required for the actual machining was a small proportion of the total energy consumed during the process. Most of the energy requirements are due to additional functions of the machine tools, such as cooling.

Kara and Li (2011) presented and tested an empirical energy model that depended on the process variables for material removal processes on several turning and milling machine tools. Aramcharoen and Mativenga (2014) proposed an energy model for estimating the energy consumed in a machining process for a discrete component and obtained 95% accuracy in their results when compared to online monitoring. It was also demonstrated that energy consumption could be reduced by selecting an appropriate tool path.

Velchev et al. (2014) presented a direct energy consumption model expressed by means of the cutting parameters in turning operations. In this model, the optimum cutting parameters are determined by applying the minimum energy criterion.

Life cycle assessment (LCA) principles were used by Cao et al. (2012) to quantify the carbon emissions of machine tools. The LCA took into account the manufacture, use, transportation and recycling of the tools. The most dominant carbon emissions were due to electricity consumption during the use phase.

^{*} Corresponding author. C/Maria Aurèlia Capmany, 61 (Edifici P2 Campus Montilivi), 17071 Girona, Spain. Tel.: +34 972418265; fax: +34 972418098.

E-mail address: mluisa.gromeu@udg.edu (M.L. Garcia-Romeu).

List of symbols			
C_{ISF}	total cost of the ISF process	t_{setup}	time required to set up the tooling framework
C_{RM}	raw material cost	C_{man1}	cost per hour of a skilled operator
C_{setup}	total cost of the experimental setup needed to develop the ISF process	t_{pr}	time necessary to develop a part program
C_{man}	operator cost	C_f	forming cost
C_{mach}	machine availability cost	C_s	setup cost
V_{setup}	volume of the experimental setup	C_i	cost of workpiece and equipment handling
$C_{manufacturing}$	manufacturing cost of the experimental setup per volume unit	C_t	tooling cost
$K_{complexity}$	coefficient for estimating the complexity of the ISF experimental setup	C_{MD}	direct material cost
N_{parts}	number of parts to be manufactured	C_{MID}	indirect material cost
R_{man}	labour cost per hour	C_{ED}	direct energy cost
t_{man}	labour time	C_{EA}	ancillary energy cost
N_{man}	number of employees	C_{env}	environmental burden cost
R_{mach}	machine cost per hour	t_f	forming time
t_{part}	processing time in incremental sheet forming operation	L_f	labour rate
I_u	utilization index of CNC machine operator	B_f	burden rate including depreciation, maintenance, taxes, interest rate
C_{pow}	power supply cost	K_f	forming cost rate including L_f and B_f
C_{ind}	general industrial cost	N_p	number of parts
t_{ISF}	processing time in incremental sheet forming operation	t_s	setup time
Q	production lot size	t_i	idling time
C_{pos}	positioning costs	t_c	time required to change tool
C_{pr}	cost of the part program development for the CNC code	K_t	tool cost
C_{tool}	tool cost	T	tool life
MS	net monthly salary of the worker	K_M	cost of workpiece material
P_{pow}	nominal power of the CNC milling machine	MD	direct material used
K_u	effective utilisation coefficient of the power	K_{LOf}	cost of forming lubricant
u_{pow}	unit cost of the power	LO_f	quantity of forming lubricant used
i	substitution rate for the machine tool	K_{LO}	cost of machine lubricant
n	useful life of the machine	LO	quantity of machine lubricant used
CM	investment cost of the machine tool	K_E	cost of electricity
λ	coefficient to calculate the general industrial cost	E_D	direct energy consumed
t_{pos}	time necessary to clamp the blank on the machine tool	E_A	ancillary energy consumed
		E_{CO_2}	CO ₂ emitted due to energy
		LO_{fCO_2}	CO ₂ emitted due to forming lubricant
		LO_{CO_2}	CO ₂ emitted due to machine lubricant
		TL_{CO_2}	CO ₂ emitted due to the tool
		ML_{CO_2}	CO ₂ emitted due to direct material
		K_{CO_2}	carbon cost

There are, however, other manufacturing processes that use these kinds of machines, one of which is incremental sheet forming (ISF). This is the process addressed in the present work.

The ISF process can be conducted in any computer numerically controlled (CNC) 3-axis machine, as they allow for high feed rates, significant work volume and the required stiffness. Indeed, a CNC milling machine is one of most commonly-used machines for ISF because it is already installed in most workshops, so there is no need to make a large investment in other machinery (Jeswiet et al., 2005a). Besides the forming tool, all that is required is a clamping system to convert a milling machine into an ISF system, and this is a relatively inexpensive solution.

Commonly, the materials used in ISF are metallic materials, such as aluminum alloys (AA1050 or AA3003, among others) or certain steels (DC04, AISI304, etc.) (Aerens et al., 2010). This is mainly because they are relatively easy to form at room temperature if good lubrication conditions are maintained. More recently, other metallic materials which require an additional heating system in order to ensure good formability, such as titanium alloys (Fiorentino et al., 2012) or magnesium alloys (Ambrogio et al., 2008), have been used.

However, as recent publications have shown, there is an increasing interest in forming polymer materials, especially thermoplastic materials. The main advantage of applying ISF to polymers is that the process can be performed at room temperature. The first polymer used in single point incremental forming (SPIF) was PVC in a study by Franzen et al. (2008). The formability limits were characterized using variable wall angle geometry and new deformation mechanisms associated with the polymer behavior were identified. The work of Martins et al. (2009) focused on evaluating the suitability of various polymers (POM, HDPE, PA, PVC and PC) in the SPIF process. For each material, Fracture Forming Limit Diagrams (FFLDs) were obtained as well as failure modes, strain at failure, accuracy of the shaped parts and color variation. Criteria for selecting the best polymer were presented which considered ductility, springback (elastic recovery), color variation (aesthetic factor) and price.

The costs involved in these processes have also been investigated. Three cost models have been proposed for ISF and the equations of these models are summarized in Table 1. The advantage of the first, developed by Hirt et al. (2003), is that their proposed equation is very simple, as it considers only the costs of raw

Table 1
ISF cost models equations.

	Equation
Hirt et al., 2003	$C_{ISF} = C_{RM} + C_{setup} + C_{man} + C_{mach}$ $C_{setup} = \frac{V_{setup} \cdot C_{manufacturing} \cdot K_{complexity}}{N_{parts}} \rightarrow K_{complexity} = 0.7 \text{ for ISF}$ $C_{man} = R_{man} \cdot t_{man} \cdot N_{man} \rightarrow N_{man} = 0.3 \text{ for ISF}$ $C_{mach} = R_{mach} \cdot t_{part}$
Ambrogio et al., 2003	$C_{ISF} = (C_{man} \cdot I_u + C_{pow} + C_{mach} + C_{ind}) \cdot t_{ISF} \cdot Q + (C_{RM} + C_{pos}) \cdot Q + (C_{setup} + C_{pr} + C_{tool})$ $C_{man} = \frac{MS \cdot 13 \cdot 1.5}{250 \cdot 8}$ $C_{pow} = P_{pow} \cdot K_{U} \cdot U_{pow}$ $C_{mach} = \frac{(1+i)^{-1} \cdot i}{(1+i)^n - 1} \cdot \frac{C_M}{2000}$ $C_{ind} = (C_{pow} + C_{man}) \cdot \lambda$ $M = C_{man} + C_{mach} + C_{ind}$ $C_{pos} = t_{pos} \cdot M$ $C_{setup} = t_{setup} \cdot M$ $C_{pr} = C_{man1} \cdot t_{pr}$
Branker, 2011	$C_{ISF} = C_f + C_s + C_t + C_{MD} + C_{MID} + C_{ED} + C_{EA} + C_{env}$ $C_f = t_f \cdot (L_f + B_f) = t_f \cdot K_f$ $C_s = \frac{K_s}{N_p} \cdot t_s$ $C_t = t_t \cdot K_f$ $C_t = (K_f \cdot t_c + K_t) \cdot \frac{t_f}{T}$ $C_{MD} = K_M \cdot MD$ $C_{MID} = K_{LOF} \cdot LOF + K_{LO} \cdot LO$ $C_{ED} = K_E \cdot E_D$ $C_{EA} = K_E \cdot E_A$ $C_{env} = (E_{CO_2} + LOF_{CO_2} + LO_{CO_2} + TL_{CO_2} + ML_{CO_2}) \cdot k_{CO_2}$

material (C_{RM}), equipment (C_{setup}), labour (C_{man}) and manufacturing (C_{mach}). Ambrogio et al. (2003) included more factors that affect the cost of the process, such as the power cost (C_{pow}) estimated by an effective use coefficient and the nominal power of the machine; general industrial costs (C_{ind}) calculated as a proportion of the manpower and power costs; the cost of positioning the part to be manufactured (C_{pos}); the cost of developing the CNC code (C_{pr}) and the tool cost (C_{tool}). Recently, Branker (2011) proposed the most complete and accurate equation for estimating the ISF cost to date. Not only does it consider all the terms specified in Ambrogio's equation – with some improvements, such as the measurement of the energy consumed during the process, rather than an estimation – but it also considers the indirect material costs (C_{MID}), the ancillary energy (C_{EA}) and the environmental burden (C_{env}).

A number of studies have investigated environmental and sustainability issues involving material removal processes whereas, in contrast, in the case of sheet forming processes, such issues have been addressed in only a few studies (Ingarao et al., 2011). Anghinelli et al. (2011) carried out a functional disaggregation of the SPIF process in phases in order to quantify the inputs and outputs of raw materials, energy and lubricants, from which they calculated the CO_2 emissions. Ingarao et al. (2012) compared a traditional forming process (stamping) with ISF from the point of view of sustainability, more specifically considering waste material and energy consumption. Recently, a series of experiments by Ingarao et al. (2014) compared the SPIF process on metallic materials performed using a CNC milling machine, a robot and an Amino machine. The power and energy consumption during the different phases of the process was evaluated. They also proposed a model to predict the energy consumption depending on the geometry and the material in the SPIF process. However, this model cannot be applied when a CNC milling machine is used because it is not material-dependant.

The background in this field outlined by this review of the literature on environmental issues and the authors' extensive experience in ISF in recent years have led to the work developed in this paper, which has three main objectives. The first is to analyze the time share, power and energy consumption during the SPIF process under different manufacturing conditions, which will be used to discuss the influence of the spindle speed, the material and

the process time. The second aim is to obtain the most suitable process parameters to achieve the best compromise between final depth, surface roughness and energy consumption. The third and final objective is to analyze the experiments from an economical point of view and to propose an empirical equation for accurately predicting the energy consumption of the machine used in the present work.

2. Methodology

In order to achieve the goals of this study, several experimental tests were carried out. This section will describe the methodology that was followed and the experimental equipment in detail.

The geometry of the selected part was a pyramidal frustum with circular generatrix, which means there is a variable wall angle at each depth increment. The length of the edges of the pyramid was 105 mm, the initial wall angle was 45° and the generatrix radius was set to 80 mm. The ISF tests were carried out on a Kondia[®] HS1000 3-axis milling machine equipped with Fidia[®] numerical control. A table-type dynamometer Kistler[®] 9257B was mounted on the machine worktable in order to measure the forming forces that occur during the process. The force data was acquired using a DaqBoard[®] 505 data acquisition card and the DaqView[®] 9.0.0 software.

A fixture system composed of a bottom plate, four supports, a clamping plate and a top plate was bolted onto the force measurement system. The blank sheet was placed between the clamping plate and the top plate, without any backing plate, as shown in Fig. 1. The dimensions of the blank were 150×150 mm and the effective working area was 120×120 mm. In order to reduce friction, liquid lubricant for cold forming was applied over the upper surface of the blanks.

The tool path was defined, taking the bidirectional countering into consideration in order to avoid torsion of the part. A Python subroutine generated the bidirectional contouring tool trajectory and translated it into CNC format for the physical process.

In order to analyze the energy consumption during the SPIF process it was necessary to register the intensity of the machine, using the following equipment: (i) a 25/5 A current transformer in order to reduce the ampere rating at the input range of the voltage transformer; (ii) an AmperFlex 67.374 voltage transformer which

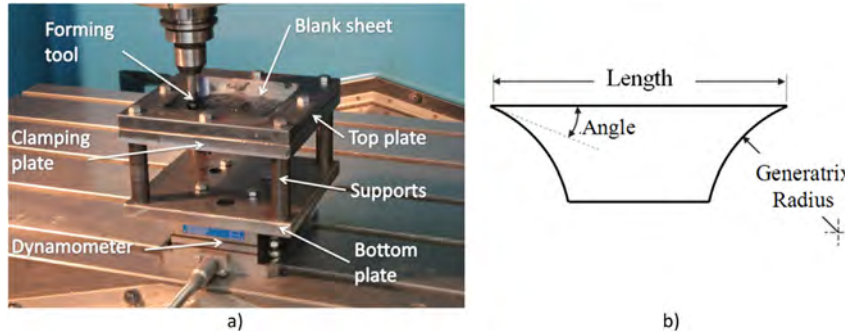


Fig. 1. a) Experimental setup used on a 3 axis CNC milling machine. b) Design of the pyramidal frusta with a circular generatrix.

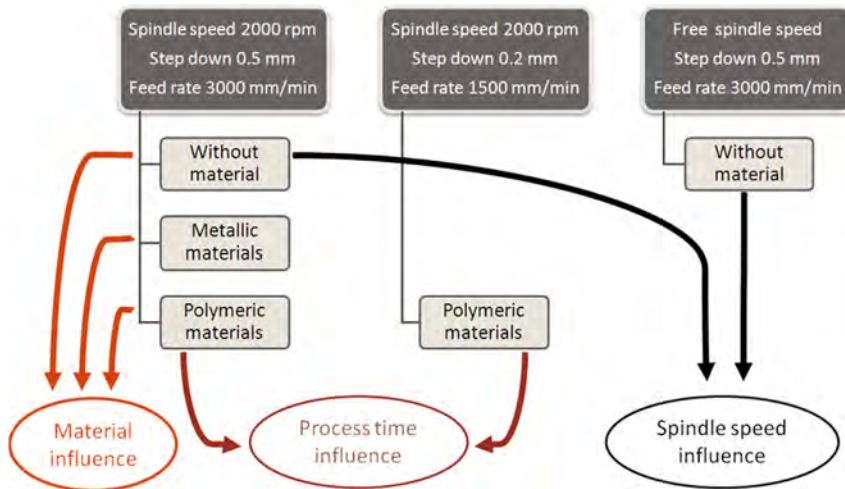


Fig. 2. Summary of the experimental tests for the energy study.

transformed the AC intensity signal to DC voltage signal from 0 to 10 V; this signal was sent to (iii) the data acquisition card and finally (iv) the signal was processed and converted once again into intensity values at a frequency of 20 Hz using the Labview software.

2.1. Preliminary tests

The first step of the study was to analyse the *time contribution* for all stages of the process and the *energy consumed* in producing a single part. In order to identify how these two factors were

influenced by the *material used*, the *total process time* and the *spindle speed*, a number of tests were carried out:

- **Material influence:** five tests were carried out with the following setup: 2000 rpm spindle speed, step down of 0.5 mm and feed rate of 3000 mm/min. One test without material, then two with metallic materials (AA1050 and AISI304) and two with polymer materials (PVC and PC).
- **Process time influence:** the process time depends mainly of the step down value and feed rate, therefore, two tests were carried

Table 2 Design of experiments.

ID	Step down (mm)	Tool diameter (mm)	Feed rate (mm/min)	Spindle speed (rpm)	Sheet thickness (mm)
1	0.2	6	3000	Free	1.5
2	0.2	6	1500	2000	1.5
3	0.5	10	3000	2000	2.0
4	0.2	6	1500	Free	2.0
5	0.5	10	1500	Free	2.0
6	0.5	6	3000	2000	1.5
7	0.5	6	1500	2000	2.0
8	0.5	6	1500	Free	1.5
9	0.5	10	1500	2000	1.5
10	0.2	6	3000	2000	2.0
11	0.2	10	1500	Free	1.5
12	0.2	10	1500	2000	2.0
13	0.5	6	3000	Free	2.0
14	0.2	10	3000	2000	1.5
15	0.2	10	3000	Free	2.0
16	0.5	10	3000	Free	1.5

out: the shortest (step down of 0.5 mm and feed rate of 3000 mm/min) and the longest (step down of 0.2 mm and feed rate of 1500 mm/min), both at spindle speeds of 2000 rpm using a polymer material.

- **Spindle speed influence:** two tests were compared, one with the spindle in the 'free' position (the tool rotates depending on the friction upon contact with the blank), the other with a spindle speed of 2000 rpm.

The preliminary tests are summarized in the graph in Fig. 2. The results will be discussed in section 3.1.

2.2. Design of experiments

In the second step of the experimental work, tests with PVC (polyvinylchloride) and PC (polycarbonate) were performed. Two different thicknesses were available for each material, 1.5 and 2 mm. Both of these thermoplastic materials have an amorphous structure with polar chlorine atoms in the molecular structure. The glass transition temperature, Tg, of the two polymers are 82 °C and 155 °C, respectively. Thus, at room temperature PVC and PC are below Tg and they can be considered glassy (with a linear elastic response followed by yielding).

Therefore, the experiments focused on the following five pairs of forming parameters based on experience from previous research (Bagudanch et al., 2015): two step down settings (0.2 and 0.5 mm); two tool diameters (6 and 10 mm), two feed rate settings (1500 and 3000 mm/min), two spindle speed settings (2000 rpm or free), and finally two different sheet thicknesses (1.5 and 2.0 mm).

A 2⁵⁻¹ factorial design of experiments was defined in 16 runs. Also, three replications for each experiment were considered so that a total of 48 tests for each material were planned (Table 2).

During the recording of the experimental data, the following readings were registered:

- **Maximum forming force in the vertical direction (Fz max).** The estimation of forming forces in ISF is especially important in the case of using machinery adapted for the process, such as milling centres and robots. It has been demonstrated that the predominant force in ISF is developed in the axial direction of the tool (Jeswiet et al., 2005b) while this, in general, is not the case in milling. As a consequence, an accurate estimation of the maximum axial force developed during the forming process is required in order to ensure the safe utilization of the hardware. Another reason to study forming forces is their direct relationship with the structural integrity of the work piece. The forming forces were collected with a frequency of 10 values per second

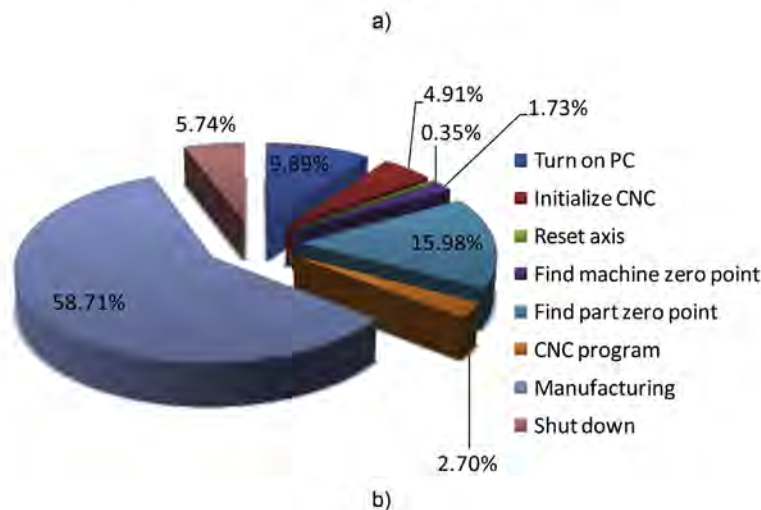
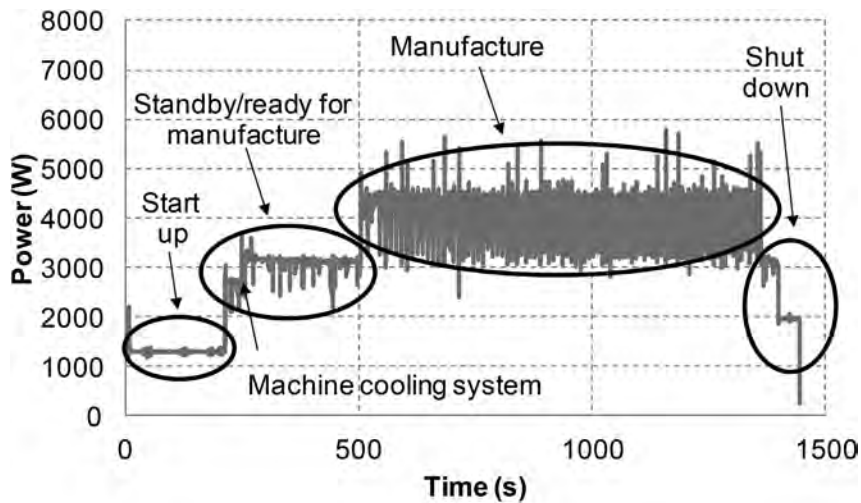


Fig. 3. a) Example of power consumption profile. b) Time share for start up (turn on PC and initialize CNC), standby/ready for manufacture (four operations), manufacturing and shut down.

using the dynamometric table. Subsequently, its magnitudes were filtered using Matlab® to obtain its maximum value.

- **Maximum depth (Z_{max}).** This value is used as an indicator of the material formability under certain process conditions. The maximum depth is obtained directly from the Computer Numerical Control (CNC) of the machine. The reading of its value is recorded at the moment that the failure of the sheet appears.
- **Surface roughness (R_a).** It is important to ensure that the final part manufactured by ISF is able to meet the requirements regarding the surface finishing. The measurements of the surface roughness are obtained with a Mitutoyo Surftest SV-2000 profilometer using the following parameters: (i) measured length: 8.8 mm; (ii) profile type: R; (iii) evaluation length: 0.8 mm; (iv) sampling length: 8.0 mm.
- **Maximum temperature (T_{max}).** Due to the friction between the tool and the blank there is an increase in temperature during

the forming process. This temperature may cause variations on the material properties, especially in polymer materials. The temperature was acquired using a thermographic camera IRBIS ImageIR® 3300.

The results were analyzed with the aim of proposing a set of the most suitable process parameters for achieving the best surface roughness and the highest final depth while consuming the minimum amount of energy (Section 3.2).

3. Results and discussion

3.1. Time share, power and energy consumption

In order to identify the different operational modes involved in the SPIF manufacturing process, several tests were performed. In a previous work by the authors (Bagudanch et al., 2015), spindle speed was shown to have a significant influence on the forming force and formability. Therefore, to determine whether spindle speed also influenced energy and/or environmental parameters, two tests were performed without any material, from initial stage (machine start-up) to final stage (machine shut-down). During this process the power intensity was acquired, as described in the previous section, and the time contribution of each stage was also analyzed. The tests were carried out using a step down of 0.5 mm, a feed rate of 3000 mm/min and two spindle speeds (free and 2000 rpm).

As can be seen from Fig. 3a, four stages of power consumption can be differentiated, some of which may involve several operations. The four are similar to those found in Ingarao et al. (2014). The first stage is the *start up*, i.e., when the electricity is supplied to the milling machine. This stage involves two operations: *turn on the computer and initialize the CNC*.

The second stage is the *standby/ready for manufacture*. During this stage the engines and the pneumatic circuit are activated, which is clearly identifiable as it produces a sharp rise in power consumption. Then, the machine zero point is set. After that, the machine operator has to determine and set the part zero point. The duration of this operation may be different in each case according to the operator's experience and ability. Finally, the CNC program is loaded and prepared for running. During this operation, an increase in power can be distinguished due to the fact that the spindle must be turned on. There is also another increase in power consumption early in the *standby/ready for manufacture* stage because the machine cooling system is turned on or shut down cannot be controlled and can occur at any time during the process.

The third stage is the *part's manufacture*. This is the most time-consuming stage, as can be seen in Fig. 3b, and power remains nearly constant throughout. However, several peaks can be observed. They appear due to the bidirectional countering, in which the tool rotation changes in each loop according to the clockwise or counter-clockwise movement. The bidirectional countering is performed in order to avoid the torsion of the part.

The final stage of the SPIF process is the *shut down*. In the first part of this stage the CNC program is finished and the machine is ready to continue with the part's manufacture if needed. If not, the engines and the pneumatic circuit are disabled and the machine is completely shut down.

Fig. 4 compares the SPIF process power profiles under the different process parameters defined in Section 2.1. Fig. 4a shows the power profile during the same test run with *no material*, with *metallic materials* and *polymer materials*. There was, in fact, no influence of material used on power consumption because the same level of power is required each time, a fact also demonstrated in

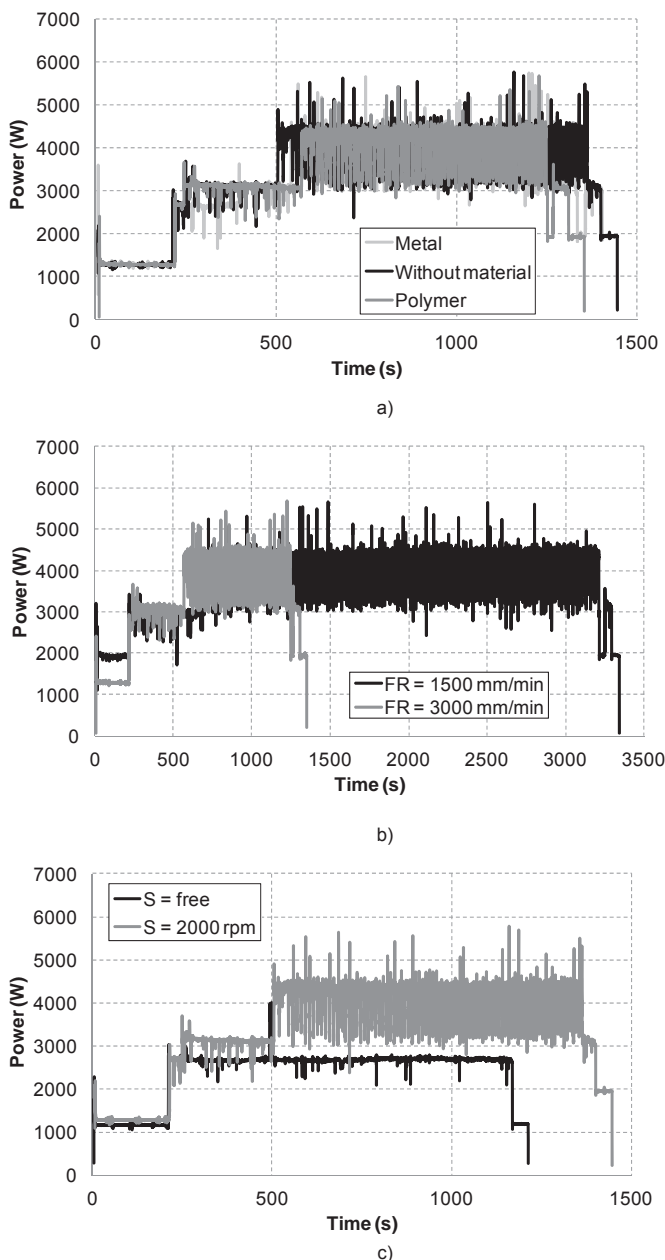


Fig. 4. a) Material influence. b) Process time influence. c) Spindle speed influence.

Table 3
DOE mean results for PC and PVC.

ID	PC						PVC					
	t_f (s)	E (kJ)	T (°C)	Fz max (N)	Z max (mm)	Ra (μ m)	t_f (s)	E (kJ)	T (°C)	Fz max (N)	Z max (mm)	Ra (μ m)
1	1162	3526.30	47.67	311.48	26.93	0.073	1444	4048.76	45.49	288.27	36.00	0.377
2	2776	11396.63	84.87	397.55	31.07	0.193	3222	13684.58	76.06	323.79	35.41	0.359
3	623	2302.82	85.29	444.40	31.17	1.195	829	3202.95	85.29	459.96	42.63	0.794
4	2066	5617.42	46.49	421.56	27.00	0.067	2327	6768.07	42.39	410.94	36.79	0.321
5	1048	3135.01	51.83	738.21	37.17	0.175	1000	2985.50	47.38	547.82	40.11	0.359
6	752	3091.46	81.05	400.26	35.50	0.135	803	3372.47	78.12	248.50	39.02	0.443
7	1212	5061.49	85.13	400.99	36.33	0.839	1290	5140.87	79.54	367.96	40.63	1.374
8	916	2430.27	45.80	409.03	31.83	0.107	958	2752.60	40.58	313.86	35.24	0.422
9	1013	4052.28	85.33	350.71	30.17	0.721	1327	5478.86	85.41	317.29	39.97	1.611
10	1740	7214.96	84.80	384.58	31.53	0.135	2100	8794.79	75.79	379.48	41.89	1.002
11	2412	7037.84	48.92	474.93	30.80	0.136	2413	6689.61	41.04	395.79	34.17	0.352
12	2208	9325.57	85.30	413.05	28.33	0.865	2901	12046.27	85.29	368.55	40.54	0.493
13	554	1663.81	62.70	483.26	32.83	0.135	635	1784.16	56.61	383.51	41.87	0.889
14	1619	6709.17	84.78	341.95	30.80	0.623	2105	8703.51	83.07	303.06	42.35	0.374
15	1343	3942.54	57.08	537.85	32.57	0.156	1565	4232.19	51.18	480.12	39.19	0.388
16	587	1762.92	68.15	545.46	36.33	0.222	628	1856.29	53.67	342.03	42.75	0.408

Ingarao et al. (2014). To make the graph clearer, therefore, the test results of only one metallic (AISI304) and one polymeric (PC) material are shown. Fig. 4b compares the power profiles of the shortest test setup (feed rate of 3000 mm/min and step down of 0.5 mm) and the longest (feed rate of 1500 mm/min and step down of 0.2 mm). The level of power reached in each case is the same; however, the significantly increased process time obviously leads to an important increase in the energy consumption. The same trend was observed by Ingarao et al. (2014) and they demonstrated that the energy consumption varied linearly with these variables. Finally, to determine the influence of the spindle speed on power consumption, two tests were carried out at *free* and 2000 rpm settings, in each case without material. The main difference is observed during the manufacturing stage (Fig. 4c). When the spindle speed is set to *free*, there is a notable reduction in power consumption and, therefore, in the energy required to obtain the part. In order to analyze this variation in power consumption with respect to spindle speed, an additional test at 1000 rpm was performed. Then, the mean intensity during the manufacturing stage was obtained in each case (5.07 A for free spindle speed, 6.26 A for 1000 rpm and 7.05 A for 2000 rpm). These values have been adjusted using a linear regression which obtained a R^2 value of 0.9866, demonstrating that the spindle speed has a linear influence on energy consumption.

3.2. Selection of the best process parameters

This section gives the test results of the design of experiments (DOE) (Table 3), that takes into consideration the total time (t_f), total energy consumption (E), the maximum temperature achieved during the forming process (T), the maximum forming force in the axial direction (Fz max), the maximum depth of the part (Z max) and the surface roughness (Ra). The results have been statistically analyzed using ANOVA in order to determine and then discuss the most influential process parameters for each response. The factors

Table 4
Identification of the best and worst case scenario for the analyzed responses.

Response	Best case (100%)	Worst case (0%)
Energy	Minimum	Maximum
Temperature	Maximum	Minimum
Force	Minimum	Maximum
Final depth	Maximum	Minimum
Surface roughness	Minimum	Maximum

that have a significant effect on the analyzed responses are those with a P-value less than 0.05 and will be discussed in the following paragraphs. Finally, the best process parameters will be selected, maximizing the properties of the final part (achieved depth and surface roughness) and minimizing the energy requirements.

As mentioned previously, in Section 3.1, when using an adapted milling machine to perform the SPIF process, power consumption is not influenced by the behaviour of the material. The energy results for both polymer materials, PC and PVC, presented in Table 3, have practically identical orders of magnitude. The slight differences than can be found are mainly due to the fact that, in general, PC parts break before PVC parts under the same process parameters, therefore, the process time and energy consumption are lower.

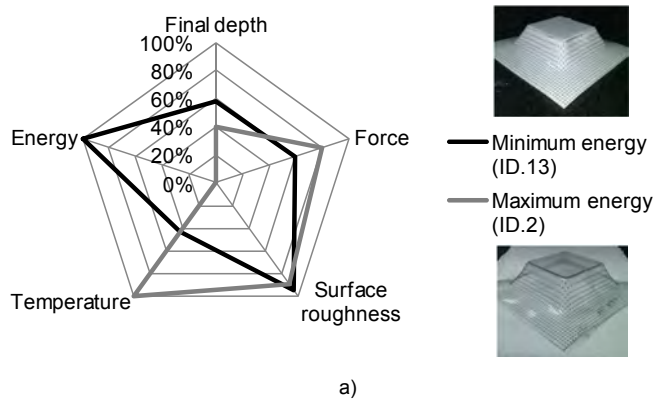
Two of the analyzed process parameters (tool diameter and sheet thickness) do not have any influence on the energy consumption required to produce the part while the variation among the remaining ones is significant. More specifically, with the increase of the feed rate and step down there is a decrease in energy requirements due to a reduction in the process time, while an increase in spindle speed involves an increase in energy consumption as was previously quantified. Taking into account these results, it is possible to conclude that the best case scenario in terms of reducing the energy consumption would be to use the free spindle speed along with the highest step down and highest feed rate.

By analyzing the maximum temperature achieved during the forming process of the SPIF parts for both thermoplastic materials (Table 3), it can be seen that there is only one process parameter that has a significant influence on the temperature variation, and that is the spindle speed. The friction between the tool and the blank during the forming operation generates heat and therefore increases the temperature. This phenomenon was first observed by Bagudanch et al. (2015), who demonstrated that even a slight variation in temperature during the SPIF process could drastically change the thermoplastic material properties, forming forces, maximum depth and surface roughness.

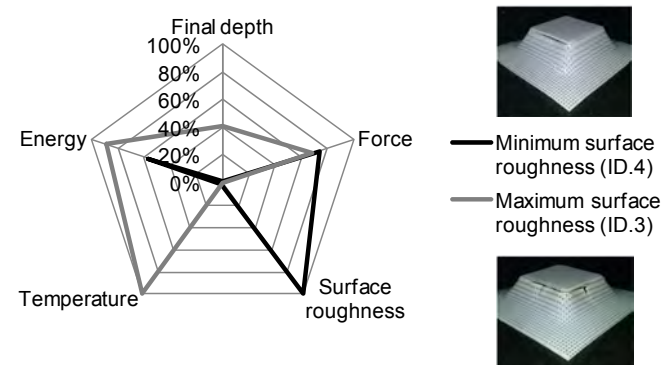
In certain specific cases, it was observed that some tests achieved temperatures higher than the glass transition temperature. When this temperature is reached, the polymer exhibits a more rubbery behaviour and it is possible to observe some imperfections on the surface. However, for higher temperatures, the forming force decreases which could be an advantage when using an adapted milling machine in order to guarantee safe operation conditions and to prevent damage to the machinery. Furthermore, formability at higher temperatures is increased and it is easier to achieve the desired depth. Therefore, the best scenario would be to obtain a

specific increase in temperature to achieve a decrease in the forming force and an increase in formability while at the same time ensuring that the glass transition temperature of the polymer is not exceeded.

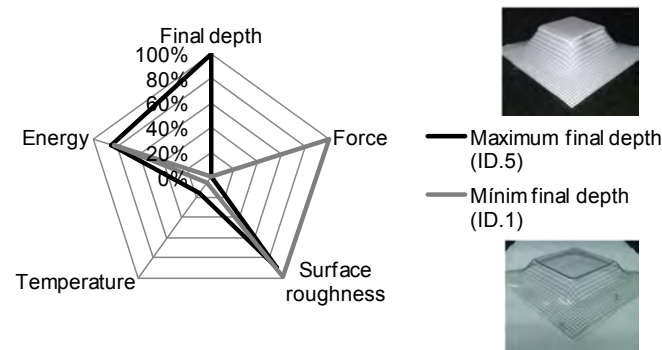
The effect of the process parameters on the forming force for PVC was discussed in depth in a previous work by the authors (Bagudanch et al., 2015). The main conclusions of that study were that the tool diameter, sheet thickness and spindle speed were the most influential parameters. In the present paper, the same trend has been observed for the other thermoplastic material, PC. For the purpose of providing guidelines or best process parameters, it should be noted that the forming force should always be lower than the maximum allowed by the machinery, but there are no other limitations of the force value.



a)



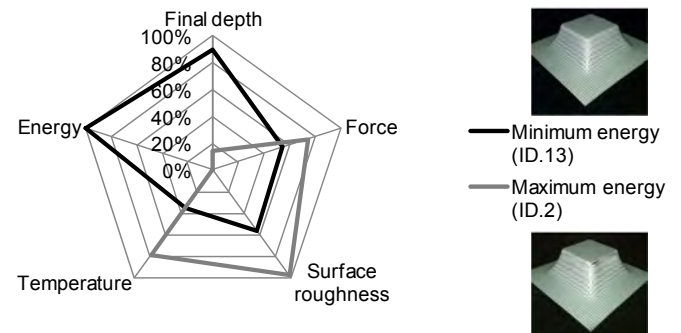
b)



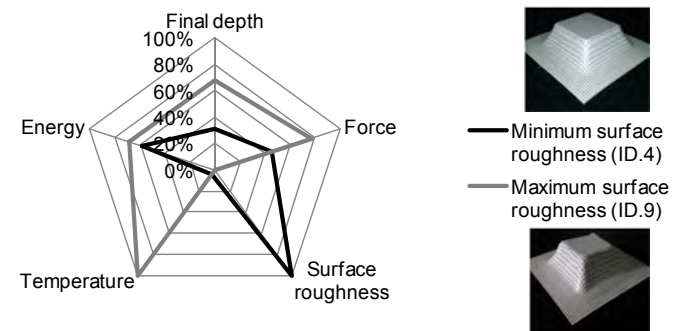
c)

In order to give a global analysis of the best process parameters, the following methodology was chosen: first, the best and the worst case scenario for each response was identified in line with the previous discussion and summarized in Table 4; next, the results for each material were weighted from 0 to 100% according to these criteria; finally, they were represented graphically on web charts, because these charts allow the five responses to be monitored and evaluated simultaneously (Figs. 5 and 6).

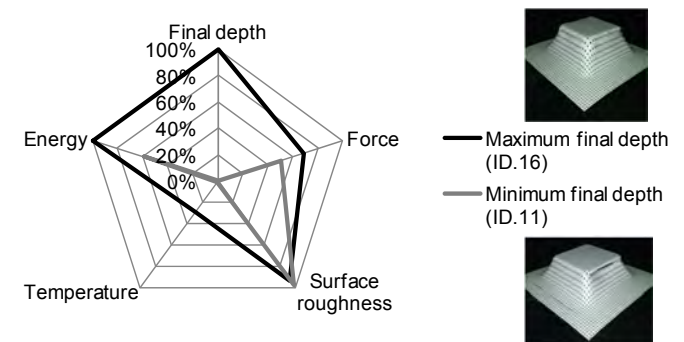
Fig. 5 represents graphically the best and worst case scenarios with the PC polymer for three parameters: energy consumed, final depth and surface roughness (with best case being as close to 100% as possible). With regard to temperature and forming force, it is not crucial to obtain 100% best case as it is only important that they do not exceed the glass transition temperature and the maximum force allowed for the experimental equipment. In case of temperatures coming close to the glass transition temperature (for example in the case of PVC tests 3, 9, 12 and 14 in the present work)



a)



b)



c)

Fig. 5. Analysis of the extreme scenarios for PC: a) Energy. b) Surface roughness. c) Final depth.

Fig. 6. Analysis of the extreme scenarios for PVC: a) Energy. b) Surface roughness. c) Final depth.

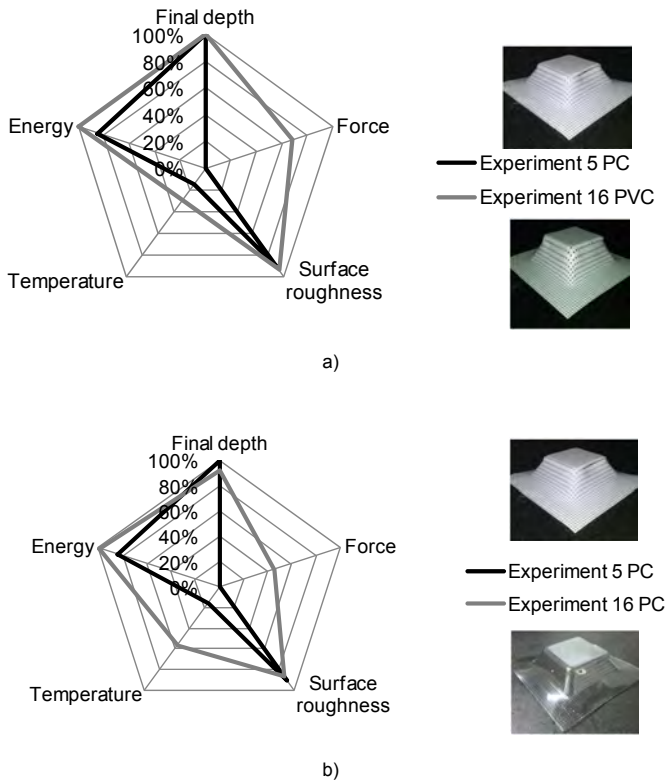


Fig. 7. a) Comparison of the best tests for PC and PVC. b) Comparison of tests 5 and 16 in PC.

Table 5
Parameters used to calculate the cost of each part.

Parameter	Value	Observations
t_r (s)	Defined in Table 3 for each experiment	Time needed to produce each part
K_f (€/h)	70	This value considers the investment cost of the machine, the useful life and indirect costs such as rent of the building, taxes, etc.
N_p (u)	96	The total number of parts produced, 48 tests for PVC and 48 for PC.
t_s (s)	2500	Time needed for fixing the framework and turning on the machine.
t_l (s)	300	Time required for loading/unloading the workpiece
T (h)	10000	In the present paper the time required to change the tool is not considered because, for a single part, only one tool is required.
K_t (€/u)	65	In Branker's cost model (Branker, 2011) K_M is given as \$/kg, therefore, in order to obtain C_{MD} this value is multiplied by the amount of material used in kg (MD). In the present case, the material cost is given in €/sheet, thus, $K_M = C_{MD}$.
K_M (€/u)	2.60 for 1.5 mm PVC 2.75 for 2 mm PVC 3.50 for 1.5 mm PC 4.00 for 2 mm PC	
K_{LOf} (€/L)	15	To calculate the indirect material costs, the quantity of machine lubricant used has been ignored because the lubricant use rate is close to zero, therefore, the contribution on the total cost will be negligible.
LO_f (mL)	30	
K_E (€/kWh)	0.18	In the present paper, the measurements of energy consumed include the direct energy (from the electricity used in the forming process) and the ancillary energy (associated with peripheral equipment such as cooling of the machine, CNC computer, etc.).
E (kJ)	Defined in Table 3 for each experiment	
E_{CO_2} (kg CO ₂)	Calculated using E (kJ) defined in Table 3 and the value obtained using the CES equation, 10.89 kg CO ₂ /Gj. The parameters of the CES equation are specified in the present section.	
LO_{fCO_2} (kg CO ₂)	0.09885	The emission intensity of the forming lubricant has been determined as 3.295 kg CO ₂ /L (Branker, 2011). The contribution of the CO ₂ emissions of the machine lubricant was ignored.
TL_{CO_2} (kg CO ₂)	0.2575 for 6 mm tool diameter 0.3292 for 10 mm tool diameter	The emission intensity of the forming tool has been determined as 6.4 kg CO ₂ /kg (Branker, 2011). The weight of the 6 mm diameter tool is 40.24 g and the weight of the 10 mm diameter tool is 51.44 g.
ML_{CO_2} (kg CO ₂)	0.394 for 1.5 mm PVC 0.525 for 2 mm PVC 0.558 for 1.5 mm PC 0.743 for 2 mm PC	In order to produce PVC 65.86 MJ/kg PVC are required, and the carbon emissions are 2.5 kg CO ₂ /kg PVC (Plastics Europe: Polyvinyl, 2006). In the case of PC, the energy needed for producing this material is estimated as 104.6 MJ/kg PC, the carbon emissions are 4.13 kg CO ₂ /kg PC (Plastics Europe: Polycarb, 2011).

the temperature of reference will be T_g while in the other cases, the temperature of reference will be at the maximum level.

In the best energy scenario (Fig. 5a), the surface roughness is very high (nearly 100%), but the final depth is only around 60%. In the best surface roughness scenario (Fig. 5b), the energy is far from ideal (40%) and the final depth is the worst one of the three, therefore, this set up would obviously not be included in the list of suitable combinations of process parameters. Finally, in the best final depth scenario (Fig. 5c), energy consumption is close to ideal at around 85% and surface roughness reaches 90%; this means that with the parameters of test number 5, it is possible to obtain the best compromise among the desired responses.

Similarly, the results for PVC are presented in Fig. 6. In the best energy scenario (100% best case = minimum energy consumption), shown in Fig. 6a, around 90% of final depth can be achieved, however, surface roughness is relatively low (60%). In the best surface roughness scenario, Fig. 6b, the energy and final depth reach only 30% of their best case values. The best compromise is obtained with the set up in test 16, Fig. 6c, where all three parameters are close to 100% best case.

Accordingly, the best results will be obtained using very similar process parameters: step down of 0.5 mm, free spindle speed, tool diameter of 10 mm and a feed rate of 1500 mm/min for PC (Experiment 5) and 3000 mm/min for PVC (Experiment 16). Fig. 7a shows the comparison of the results obtained in these two cases.

In order to identify whether it is possible to improve the productivity by increasing the feed rate and therefore decrease the energy consumption due to a lower process time, Fig. 7b shows the comparison of the results of test 5 (1500 mm/min) and 16 (3000 mm/min) for PC. In test 16, the final depth and surface roughness are slightly worse compared with those of test 5, but the

Table 6
Total cost of the parts produced using ISF in PC and PVC.

ID	C _{ISF} (€) for PC	C _{ISF} (€) for PVC
1	33.10	37.70
2	64.90	72.79
3	23.06	25.85
4	51.29	55.17
5	31.36	29.17
6	25.10	25.20
7	34.65	34.92
8	28.25	28.18
9	30.23	35.50
10	45.03	50.86
11	57.59	56.69
12	54.25	66.61
13	21.68	22.01
14	42.15	50.80
15	37.14	40.22
16	21.82	21.72

energy consumption is improved. Therefore, the parameters of test 16 can be considered as the best combination for both materials.

3.3. Economic cost

This section gives details of the economic cost of the ISF process for obtaining the parts with the different process parameters proposed in the paper. In order to calculate the costs, the methodology proposed by Branker (2011) described in the introduction section (Table 1) will be followed. A few assumptions and modifications have been made which are summarized in Table 5. With the cost calculation, it will be possible to determine whether the best process parameters identified in the previous section can be used to obtain the cheapest part or not.

In the current context, where it is increasingly important to protect the environment, the CES (Carbon Emission Signature) indicator has emerged as a way of accounting for carbon emissions in systems that use electric power grids (Jeswiet and Kara, 2008). The equation for the CES calculation is as follows:

$$CES = (1/\eta)(112C + 49N + 66P) \quad (1)$$

Where η is an efficiency coefficient, which is different for each country; $(1/\eta)$ is usually between 0.25 and 0.35; for Spain, it is 0.34 (Anghinelli et al., 2011). C, N and P, are, respectively, the percentages of coal, oil and natural gas used to produce energy in a particular country or by a supplying electricity company.

CO₂ emissions due to electrical consumption depend on the supplier (ENDESA ENERGIA, S.A., in the present case). The energy mix which the supplier provides to their customers was determined. With these values (18.0% C, 2.9% N and 20.3% P) and Equation (1), the CES value of the shop floor energy consumption was estimated at 102.88 kg CO₂/GJ. This value will be applied to energy consumption in order to calculate CO₂ emissions due to electrical consumption.

Table 7
Mean consumption intensity during the entire experimental campaign.

	Free spindle speed	2000 rpm spindle speed
Machine cooling system turn on (65% of time)	5.05 A	7.07 A
Machine cooling system shut down (35% of time)	4.39 A	6.37 A

By applying the equations proposed by Branker (2011) using the terms specified in Table 5, it is possible to determine the cost of each test setup performed in the present work. The results are presented in Table 6. In the previous section, it was found that the most suitable part was obtained using the process parameters of Experiment 16. Table 6 shows that this combination of parameters provides the cheapest part in the case of using the PVC material (21.72 €). For the PC material, the cost of producing the part using the parameters in Experiment 16 is 21.82 €, while with Experiment 13, the cost is slightly cheaper at 21.68 €. However, the part obtained in Experiment 13 is considered inadequate because the final depth was far from ideal. Therefore, it can be concluded that the parameters used in Experiment 16 will produce the cheapest parts with the best final results in terms of energy consumed, final depth and surface roughness.

Fig. 8 shows the contribution of each item in the Branker cost model to the total cost of the ISF process for two extreme cases: the most expensive experiment (Fig. 8a) and the cheapest experiment (Fig. 8b). As can be seen, the forming cost (C_f) is the biggest cost contribution, ranging from 52.3% to 83.2%. This illustrates an important difference between ISF and other traditional sheet forming processes, such as deep drawing, where the biggest cost contribution is due to the tooling and experimental equipment required for the process. In ISF, the C_f cost basically depends on the forming time, which can be controlled by two process parameters: feed rate and depth step. Therefore, slight variations of these parameters have a significant influence on the overall cost.

Using the aforementioned methodology, the economic cost of the ISF process can only be calculated after the part is produced in order to obtain the real energy consumption. However, it would be better to be able to estimate the cost before the part's production in order to determine whether it is profitable or not in economic terms.

Hence, during the campaign of experiments, the time consumed by each manufacturing stage was recorded. Furthermore, the intensity peaks were all analyzed and assigned to a certain machine subunit or a certain manufacturing stage. During this detailed evaluation, it was possible to quantify that the machine cooling system was turned on, on average, 65% of time while the remaining 35% of time it was shut down. The mean consumption intensity of the machine, considering the values registered during the whole experimental work, is presented in Table 7.

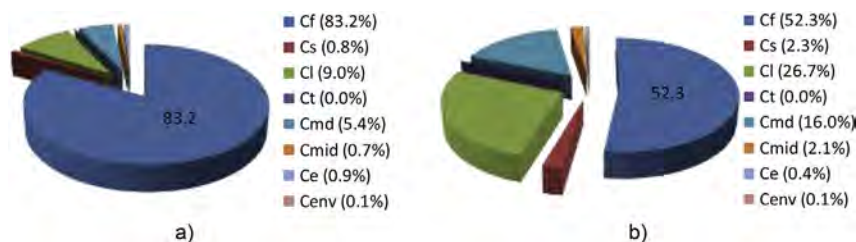


Fig. 8. Contribution of the Branker cost model items to total cost for: a) the most expensive experiment and b) the cheapest experiment.

Table 8

Energy consumption measured during the experimental campaign and calculated using Equation (2) (below).

ID	PC			PVC		
	E _{exp} (kJ)	E _{eq} (kJ)	Error (%)	E _{exp} (kJ)	E _{eq} (kJ)	Error (%)
1	3526.30	3317.05	-5.93	4048.76	4122.04	1.81
2	11396.63	11211.15	-1.63	13684.58	13012.37	-4.91
3	2302.82	2516.05	9.26	3202.95	3348.00	4.53
4	5617.42	5897.60	4.99	6768.07	6642.65	-1.85
5	3135.01	2991.62	-4.57	2985.50	2854.60	-4.38
6	3091.46	3037.03	-1.76	3372.47	3243.00	-3.84
7	5061.49	4894.78	-3.29	5140.87	5209.79	1.34
8	2430.27	2614.81	7.59	2752.60	2734.71	-0.65
9	4052.28	4091.10	0.96	5478.86	5359.22	-2.18
10	7214.96	7027.16	-2.60	8794.79	8481.06	-3.57
11	7037.84	6885.30	-2.17	6689.61	6888.15	2.97
12	9325.57	8917.23	-4.38	12046.27	11715.98	-2.74
13	1663.81	1581.45	-4.95	1784.16	1812.67	1.60
14	6709.17	6538.49	-2.54	8703.51	8501.25	-2.32
15	3942.54	3833.73	-2.76	4232.19	4467.45	5.56
16	1762.92	1675.65	-4.95	1856.29	1792.69	-3.43

With the information in Table 7, it is possible to obtain a general equation (Equation (2)) for calculating the energy consumption (E, in J), specifically for the Kondia HS1000 milling machine used in the present work, in which S is the spindle speed in rpm (0 or 2000 rpm in this case) and t is the forming time in seconds, which can be easily obtained from the CNC code using, for example, CAM software. Table 8 compares the energy experimentally measured (E_{exp}) with the energy calculated using Equation (2) (E_{eq}) for both materials and shows that the error in the calculated value is always less than 10% (with a mean error of 3.5%), thus demonstrating the reasonable degree of reliability of the equation.

$$E = (2854.6 + 0.592 \cdot S) \cdot t \quad (2)$$

3.4. General process guidelines

In this section, the results presented throughout the paper are summarized in order to provide a general view of the relationship between the process parameters and the output variables. This information can be used as general process guidelines in the case of forming polymers by SPIF.

Table 9 qualitatively presents the overall influence of the SPIF process parameters on the process outputs: environmental costs (energy), running processes (temperature and maximum forming force), part quality (maximum depth and surface roughness) and economic costs, by identifying whether they are directly

Table 9

Relationship between the process parameters and the process outputs.

	Step down	Tool diameter	Feed rate	Spindle speed	Sheet thickness
Energy	⇓	⇐	⇓	⇑	⇐
Temperature	⇐	⇐	⇐	⇑	⇐
Maximum forming force	⇑	⇑	⇐	⇓	⇑
Maximum depth	⇑	⇑	⇐	⇑	⇑
Surface roughness	⇑	⇐	⇐	⇑	⇑
Cost	⇓	⇐	⇓	⇑	⇐

proportional (⇑), inversely proportional (⇓) or independent (⇐). When the dependence between a process parameter and a process output is strong, this is indicated using two arrows, for example, increased spindle speed strongly increases energy consumption (⇑⇑).

4. Conclusions

In this paper, the energy consumption during the SPIF process has been analyzed from several perspectives. The first part of the work focused on the identification of the stages and operations needed during the manufacturing process and on evaluating the power consumption profile and the time share of each one of these stages under different process conditions. The results demonstrated that an increase in the *step down* and the *feed rate* lead to a decrease in energy consumption, a result also found in the work of Ingarao et al. (2014). Additionally, a decrease in the *spindle speed* was found to cause a decrease in energy consumption.

In the second part of the work, an experimental campaign for two polymer materials (PC and PVC) was planned and carried out. The results regarding the energy consumption, maximum temperature, maximum axial forming force, maximum depth and surface roughness were discussed. A methodology to determine a set of the most suitable process parameters in order to obtain the most satisfactory final part (in terms of energy consumption, final depth and surface roughness) was proposed. According to this methodology, the most suitable process parameters are: a step down of 0.5 mm, 10 mm tool diameter, a feed rate of 3000 mm/min and a free spindle speed (Experiment 16).

Then, the economic cost for each experiment was calculated following the cost estimation model proposed by Branker (2011). It was demonstrated that by using the parameters of Experiment 16, it is possible to obtain not only the best final part but also the cheapest. Finally, an empirical equation to accurately predict the energy consumption in the Kondia HS1000 3-axis milling machine was derived with the aim of simplifying the economic evaluation of the ISF process.

Acknowledgements

The research leading to these results has received funding from the Spanish Ministry of Education, research project DPI2012-36042. The first author gratefully acknowledges the support provided by grant FPU12/05402, also from the Spanish Ministry of Education. The authors would like to thank Aleix Lleget for his collaboration during the experimental campaign.

References

- Aerens, R., Eyckens, P., Van Bael, A., Duflou, J.R., 2010. Force prediction for single point incremental forming deduced from experimental and FEM observations. *Int. J. Adv. Manuf. Technol.* 46 (9–12), 969–982.
- Ambrogio, G., Di Lorenzo, R., Micari, F., 2003. Analysis of the economical effectiveness of incremental forming processes: an industrial case study. In: VI AITeM Conference, Gaeta, Italy.
- Ambrogio, G., Filice, L., Manco, G.L., 2008. Warm incremental forming of magnesium alloy AZ31. *CIRP Ann. Manuf. Technol.* 57 (1), 257–260.
- Anghinelli, O., Ambrogio, G., Di Lorenzo, R., Ingarao, G., 2011. Environmental costs of single point incremental forming. *Steel Res. Int.* 525–530.
- Aramcharoen, A., Mativenga, P.T., 2014. Critical factors in energy demand modeling for CNC milling and impact of toolpath strategy. *J. Clean. Prod.* 78, 63–74.
- Bagudanch, I., Garcia-Romeu, M.L., Centeno, G., Elías-Zúñiga, A., Ciurana, J., 2015. Forming force and temperature effects on single point incremental forming of polyvinylchloride. *J. Mater. Process. Technol.* 219, 221–229.
- Branker, K., 2011. A Study of Energy, Carbon Dioxide Emissions and Economics in Machining: Milling and Single Point Incremental Forming (PhD thesis). Queen's University, Kingston, Ontario, Canada.
- Cao, H., Li, H., Cheng, H., Luo, Y., Yin, R., Chen, Y., 2012. A carbon efficiency approach for life-cycle carbon emission characteristics of machine tools. *J. Clean. Prod.* 37, 19–28.

- Duflou, J.R., Sutherland, J.W., Dornfeld, D., Herrmann, C., Jeswiet, J., Kara, S., Hauschild, M., Kellens, K., 2012. Towards energy and resource efficient manufacturing: a processes and systems approach. *CIRP Annals Manuf. Technol.* 61, 587–609.
- Fiorentino, A., 2014. Cost drivers-based method for machining and assembly cost estimations in mould manufacturing. *Int. J. Adv. Manuf. Technol.* 70 (5–8), 1437–1444.
- Fiorentino, A., Marzi, R., Ceretti, E., 2012. Preliminary results on Ti incremental sheet forming (ISF) of biomedical devices: biocompatibility, surface finishing and treatment. *Int. J. Mechatron. Manuf. Syst.* 5 (1), 36–45.
- Franzen, V., Kwiatkowski, L., Martins, P.A.F., Tekkaya, A.E., 2008. Single point incremental forming of PVC. *J. Mater. Process. Technol.* 209 (1), 462–469.
- Gutowsky, T., Dahmus, J., Thiriez, A., 2006. Electrical energy requirements for manufacturing processes. In: *Proceedings of the 13th CIRP International Conference on Life Cycle Engineering*, Leuven.
- Hirt, G., Ames, J., Bambach, M., 2003. Economical and ecological benefits of CNC incremental sheet forming (ISF). In: *International Committee of Environmental and Manufacturing 9th International Workshop on Ecology and Economy in Manufacturing*, Hungary.
- Ingarao, G., Di Lorenzo, R., Micari, F., 2011. Sustainability issues in sheet metal forming processes: an overview. *J. Clean. Prod.* 19, 337–347.
- Ingarao, G., Ambrogio, Gagliardi, F., Di Lorenzo, R., 2012. A sustainability point of view on sheet metal forming operations: material wasting and energy consumption in incremental forming and stamping processes. *J. Clean. Prod.* 29–30, 255–268.
- Ingarao, G., Vanhove, H., Kellens, K., Duflou, J.R., 2014. A comprehensive analysis of electric energy consumption of single point incremental forming processes. *J. Clean. Prod.* 67, 173–186.
- Jeswiet, J., Kara, S., 2008. Carbon emissions and CESTM in manufacturing. *CIRP Annals Manuf. Technol.* 57, 17–20.
- Jeswiet, J., Micari, F., Hirt, G., Bramley, A., Duflou, J., Allwood, J., 2005. Asymmetric single point incremental forming of sheet metal. *CIRP Ann. Manuf. Technol.* 54 (2), 88–114.
- Jeswiet, J., Duflou Joost, R., Szekeres, Alexander, 2005. Forces in single point and two point incremental forming. *Adv. Mater. Res.* 6–8, 449–456.
- Kara, S., Li, W., 2011. Unit process energy consumption models for material removal processes. *CIRP Annals Manuf. Technol.* 60, 37–40.
- Martins, P.A.F., Kwiatkowski, L., Franzen, V., Tekkaya, A.E., Kleiner, M., 2009. Single point incremental forming of polymers. *CIRP Ann. Manuf. Technol.* 58 (1), 229–232.
- Plastics Europe: Polycarbonate PC. *Eco-profiles and Environmental Product Declarations of the European Plastics Manufacturers*. Brussels, March 2011.
- Plastics Europe: Polyvinylchloride PVC (Emulsion Polymerisation), April 2006. *Eco-profiles of the European Plastics Industry*, Brussels.
- Velchev, S., Kolev, I., Ivanov, K., Gechevski, S., 2014. Empirical models for specific energy consumption and optimization of cutting parameters for minimizing energy consumption during turning. *J. Clean. Prod.* 80, 139–149.

Chapter 5. Polymer incremental sheet forming process: temperature analysis using response surface methodology

Chapter 5 studies deeply the effect of the main process parameters (tool diameter, spindle speed, feed rate and step down) on the maximum forming temperature for three non-biocompatible polymers (PVC, PC and PP -polypropylene-) and two biocompatible polymers (UHMWPE -ultra-high molecular weight polyethylene- and PCL -polycaprolactone-).

This study was presented in an article entitled “*Polymer incremental sheet forming process: temperature analysis using response surface methodology*”, published in *Materials and Manufacturing Processes* (Bagudanch et al., 2017a).

Bagudanch, I., Vives-Mestres, M., Sabater, M., Garcia-Romeu, M.L., 2017. Polymer incremental sheet forming process: Temperature analysis using response surface methodology. *Materials and Manufacturing Processes* 32, 44-53.

<http://www.tandfonline.com/doi/abs/10.1080/10426914.2016.1176191?journalCode=lmmp20>

<https://doi.org/10.1080/10426914.2016.1176191>

Received 12 Jan 2016, Accepted 12 Feb 2016, Accepted author version posted online: 27 Apr 2016,
Published online: 27 Sep 2016

© Taylor and Francis, 2017

Abstract

To reduce costs associated with the manufacturing of customized products, several innovative forming processes have been developed. Incremental sheet forming (ISF) is one of these new technologies, becoming, in the past decade, more interesting for the academic and industrial community. The influence of main process parameters, namely, tool diameter, spindle speed, feed rate, and step down, is studied in depth in this paper. The maximum temperature achieved during the forming process of a truncated pyramid frustum with a circular generatrix using three nonbiocompatible and two biocompatible polymer materials is measured. Box–Behnken design of experiments and the response surface methodology have been utilized to statistically analyze the results and to provide models able to predict the maximum temperatures.

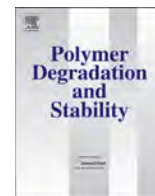
Keywords

Biocompatible, forming, incremental, parameters, point, process, single, temperature

Chapter 6. Revisiting formability and failure of polymeric sheets deformed by single point incremental forming

Chapter 6 aims to evaluate the overall formability of a series of polymeric sheets in the SPIF process, including non-biocompatible and biocompatible materials, considering a variety of process parameters including spindle speed, which has been revealed as the most relevant in polymers deformed by Incremental Sheet Forming (ISF).

This study was presented in an article entitled “*Revisiting formability and failure of polymeric sheets deformed by single point incremental forming*”, published in *Polymer Degradation and Stability* (Bagudanch et al., 2017a).



Revisiting formability and failure of polymeric sheets deformed by Single Point Incremental Forming



I. Bagudanch ^a, G. Centeno ^b, C. Vallengano ^b, M.L. Garcia-Romeu ^{a,*}

^a Department of Mechanical Engineering and Industrial Construction, University of Girona, Girona, Spain

^b Department of Mechanical and Manufacturing Engineering, University of Seville, Seville, Spain

ARTICLE INFO

Article history:

Received 13 June 2017

Received in revised form

28 July 2017

Accepted 15 August 2017

Available online 17 August 2017

Keywords:

Incremental Sheet Forming

Formability

Failure

Thermal properties

Polymers

ABSTRACT

Single Point Incremental Forming (SPIF) has been intensively investigated in the last two decades. It is a versatile and economical manufacturing technology that is especially viable for small and medium-sized batches, with a great potential for manufacturing highly customized parts. One of the most important advantages of this technology is the greater formability it can attain compared to conventional sheet forming processes. The aim of this paper is to evaluate the overall formability of a series of polymeric sheets deformed by SPIF process, including biocompatible and non-biocompatible materials, while considering a variety of process parameters including *spindle speed* which, in previous studies on polymers formed by Incremental Sheet Forming (ISF), has been shown to be the most influential process parameter. The results show that variations in spindle speed caused a variation in the forming temperature and the material forming limits. For a better understanding of the deformation mechanism and the failure process of polymers during SPIF, a fractographic analysis using optical microscopy was carried out, as well as a Differential Scanning Calorimetry (DSC) analysis to determine the glass transition and melting temperatures and the degree of crystallinity of the polymers.

© 2017 Published by Elsevier Ltd.

1. Introduction

Incremental Sheet Forming (ISF) has been recognized as a process that has the potential to change radically the production system involved in manufacturing prototypes, small batches or customized sheet products. The evolution of ISF and the different varieties, applications and advantages, as well as the process parameters affecting it have been comprehensively described in a series of review and state-of-the-art research papers [1–4]. Additionally, ISF has been shown to be a more environmentally friendly process compared to conventional technologies [5]. As a result, during the past few decades, ISF has attracted the attention of numerous research groups trying to overcome the various problems that limit the more widespread use of the technology as a manufacturing process.

Formability is a measure of the degree to which a certain material can undergo plastic deformation before failure occurs. With the aim of evaluating formability in ISF, several researchers have

used the maximum achievable wall angle as an indicator of the material forming limits [6,7]. However, the pioneering work of Silva et al. [8] demonstrated that, in order to determine formability in Single Point Incremental Forming (SPIF), it is preferable to carry out a principal strain analysis within Forming Limit Diagrams or FLDs. This consists of locating graphically the principal strain states of different points on the outer surface of the manufactured sheet part in a Cartesian plane bounded by the major versus minor principal strains axes. Such representations have been more recently depicted in combination with curves indicating the principal failure strains caused by necking or fracture of the sheet material, including those corresponding to mode I and II fractures described in fracture mechanics [9].

As a consequence, formability in ISF (as with conventional sheet metal forming) is commonly analyzed nowadays within FLDs [10] for most applications in which failure involves mode I fractures (in-plane tension). An FLD diagram needs to show the limit strains characterized by the combinations of strains (i) at the onset of local necking, i.e., the FLD at necking or the *Forming Limit Curve* (FLC), and (ii) at the beginning of ductile fracture, i.e., the FLD at fracture or the *Fracture Forming Line* (FFL). On the contrary to the failure controlled by necking that usually takes place in conventional sheet

* Corresponding author. C/Maria Aurèlia Capmany, 61 (Edifici P2 Campus Montilivi), 17003 Girona, Spain.

E-mail address: mluisa.gromeu@udg.edu (M.L. Garcia-Romeu).

metal forming processes, metal sheets deformed by ISF within a certain range of process parameters suffer a stable straining above the FLC that seems to lead directly to ductile fracture [11]. The stabilization mechanisms that can delay or even suppress necking, providing the formability enhancement usually observed in ISF, are comprehensively discussed in the paper by Emmens and van den Boogaard [12]. Besides, recent studies [13–15] have demonstrated that failure strains in ISF are within a scatter band of the FFL in a certain range of process parameters avoiding the onset of necking. In this sense, the effect of the localized bending induced by the forming tool, via the t_0/R ratio, in the stabilization of plastic deformation above the FLC during ISF has been also studied by the authors of this article [11] for stainless steel sheets. It was observed that for high tool diameters, the failure mode was due to necking followed by ductile fracture. However for the lowest tool diameters considered, failure occurred by fracture in the absence of necking.

In this scientific context, the simplest ISF technology is the variety known as axisymmetric Single-Point Incremental Forming or SPIF. As shown in Fig. 1, the SPIF process consists of a hemispherical end-forming tool driven by a numerical control machine that progressively follows a pre-established trajectory, deforming a peripherally clamped sheet blank into a final component without the use of any specific forming die.

As discussed above, ISF processes including SPIF have historically been applied mainly to metal sheets, either working at room temperature or at elevated temperatures to increase formability [16–18]. However, in the recent years, there has been increasing interest in this process for forming polymeric materials. In this context, SPIF applied to polymeric sheets is equally capable of achieving the high levels of principal strain that it has been widely shown to have in metals. In this regard, the pioneering work of Martins et al. [19] was one of the first studies that evaluated the formability of thermoplastic materials processed using SPIF. Fracture Forming Limit Diagrams or FFLD's were employed to characterize the materials considered, due to the absence of necking previous to failure. A similar study was carried out by Marques et al. [20], in which the experimental tests were performed using truncated conical and pyramid geometries. For PC (polycarbonate) and PVC (polyvinyl chloride), the strains at fracture corresponded to the calculated FFL, whereas PET (polyethylene terephthalate) had even higher levels of formability (no fracture was observed) and PA (polyamide) had higher formability and failure was caused by wrinkling rather than by fracture. It was also pointed out that formability was increased with an increase in sheet thickness and a decrease in tool radius. Later, hole-flanges in PET and PC sheets were produced by multi-stage SPIF [21] in an analysis of formability using FFLD's. It was concluded that two modes of deformation are involved in incremental hole-flanging: (i) in-plane stretching under plane strain conditions and (ii) in-plane stretching combined with

bending near the hole. PET had better formability than PC due to its higher fracture toughness and a more effective rearrangement of the plastic chains during plastic deformation.

The work by Bagudanch et al. [22] was the first to demonstrate the effect that spindle speed had on SPIF when using a sheet of polymer material (in this case, PVC). Their results showed that by increasing the spindle speed it was possible to reduce the forming force and to increase formability because of the heat generated by the friction between tool and sheet. In a subsequent work [23], the study was extended to five polymers and empirical equations to predict the maximum temperature during the SPIF process were provided. Davarpanah et al. [24] also confirmed that spindle speed (or “tool rotation speed”) influences the forming force for PVC and PLA (polylactic acid). Very recently, Davarpanah et al. [25] investigated the effect of the step down and spindle speed on the mechanical properties, the degree of crystallinity and the chain orientation of PVC and PA parts formed by SPIF, concluding that SPIF induced a chain reorientation that causes an improvement in ductility and toughness.

Regarding the potential of ISF for manufacturing polymeric parts, Centeno et al. [26] proposed a complete methodology for the design and manufacture of customized cranial prostheses made from polymers using SPIF technology based on patients' CAT (Computed Axial Tomography) scans, demonstrating the considerable potential of SPIF for manufacturing highly-individualized polymeric prostheses. On the other hand, Bagudanch et al. [27] showed the capability of ISF for manufacturing customized cranial implants using a biocompatible polymer, UHMWPE (ultra-high molecular weight polyethylene). Two cranial implants were produced using SPIF and TPIF (Two-Point Incremental Forming) processes, modifying the spindle speed as the most important process parameter. Using 3D scanning, it was shown that with higher spindle speeds and using TPIF, more accurate parts could be obtained. Additionally, the total costs of producing a customized cranial implant were calculated, from the design stage to its fabrication using ISF, which took into consideration all the factors involved (energy, raw material, processing time, etc.). It was shown that implants made using TPIF would be an attractive approach for repairing cranial defects at low costs as well as with low lead times.

In this paper, the overall formability of a series of polymeric sheets undergoing the SPIF process is evaluated, including non-biocompatible (PVC, PC and PP –polypropylene–) and also biocompatible materials (PCL –polycaprolactone– and UHMWPE, which have demonstrated their biocompatibility, as can be seen for instance in Refs. [28] and [29] respectively) whose formability in SPIF was never studied before, thus increasing current knowledge on formability and failure regarding such materials with the aim of identifying the feasibility of applying them, for example, to the manufacturing of customized medical devices and prostheses. The

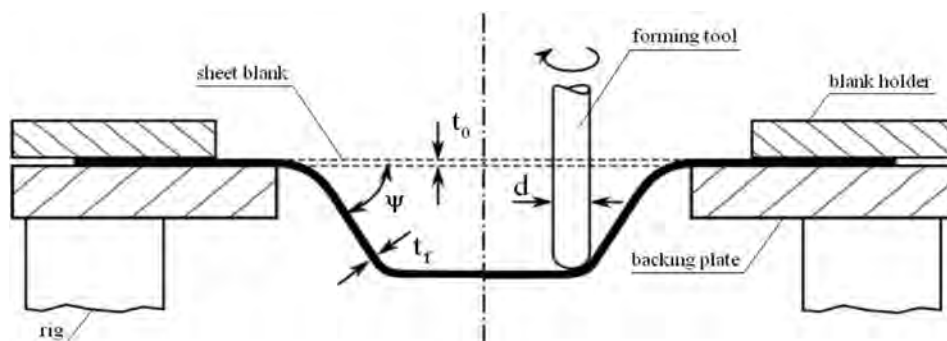


Fig. 1. Schematic representation of Single-Point Incremental Forming.

results show that spindle speed causes a variation in the forming temperature and the material forming limits, and this relationship between temperature and formability is evaluated in detail for each one of the polymeric materials considered. For a better understanding of the failure process in SPIF of polymers, a fractographic study using microscopy was performed along with a DSC (Differential Scanning Calorimetry) analysis to determine the glass transition temperature and the degree of crystallinity of the polymers. To sum up, this work demonstrates the potential -in terms of formability- for manufacturing complex geometrical parts in polymeric sheets using SPIF. It has also been pointed out the importance of evaluating the formability of polymers within a proper range of process parameters in order to provide catalogues of material formability and thus provide safe formability ranges of deformation within their corresponding FFLDs.

2. Methodology

2.1. Material characterization

Tensile tests were carried out at testing speeds of 5, 50 and 500 mm/min on the selected polymer materials in an MTS Insight universal testing machine with a 10 kN load cell. Three replications of each test were performed until the specimen failed, following the specifications of standard test ASTM D638-14. The tests were performed at room temperature, 40 °C and 60 °C in order to analyze the influence of the temperature variation on the behavior of the polymer.

2.2. SPIF experimental tests

The process parameters values considered for the experimental tests are summarized in Table 1. Box-Behnken designs (BBD) are three-level design of experiments that allow second order response surfaces to be fitted efficiently. In this case, the four-factor design consists of 27 experimental runs (Table 2) that can be split into three blocks with one center point at each. This experimental plan was carried out for each of the five different materials analyzed in the present work: polyvinylchloride (PVC), polycarbonate (PC), polypropylene (PP), polycaprolactone (PCL) and ultra-high molecular weight polyethylene (UHMWPE). The tests were performed on 2 mm thickness sheet blanks. Four of the tested materials were commercially available in sheet form (PVC, PC, PP and UHMWPE). The PCL sheets were produced by compression molding. Around 55 g of PCL pellets (Sigma Aldrich, ≈ 3 mm, average Mn = 80,000) were positioned into a stainless steel cast cavity of $150 \times 150 \times 2$ mm³ which was previously warmed to a set temperature between 60 and 80 °C inside a heating hydraulic press. A low load was applied for a fixed time to guarantee the complete melting of the material. Subsequently, the load was increased, thus keeping the sheet in place for a few more minutes to complete the final compaction of the fused polymer. Finally, the pressure was retired and the cast cooled to room temperature by placing it in a cooling press.

The ISF tests were carried out on a Kondia[®] HS1000 3-axis milling machine equipped with Fidia[®] numerical control. A table-

Table 1
Values considered for the process parameters analysis.

Tool diameter d_t (mm)	Feed rate F (mm/min)	Step down Δz (mm)	Spindle speed S (rpm)
6	1500	0.2	Free
10	2250	0.35	1000
14	3000	0.5	2000

Table 2
Box-Behnken design of experiments.

ID	Tool diameter d_t (mm)	Feed rate F (mm/min)	Step down Δz (mm)	Spindle speed S (rpm)
1	6	2250	0.35	Free
2	14	2250	0.35	Free
3	6	2250	0.35	2000
4	14	2250	0.35	2000
5	10	1500	0.2	1000
6	10	3000	0.2	1000
7	10	1500	0.5	1000
8	10	3000	0.5	1000
9	10	2250	0.35	1000
10	6	2250	0.2	1000
11	14	2250	0.2	1000
12	6	2250	0.5	1000
13	14	2250	0.5	1000
14	10	1500	0.35	Free
15	10	1500	0.35	2000
16	10	3000	0.35	Free
17	10	3000	0.35	2000
18	10	2250	0.35	1000
19	6	1500	0.35	1000
20	14	1500	0.35	1000
21	6	3000	0.35	1000
22	14	3000	0.35	1000
23	10	2250	0.2	Free
24	10	2250	0.2	2000
25	10	2250	0.5	Free
26	10	2250	0.5	2000
27	10	2250	0.35	1000

type dynamometer Kistler[®] 9257B was mounted on the machine worktable in order to measure the forming forces that occur during the process. The force data was acquired using a DaqBoard[®] 505 data acquisition card and the DaqView[®] 9.0.0 software. A fixture system composed of a bottom plate, four supports, a clamping plate and a top plate was bolted onto the force measurement system. The blank sheet was placed between the clamping plate and the top plate, without any backing plate, as shown in Fig. 2a. The dimensions of the blank were 150×150 mm² and the effective working area was 120×120 mm². In order to reduce friction, liquid lubricant for cold forming (Houghton TD-52) was applied over the upper surface of the blanks. A thermographic camera IRBIS Image IR13300, was used to acquire the temperature variation in the material during the forming operation, at a frequency of 1 image per 10 s. The temperature distribution over the sheet during the entire experimental tests was registered. This information was processed in order to obtain the maximum reached temperature for each test of the materials analyzed.

The selected geometry, a pyramidal frustum, had the following specifications: initial wall angle: 45°, generatrix radius: 80 mm, length of the pyramid edges: 105 mm and a final desired depth of 43 mm (Fig. 2b).

2.3. Methodology for strain analysis

The principal strain state of the finished part was evaluated via circle grid analysis by using the 3D deformation digital measurement system ARGUS[®]. Prior to the tests, the circle grid had to be printed on the sheet blank by a serigraphy process. The analysis of the tested sheets performed using ARGUS[®] provided the contour of the principal strains on the outer surface of the finished part. As expected, the zone with highest major strains was located at the vicinity of the crack. The measurement system was able to capture the deformation of ellipses both above and below it and, therefore, able to interpolate the strains throughout the crack.

The first step of the procedure for constructing the FFL, applied

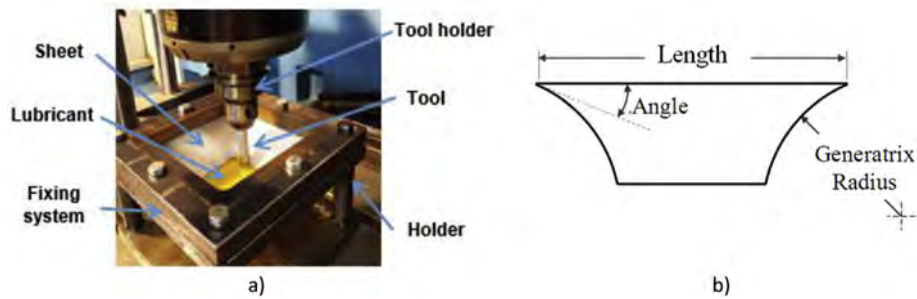


Fig. 2. a) Experimental setup used on the 3 axis CNC machine. b) Design of the pyramidal frusta with a circular generatrix.

by the authors in previous research on metals [11] and based on the work of Atkins [30], is to measure the thickness at fracture at several places along the crack in order to obtain the average thickness strain. This average thickness strain is then evaluated at both sides of the crack for every tested specimen. In addition, some tested specimens were cut and polished perpendicularly to the crack and the thickness was measured from a profile view in order to validate the fracture strains calculated from the thickness measurements along the crack. The measurements were done with a Stereomicroscope Nikon SMZ800 with $\times 20$ magnification and analyzed using KAPPA Image Base Metro 2.7.2. The average minor strain was evaluated at certain locations on the outer sheet surface close to the crack appearance. The major strain was then calculated by volume constancy as follows:

$$\bar{\epsilon}_{1,f} = -(\bar{\epsilon}_{2,f} + \bar{\epsilon}_{3,f}) \quad (1)$$

where $\bar{\epsilon}_{2,f}$ and $\bar{\epsilon}_{3,f}$ are, respectively, the average minor and thickness strains evaluated in a series of points along the crack.

According to previous research work, spindle speed is the most influential factor on the results concerning forming force, maximum temperature, surface roughness and maximum achieved depth [5,22,23]. Therefore, in order to determine the influence of the spindle speed on formability, the present paper will focus on the Tests 25 and 26 shown in Table 2, carried out for each considered material. In other words, the process parameters selected for consideration in the formability analysis for each material shall be those shown in Table 3 below.

2.4. Differential Scanning Calorimetry (DSC)

As previously shown in research by Davarpanah et al. [24], DSC tests are useful for obtaining the transition temperatures of polymers as well as their degree of crystallinity. Five samples for each material were considered for the DSC measurements: two from the biaxial strain zone and two from the plane strain zone (with spindle speeds set at *free* and 2000 rpm in each case) and one from the unformed material. Fig. 3 schematically illustrates the location of the DSC samples.

The DSC measurements were performed using the TA Instruments Q2000 model. The sample size was between 6 and 10 mg. The pan was aluminum. The samples of PVC, PC and PP and

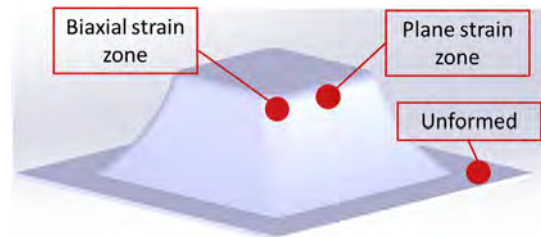


Fig. 3. Identification of the DSC samples locations.

UHMWPE were heated from 25 to 200 °C with a 10°C/min temperature ramp, while in the case of PCL, the maximum temperature was 80 °C. The environment for measuring samples was purged with highly pure nitrogen gas at a rate of 50 ml/min. For the amorphous polymers the glass transition temperature (T_g) was recorded whereas for the semicrystalline polymers the melting temperature (T_m) was recorded, as well as the melting enthalpy (ΔH_m) which was used to calculate the degree of crystallinity (X_c) using the following equation:

$$X_c = \frac{\Delta H_m}{\Delta H_m^0} \times 100 \quad (2)$$

where ΔH_m^0 is the heat of fusion of 100% crystalline polymer.

3. Results and discussion

3.1. Material characterization

Table 4 summarizes the main mechanical properties obtained for PVC, PC and PCL. As will be seen in the following section, in the case of PP and UHMWPE, the test geometry was successfully formed without fracture and, consequently, from the point of view of spifability (i.e., formability in SPIF) and failure strain analysis, these materials are of little interest. Therefore, the results regarding material characterization will be presented only for the ones that are prone to fail. It was noticed that the material samples experienced a linear elastic response followed by a yielding, softened behavior.

Table 3
Selected process parameters for formability analysis.

Tool diameter d_t (mm)	Feed rate F (mm/min)	Step down Δz (mm)	Spindle speed S (rpm)
10	2250	0.5	Free 2000

Table 4
Mechanical properties of the polymeric sheets.

Material	Young modulus E (MPa)	Yield stress σ_y (MPa)	Yield point ϵ_y (%)
PVC	2696	55.52	3.20
PC	2344	64.32	5.87
PCL	375	15.20	12.20

Fig. 4 illustrates the PVC material response when subjected to a simple uniaxial load in the tensile tests at different testing speeds and temperatures. As can be seen from Fig. 4, these experimental tests show that at higher testing speeds, the Young modulus (E) and the yield stress (s_y) are increased, whereas the strain values at the yield point (e_y) and at the material fracture are reduced, i.e. there is lower formability of the material. Therefore, increasing the feed

rates during the manufacturing in SPIF would decrease sheet formability. In order to explore the worst case scenario and to evaluate the capability of this methodology, a feed rate of 2250 mm/min was set in all the SPIF tests described hereafter (agreeing with Table 3). Furthermore, when the testing temperature is increased, the Young modulus and the yield stress value also diminish. This strain-rate and temperature-dependent behavior is

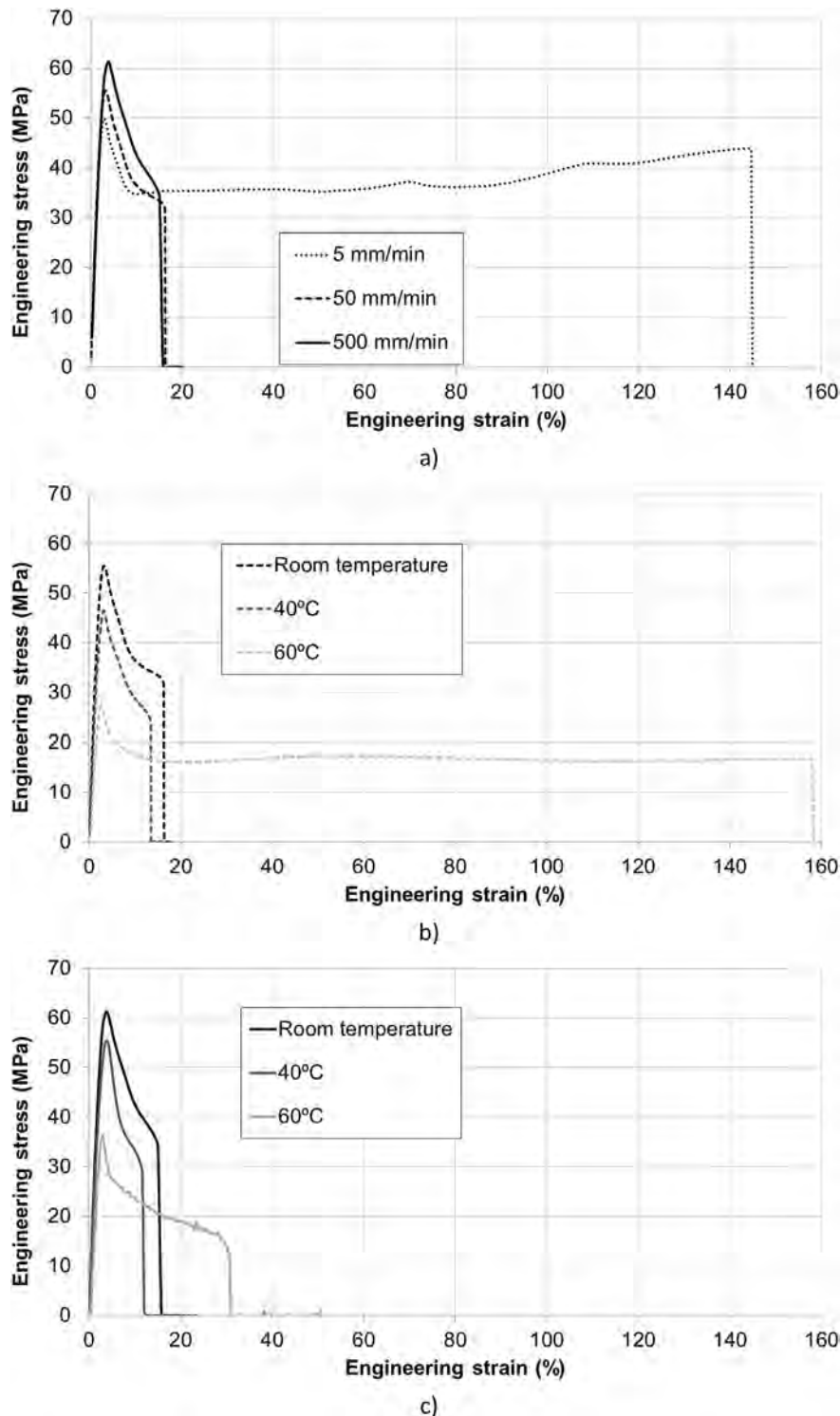


Fig. 4. Stress strain curve for PVC: (a) under different testing speeds at room temperature; (b) at 50 mm/min at various temperatures and (c) at 500 mm/min at various temperatures.

very common for thermoplastic materials. Similar behavior in a quantitative sense has been obtained for PC and PCL.

3.2. SPIF tests and failure strains

Table 5 summarizes the results of maximum achieved depth, maximum angle and failure occurrence and mode of failure for the different SPIF tests. As it was mentioned earlier, neither PP nor UHMWPE failed during the SPIF tests and, therefore, they will not be further analyzed in terms of spifability and failure strains.

As above exposed, the strain state of the tested polymeric sheets was measured off-line on the finished part by using the 3D deformation digital measurement system ARGUS[®] via circle grid analysis. This allows the principal strains on the outer surface to be represented within the principal strain space. It depicts different strain paths corresponding to meridional sections along the final part labeled as S_0 , S_1 and S_2 . Section S_0 is the closest to the equibiaxial strain state, S_1 corresponds to biaxial strain and S_2 coincides with plane strain (see final parts views in Fig. 5).

As can be seen in Fig. 5, the failure strains were analyzed in two different places along the fracture line, corresponding to plane strain and biaxial strain conditions. The fracture strains were evaluated directly on the final specimens by microscope following the previously mentioned procedure.

Fig. 5 presents the FFLD for PVC, PC and PCL with spindle speed set at *free* and 2000 rpm. In general terms, it can be observed that for the higher spindle speed, the forming limits of the material can be increased. This behavior most notable in PC because both tests failed by ductile fracture and the limit major strains under plane-strain state were increased from 0.75 to 0.84 with a spindle speed of 2000 rpm. This occurs because when increasing the spindle speed, the friction between the tool and the sheet increases and there is a rise in temperature during the forming process. It is also notable that PVC is the material with the highest formability, followed by PCL and PC. Table 6 summarizes the fracture strains or the maximum strains obtained without fracture in the experiments analyzed.

Notice that, in the case of PCL (Fig. 5e and f), the FFL is represented with a red dashed line. This differentiation was made because the failure in PCL was due to the appearance of several small cracks rather than a ductile fracture (more details of this sort of failure are given in the next section). Therefore, the strains were evaluated in the maximum thinning zone and at the precise places where these small cracks appeared, not at the fracture zone. Thus, the limit line cannot be considered as the common FFL.

3.3. Modes of failure

As already seen in Table 5, the SPIF tests on PP and UHMWPE (tests 7 to 10) were completed successfully without failure and, therefore, no formability analysis was carried out on these two

materials. In contrast, for PVC, PC and PCL (tests 1 to 6), fracture occurred during 3 of the tests while in the other 3 cases there was evidence of another sort of failure, i.e., twisting and/or the appearance of small cracks. In this section, the different modes of failure found in these materials are presented using the fractographies captured in the microscope in order to measure the thickness reduction and to calculate the strains at failure, which, in turn, were used to obtain the FFLs shown in the previous section.

As can be observed in Fig. 6, for PVC and PC with a spindle speed set at *free* and for PC with a spindle speed of 2000 rpm (Fig. 6a, c and d, respectively), the failure mode was ductile fracture without previous necking in the plane strain and biaxial strain sections. Furthermore, in the vicinity of the fracture, it can be observed an indentation corresponding to the plastic deformation caused by the tool radius. Fig. 6d shows the detail of the fracture in the plane strain zone, where it is possible to observe the formation of a small burr (indicated by the red arrow), caused by the increased temperature. Fig. 6d also shows the three thickness measurements carried out in order to obtain the average thickness strain, as it has been explained in the procedure for the construction of the FFL (Section 2.4). In the case of the PVC part manufactured at 2000 rpm (Fig. 6b), the failure was the result of twisting without fracture due to the rise in temperature during the forming operation which caused an increase in formability.

PCL failed due to the appearance of small cracks in both tests, at *free* and 2000 rpm spindle speeds. With *free* spindle speed set at *free*, the small cracks are not located in the zone of maximum strain. Instead, they appear below this zone, as highlighted in Fig. 6e, which suggests that it is due to the degradation of the material. At a spindle speed of 2000 rpm (Fig. 6f), these cracks do appear where the maximum strain occurs. Therefore, the thickness at this point is used to obtain the average thickness strains to represent the limit line, which should not be considered as the FFL itself, as explained in the previous section. It is worth mentioning that, in this case, an increase in formability could not be found despite the rise in temperature due to spindle speed.

3.4. Crystallinity and glass transition temperatures

Table 7 shows the maximum reached temperature during the forming process (T_f) as well as the data provided by the DSC thermograms, from which it was possible to obtain the glass transition temperature (T_g), the melting temperature (T_m) and degree of crystallinity (X_c) at different spindle speeds (*free* and 2000 rpm) and strain conditions (unformed (U), plane strain (P) and biaxial strain (B)) for all the materials tested. Furthermore, the maximum standard deviation of the measurements is included.

Some data was not available (n/a) because the degree of crystallinity could not have been obtained for the amorphous polymers (PVC and PC), since crystal morphology was not observed and only T_g was measured. As Table 7 shows, there is no evidence of a

Table 5
SPIF experimental results.

Test	Materials	Spindle speed S (rpm)	Maximum depth (mm)	Maximum angle (°)	Failure?
1	PVC	Free	42.5	89.5	YES
2		2000	43	90	Twisting without fracture
3	PC	Free	29	79.8	YES
4		2000	32.5	82.5	YES
5	PCL	Free	43	90	Small cracks and twisting
6		2000	43	90	Small cracks
7	PP	Free	43	90	NO
8		2000	43	90	NO
9	UHMWPE	Free	43	90	NO
10		2000	43	90	NO

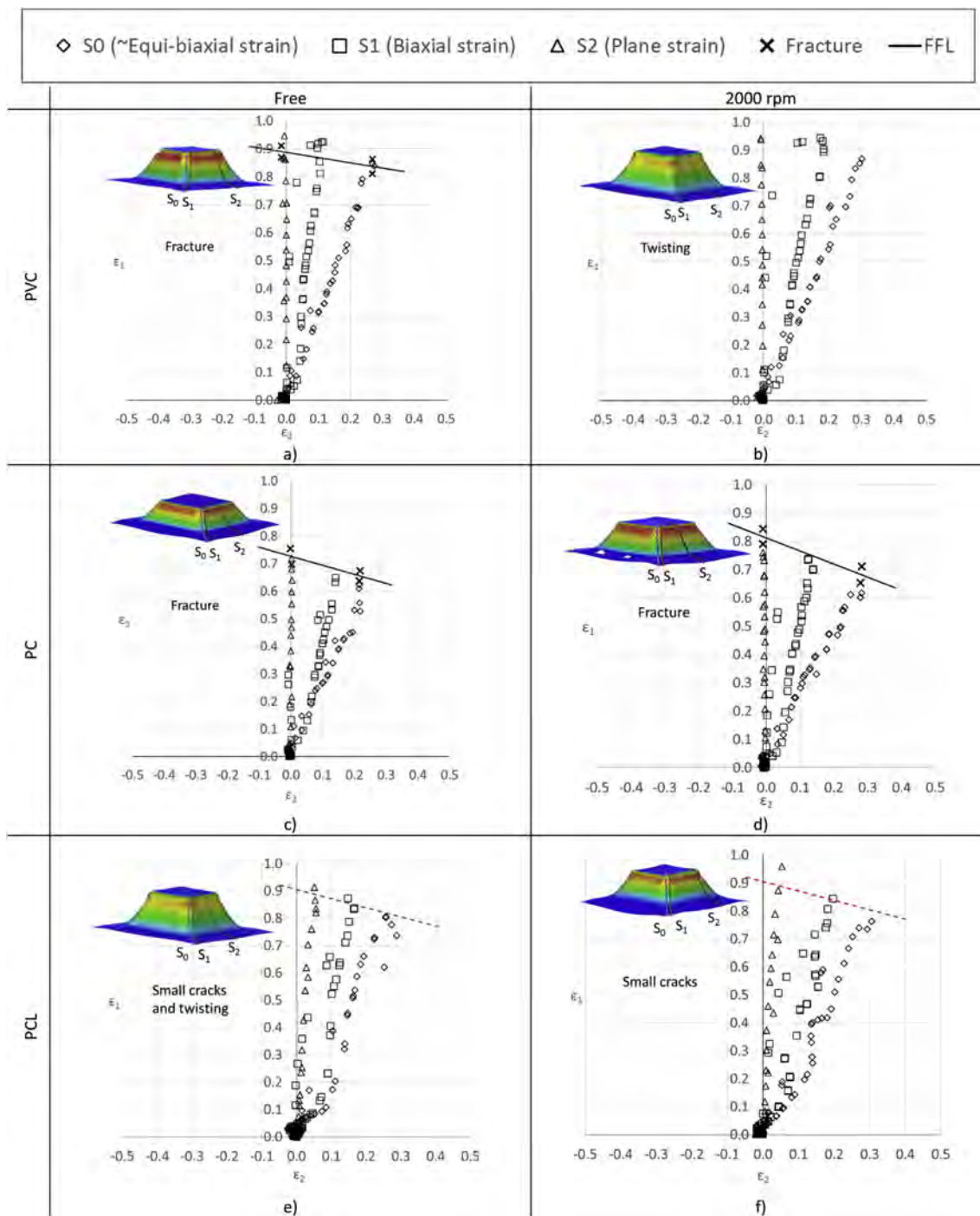


Fig. 5. FFLD for PVC, PC and PCL with spindle speeds set at *free* and 2000 rpm.

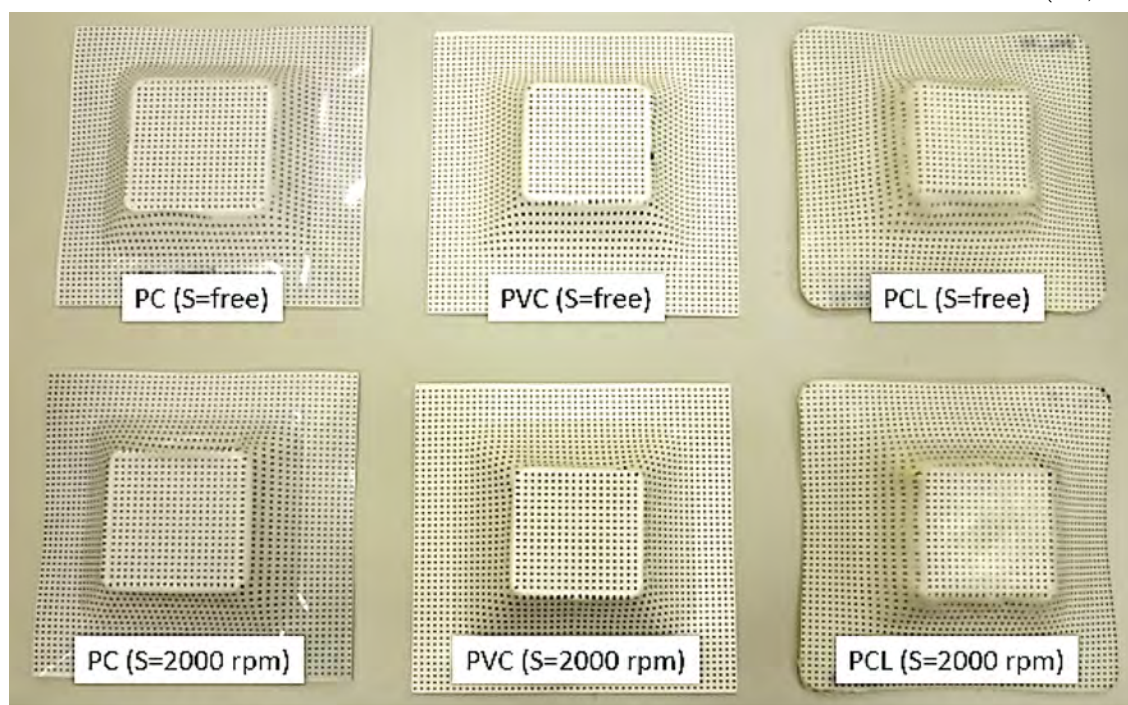
significant variation in the glass transition temperature, either with spindle speed, or due to the strain conditions. For these two polymers, the exact T_m was not obtained because it is significantly far from the forming temperatures (around 210 °C for PVC and 225 °C for PC).

For PCL, PP and UHMWPE, the glass transition temperature is lower than the room temperature (approximately, -60 °C, -10 °C and -160 °C, respectively). Therefore, Table 7 only presents their melting temperature, since they are in the range of the temperatures achieved in the SPIF process. In order to calculate the degree of crystallinity X_c , the heat of fusion of 100% crystalline polymer

(ΔH_m^0) is required, which is considered to be 139.5 J/g for PCL [31], 209 J/g for PP [32] and 290 J/g for UHMWPE [33]. Once again, no clear trend could be found because the melting temperature and the degree of crystallinity were nearly the same for each material independently of spindle speed and strain conditions. Similar results regarding the effect of spindle speed on crystallinity were found recently by Davarpanah et al. [25]. Finally, Table 7 also provides the maximum standard deviation obtained in the measurement of the glass transition temperature and the degree of crystallinity, respectively. As can be seen, they show a reduced experimental scatter in all cases.

Table 6
Failure or maximum strains without fracture obtained in the SPIF tests.

Test	Materials	Spindle speed S (rpm)	Fracture strains ($\epsilon_{1,f}$, $\epsilon_{2,f}$)		Maximum strains without failure (ϵ_1 , ϵ_2)	
			Plane strain	Biaxial strain	Plane strain	Biaxial strain
1	PVC	Free	(0.91, -0.01)	(0.86, 0.27)	n/a	n/a
2		2000	no fracture	no fracture	(1.04, -0.01)	(0.86, 0.30)
3	PC	Free	(0.75, 0.00)	(0.67, 0.22)	n/a	n/a
4		2000	(0.84, 0.00)	(0.71, 0.28)	n/a	n/a
5	PCL	Free	no fracture	no fracture	(0.91, 0.05)	(0.80, 0.26)
6		2000	no fracture	no fracture	(0.88, 0.05)	(0.80, 0.30)



*n/a means not applicable.

Fig. 7 shows the typical DSC thermograms for an amorphous polymer, corresponding to the biaxial section of PVC (Fig. 7a), and a semicrystalline one, which corresponds to the biaxial section of PCL (Fig. 7b), both manufactured at a spindle speed of 2000 rpm. Notice that melting in polymers can take place during a wide temperature range, although the peak value is considered as the reference melting temperature. For example, in the case of PCL sheets the temperature ranges from 40 °C to 66 °C (see Fig. 7b).

3.5. Discussion

It is well known that temperature has an important role in the polymers behavior and their performance during the forming process. As has been mentioned throughout this paper, spindle speed has a significant impact on polymers deformed by SPIF, as was expected from previous research works [5,22,23]. This section aims to clarify in which cases formability can be then improved by increasing spindle speed, and consequently the reached temperature, in relation with the characteristic temperatures of each polymeric sheet.

The experimental tests described here have revealed that the temperature increased by between 12 and 30 °C in most cases, even up to 65 °C in the case of PP, when the highest spindle speed was employed (Table 7). This considerable rise in temperature has

several consequences from the point of view of formability and failure:

- In the case of PVC, it led to higher strains being reached, but also to the presence of wrinkles, which became the mode of failure of the manufactured part. This effect is due to reaching a forming temperature being closer to T_g , which may have altered the material properties.
- Regarding the PC sheets, the temperature increase significantly improved the material's formability without modifying the mode of failure, the only difference observed is slight, resulting in the formation of a burr on the part manufactured at 2000 rpm. The glass transition temperature of PC is the highest of the five materials tested, and even in Test 4 (at 2000 rpm), the maximum forming temperature was still far from T_g . This means that PC is not as prone as PVC to failure by twisting, even when reaching these temperatures.
- The glass transition temperature of PCL (around -60 °C) is well below the room temperature, whereas the temperature reached during Tests 5 and 6 were close to the range of temperature where melting takes place (see Fig. 7b), especially in the case of Test 6. This approximation to the melting temperature might have caused localized melting of the crystalline lattices. Furthermore, it should be pointed out again that PCL sheets

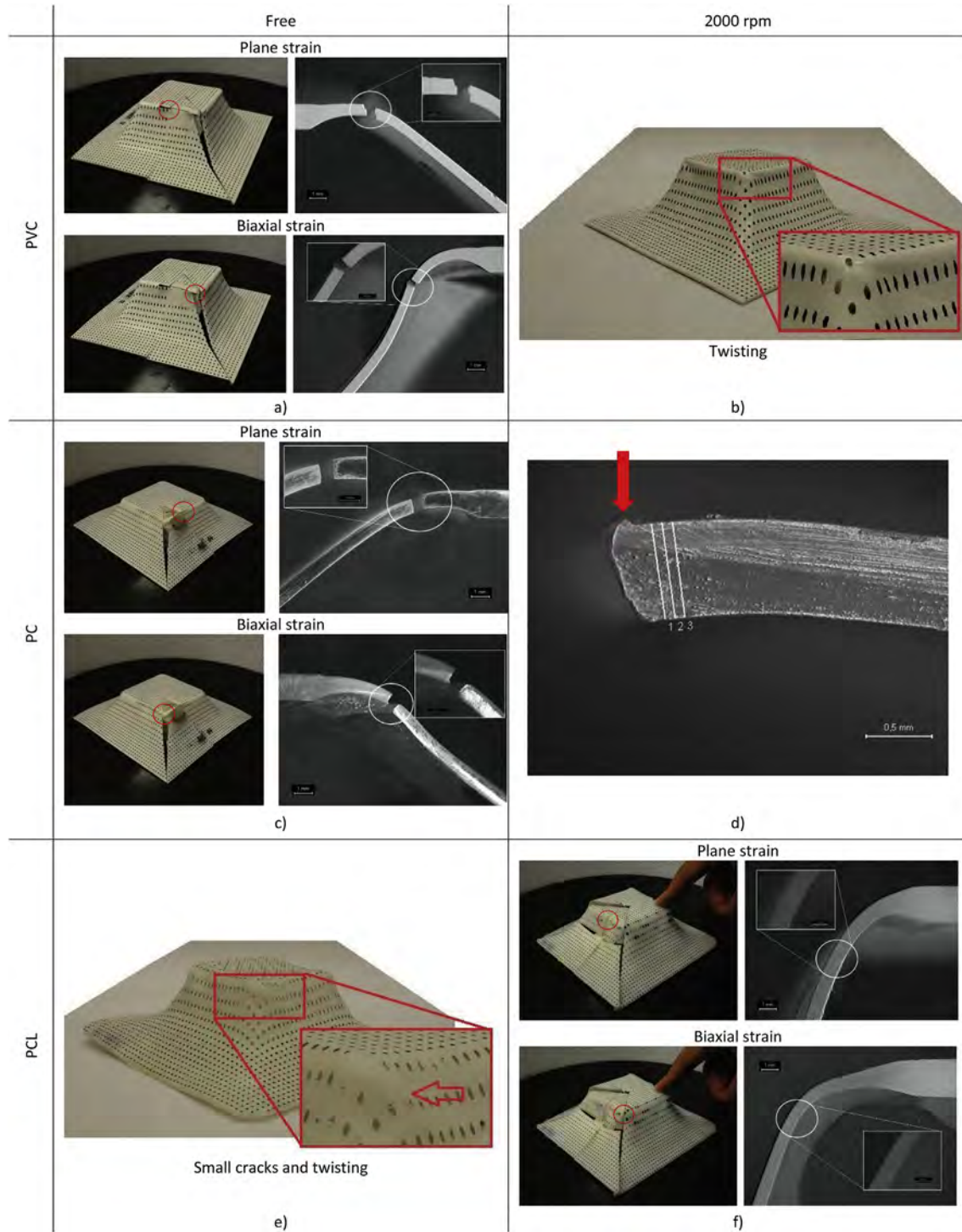


Fig. 6. Summary of modes of failure for PVC, PC and PCL with spindle speeds set at *free* and 2000 rpm.

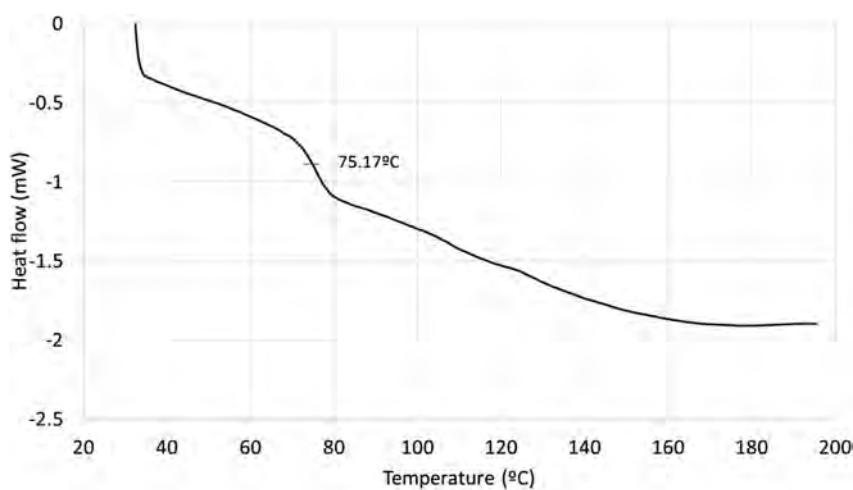
were manufactured from pellets by compression molding. Therefore, the sheets might be less homogeneous compared to the other materials, which were commercially available in sheet form, being possible to have zones with lower thickness or an inappropriate cohesion between pellets. A combined effect of both approaches (i.e. the localized melting and the heterogeneous sheet) might explain why PCL failed by the appearance of small cracks rather than ductile fracture, which was expected from previous experiences in polymers deformed by SPIF.

- PP and UHMWPE are semi-crystalline polymers with a relatively high melting temperature. At room temperature, they are above their glass transition temperatures, which are approximately $-10\text{ }^{\circ}\text{C}$ for PP and $-160\text{ }^{\circ}\text{C}$ for UHMWPE. The test geometry was successfully manufactured from these materials without failure (no fracture, no twisting) independently of the spindle speed used because the temperature reached in the experiments remained well below T_m , meaning that melting did not occur in the crystalline regions of these polymers.

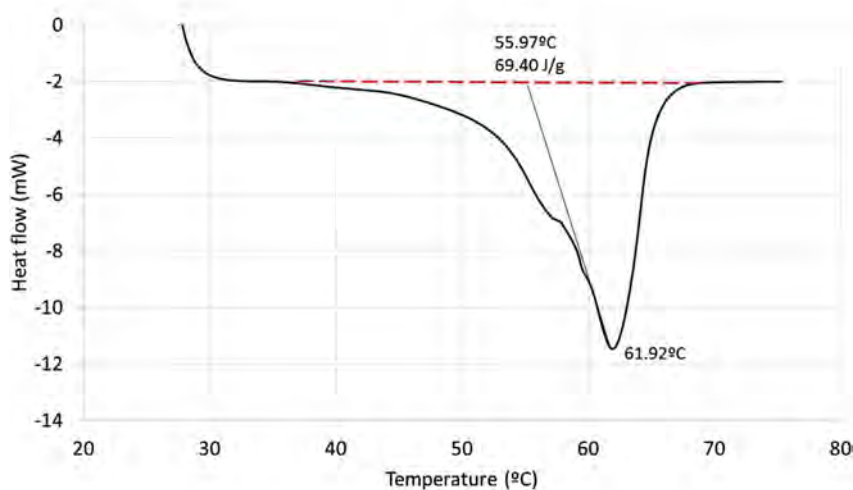
Table 7
Maximum reached temperature and DSC results.

Test	Materials	S (rpm)	T_f (°C)						
				U	P	B	U	P	B
Amorphous polymers									
				T_g (°C)			X_c (%)		
1	PVC	Free	41.23	76.55	77.76	76.99	n/a	n/a	n/a
2		2000	53.96		76.48	75.17		n/a	n/a
3	PC	Free	47.37	149.38	147.91	148.75	n/a	n/a	n/a
4		2000	70.56		147.62	147.96		n/a	n/a
Semicrystalline polymers									
				T_m (°C)			X_c (%)		
5	PCL	Free	36.58	63.93	59.07	61.38	45.24	46.32	47.81
6		2000	54.18		61.83	61.92		49.00	49.75
7	PP	Free	39.85	162.26	160.69	162.56	42.94	42.43	41.30
8		2000	104.10		162.42	163.07		42.35	42.60
9	UHMWPE	Free	44.93	136.22	138.72	139.30	45.90	42.06	44.79
10		2000	77.91		140.39	136.52		47.55	41.89

*U, P and B refer to the location of the DSC samples with different strain conditions in the pyramidal part, which are the unformed, plane strain and biaxial strain zones respectively.



a)



b)

Fig. 7. DSC thermograms for: a) PVC at 2000 rpm in the biaxial section and b) PCL at 2000 rpm in the biaxial section.

4. Conclusions

Previous studies have revealed the influence of spindle speed on polymers deformed by SPIF regarding the variation of forming forces [22], energy consumption [5] and forming temperature [23]. The study described in this paper has further underlined the importance of spindle speed, while at the same time presenting an evaluation of the overall formability of a series of polymeric sheets during the SPIF process, including non-biocompatible and biocompatible materials, thus increasing the current knowledge in formability and failure in these kinds of materials.

In this context, this research work clarifies the likely increase of formability of the polymeric sheet related to the spindle speed, explaining: (i) in which cases this effect allows leading with a higher level of strains, or even suppressing failure in the test conditions considered, and (ii) in which cases the increase of the spindle speed has not a significant effect in the formability and failure of the polymeric sheet. It has been pointed out that the effect of the spindle speed needs to be analyzed in relation with the characteristic temperatures of the polymeric material, i.e. the glass transition and the melting temperatures. In this sense, a series of main contributions can be highlighted from the results presented throughout the paper:

- For polymers with a glass transition temperature above the forming temperature (PVC and PC in the present case), an increase in spindle speed leads to a significant increase in formability and the expected mode of failure is ductile fracture without previous necking. In contrast, if the process conditions involve temperatures very close to or even greater than T_g , the part could fail by twisting.
- Polymers with T_g below room temperature (PP and UHMWPE), enhanced formability with increased spindle speed is not as pronounced. Moreover, if the polymer has a low melting temperature (e.g. PCL), the temperature reached during the forming process could initiate localized melting process, compromising the formability.

Acknowledgements

The research leading to these results has received funding from the University of Girona (MPCUdG2016/036) and the Spanish Ministry of Education (DPI2016-77156-R and DPI2015-64047-R). The first author gratefully acknowledges the support from the Spanish grant FPU12/05402. The work of Jaime Domínguez MSc is also gratefully acknowledged.

References

- [1] A.K. Behera, R.A. de Sousa, G. Ingarao, V. Oleksik, Single point incremental forming: an assessment of the progress and technology trends from 2005 to 2015, *J. Manuf. Process.* 27 (2017) 37–62, <http://dx.doi.org/10.1016/j.jmapro.2017.03.014>.
- [2] S. Gatea, H. Ou, G. McCartney, Review on the influence of process parameters in incremental sheet forming, *Int. J. Adv. Manuf. Technol.* (2016), <http://dx.doi.org/10.1007/s00170-016-8426-6>.
- [3] W.C. Emmens, G. Sebastiani, A.H. van den Boogaard, The technology of Incremental Sheet Forming—a brief review of the history, *J. Mater. Process. Technol.* 210 (2010) 981–997, <http://dx.doi.org/10.1016/j.jmatprotec.2010.02.014>.
- [4] J. Jeswiet, F. Micari, G. Hirt, A. Bramley, J. Dufflou, J. Allwood, Asymmetric single point incremental forming of sheet metal, *CIRP Ann. - Manuf. Technol.* 54 (2005) 88–114, [http://dx.doi.org/10.1016/S0007-8506\(07\)60021-3](http://dx.doi.org/10.1016/S0007-8506(07)60021-3).
- [5] I. Bagudanch, M.L. Garcia-Romeu, M. Sabater, Incremental forming of polymers: process parameters selection from the perspective of electric energy consumption and cost, *J. Clean. Prod.* 112 (2016) 1013–1024, <http://dx.doi.org/10.1016/j.jclepro.2015.08.087>.
- [6] G. Hussain, L. Gao, N. Dar, An experimental study on some formability evaluation methods in negative incremental forming, *J. Mater. Process. Technol.* 186 (2007) 45–53, <http://dx.doi.org/10.1016/j.jmatprotec.2006.12.005>.
- [7] G. Hussain, L. Gao, N. Hayat, N.U. Dar, The formability of annealed and pre-aged AA-2024 sheets in single-point incremental forming, *Int. J. Adv. Manuf. Technol.* 46 (2009) 543–549, <http://dx.doi.org/10.1007/s00170-009-2120-x>.
- [8] M.B. Silva, M. Skjoeedt, A.G. Atkins, N. Bay, P.A.F. Martins, Single-point incremental forming and formability–failure diagrams, *J. Strain Anal. Eng. Des.* 43 (2008) 15–35, <http://dx.doi.org/10.1243/03093247JSA340>.
- [9] K. Isik, M.B. Silva, A.E. Tekkaya, P.A.F. Martins, Formability limits by fracture in sheet metal forming, *J. Mater. Process. Technol.* 214 (2014) 1557–1565, <http://dx.doi.org/10.1016/j.jmatprotec.2014.02.026>.
- [10] A.J. Martínez-Donaire, F.J. García-Lomas, C. Vallengano, New approaches to detect the onset of localised necking in sheets under through-thickness strain gradients, *Mater. Des.* 57 (2014) 135–145, <http://dx.doi.org/10.1016/j.matdes.2014.01.012>.
- [11] G. Centeno, I. Bagudanch, A.J. Martínez-Donaire, M.L. Garcia-Romeu, C. Vallengano, Critical analysis of necking and fracture limit strains and forming forces in single-point incremental forming, *Mater. Des.* 63 (2014) 20–29, <http://dx.doi.org/10.1016/j.matdes.2014.05.066>.
- [12] W.C. Emmens, A.H. van den Boogaard, An overview of stabilizing deformation mechanisms in incremental sheet forming, *J. Mater. Process. Technol.* 209 (2009) 3688–3695, <http://dx.doi.org/10.1016/j.jmatprotec.2008.10.003>.
- [13] M.B. Silva, P.S. Nielsen, N. Bay, P.A.F. Martins, Failure mechanisms in single-point incremental forming of metals, *Int. J. Adv. Manuf. Technol.* 56 (2011) 893–903, <http://dx.doi.org/10.1007/s00170-011-3254-1>.
- [14] T. Madeira, C.M.A. Silva, M.B. Silva, P.A.F. Martins, Failure in single point incremental forming, *Int. J. Adv. Manuf. Technol.* (2015) 1471–1479, <http://dx.doi.org/10.1007/s00170-014-6381-7>.
- [15] J.M.C. Soeiro, C.M.A. Silva, M.B. Silva, P.A.F. Martins, Revisiting the formability limits by fracture in sheet metal forming, *J. Mater. Process. Technol.* 217 (2015) 184–192, <http://dx.doi.org/10.1016/j.jmatprotec.2014.11.009>.
- [16] G. Palumbo, M. Brandizzi, Experimental investigations on the single point incremental forming of a titanium alloy component combining static heating with high tool rotation speed, *Mater. Des.* 40 (2012) 43–51, <http://dx.doi.org/10.1016/j.matdes.2012.03.031>.
- [17] G. Ambrogio, L. Filice, F. Gagliardi, Formability of lightweight alloys by hot incremental sheet forming, *Mater. Des.* 34 (2012) 501–508.
- [18] D.K. Xu, B. Lu, T.T. Cao, H. Zhang, J. Chen, H. Long, et al., Enhancement of process capabilities in electrically-assisted double sided incremental forming, *Mater. Des.* 92 (2016) 268–280, <http://dx.doi.org/10.1016/j.matdes.2015.12.009>.
- [19] P.A.F. Martins, L. Kwiatkowski, V. Franzen, A.E. Tekkaya, M. Kleiner, Single point incremental forming of polymers, *CIRP Ann. - Manuf. Technol.* 58 (2009) 229–232, <http://dx.doi.org/10.1016/j.cirp.2009.03.095>.
- [20] T.A. Marques, M.B. Silva, P.A.F. Martins, On the potential of single point incremental forming of sheet polymer parts, *Int. J. Adv. Manuf. Technol.* 60 (2012) 75–86.
- [21] M.B. Silva, T.M. Martinho, P.A.F. Martins, Incremental forming of hole-flanges in polymer sheets, *Mater. Manuf. Process.* 28 (2013) 330–335, <http://dx.doi.org/10.1080/10426914.2012.682488>.
- [22] I. Bagudanch, M.L. Garcia-Romeu, G. Centeno, A. Elías-Zúñiga, J. Ciurana, Forming force and temperature effects on single point incremental forming of polyvinylchloride, *J. Mater. Process. Technol.* 219 (2015) 221–229, <http://dx.doi.org/10.1016/j.jmatprotec.2014.12.004>.
- [23] I. Bagudanch, M. Vives-Mestres, M. Sabater, M.L. Garcia-Romeu, Polymer incremental sheet forming process: temperature analysis using response surface methodology, *Mater. Manuf. Process.* 32 (2017) 44–53, <http://dx.doi.org/10.1080/10426914.2016.1176191>.
- [24] M.A. Davarpanah, A. Mirkouei, X. Yu, R. Malhotra, S. Pilla, Effects of incremental depth and tool rotation on failure modes and microstructural properties in Single Point Incremental Forming of polymers, *J. Mater. Process. Technol.* 222 (2015) 287–300, <http://dx.doi.org/10.1016/j.jmatprotec.2015.03.014>.
- [25] M.A. Davarpanah, S. Bansal, R. Malhotra, Influence of single point incremental forming on mechanical properties and chain orientation in thermoplastic polymers, *J. Manuf. Sci. Eng.* 139 (2017) 21012–21019, <http://dx.doi.org/10.1115/1.4034036>.
- [26] G. Centeno, D. Morales-Palma, B. Gonzalez-Perez-Somarrriba, I. Bagudanch, J.J. Egea-Guerrero, L.M. Gonzalez-Perez, et al., A functional methodology on the manufacturing of customized polymeric cranial prostheses from CAT using SPIF, *Rapid Prototyp. J.* 23 (2017), <http://dx.doi.org/10.1108/RPJ-02-2016-0031>.
- [27] I. Bagudanch, M.L. Garcia-Romeu, I. Ferrer, J. Ciurana, Customized cranial implant manufactured by Incremental Sheet Forming using a biocompatible polymer, *Rapid Prototyp. J.* (2017), <http://dx.doi.org/10.1108/RPJ-06-2016-0089>.
- [28] A.J. Guerra, J. Ciurana, Effect of fibre laser process on in-vitro degradation rate of a polycaprolactone stent a novel degradation study method, *Polym. Degrad. Stab.* 142 (2017) 42–49, <http://dx.doi.org/10.1016/j.polymdegradstab.2017.05.028>.
- [29] L.M. Gonzalez Perez, B. Gonzalez-Perez-Somarrriba, G. Centeno, C. Vallengano, J.F. Montes-Carmona, Evaluation of total allopastic temporo-mandibular joint replacement with two different types of prostheses: a three-year prospective study, *Med. Oral, Patol. Oral Y Cirugía Bucal* 21 (2016) 766–775, <http://dx.doi.org/10.4317/medoral.21189>.
- [30] A.G. Atkins, Fracture in forming, *J. Mater. Process. Technol.* 56 (1996) 609–618, [http://dx.doi.org/10.1016/0924-0136\(95\)01875-1](http://dx.doi.org/10.1016/0924-0136(95)01875-1).

- [31] G. Zhu, Q. Xu, R. Qin, H. Yan, G. Liang, Effect of gamma-radiation on crystallization of polycaprolactone, *Radiat. Phys. Chem.* 74 (2005) 42–50, <http://dx.doi.org/10.1016/j.radphyschem.2004.11.006>.
- [32] S.A.S. Alariqi, A.P. Kumar, B.S.M. Rao, R.P. Singh, Effect of γ -dose rate on crystallinity and morphological changes of γ -sterilized biomedical polypropylene, *Polym. Degrad. Stab.* 94 (2009) 272–277, <http://dx.doi.org/10.1016/j.polymdegradstab.2008.10.027>.
- [33] F.J. Medel, F. García-Álvarez, E. Gómez-Barrera, J.A. Puértolas, Microstructure changes of extruded ultra high molecular weight polyethylene after gamma irradiation and shelf-aging, *Polym. Degrad. Stab.* 88 (2005) 435–443, <http://dx.doi.org/10.1016/j.polymdegradstab.2004.11.015>.

Chapter 7. A functional methodology on the manufacturing of customized polymeric cranial prostheses from CAT using SPIF

Chapter 7 proposes a functional methodology to produce cranial prosthesis in non-biocompatible polymeric sheet (PC), analyzing the formability of a series of polymeric materials in SPIF with the aim of determining the capability of this process to obtain a partial cranial prosthesis.

This study was presented in an article entitled “*A functional methodology on the manufacturing of customized polymeric cranial prostheses from CAT using SPIF*”, published in Rapid Prototyping Journal (Centeno et al., 2017).

Centeno, G., Morales-Palma, D., Gonzalez-Perez-Somarriba, B., Bagudanch, I., Egea-Guerrero, J.J., Gonzalez-Perez, L.M., Garcia-Romeu, M.L., Vallellano, C., 2017. A functional methodology on the manufacturing of customized polymeric cranial prostheses from CAT using SPIF. *Rapid Prototyping Journal* 23(4), 771-780.

<http://www.emeraldinsight.com/doi/full/10.1108/RPJ-02-2016-0031>

<https://doi.org/10.1108/RPJ-02-2016-0031>

© Emerald Publishing Limited 2017

Abstract

Purpose

This paper aims to propose a functional methodology to produce cranial prostheses in polymeric sheet. Within the scope of rapid prototyping technologies, the single-point incremental forming (SPIF) process is used to demonstrate its capabilities to perform customized medical parts.

Design/methodology/approach

The methodology starts processing a patient's computerized axial tomography (CAT) and follows with a computer-aided design and manufacture (CAD/CAM) procedure, which finally permits the successful manufacturing of a customized prosthesis for a specific cranial area.

Findings

The formability of a series of polymeric sheets is determined and the most restrictive material among them is selected for the fabrication of a specific partial cranial prosthesis following the required geometry. The final strain state at the outer surface of the prosthesis is analysed, showing the high potential of SPIF in manufacturing individualized cranial prostheses from polymeric sheet.

Originality/value

This paper proposes a complete methodology to design and manufacture polymer customized cranial prostheses from patients' CATs using the novel SPIF technology. This is an application of a new class of materials to the manufacturing of medical prostheses by SPIF, which to this purpose has been mainly making use of metallic materials so far. Despite the use of polymers to this application is still to be validated from a medical point of view, transparent prostheses can already be of great interest in medical or engineering schools for teaching and research purposes.

Keywords

Rapid prototyping, Computerized axial tomography (CAT), Cranial prostheses, Formability limits, Single-point incremental forming (SPIF)

Chapter 8. Customized cranial implant manufactured by Incremental Sheet Forming using a biocompatible polymer

Chapter 8 demonstrates the feasibility of ISF considering the SPIF and TPIF process variants to produce customized cranial implants using a biocompatible polymer (UHMWPE), ensuring an appropriate geometric accuracy and low cost.

This study was presented in an article entitled “*Customized cranial implant manufactured by Incremental Sheet Forming using a biocompatible polymer*”, accepted for publication in Rapid Prototyping Journal on May 2017, doi: 10.1108/RPJ-06-2016-0089 (Bagudanch et al., 2018)

Customized cranial implant manufactured by Incremental Sheet Forming using a biocompatible polymer

I. Bagudanch, M.L. Garcia-Romeu, I. Ferrer, J. Ciurana

University of Girona - Department of Mechanical Engineering and Industrial Construction, Girona (Spain)

Abstract

Purpose – This work aims to demonstrate the feasibility of Incremental Sheet Forming (ISF), using the most common variants, Single Point Incremental Forming (SPIF) and Two Point Incremental Forming (TPIF), to produce prototypes of customized cranial implants using a biocompatible polymer (ultrahigh molecular weight polyethylene, UHMWPE), ensuring an appropriate geometric accuracy and cost.

Design/methodology/approach – The cranial implant is designed based on computerized tomographies (CT) of the patient, converting them into a 3D model using the software InVesalius. To generate the toolpath for the forming operation Computer Aided Manufacturing (CAM) software is employed. Once the cranial implant is manufactured, a 3D scanning system is used to determine the geometric deviation between the real part and the initial design.

Findings – The results corroborate that it is possible to successfully manufacture a customized cranial implant using ISF, being able to improve the geometric accuracy using the TPIF variant with a negative die.

Originality/value – This paper is one of the first research works in which a customized cranial implant is successfully manufactured using a flexible technology, ISF, and a biocompatible polymer. The use of polymeric implants in cranioplasty is advantageously because of their lightweight, low heat conductivity and mechanical properties similar to bone. Furthermore, the cost of the implant has been calculated considering not only the raw materials and manufacturing time, but also the environmental impact, revealing that it is a cheap process with a low lead-time.

Keywords: Incremental sheet forming, geometric accuracy, 3D scanning, UHMWPE, rapid prototyping, additive manufacturing

Paper type: research paper

1 Introduction

Cranial bone defects can be classified as congenital or acquired, depending on their origin. The acquired defects can be caused by a traumatic injury (being the most common cause), cranial bone tumors originated in the skull bone (primary tumors) or in the neighboring (secondary tumors), osteomyelitis (bone infection) or a cranial bone resorption (Stula, 1984). A surgical procedure, cranioplasty, is utilized to remove and substitute the damaged area of the skull bone using a cranial implant.

Appropriate material to be used as a reconstruction material for the damaged cranial bone should meet the following requirements: biocompatibility, strong but lightweight, easy to shape, low electric and thermal conductivity, enable osteointegration (bone ingrowth), and with a low manufacturing cost (Piitulainen, 2015; Aydin et al., 2011; Bani et al., 1991). Furthermore, the cranial implant should have a mechanical behavior similar to the adjacent bone.

The materials commonly used in cranioplasty can be: (i) autografts, (ii) allografts or (iii) synthetic (Figure 1). An autograft is a bone retrieved from another part of the patient's body such as tibia, sternum and rib. It is worth mentioning that the biocompatibility and osteointegration of autografts are very advantageous, therefore, they are the preferable choice for the skull bone replacement. However, autografts cannot always be used because of the amount needed or the patient's health (Song et al., 2015). Second option is to use allografts (cadaver bone donation) but they have major problems regarding risk of infection (Bonda et al., 2015) and limited strength (Shah et al., 2014).

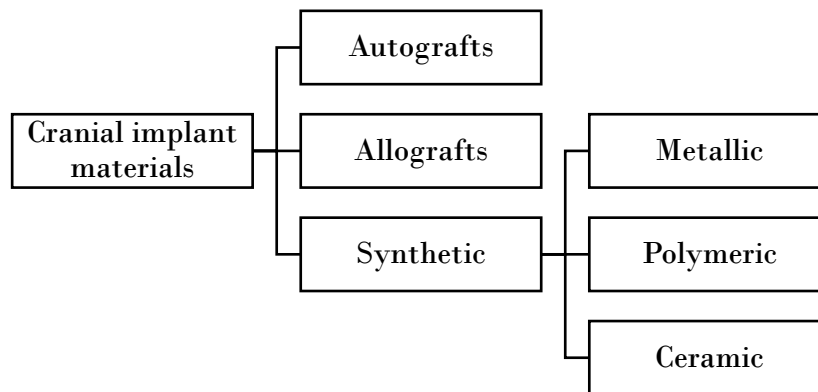


Figure 1. Material classification for cranial bone replacement.

Synthetic materials such as metallic, polymeric and ceramic seem to be good alternative in cranioplasty as they can skip all disadvantages of autografts and allografts. In the former cranioplasty surgeries using metallic materials, the implants were commonly made of gold, silver or stainless steel. Nowadays, titanium alloys, mainly grade 5 surgical alloy Ti6Al4V, are the most widely used metallic materials (Andani et al., 2014). In cranioplasty, titanium can be applied for fixation devices and for the manufacturing of meshed or solid plates. Although it has remarkable biocompatibility and corrosion resistance properties, it has significant drawbacks such as the heat conduction and the higher mechanical properties compared to the cranial bone (elastic modulus of 110 GPa, (Majumdar et al., 2008)). The elastic behavior of the bone depends on its location and quality, but an average elastic modulus of 10.77 ± 9.38 GPa (tested at 1.0 m/s) has been considered as a reference in the literature (Motherway et al., 2009). Due to the differences in the mechanical behavior, a titanium implant may be the cause of contiguous bone fracture under certain stress/strain conditions.

Polymeric materials for cranial implants are nonabsorbable polymers such as polymethylmethacrylate (PMMA), polyetheretherketone (PEEK) and polyethylene (PE), and absorbable polymers such as polycaprolactone (PCL) and polylactic acid (PLA) (Piitulainen, 2015), the nonabsorbable polymers being the most frequently utilized in the clinical procedures. In general terms, polymeric implants have several benefits compared to metallic ones such as lightweight (with a density from 3 to 5 times lower than titanium), low heat conductivity and mechanical properties similar to bone. Main advantages and disadvantages of PMMA, PEEK and PE are summarized in Table 1.

Regarding the ceramics, the most common used for cranial implants is hydroxyapatite (hexagonal form of calcium phosphate). It has very good osteointegration because this material is present in human bone tissue. However, it has poor mechanical properties and the cranial implant is fragile.

Taking into account the aforementioned properties, advantages and disadvantages of the materials, the selection of the most appropriate material to heal the defect of the skull bone has to be done. In the case of using a synthetic material, the next step is to decide which will be the manufacturing process that will be used to obtain the implant from the raw material, ensuring an accurate fitting of the implant with the adjacent bone in order to reduce the surgical procedure time, cost and risk of infection. The development of advanced manufacturing technologies (mainly additive manufacturing, AM, processes) linked with the evolution of digital modelling techniques for tissue reconstruction has resulted in the possibility of producing customized medical implants in a relatively short time-to-market (Maji et al., 2014, Leordean et al., 2015).

Table 1. Comparison of nonabsorbable polymers for cranial implants.

Polymer	Advantages	Disadvantages
PMMA	<ul style="list-style-type: none"> - Biocompatible and biostable - No resorption - Low cost - Elastic modulus similar to the skull bone (between 3.0 and 3.4 GPa) (Rösler et al., 2007) - Large amount of heat is required to mold the part, which could damage surrounding tissues 	<ul style="list-style-type: none"> - Fracture due to impact trauma - Tissue ingrowth is not possible - Migration
PEEK	<ul style="list-style-type: none"> - Strong, inert and biocompatible - Density, mechanical strength and elastic modulus (3.24 GPa) (Barbero, 2010), comparable to cortical bone 	<ul style="list-style-type: none"> - Lack of osteointegration - High cost
PE	<ul style="list-style-type: none"> - Bone ingrowth for porous PE enhancing biocompatibility - Elastic modulus between 0.3 and 1.0 GPa (Rösler et al., 2007) - Easy to shape 	<ul style="list-style-type: none"> - Risk of infection

Additive manufacturing describes a group of technologies based on the same principle of producing 3D objects by adding material layer-by-layer. Some of the most widespread technologies are Selective Laser Sintering (SLS), Direct Metal Laser Sintering (DMLS), Fused Deposition Modeling (FDM), Stereolithography Apparatus (SLA), or 3D Printing

(3DP). In the paper of Jardini et al. (2014) two of these additive manufacturing technologies were used to be able to heal an injured area of the cranial bone. With the data obtained from patient's computerized tomography (CT) it was possible to reconstruct a 3D biomodel of the damaged skull manufactured by 3DP. Then, using DMLS, a titanium implant was fabricated and placed on the 3D biomodel to verify the adjustment. With some of these AM technologies it is not possible to directly manufacture biocompatible implants, because they cannot work using biocompatible materials. However, they can be useful, for example, for the production of customized cranial implant molds. Gopakumar (2004) and Ruiz-Huerta et al. (2016) used FDM machine to obtain a mold made of ABS and PC, respectively. After that, the PMMA implant was cured, polished, sterilized and ready to use in the cranioplasty.

There are other advanced manufacturing processes that can be suitable for producing customized implants, such as Incremental Sheet Forming (ISF), which is a relatively new rapid prototyping technology useful to manufacture full or scale size prototypes as well as small batch or one-of-a-kind sheet products. In ISF, the blank, fixed by a clamping device, is progressively deformed using a hemispherical end-forming tool. The movement of the tool is driven by a CNC machine or robot following the toolpath described by Computer Aided Manufacturing (CAM) software. Depending on the existence or absence of a die, or support post, the two main variants of the process are identified as Single Point Incremental Forming (SPIF) or Two Point Incremental Forming (TPIF). In turn, the TPIF variant can be classified as negative or positive. Furthermore, in TPIF it is possible to use a full die or a partial die.

ISF technology has been mainly applied in the automotive and aeronautic sectors, either to obtain functional parts or prototypes. However, there are other fields that have growing interest in this manufacturing process; such as the biomedical field, which requires a technology capable to produce unique parts in a short time and at reasonable cost. Several works in the literature used ISF to produce ankle prosthesis (Ambrogio et al., 2005), cranial implants (Duflou et al., 2005; Göttmann et al., 2012; Lu et al., 2014), palate implant (Tanaka et al., 2007), a part for a knee implant (Oleksik et al., 2010) and most recently several maxillofacial implants (Duflou et al., 2013; Araújo et al., 2014). There are also some preliminary studies that use ISF for producing medical devices, such as mesoforceps for biopsy (Garcia-Romeu et al., 2012). All of these applications have been manufactured using metallic materials. These biocompatible metallic materials such as titanium are very difficult to deform at room temperature. Therefore, it is necessary to use an additional heating system to increase the formability in order to be able to produce the desired part.

Nowadays, there are few publications dealing with the production of any biomedical device or prosthesis manufactured with ISF using biocompatible polymers. Fiorentino et al. (2012) manufactured a palate prosthesis using a titanium alloy and PCL (polycaprolactone). Although their results were promising an optimization of the process parameters should be done in order to increase the accuracy of the part. Customized cranial implants manufactured in polymeric sheet by SPIF can be found in the literature, which are mainly focused on the evaluation of the formability (Centeno et al., 2015) and the accuracy of cranial prostheses in polycarbonate (Bagudanch et al., 2014) or polycaprolactone

(Bagudanch et al., 2015a). However, in order to achieve better accuracy results the TPIF variant should be used. Thus, a niche market where the use of biocompatible polymers manufactured by ISF can provide remarkable advantages in terms of low cost and reduced time to market has been identified.

The aim of the present paper is to demonstrate the feasibility of the ISF technology, including SPIF and TPIF process variants, to produce prototypes of a customized cranial implant with biocompatible polymer (ultrahigh molecular weight polyethylene, UHMWPE) to get an appropriate geometric accuracy (section 3.1) in a short time-to-market and low cost (section 3.2). For the present case study, the cost of the customized implant is calculated adapting the methodology proposed by Branker (2011) for manufacturing simple geometries in SPIF and taking into account additional terms related to the particularities of the customized implant design and manufacturing.

2 Methodology

The methodology followed in order to achieve the objectives of the paper is summarized in Figure 2 and explained in detail in the following subsections. Note that it is not necessary for the die fabrication stage when SPIF technology is used.

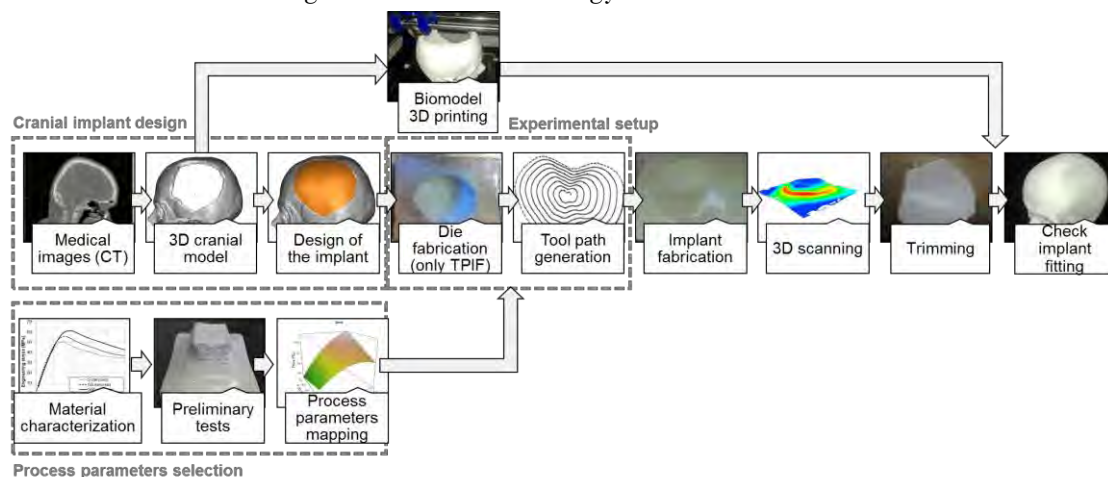


Figure 2. Methodology for manufacturing a customized cranial implant by ISF.

2.1 Cranial implant design

In order to produce a customized cranial implant, the first step is to obtain medical images using computerized tomography (CT). These images are processed in specific software called InVesalius to obtain the 3D model. The images obtained from the CT were exported using DICOM (Digital Imaging Communication in Medicine) protocol. InVesalius recognizes the different tissues (cortical or trabecular bone, blood, muscle, among others) obtained from the CT images, defining each one according to the Hounsfield scale. The model generated from the skull bone was exported as a StL file. Using Rhinoceros® and following the BioCAD methodology (Kemmoku et al., 2012) it was possible to have the geometry of the healthy skull bone. The cranial implant was designed following the anatomic lines of the healthy zone (Figure 3) and the CAD model in a sheet form was obtained (Figure 4) with some additional curvatures required to progressively reach the desired shape in the ISF

process. After forming the sheet, the cranial implant must be cut in order to eliminate the excess of material.

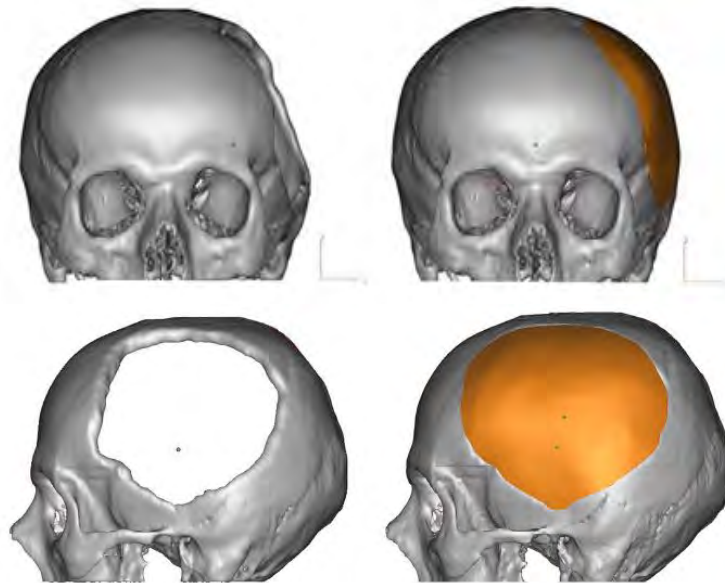


Figure 3. Cranial fracture (left) and prosthesis (right). Source: Centro de Tecnologia de Informação Renato Archer (CTI).

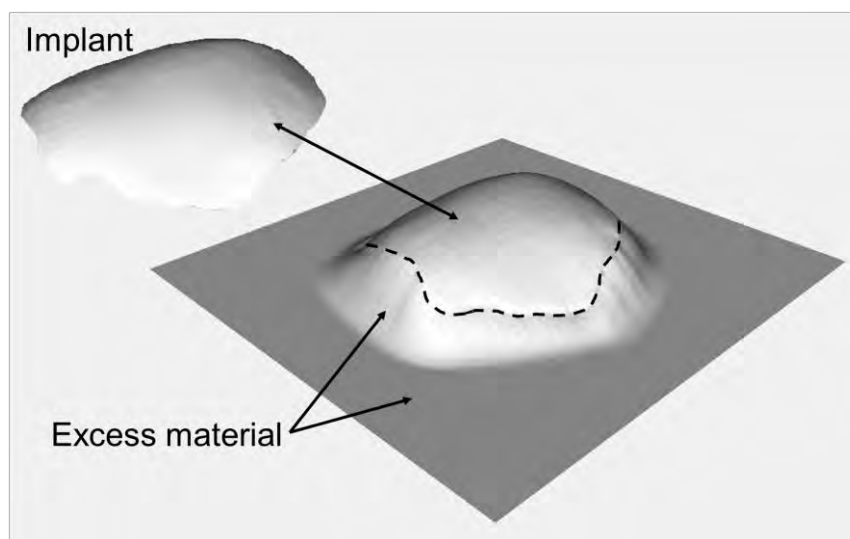


Figure 4. CAD model of the cranial implant.

2.2 Material

In this paper, 200x200 mm UHMWPE sheets have been used in order to produce the desired cranial implant. The thickness of the sheets is 2 mm. UHMWPE is a biocompatible polymer, commonly used for orthopedic applications. It is a lightweight material, with good wear resistance and chemical stability (Firouzi et al., 2014). This material is mainly processed using the compression molding technique, requiring high temperature (around 300°C) and long time (approximately 3h) to obtain the part (Huang et al., 2014).

2.3 Experimental setup

The ISF experimental tests have been carried out on a Kondia® HS1000 3-axis milling machine equipped with Fidia® numerical control. For the SPIF configuration (Figure 5a), toggle clamps are used for the sheet clamping system. In the case of TPIF, the cranial implant die is manufactured using wood agglomerate (Figure 5b), in a Deckel Maho 64V Linear milling machine. This die is bolted in the machine work table. In order to reduce friction during the forming process, lubricant for cold forming has been applied over the upper surface of the blanks. The tool path has been generated using CAM software (PTC Creo) considering a contouring tool trajectory.

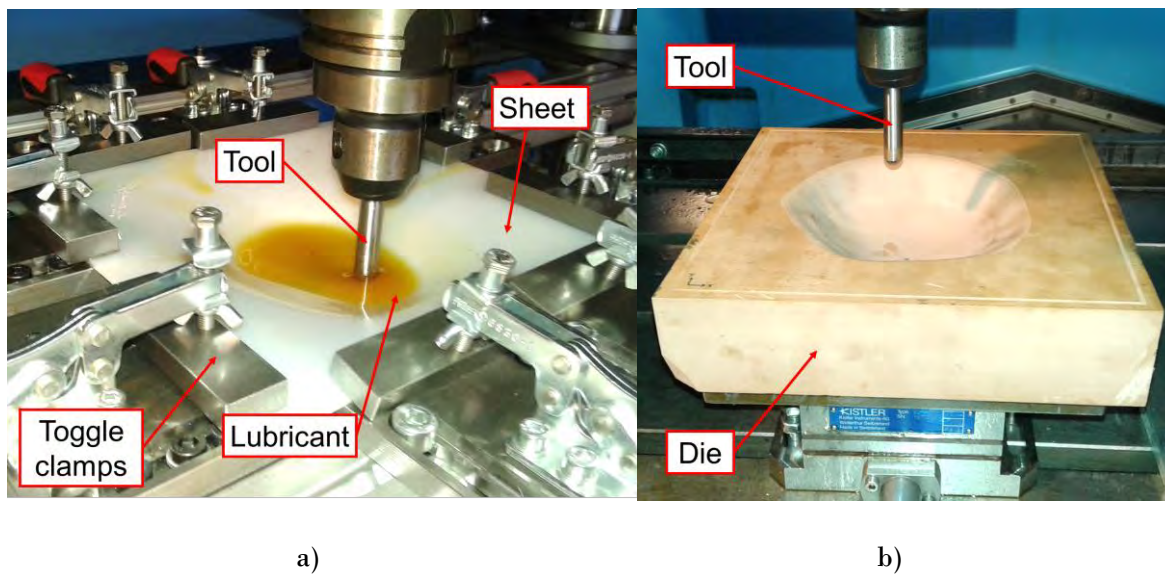


Figure 5. Setup for manufacturing the cranial implant using SPIF (a) and TPIF (b) variants.

2.4 Process parameters selection

The process parameters selection has been done according to results obtained in previous research works (Bagudanch et al., 2015b; Bagudanch et al., 2016a; Bagudanch et al., 2016b), where it was demonstrated that the variation of feed rate and step down does not significantly influence the material formability or the geometric accuracy obtained in polymers formed by ISF. Therefore, in order to manufacture the cranial implants the values are chosen aiming to reduce the forming time and costs, i.e. 3000 mm/min feed rate and 0.5 mm step down. As revealed in the same literature, the spindle speed is the factor with the major influence on the results concerning forming force, maximum temperature, surface roughness and formability. In this regard, two cranial implants for each ISF variant have been manufactured considering two different spindle speeds (free and 2000 rpm) to determine its influence on the geometric accuracy. Two replicas of each test have been carried out. A hemispherical tool of 10 mm diameter made of Vanadis 23 has been used for all the tests.

2.5 Scanning system

Once the parts have been fabricated, mobile 3D scanner which employs Structured Light technology (David SLS-2) is used to acquire the final dimensions and compare them with the theoretical CAD model. This comparison is done using Shape Analysis Library (SAL 3D) software and the deviations between both surfaces (the real and the theoretical one) are analyzed in order to determine the geometric accuracy of the process.

2.6 Biomodel

The biomodel of the patient's skull has been manufactured using 3DP technology (RepRap BCN3D+) in PLA. The biomodel is used to check the fitting of the customized cranial implant after trimming and removing the excess material.

3 Results and discussion

3.1 Geometric accuracy

Figure 6 and Figure 7 depict the geometric accuracy obtained for the cranial implants manufactured by SPIF and TPIF respectively, using free spindle speed (Figure 6a and 7a) and spindle speed fixed at 2000 rpm (Figure 6b and 7b). On the left side of the images the top view of the implants and on the right side the 3D perspective are shown. The colors represent zones which have different deviation ranges (in mm) of the real part referred to the theoretical one. Negative values indicate that the manufactured part has not reached the designed depth while positive values indicate that the real part has overpassed the desired profile.

Using the simplest ISF variant, SPIF (Figure 6), the cranial implants are far from the desired geometry, with deviations ranging between -10 and 6 mm (spindle speed of 2000 rpm) and -7 and 7 mm (free spindle speed), due to the extremely significant springback effect that this polymeric material exhibits. In TPIF (Figure 7), as it can be observed in both cases, the deviation varies from -4.5 to 4.5 mm, which is still unacceptable considering that the tolerance process window for ISF when using metallic materials is 2 mm (Allwood et al., 2005). It is, however, worth noting that in the case of using a higher spindle speed (Figure 7b) there are less extreme regions (dark blue or red), meaning that the implant is closer to the desired geometry and that the springback effect, which appears when the sheet is released from the clamping system, is slightly reduced.

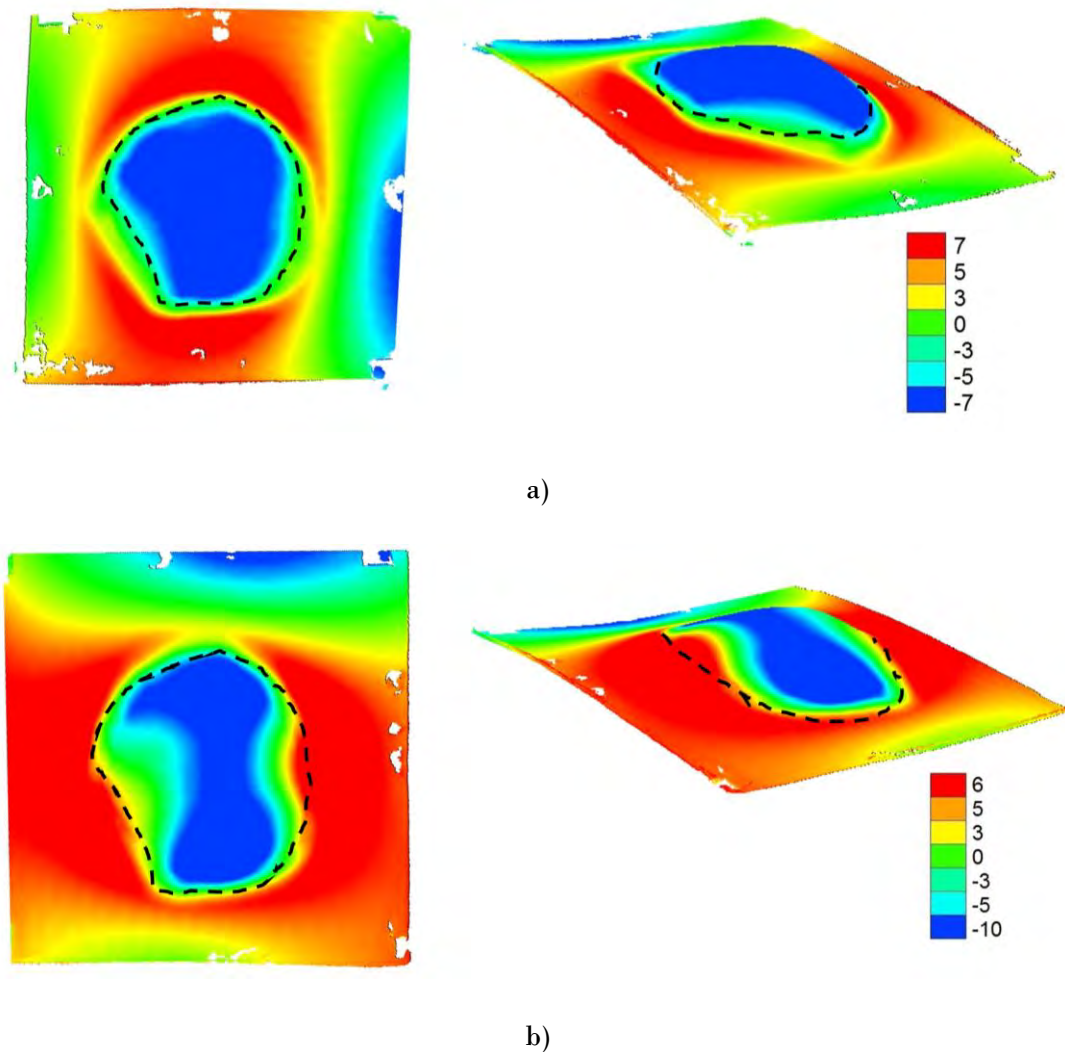


Figure 6. Geometric deviation (in mm) for the cranial implant manufactured using SPIF at a free spindle speed (a) and at 2000 rpm spindle speed (b).

It should be considered that the excess material shown in Figure 4 must be cut in order to finally obtain the implant which is marked as dashed line. This post-process operation will eliminate some of the zones with higher deviations. Figure 8 shows the geometric deviations measured after trimming the cranial implants manufactured at 2000 rpm spindle speed for both variants, SPIF and TPIF, Figure 8a and 8b respectively. It has been possible to improve the global accuracy of the implants, mainly in the case of TPIF, whereas the SPIF variant still remains on ± 4 mm deviation. Therefore, the use of the simplest variant is not recommended for manufacturing customized cranial implants due to the significant disagreement between the designed and manufactured implants.

The geometric tolerances for this kind of application are usually wide, because one of the implant's objective is to repair the damaged area ensuring an appropriate aesthetic finishing, considering the anatomic lines of the patient and being as symmetric as possible. Therefore, even though the deviations of the manufactured implants respect to the designed one are around ± 1.5 mm in some parts of the geometry, it could still be suitable for cranioplasty, as observed in Figure 9, since the aesthetical differences to the human eye will be practically negligible and the psychological and emotional repercussions for the patient

will be improved. Table 2 summarizes the geometric deviations obtained in the cranial implants manufactured in this paper before and after the trimming operation.

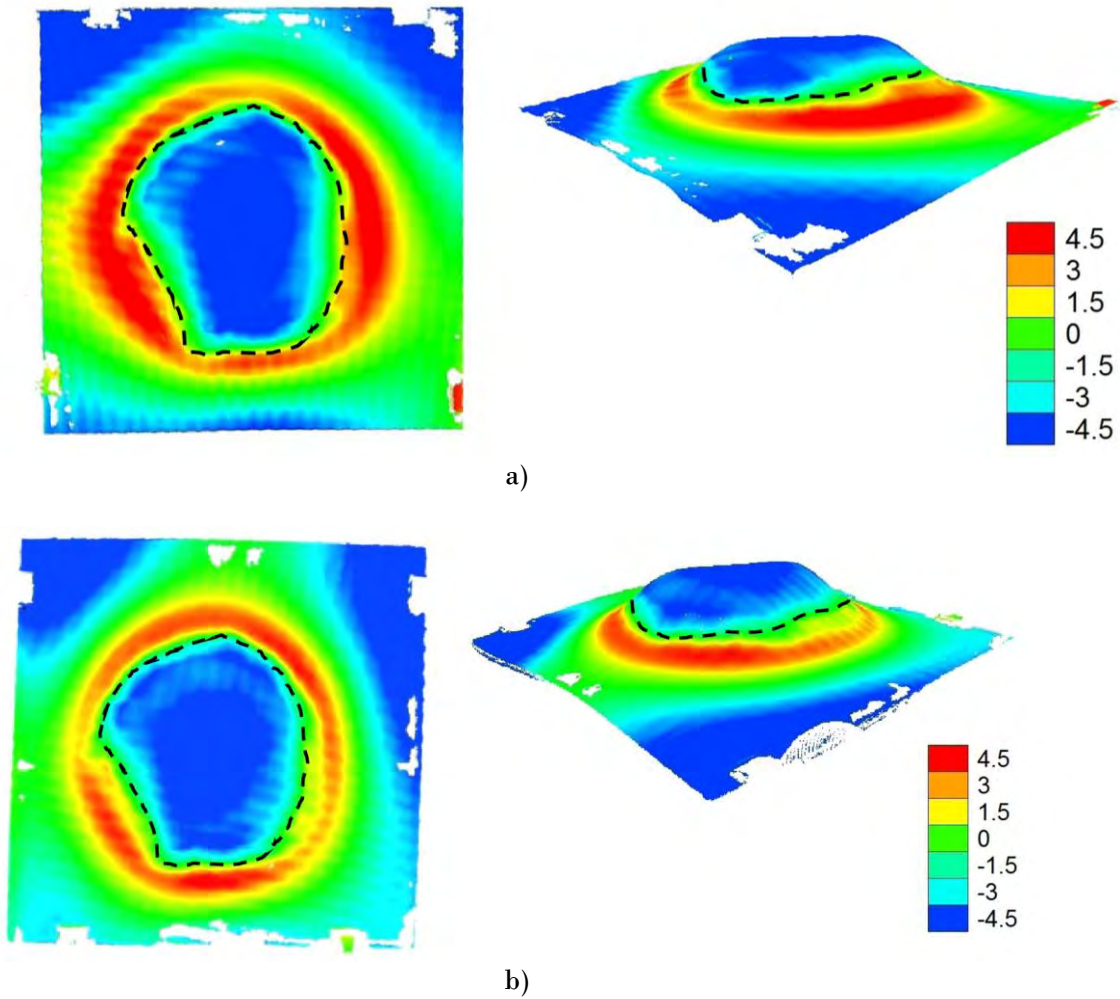


Figure 7. Geometric deviation (in mm) for the cranial implant manufactured using TPIF at a free spindle speed (a) and at 2000 rpm spindle speed (b).

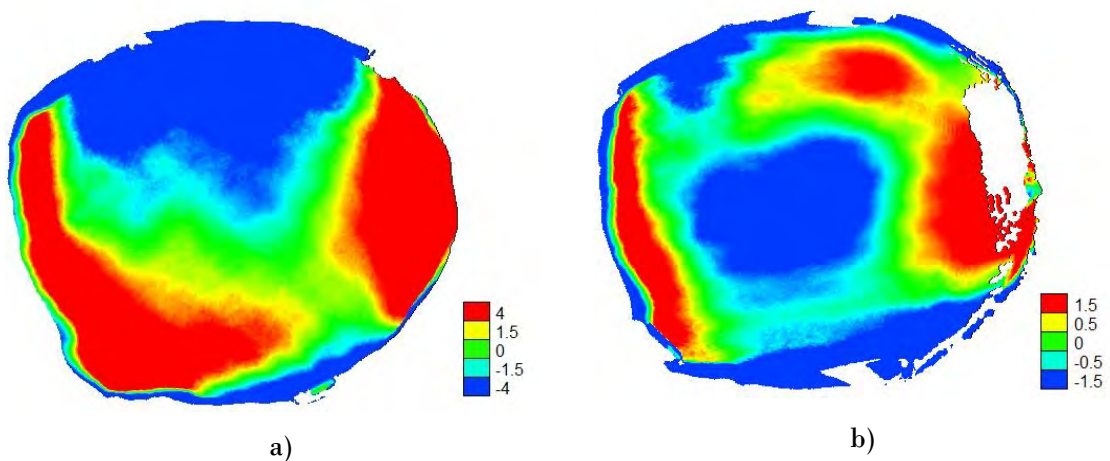


Figure 8. Geometric deviation (in mm) for the trimmed cranial implants manufactured at 2000 rpm spindle speed using SPIF (a) and TPIF (b).

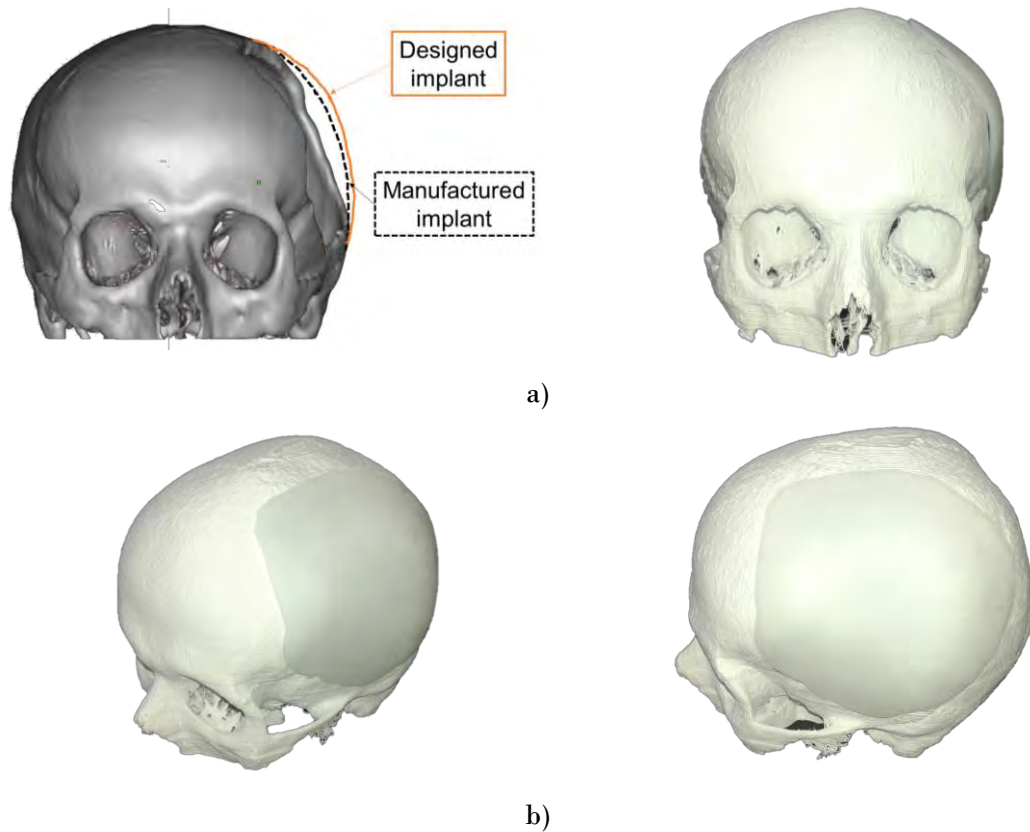


Figure 9. a) Front view showing the deviation between the designed and manufactured implants. b) Adjustment of the customized implant to the biomodel.

Table 2. Summary of the deviation ranges obtained in all the experiments.

		Spindle speed	
		Free	2000 rpm
SPIF	Before trimming	± 7 mm	From -10 to 6 mm
	After trimming	± 4 mm	± 4 mm
TPIF	Before trimming	± 4.5 mm	± 4.5 mm
	After trimming	± 2 mm	± 1.5 mm

3.2 Economic cost

In the previous section it has been demonstrated that the ISF technology is able to fulfill the accuracy requirements for a customized cranial implant. It is also important to focus on the cost, in order to ensure that the ISF approach meets not only the technological requirements but the economic viability as well. Recently, Branker (2011) proposed the most complete and accurate equation for estimating the ISF cost to date, considering the forming costs (C_f), the setup costs (C_s), the workpiece handling costs (C_l), the tooling costs (C_t), the direct material costs (C_{MD}), the indirect material costs (C_{MID}), the energy consumed during the process (C_{ED}), the ancillary energy (C_{EA}) and the environmental burden (C_{env}). However, this is a good approach for the SPIF variant to produce simple geometries, for a customized geometry it should include an additional cost due to the design stage of a customized implant (C_{design}). The trimming cost (C_{cut}) and the biomodel fabrication (C_{bm}) have been also taken into account (Equation (1)). The cost for the TPIF variant (C_{TPIF}) will be the SPIF cost plus the die manufacturing cost using a milling operation and the die

material cost (C_{die})(Equation (2)). The cranial implant cost manufactured by ISF is summarized in Table 3.

$$C_{SPIF} = C_f + C_s + C_l + C_t + C_{MD} + C_{MID} + C_{ED} + C_{EA} + C_{env} + C_{design} + C_{cut} + C_{bm} \quad (1)$$

$$C_{TPIF} = C_{SPIF} + C_{Die} \quad (2)$$

The contribution of each cost to the total ISF cost for a customized cranial implant is shown in Figure 10. The cost for the SPIF variant is around 360€ while the cost for TPIF is 520€. It is evident that the implants manufactured with SPIF will be cheaper because the die manufacturing has a significant cost contribution. However, this increase of the cost is balanced with parts accuracy improvement. It is also worth noting that the cost can be easily reduced if the 3D biomodel is not manufactured, nevertheless its use is recommended for ensuring an adequate fitting of the implant. Although the implant sterilization cost must be also considered, which will increase the total cost, it is remarkable that the TPIF process is a promising alternative for manufacturing customized polymer implants in a short time (1 day approximately) and at a competitive cost, since currently the customized implants cost for cranioplasty range from 300€ to 5000€ depending on the implant material and defect size (Sundseth and Berg-Johnsen, 2013).

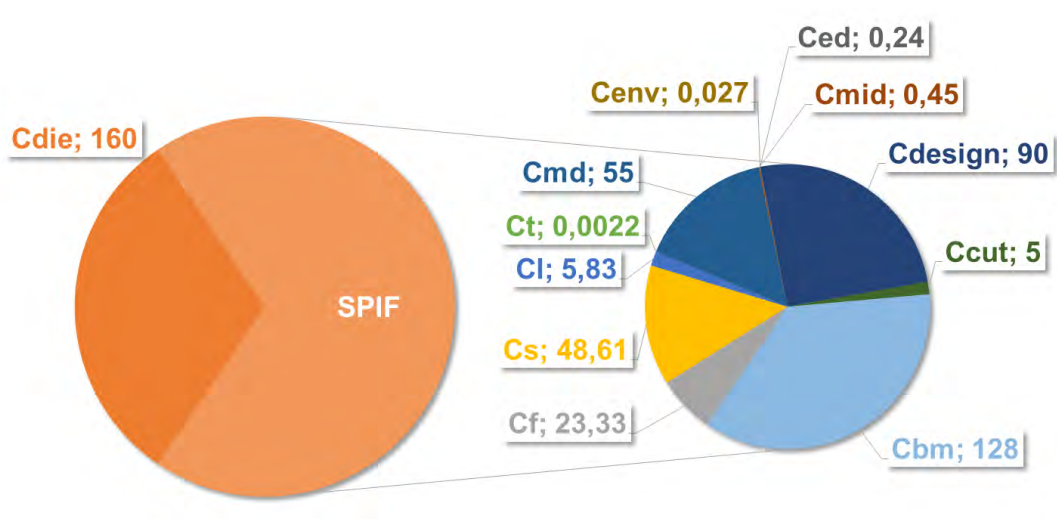


Figure 10. Contribution of the cost model items to total cost.

Table 3. Parameters used to calculate the cost of the cranial implant.

Cost (€)	Parameter	Value	Observations
$C_f = t_f \cdot K_f = 23.33$	t_f (s)	1200	Time needed to produce each part.
	K_f (€/h)	70	This value considers the investment cost of the machine, the useful life and indirect costs such as rent of the building, taxes, etc.
$C_s = \frac{K_f}{N_p} \cdot t_s = 48.61$	N_p (u)	1	The total number of parts produced.
	t_s (s)	2500	Time needed for fixing the framework and turning on the machine.
$C_l = t_l \cdot K_f = 5.83$	t_l (s)	300	Time required for loading/unloading the workpiece.
$C_t = (K_f \cdot t_c + K_t) \cdot \frac{t_f}{T} = 0.0022$	T (h)	10000	In the present paper the time required to change the tool (t_c) is not considered because, for a single part, only one tool is required. T is the tool life and K_t the tool cost.
	K_t (€/u)	65	
$C_{MD} = K_M \cdot MD = 55$	K_M (€/u)	55	In Branker (2011) K_M (material cost) is given as \$/kg, therefore, in order to obtain C_{MD} this value is multiplied by the amount of material used in kg (MD). In the present case, the material cost is given in €/sheet, thus, $K_M=C_{MD}$.
$C_{MID} = K_{LOf} \cdot LO_f + K_{LO} \cdot LO = 0.45$	K_{LOf} (€/L)	15	To calculate the indirect material costs, the quantity of machine lubricant used (LO) has been ignored because the lubricant use rate is close to zero, therefore, the contribution on the total cost will be negligible. Only the forming lubricant is needed (LO_f) and its cost (K_{LOf}).
	LO_f (mL)	30	
$C_{ED} = K_E \cdot E_D = 0.24$	K_E (€/kWh)	0.18	Electricity cost.
	E (kJ)	4846.32	In the present paper, the measurements of energy consumed include the direct energy (E_D , from the electricity used in the forming process) and the ancillary energy (E_A , associated with peripheral equipment such as cooling of the machine, CNC computer, etc.). The energy consumed (in J) has been calculated using an empirical equation obtained in a previous work of the authors (Bagudanch et al., 2016a) which depends on the spindle speed and the forming time. $E=(2854.6+0.592 \cdot S) \cdot t_f$
$C_{env} = (E_{CO_2} + LO_{fCO_2} + LO_{CO_2} + TL_{CO_2} + ML_{CO_2}) \cdot k_{CO_2} = 0.027$	E_{CO_2} (kg CO ₂)	0.4986	Calculated using E (kJ) and the value obtained using the CES equation, 102.88 kg CO ₂ /GJ (Bagudanch et al., 2016a).
	LO_{fCO_2} (kg CO ₂)	0.0989	The emission intensity of the forming lubricant has been determined as 3.295 kg CO ₂ /L (Branker, 2011). The contribution of the CO ₂ emissions of the machine lubricant was ignored (LO_{CO_2}).
	TL_{CO_2} (kg CO ₂)	0.3292	The emission intensity of the forming tool has been determined as 6.4 kg CO ₂ /kg (Branker, 2011). The weight of the 10 mm diameter tool is 51.44g.
	ML_{CO_2} (kg CO ₂)	0.1662	In order to produce UHMWPE the carbon emissions are 1.96 kg CO ₂ /kg UHMWPE (Plastics Europe, 2008). The weight of a 200x200x2 mm sheet is 84.80 g.
	k_{CO_2} (€/kg CO ₂)	0.025	Carbon cost.
$C_{design} = t_{design} \cdot K_{design} = 90$	t_{design} (h)	3	Time needed to design a customized implant from the DICOM files obtained in a CT.
	K_{design} (€/h)	30	Design cost rate.
$C_{cut} = t_{cut} \cdot K_{cut} = 5$	t_{cut} (h)	0.25	Time needed to trim the cranial implant
	K_{cut} (€/h)	20	Trimming cost rate
$C_{bm} = t_{bm} \cdot K_{bm} + K_{PLA} \cdot MD_{PLA} = 128$	t_{bm} (h)	24	Time needed to 3D print the cranial biomodel.
	K_{bm} (€/h)	5	Biomodel manufacturing cost rate.
	K_{PLA} (€/kg)	20	Cost of the biomodel raw material (polylactic acid, PLA).
	MD_{PLA} (kg)	0.4	Direct material used for manufacturing the biomodel.
$C_{SPIF} = 356.49$			
$C_{Die} = t_{Mill} \cdot K_{Mill} + K_{Die} = 160$	t_{Mill} (h)	2	Time needed to manufacture the die in a milling machine.
	K_{Mill} (€/h)	70	This value considers the investment cost of the milling machine, the useful life and indirect costs such as rent of the building, taxes, etc.
	K_{Die} (€)	20	Cost of the die's raw material.
$C_{TPIF} = 516.49$			

4 Conclusions

The present paper has focused on the capability of the ISF technology for manufacturing customized cranial implants using biocompatible polymers. ISF is a very flexible technology, having a great potential in the biomedical field, and polymeric materials can be easily formed without additional heating systems. Furthermore, the use of polymers in cranioplasty is advantageously because they have mechanical properties more similar to the cranial bone, they are less expensive and more lightweight.

Two cranial implants have been produced for each process variant, modifying spindle speed as the most important process parameters in incrementally formed parts using polymers. Using a 3D scanning system it has been shown that with higher spindle speeds and TPIF it is possible to obtain more accurate parts. This fact is due to the heat originated from the friction between the tool and the sheet, increasing material formability and reducing the springback effect.

In the case of severe cranial injuries, the discrepancies between the manufactured and designed implants are not a limiting factor, especially if these deviations are of about ± 1.5 mm (which were the better results found in the present paper). Here, the priority is to heal the damaged area to protect the brain, ensure the symmetry in the patient's skull and improve the emotional and psychological repercussion for the patient.

Additionally, the cost of producing a customized cranial implant, since the design stage until its fabrication using ISF, has been calculated considering all the involved factors (energy, raw material, processing time, etc.), demonstrating that TPIF is an interesting approach for repairing cranial defects at a low cost and low lead time.

Future work will be focused on: (i) producing the cranial implants in TPIF using a full positive die, (ii) the development of tool-path correction strategies able to decrease the geometric deviation of the manufactured implants, ensuring a better fitting in the health skull bone, and (iii) besides the research in order to improve the process and the part obtained it is also necessary to verify the implant's behavior in vivo, for example, in animals.

5 References

Allwood, J.M., King, G.P.F. and Duflou, J. (2005), "A structured search for applications of the incremental sheet-forming process by product segmentation", *Proceedings of the Institution of Mechanical Engineers, Part B: Journal of Engineering Manufacture*, Vol. 219, pp. 239–244.

Ambrogio, G., Denapoli, L., Filice, L., Gagliardi, F. and Muzzupappa, M. (2005), "Application of Incremental Forming process for high customised medical product manufacturing", *Journal of Materials Processing Technology*, Vol. 162-163, pp. 156-162.

Andani, MT., Moghaddam, NS., Haberland, C., Dean, D., Miller, MJ. and Elahinia, M. (2014), "Metals for bone implants. Part 1. Powder metallurgy and implant rendering", *Acta Biomaterialia*, Vol. 10 No. 10, pp. 4058-4070.

Araújo, R., Teixeira, P., Silva, M.B., Reis, Al. and Martins, P.A.F. (2013), "Single point incremental forming of a medical implant", *Key Engineering Materials*, Vol. 544-557, pp. 1388-1393.

Aydin, S., Kucukyuruk, B., Abuzayed, B., Aydin, S. and Zihni Sanus, G. (2011), "Cranioplasty: review of materials and techniques", *Journal of Neurosciences in Rural Practice*, Vol. 2 No. 2, pp. 162-167.

Bagudanch, I., Garcia-Romeu, M.L. and Ferrer, I. (2014), "Manufacturing of thermoplastic cranial prosthesis by incremental sheet forming", in *Proceedings of the 2nd International Conference on Design and Processes for Medical Devices (PROMED)*, in Monterrey, Mexico, 2014.

Bagudanch I., Lozano M., Puigpinós L., Sabater M., Elizalde L.E., Elías-Zúñiga A. and Garcia-Romeu M.L. (2015a), "Manufacturing of polymeric biocompatible cranial geometry by single point incremental forming", *Procedia Engineering*, Vol. 132, pp. 267-273.

Bagudanch, I., Garcia-Romeu, M.L., Centeno, G., Elías-Zúñiga, A. and Ciurana, J. (2015b), "Forming force and temperature effects on single point incremental forming of polyvinylchloride", *Journal of materials processing technology*, Vol. 219, pp. 221-229.

Bagudanch, I., Sabater, M. and Garcia-Romeu, M.L. (2016a), "Incremental forming of polymers: process parameters selection from the perspective of electric energy consumption and cost", *Journal of Cleaner Production*, Vol. 112, pp. 1013-1024.

Bagudanch, I., Vives-Mestres, M., Sabater, M., Garcia-Romeu, M.L. (2016b), "Polymer incremental sheet forming process: temperature analysis using response surface methodology", *Materials and Manufacturing Processes*, in press.

Bani, G.G., Torcello, L., Ferraresi, S., Griffini, C., Pinto, N. and Cassinari, V. (1991), "Skull bone defects, preliminary results using a new prosthesis", *Acta Neurochirurgica*, Vol. 109, pp. 72-75.

Barbero, E.J. (2010), "Introduction to composite materials design, second edition". CRC Press.

Bonda, D.J., Manjila, S., Selman, W.R. and Dean, D. (2015), "The recent revolution in the design and manufacture of cranial implants: modern advancements and future directions". *Neurosurgery*, Vol. 77 No. 5, pp. 814-824.

Branker, K. (2011), "A study of energy, carbon dioxide emissions and economics in machining: milling and single point incremental forming", *PhD thesis*, Queen's University, Kingston, Ontario, Canada.

Centeno, G., Morales-Palma, D., Bagudanch I., Martínze-Donaire, A.J., Garcia-Romeu M.L., Vallellano, C. (2015) “Experimental strain analysis on the manufacturing of polymer cranial prosthesis by single point incremental forming”, *Proceedings of the Manufacturing Engineering Society International Conference, MESIC 2015*, in Barcelona, Spain, 2015.

Duflou, J.R., Lauwers, B., Verbert, J., Gelaude, F. and Tunckol, Y. (2005), “Medical application of single point incremental forming: Cranial plate manufacturing”, *Virtual Modelling and Rapid Manufacturing - Advanced Research in Virtual and Rapid Prototyping*, pp. 161-166.

Duflou, J.R., Behera, A.K., Vanhove, H. and Bertol, L.S. (2013), “Manufacture of accurate titanium cranio-facial implants with high forming angle using single point incremental forming”, *Key Engineering Materials*, Vol. 549, pp. 223-230.

Fiorentino, A., Marenza, G.P., Marzi, R., Ceretti, E., Kemmoku, D.T. and Lopes da Silva, J.V. (2012), “Rapid prototyping techniques for individualized medical prosthesis manufacturing”, *Proceedings of the 5th International Conference on Advanced Research and Rapid Prototyping*, pp. 589-594.

Firouzi, D., Youssef, A., Amer, M., Srouji, R., Amleh, A., Foucher, D.A. and Bougherara, H. (2014), “A new technique to improve the mechanical and biological performance of ultra high molecular weight polyethylene using a nylon coating”, *Journal of the mechanical behaviour of biomedical materials*, Vol. 32, pp. 198-209.

Garcia-Romeu, M.L., Perez-Santiago, R., Bagudanch, I. and Puigpinós, L. (2012), “Fabrication of a Biopsy Micro-Forceps prototype with Two Point Incremental Forming”, *Proceedings of the 1st International Conference on Design and Processes for Medical Devices (PROMED)*, pp. 103-106.

Gopakumar, S. (2004), “RP in medicine: a case study in cranial reconstructive surgery”, *Rapid Prototyping Journal*, Vol. 10 No. 3, pp. 207-211.

Göttmann, A. Korinth, M., Taleb-Araghi, B., Bambach, M. and Hirt, G. (2012), “Manufacturing of cranial implants using incremental sheet metal forming”, *Proceedings of the 1st International Conference on Design and Processes for Medical Devices (PROMED)*, pp. 287-290.

Huang, Y.F., Xu, J.Z., Li, J.S., He, B.X., Xu, L. and Li, Z.M. (2014), “Mechanical properties and biocompatibility of melt processed, self-reinforced ultrahigh molecular weight polyethylene”, *Biomaterials*, Vol. 35 No.25, pp. 6687-6697.

Jardini, A.L., Larosa, M.A., Filho, R.M., Carvalho Zavaglia, C.A., Bernardes, L.F., Lambert, C.S., Calderoni, D.R. and Kharmandayan, P. (2014), “Cranial reconstruction: 3D biomodel and custom-built implant created using additive manufacturing”, *Journal of Cranial-maxillofacial Surgery*, Vol. 42 No. 8, pp. 1877-1884.

Kemmoku, D.T., Laureti, C.A.R., Noritomi, P.Y. and Silva, J.V.L. (2012), “BioCAD techniques: example on maxilla for rapid expansion simulation”, *Innovative Developments in Virtual and Physical Prototyping*, pp. 715-718.

Maji P.K., Banerjee A.J., Banerjee P.S. and Karmakar S. (2014), “Additive manufacturing in prosthesis development - a case study”, *Rapid Prototyping Journal*, Vol. 20 No. 6, pp. 480-489.

Majumdar, P., Singh, S.B. and Chakraborty, M. (2008), “Elastic modulus of biomedical titanium alloys by nano-indentation and ultrasonic techniques – a comparative study”, *Materials and Science Engineering: A*, Vol. 489 No. 1-2, pp. 419-425.

Motherway, J.A., Verschuere, P., Van der Perre, G., Vander Sloten, J. and Glichrist, M.D. (2009), “The mechanical properties of cranial bone: the effect of loading rate and cranial sampling position”, *Journal of Biomechanics*, Vol. 42 No. 13, pp. 2129-2135.

Leordean D., Dudescu C., Marcu T., Berce P. and Balci N. (2015), "Customized implants with specific properties, made by selective laser melting", *Rapid Prototyping Journal*, Vol. 21 No. 1, pp. 98-104.

Lu, B., Ou, H., Shi, S.Q., Long, H. and Chen, J. (2014), “Titanium based cranial reconstruction using incremental sheet forming”, *International Journal of Material Forming*, doi. 10.1007/s12289-014-1205-8.

Oleksik, V., Pascu, A., Deac, C., Fleaca, R., Roman, M. and Bologa, O. (2010), “The influence of geometrical parameters on the incremental forming process for knee implants analyzed by numerical simulation”, *AIP Conference Proceedings*, Vol. 1252, pp. 1208-1215.

Piitulainen, J. (2015), “Reconstruction of cranial bone defects with fiber-reinforced composite-bioactive glass implants”, *PhD thesis*, University of Turku, Finland.

Plastics Europe (2008), “High density polyethylene HDPE”, *Eco-profiles of the European Plastics Industry*. Brussels, November 2008.

Rösler, J., Harders, H. and Bäker, M. (2007), “Mechanical Behaviour of Engineering Materials. Metals, Ceramics, Polymers and Composites”. Berlin, Springer-Verlag.

Ruiz-Huerta, L., Almanza-Arjona, Y.C., Caballero-Ruiz, A., Castro-Espinosa, H.A., Díaz-Aguirre, C.M. and Echevarría y Pérez, E. (2016), "CAD and AM-fabricated moulds for fast cranio-maxillofacial implants manufacture", *Rapid Prototyping Journal*, Vol. 22 Iss 1 pp. 31 – 39.

Shah, A.M., Jung, H. and Skirboll, S. (2014), “Materials used in cranioplasty: a history and analysis”, *Neurosurgical Focus*, Vol. 36 No. 4, pp. 1-7.

Song, T., Qiu, Z.Y. and Cui, F.Z. (2015), “Biomaterials for reconstruction of cranial defects”, *Frontiers of Materials Science*, Vol. 9 No. 4, pp. 346-354.

Stula, D. (1984), "Cranioplasty: Indications, techniques and results". Wien; New York: Springer-Verlag.

Sundseth, J. and Berg-Johnsen, J. (2013), "Prefabricated patient-matched cranial implants for reconstruction of large skull defects", *Journal of Central Nervous System Disease*, Vol. 5, pp. 19-24.

Tanaka, S., Nakamura, T., Hayakawa, K., Nakamura, H. and Motomura, K. (2007), "Residual stress in sheet metal parts made by incremental forming process", *AIP Conference Proceedings*, Vol. 908, pp. 775-780.

Chapter 9. Discussion

This chapter will compare and discuss some of the main findings of each paper presented as separate chapters (from 3 to 8). The discussion will be divided in two main sections: the first one is related to the study of the process parameters influence in polymer SPIF and the second one is about the application of ISF to produce customized cranial implants. At the end of this chapter, a list of additional publications related to ISF but not included as chapters of the thesis is provided.

9.1 Study of the influence of process parameters on basic geometries manufactured by SPIF

This first part of the discussion covers from chapter 3 to 6. The main idea of the four papers presented under this section was to increase the existing knowledge on how the process parameters in SPIF affect the manufacturing of basic geometries. They are presented in chronological order as the research progressed and as the need of covering new gaps of knowledge or deepening in the contributions of previous works appeared.

Chapter 3 presented an experimental work mainly focused on the evaluation of the forming force in PVC parts manufactured by SPIF considering five process parameters: sheet thickness, tool diameter, step down, feed rate and spindle speed. It was found that the parameter that had the most important effect was the spindle speed, which was an

interesting contribution since at the moment the paper was published, this effect had not been previously studied in SPIF of polymers. On the light of this finding, additional tests were carried out in order to demonstrate that the increase of the spindle speed caused a rise of the temperature during the forming process due to the increase of the friction between the tool and the sheet. Furthermore, the effect of the aforementioned process parameters on the surface roughness and final achieved depth were also studied, being again the spindle speed one of the most significant factors.

Since then, the research aimed to corroborate and deepen in the importance of the spindle speed in the case of forming polymers. In the second paper (Chapter 4), the same DOE of the previous paper was used, including one additional material, PC. The outputs analyzed were maximum forming force, surface roughness, maximum achieved depth and, as a novelty, the maximum temperature reached during the forming process and the energy consumption. The importance of the spindle speed was verified and the main contributions of that work were (i) the significant reduction on the energy consumption when a free spindle speed is used; (ii) the methodology to determine the set of the most suitable process parameters to obtain the most satisfactory final part; (iii) the demonstration that by using the best combination of process parameters it was also possible to obtain the cheapest part and (iv) the proposal of an empirical equation to predict the energy consumption mainly dependent on the forming time and the spindle speed.

The influence of the spindle speed, among other process parameters, on the variation of the temperature during the forming process was deeply studied in the subsequent work presented in Chapter 5. The range of materials used was widened, including three non-biocompatible polymers (PVC, PC and PP) and two biocompatible polymers (PCL and UHMWPE). A Box-Behnken design of experiments was used, considering four process parameters (step down, feed rate, tool diameter and spindle speed) and three levels for each parameter, which allowed to determine if the effects were linear or not. It was shown that increasing the tool diameter and the spindle speed, the temperature increased, while the variation of the feed rate and the step down did not affect the maximum temperature reached. Furthermore, empirical models to predict the maximum temperature were proposed for each material, being possible to control the temperature reached and the changes in the material properties. Therefore, the material formability could be increased and ensure that the level of forming forces will not exceed the machine operating limits. Moreover, it would be possible to predict which will be the increase of the temperature under new process conditions, determining, for example, whether the material will overpass the glass transition or melting temperatures ensuring that they are appropriate for obtaining a successful part.

From the experimental task done in Chapter 5, it was possible to evaluate the formability and failure modes of the selected materials depending on the spindle speed used. The strain state of the tested polymeric sheets was measured off-line on the final part by using the 3D deformation digital measurement system ARGUS® via circle grid analysis in order to represent the principal strains on the outer surface within the principal strain space. The fractography images captured in the microscope for measuring the thickness reduction and

calculate the strains at fracture were used to analyze the different modes of failure found in the experiments. For PVC and PC using a free spindle speed and for PC deformed at 2000 rpm, there is a ductile fracture without previous necking in the plane strain and biaxial strain sections. In the case of the PVC part manufactured at 2000 rpm, the failure is caused by twisting without fracture. This effect could be because of having a forming temperature close to T_g , which could have altered the material properties. Otherwise, PCL failed by the appearance of small cracks that could be either originated by a localized melting of the crystalline lattices, as far as the temperature reached during the forming process was close to the material melting temperature, or because inhomogeneities due to the in-house manufacturing of the PCL sheets. PP and UHMWPE could be successfully formed without failure because the forming temperature was below the melting temperature. Furthermore, they are not as sensitive to the spindle speed variation because at room temperature they are well above T_g .

In the light of the results presented in the thesis, it has been proved the high potential in terms of formability of polymeric sheets manufactured by SPIF, but make also clear the importance of evaluating the polymers formability in a proper range of process parameters procuring materials formability libraries and so providing safe formability areas of deformation within the corresponding FLD's. Then, this information could be used to select the most appropriate material and/or process parameters to manufacture successfully, for example, a biomedical device. To contribute on increasing the available database regarding materials formability, the procedure depicted in Figure 9.1 is proposed when a new raw material is going to be used in ISF. Once the process parameters are selected and the characterization is complete, the experimental tests can be performed with the aim of analyzing its formability. During the tests, the forming temperature should be measured and linked with the formability results, as it has been proved to have a close relationship. If failure occurs and formability can be increased, it should be verified if the temperature reached during the tests is close to the glass transition or melting temperatures because it can affect the failure mode (as explained in Chapter 6). If it is the case, the spindle speed should be reduced in order to decrease the forming temperature. Otherwise, other process parameters can be modified, such as, depth step or tool diameter. When the part is successfully formed or when formability cannot be further improved, it is possible to determine the safe forming zone, increasing the current knowledge regarding the formability of polymers.

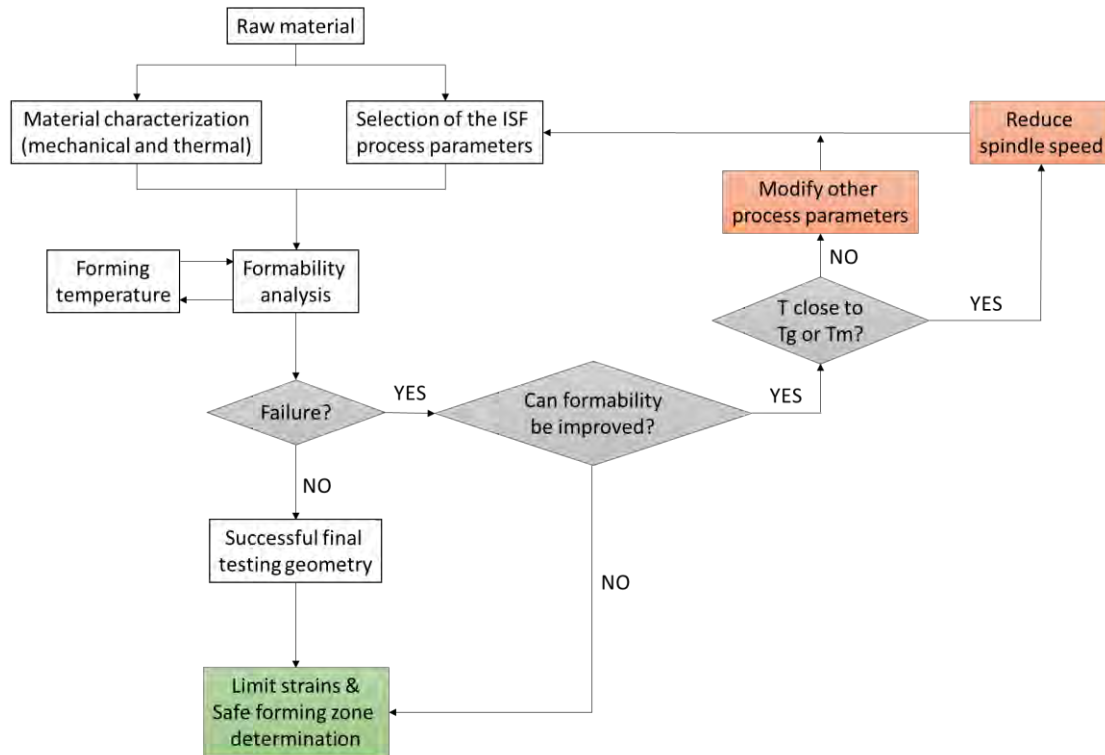


Figure 9.1. Procedure for determining the safe forming zone in SPIF.

Throughout the development of the thesis and with the exhaustive review of the state of the art for polymer ISF it has been evidenced how variable is the behavior of the thermoplastic materials depending on the process conditions, for example at different testing speeds or operating temperatures. Therefore, to be able to adequately compare the results obtained in different research works, the material characterization and the data provided should be as complete as possible.

On the contrary to the regular behavior of metal sheets deformed by SPIF (Centeno et al., 2014), it was observed in the papers presented in Chapters 3 and 4 that the formability for PVC and PC increased at larger step down values, this fact was also found in the work carried out by Davarpanah et al. (2015) for PVC and PLA, published almost in parallel with the paper of Chapter 3. This formability behavior of PVC and PC is the opposite from that found by Le et al. (2008) in the case of PP. An explanation for the difference in the formability trends could be related to the rheological properties of thermoplastic materials. It is well known that polymers exhibit a drastically different behavior depending on their molecular weight, even to the extent to observe trends that are not in accordance to those previously found in the literature, especially if two different polymers are being compared. Furthermore, it should be mentioned that a same type of thermoplastic material (for instance, PVC) can be found with different molecular weights depending on the arrangement of the polymer chains, the polymerization reaction, etc. From the literature review, it can be noticed that the polymer characterization is mainly based on the mechanical properties (Young modulus, yield stress, etc.) typically found in metallic materials. However, it is scarce regarding other inherent polymer aspects, such as the thermal or rheological characteristics (Table 9.1).

Table 9.1. Summary of the polymeric materials properties provided in the polymer ISF literature.

Legend: ● Information explicitly provided in the paper; ○ Information obtainable from figures provided in the paper; ◇ Information provided at various testing speeds and/or temperatures; - Information not available.

Author	Material	General properties		Mechanical properties								Thermal properties		Other		
		Structure	Density (kg/m ³)	E (MPa)	Poisson's ratio	Yield stress tension (MPa)	Yield stress compression (MPa)	Ultimate stress (MPa)	Elongation at yield point (%)	Elongation at fracture (%)	Fracture toughness (kJ/m ²)	FLD / Fracture strains	Tg (°C)	Tm (°C)	Biodegradability (%)	Water permeability (kg/m ² /day)
(Franzen et al., 2009)	PVC	●	-	-	-	-	-	-	-	●	-	-	●	-	-	-
(Le et al., 2008)	PP	-	-	-	-	-	-	-	-	-	-	-	-	-	-	-
(Martins et al., 2009)	POM	●	●	●	-	●	-	-	-	-	●	●	-	-	-	-
	HDPE	●	●	●	-	●	-	-	-	-	●	●	-	-	-	-
	PA	●	●	●	-	●	-	-	-	-	●	●	-	-	-	-
	PVC	●	●	●	-	●	-	-	-	-	●	●	-	-	-	-
	PC	●	●	●	-	●	-	-	-	-	●	●	-	-	-	-
(Silva et al., 2010)	PVC	●	●	●	●	●	-	-	-	-	●	-	●	-	-	-
(Marques et al., 2012)	PET	●	●	●	-	●	●	-	-	-	-	●	-	-	-	-
	PA	●	●	●	-	●	●	-	-	-	-	●	-	-	-	-
	PVC	●	●	●	-	●	●	-	-	-	-	●	-	-	-	-
	PC	●	●	●	-	●	●	-	-	-	-	●	-	-	-	-
(Fiorentino et al., 2012)	PCL	●	-	●	-	●	-	-	-	●	-	-	●	●	●	●
(Alkas Yonan et al., 2013)	PVC	-	-	-	-	○	-	-	○	-	-	-	-	-	-	-
(Silva et al., 2013)	PET	●	-	●	-	●	●	-	-	-	●	●	-	-	-	-
	PC	●	-	●	-	●	●	-	-	-	●	●	-	-	-	-
(Alkas Yonan et al., 2014)	PVC	-	-	●	-	●	●	-	-	-	●	-	-	-	-	-
(Davaranah et al., 2015)	PLA	-	-	-	-	-	-	-	-	-	-	-	-	-	-	-
	PVC	-	-	-	-	-	-	-	-	-	-	-	-	-	-	-
(Hussain et al., 2016)	PVC	●	●	-	-	●	-	●	●	-	-	-	-	●	-	-
	PE	●	●	-	-	●	-	●	●	-	-	-	-	●	-	-
(Davaranah et al., 2017)	PVC	●	-	-	-	○	-	○	○	○	-	-	-	-	-	-
	PA	●	-	-	-	○	-	○	○	○	-	-	-	-	-	-
(Lozano-Sánchez et al., 2017)	PP-MWCNTs	●	-	-	-	-	-	-	-	-	-	-	●	-	-	-
(Bagudanch et al., 2015)	PVC	●	-	◇	-	◇	-	-	-	-	-	●	●	-	-	-
(Centeno et al., 2017)	PC	-	-	◇	-	◇	-	-	◇	-	-	●	-	-	-	-
	PC	-	-	◇	-	◇	-	-	◇	-	-	●	-	-	-	-
	PVC	-	-	◇	-	◇	-	-	◇	-	-	●	-	-	-	-

These characteristics of the polymer mechanical and thermal behavior establish important drawbacks regarding the applicability of numerical methods, for example Finite Element Method (FEM), to simulate the ISF process. This is the main reason why there are very few works in the literature that are focused on the ISF simulation analysis (Alkas Yonan et al., 2014, 2013). During the development of this thesis, few attempts were done in order to identify and evaluate possible polymeric constitutive equations to be used on the simulation of polymer SPIF (Bagudanch et al., 2014b, 2013). Although a material model was found to be suitable to predict the mechanical behavior of a tensile test under different testing temperatures using PVC and PC, its application on the complex process of SPIF becomes a challenge difficult to solve. Therefore, further work is still required in order to obtain appropriate models and be able to accurately predict the experimental results.

9.2 Cases of study: approaching ISF to the manufacturing of custom cranial implants

The papers of Chapters 7 and 8 arise from some previous studies presented in several international conferences, which firstly demonstrated the feasibility of producing polymer customized cranial implants using the ISF technology. For example, Bagudanch et al. (2015b), is the first research work that presents a customized cranial implant manufactured in SPIF using a biocompatible polymer, polycaprolactone (PCL). It is a preliminary study in which a scaled implant is obtained and the geometric accuracy of the final part is measured using a 3D scanning system. PCL has an important springback effect, significantly more remarkable compared to the non-biocompatible polymers previously utilized. Therefore, some important deviations (from 2.5 to 4 mm) were obtained in the steepest parts of the geometry, while in the central part the deviations were lower (0.6-1.2 mm). Even though the high deviations, this work establishes the great potential that the technology has in order to obtain polymer cranial implants.

From these previous results, it appears the need of improving the SPIF manufacturing process to reduce as much as possible the geometric deviations. Furthermore, PCL is biodegradable, meaning that at a certain time period a cranial implant manufactured using PCL would start to degrade and reduce its mechanical properties, which of course would be a very limiting factor to be used in a real surgical procedure. Considering these key issues, the paper presented in Chapter 8 was developed.

The case studies presented in the present dissertation are mainly considered as prototypes, not as a final part ready to be used in surgical procedures. Before testing the cranial implant in humans, its medical efficiency should be verified for example in animals, and also an appropriate sterilization process is needed. Furthermore, the product must be approved according to several norms for direct implant, which is often the most limiting factor for its actual application.

Even though, the results presented here can be useful to: (i) evaluate the technical and economic feasibility of the ISF process to obtain complex and customized cranial implants, firstly using non-biocompatible polymers (Chapter 7) and afterwards using a biocompatible polymer, UHMWPE (Chapter 8), and (ii) establish the basis for future research on the topic.

The use of ISF and UHMWPE for manufacturing cranial implants is an interesting novelty in the field, providing significant advantages:

- It is a quick process and the cost of the manufactured implants is lower compared to the commercial ones.
- Polymers compared to the metallic materials used in implants are lightweight, have lower heat conductivity and mechanical properties more similar to bone.

In Chapter 8 it has been found that the minimum geometric deviations were obtained when the TPIF configuration is used and when the spindle speed is 2000 rpm. These deviations are of about ± 1.5 mm. In the case of severe cranial injuries, the discrepancies between the manufactured and designed implants are not a limiting factor. What is more important is to heal the damaged zone protecting the brain and provide and improve the emotional and psychological repercussion for the patient (Figure 2.53).

Most cranial defects will have some variable proportion of cosmetic and mechanical requirements. In the case of noticeable cranial defects (which is the case study of the present thesis), they are often interpreted by the public as signs of mental disturbance or retardation and, consequently, many patients may be inhibited from carrying out traditional psychosocial functions. Additional anxiety is precipitated by the fear of injury to the unprotected brain.

Physical properties of a material play an important role in protection and comfort provided by the implant. For patient safety, the implanted material should be similar in strength and fracture resistance (toughness) to skull bone, properties dictated by the material's strength, elastic modulus, and percentage of elongation at failure. Of particular interest to cranioplasty, with regard to patient's comfort, are the material's temperature conduction properties. Because the implant can be exposed to significant temperature changes, it is especially susceptible to passing hot or cold temperatures to the brain, causing patient discomfort. This is especially true of a material with a high heat conduction coefficient, such as most metals. Material magnetic properties and radiopacity are considerations in postoperative imaging. An implant material that is radiopaque or creates significant artefact on MR (Magnetic Resonance) images or CT scans, making them difficult to interpret, would detract from the usefulness of the material. Finally, a material that has excellent biocompatibility and physical properties would be useless if it could not be easily formed and modified to fit the skull defect. This factor is a major consideration, because it affects the time and expertise required for implantation. If the material is difficult to mold or deform, this aspect can multiply the cost of the implant.

Therefore, the two major purposes of performing a cranioplasty are to protect the brain and to provide reasonable aesthetics. The most important physical requirements of the implant

are strength similar to bone, low heat conductivity and that the material must be easy to shape. For this specific application, it is of course important to obtain an implant as close as possible to the desired shape, but is not the main aspect that should be prioritized. The proposed biocompatible and customized implant of this thesis meets all the aforementioned requirements.

The norms ASTM F 648-07 and ISO 5834-2:2011 list some of the mechanical requirements that a UHMWPE part must guarantee in order to be used in a surgical procedure. To ensure that the material used in this thesis to manufacture a customized cranial implant, several mechanical characterization tests have been performed. The obtained results and the information provided by the material data sheet are compared to the normalized requirements. Table 9.2 shows the summary of the results.

Table 9.2. Summary of the normalized mechanical requirements for a UHMWPE surgical part and the material data sheet and characterization results

	<i>ASTM F 648-07</i>	<i>ISO 5834-2:2011</i>	<i>Material data sheet</i>	<i>Results from the mechanical tests</i>
<i>Ultimate tensile strength (MPa)</i>	>40	>27	-	41
<i>Yield tensile strength (MPa)</i>	>19	>19	19	17
<i>Elongation (%) ultimate</i>	>340	>300	-	370
<i>Charpy Impact Strength (kJ/m²)</i>	>30	-	115	No fracture occurs
<i>Special Charpy Impact Strength (kJ/m²)</i>	-	>90	170	-

Even though the implant had fulfilled the abovementioned mechanical normalised requirements with satisfactory results, there are some other procedures required to obtain the legal permission for using custom made implants, not only for ISF operations but also for other advanced manufacturing techniques such as Additive Manufacturing (AM).

The request should be accompanied by a specific form for sanitary products of interest to health under medical responsibility explaining: (i) what's driving the treatment of a patient, (ii) why this sanitary product is specifically required and (iii) the justification that it is applicable and provides comparable results, among others. To justify that the product is more suitable in relation to any other possible existing alternative, the request should present a scientific literature review and, if necessary, referring to previous experience with such interventions.

The authorization will be issued only for the treatment of a certain patient. The treatment can only be carried out:

- With the patient's informed consent who must sign a document, along with the doctor.
- Prior approval of the director of medical centre.

- Under the responsibility of the doctor in charge.

Taking into account this complex procedure most of the custom-made medical implants are still far from being applicable in real cases, independently of the technology used for obtaining them. However, this does not mean that research in this sense should not be carried out, and the appearance of new materials/technologies that aim to provide a wider range of alternatives should not be limited.

9.3 List of additional publications

The following list contains other publications not included as chapters of the thesis but developed during the PhD studies.

Journals:

Bagudanch, I., Centeno, G., Vallengano, C., Garcia-Romeu, M.L., 2013a. Forming force in Single Point Incremental Forming under different bending conditions. *Procedia Engineering* 63, 354–360.

Bagudanch, I., Elías-Zúñiga, A., Garcia-Romeu, M.L., 2013b. Evaluating material constitutive equations for the simulation of Incremental Sheet Forming applied to form thermoplastic materials. *Key Engineering Materials* 554-557, 1312–1319.

Bagudanch, I., Garcia-Romeu, M.L., Ferrer, I., Lupiañez, J., 2013c. The effect of process parameters on the energy consumption in Single Point Incremental Forming. *Procedia Engineering* 63, 346–353.

Bagudanch, I., Martínez-Romero, O., Elías-Zúñiga, A., Garcia-Romeu, M.L., 2014. Identifying polymeric constitutive equations for incremental sheet forming modeling. *Procedia Engineering* 81, 2292–2297.

Bagudanch, I., Lozano-Sánchez, L.M., Puigpinós, L., Sabater, M., Elizalde, L.E., Elías-Zúñiga, A., Garcia-Romeu, M.L., 2015. Manufacturing of Polymeric Biocompatible Cranial Geometry by Single Point Incremental Forming. *Procedia Engineering* 132, 267–273.

Bagudanch, I., Sabater, M., Garcia-Romeu, M.L. 2016. Single Point versus Two Point Incremental Forming of thermoplastic materials. *Advances in Materials and Processing Technologies*, DOI: 10.1080/2374068X.2016.1250245

Centeno, G., Bagudanch, I., Martínez-Donaire, A.J., Garcia-Romeu, M.L., Vallengano, C., 2014. Critical analysis of necking and fracture limit strains and forming forces in single-point incremental forming. *Materials and Design* 63, 20–29.

Centeno, G., Bagudanch, I., Morales-Palma, D., García-Romeu, M.L., Gonzalez-Perez-Somarrriba, B., Martinez-Donaire, A.J., Gonzalez-Perez, L.M., Vallellano, C., 2017. Recent Approaches for the Manufacturing of Polymeric Cranial Prostheses by Incremental Sheet Forming. *Procedia Engineering* 183, 180–187.

Elías-Zúñiga, A., Baylón, K., Ferrer, I., Serenó, L., Garcia-Romeu, M.L., Bagudanch, I., Grabalosa, J., Pérez-Recio, T., Martinez-Romero, O., Ortega-Lara, W., Elizalde, L.E., 2014. On the rule of mixtures for predicting stress-softening and residual strain effects in biological tissues and biocompatible materials. *Materials* 7, 441–456.

Garcia-Romeu, M.L., Pérez-Santiago, R., Bagudanch, I., 2013. Fabrication of a biopsy meso-forceps prototype with incremental sheet forming variants. *International Journal of Mechatronics and Manufacturing Systems* 6, 242–253.

Martinez-Romero, O., Garcia-Romeu, M.L., Olvera-Trejo, D., Bagudanch, I., Elías-Zúñiga, A., 2014. Tool dynamics during single point incremental forming process. *Procedia Engineering* 81, 2286–2291.

Pérez-Santiago, R., Bagudanch, I., García-Romeu, M.L., Hendrichs, N., 2012. Effect of strain hardening exponent in the incremental sheet forming force, in: *Steel Research International. Special Issue*, pp. 439–442.

Puigpinós, L., Bagudanch, I., Garcia-Romeu, M.L., Perez-Santiago, R., 2012. Incremental Sheet Forming (ISF) technology applied to form thin metal sheets, in: *Steel Research International. Special Issue*, pp. 443–446.

Soria, M., Bagudanch, I., Garcia-Romeu, M.L., Perez-Santiago, R., Masqué, S., Ribatallada, J., Guillaumet, J., Ardanuy, J., Poch, R., 2012. Numerical approach of ROBOSTAMP: A new metal forming technology based on the use of industrial robots, in: *Steel Research International. Special Issue*, pp. 311–314.

Conferences:

Bagudanch, I., Garcia-Romeu, M.L., Ferrer, I., 2014. Manufacturing of thermoplastic cranial prosthesis by incremental sheet forming, in: *Proceedings of the 2nd International Conference on Design and Processes for Medical Devices (PROMED)*. Monterrey (Mexico), pp. 95–98.

Centeno, G., Morales-Palma, D., Bagudanch, I., Martínez-Donaire, A.J., Garcia-Romeu, M.L., Vallellano, C. 2015. Experimental strain analysis on the manufacturing of polymer cranial prosthesis by single point incremental forming, in: *6th Manufacturing Engineering Society International Conference (MESIC)*, Barcelona (Spain). 3rd best poster award.

Garcia-Romeu, M.L., Pérez-Santiago, R., Bagudanch, I., Puigpinós, L., 2012. Fabrication of a Biopsy Micro-Forceps prototype with Incremental Sheet Forming, in: *Proceedings of the*

1st International Conference on Design and Processes for Medical Devices (PROMED). Brescia (Italy), pp. 103–106.

Garcia-Romeu, M.L., Bagudanch, I., Lozano-Sánchez, L.M., Martinez-Romero, O., Elías-Zúñiga, A., Elizalde, L.E., 2014. On the manufacture of biomedical devices based on nanopolymer composites by single point incremental forming, in: Proceedings of the 2nd International Conference on Design and Processes for Medical Devices (PROMED). Monterrey (Mexico), pp. 49–52.

Lozano-Sánchez, L.M., Bagudanch, I., Elizalde, L.E., Garcia-Romeu, M.L., Elías-Zúñiga, A. 2015. Preparation of biocompatible polymer sheets useful in the incremental sheet forming process, in: Advances in Materials and Processing Technologies Conference (AMPT). Madrid (Spain).

Pérez-Santiago, R., García-Romeu, M.L., Bagudanch, I., 2012. Fabrication of a Biopsy Micro-Forceps Prototype with Incremental Sheet Forming, in: Innovative Developments in Virtual and Physical Prototyping - Proceedings of the 5th International Conference on Advanced Research in Virtual and Rapid Prototyping. Leiria (Portugal), pp. 429–435.

Chapter 10. Conclusions.

Chapter 10 presents the conclusion of the Thesis, summarizes the main contributions presented and points out possible further works arising from the research exposed.

10.1 General conclusions

The focus of this Thesis is to increase the knowledge regarding the use of polymeric materials in Incremental Sheet Forming in order to manufacture customized biomedical implants at a low cost and reduced time-to-market.

For this reason the issues considered in this thesis include as first approach an experimental study to determine the influence of the process parameters on basic geometries produced by Single Point Incremental Forming (SPIF) for non-biocompatible and biocompatible polymers. In Chapters 3-6 the same basic geometry is manufactured (a truncated square pyramid with a variable wall angle) using several polymeric materials, but the process parameters and the studied responses are analyzed from different perspectives, leading to the following conclusions:

- The spindle speed has an important role in polymeric materials deformed by SPIF. This effect of the spindle does not only have the capability of decreasing the maximum forming force, but also increases the sheet formability, evaluated by the

maximum depth achieved. It also has a direct relationship with the energy consumed during the forming process.

- With the variation of the spindle speed there is a change in the friction conditions, which lead to different amounts of heat generation during the tests. As a result, the polymeric material might change its mechanical behavior or even overpass the glass transition or melting temperatures.
- Analyzing more in detail the influence of the spindle speed on the formability by means of circle gird analysis, it has been demonstrated that increasing the spindle speed the formability usually improves, but it may also affect the failure mode of the material: it can be changed from ductile fracture without necking to failure by twisting if the forming temperature is close to the glass transition or even localized melting could occur appearing small cracks on the sheet surface.

The focus of Chapters 7 and 8 is to demonstrate the feasibility of producing polymer customized cranial implants by ISF.

In Chapter 7 non-biocompatible materials (PVC and PC) are used to demonstrate that it is possible to manufacture successfully a cranial implant without reaching the material forming limits in SPIF, showing the high potential of the technology. The main findings of this chapter are summarized below:

- From the material characterization and formability analysis of a series of polymeric sheets formed by SPIF it has been possible to determine the most restrictive material, i.e., PC because presents a lower formability limit.
- Once the most restrictive material has been identified, a cranial implant has been manufactured in SPIF. The maximum strains obtained in the implant are significantly below the material forming limits, showing the high potential of the technology because of the achievable enhanced formability in SPIF within a range of process parameters.
- Although the materials used in this paper are not biocompatible, it provides a good basis for future research. Moreover, this methodology has also an educational interest, as far as transparent prostheses can be of great importance in medical or nursery schools for teaching and research purposes.

The paper presented in Chapter 8 was developed using a biocompatible polymer. The principal highlights of this last part of the present thesis are:

- Since in the previous chapters it was demonstrated that the spindle speed had an important effect in the results of the final part, in this case it was decided to keep constant the rest of the process parameters (tool diameter, feed rate and step down) and only modify the spindle speed (Free and 2000 rpm). In general terms, it has been shown that using the highest value of the spindle speed the accuracy of the implants is improved.

- Two ISF variants have been used, SPIF and TPIF with a negative die. As expected, better results in terms of geometric accuracy have been obtained with the TPIF variant. After the trimming process, the final accuracy of the implant manufactured at 2000 rpm is ± 1.5 mm.
- In the case of severe cranial injuries, the discrepancies between the manufactured and designed implants are not a limiting factor, especially if these deviations are of about ± 1.5 mm (which were the best results found). In those cases, the priority is to heal the damaged area to protect the brain, ensure the symmetry in the patient's skull and improve the emotional and psychological repercussion for the patient.
- A deep cost analysis has been presented for both cases, SPIF and TPIF. Obviously, using the TPIF variant the cost of the implant becomes higher because it is required to manufacture the die. However, it is worth the cost increase due to the reduction of the geometric deviation. Furthermore, ISF has been presented as an interesting alternative for the customized cranial implants because the cost of the product is very competitive.

With the knowledge provided by these studies, the state of the art of the Incremental Sheet Forming process using polymeric materials is enhanced and enriched. In addition, this proves the economic and technological feasibility to produce customized cranial implants ensuring acceptable accuracy, surface quality and lead time.

10.2 Main contributions

The main contributions of the work presented in this Thesis are summarized below:

- The effect of key process parameters on the maximum forming force, maximum achieved temperature, surface roughness, formability, energy and cost have been investigated for the process of incremental sheet forming on three non-biocompatible polymers (PVC, PC and PP) and on two biocompatible polymers (PCL and UHMWPE). The geometry used for the tests has been a truncated square pyramid with a variable wall angle.
- A set of process parameters guidelines has been provided in order to obtain the better results in terms of the lowest energy consumption and cost and increase the maximum achievable depth.
- Statistical models for predicting the maximum temperature for the five analyzed polymers have been obtained. These models are useful for determining the most influential factors and if under certain conditions the material will reach the glass transition or melting temperatures.

- For polymers with a glass transition temperature above the forming temperature, there is a significant increase of the formability with the increase of the spindle speed and the expected mode of failure is ductile fracture without previous necking. Otherwise, if the process conditions led to reach temperatures very close or even greater than T_g , the part could fail by twisting.
- On the other hand, polymers which at room temperature are above T_g are not as much sensitive to the improvement of the formability with the increase of the spindle speed. However, if the polymer has a low melting temperature, then the temperature reached during the forming process could initiate a localized melting and the part could fail by the appearance of small cracks.
- With the presented case study it has been shown the feasibility of the technology to produce custom-made cranial implants using biocompatible polymers. ISF has a great capability not only in terms of accuracy and cost but also because of its enhanced formability limits, making it possible to produce a wide range of products.

10.3 Further work

This section suggests possible topics to continue the research and development of Incremental Sheet Forming.

- Testing of ISF using other biocompatible materials, such as polymers reinforced with nanoparticles (e.g. PLA with TiO_2 , PLA with $CaCO_3$) or copolymers (e.g. PCL-PLA or PCL-PMMA).
- Comparing the geometrical accuracy of cranial implants obtained using the TPIF positive variant with the presented in the thesis, and evaluate whether the increment of the cost associated with the major complexity of the setup is worthwhile if there is an improvement of the accuracy.
- Using ISF for manufacturing not only customized cranial implants, but also other maxillofacial or orbital implants.
- Evaluating possible post-processes to improve the implant geometrical accuracy and performance, such as heat treatments in order to release residual stresses or drilling holes in the sheet surface.
- Comparing the performance of a polymeric cranial implant manufactured using ISF with a commercial one, in terms of accuracy, resistance, biocompatibility and cost.

Chapter 11. References

- Aerens, R., Eyckens, P., Bael, A., Duflou, J.R., 2010. Force prediction for single point incremental forming deduced from experimental and FEM observations. *The International Journal of Advanced Manufacturing Technology* 46, 969–982. doi:10.1007/s00170-009-2160-2
- Alkas Yonan, S., Silva, M.B., Martins, P.A.F., Tekkaya, A.E., 2014. Plastic flow and failure in single point incremental forming of PVC sheets. *Express Polymer Letters* 8, 301–311. doi:10.3144/expresspolymlett.2014.34
- Alkas Yonan, S., Soyarslan, C., Haupt, P., Kwiatkowski, L., Tekkaya, A.E., 2013. A simple finite strain non-linear visco-plastic model for thermoplastics and its application to the simulation of incremental cold forming of polyvinylchloride (PVC). *International Journal of Mechanical Sciences* 66, 192–201. doi:10.1016/j.ijmecsci.2012.11.007
- Allwood, J.M., Braun, D., Music, O., 2010. The effect of partially cut-out blanks on geometric accuracy in incremental sheet forming. *Journal of Materials Processing Technology* 210, 1501–1510. doi:10.1016/j.jmatprotec.2010.04.008
- Allwood, J.M., Houghton, N.E., Jackson, K.P., 2005a. The design of an incremental sheet forming machine, in: *Advanced Materials Research*. Trans Tech Publications, pp. 471–478.
- Allwood, J.M., King, G.P.F., Duflou, J., 2005b. A structured search for applications of the incremental sheet-forming process by product segmentation. *Proceedings of the Institution of Mechanical Engineers, Part B: Journal of Engineering Manufacture* 219, 239–244. doi:10.1243/095440505X8145
- Ambrogio, G., Ciancio, C., Filice, L., Gagliardi, F., 2016. Theoretical model for temperature prediction in Incremental Sheet Forming – Experimental validation. *International Journal of Mechanical Sciences* 108-109, 39–48. doi:10.1016/j.ijmecsci.2016.01.030

- Ambrogio, G., Conte, R., de Napoli, L., Fragomeni, G., Gagliardi, F., 2015. Forming Approaches Comparison for High Customised Skull Manufacturing. *Key Engineering Materials* 651-653, 925–931. doi:10.4028/www.scientific.net/KEM.651-653.925
- Ambrogio, G., Costantino, I., Denapoli, L., Filice, L., Fratini, L., Muzzupappa, M., 2004. Influence of some relevant process parameters on the dimensional accuracy in incremental forming: a numerical and experimental investigation. *Journal of Materials Processing Technology* 153-154, 501–507. doi:10.1016/j.jmatprotec.2004.04.139
- Ambrogio, G., Cozza, V., Filice, L., Micari, F., 2007. An analytical model for improving precision in single point incremental forming. *Journal of Materials Processing Technology* 191, 92–95. doi:10.1016/j.jmatprotec.2007.03.079
- Ambrogio, G., Denapoli, L., Filice, L., Gagliardi, F., Muzzupappa, M., 2005. Application of Incremental Forming process for high customised medical product manufacturing. *Journal of Materials Processing Technology* 162-163, 156–162. doi:10.1016/j.jmatprotec.2005.02.148
- Ambrogio, G., Filice, L., Manco, G., 2008. Warm incremental forming of magnesium alloy AZ31. *CIRP Annals - Manufacturing Technology* 57, 257–260. doi:10.1016/j.cirp.2008.03.066
- Ambrogio, G., Gagliardi, F., 2014. Temperature variation during high speed incremental forming on different lightweight alloys. *International Journal of Advanced Manufacturing Technology* 76, 1819–1825. doi:10.1007/s00170-014-6398-y
- Ambrogio, G., Gagliardi, F., Bruschi, S., Filice, L., 2013. On the high-speed Single Point Incremental Forming of titanium alloys. *CIRP Annals - Manufacturing Technology* 62, 243–246. doi:10.1016/j.cirp.2013.03.053
- Anghinelli, O., Ambrogio, G., Di Lorenzo, R., Ingarao, G., 2011. Environmental Costs of Single Point Incremental Forming. *Steel Research International* 525–530.
- Araghi, B.T., Manco, G.L., Bambach, M., Hirt, G., 2009. Investigation into a new hybrid forming process: Incremental sheet forming combined with stretch forming. *CIRP Annals - Manufacturing Technology* 58, 225–228. doi:10.1016/j.cirp.2009.03.101
- Araujo, R., Teixeira, P., Montanari, L., Reis, A., Silva, M.B., Martins, P.A., 2014. Single point incremental forming of a facial implant. *Prosthetics and Orthotics International* 38, 369–378. doi:10.1177/0309364613502071
- ASEBIO, 2014. Situación y tendencias del sector de la biotecnología en España.
- Attanasio, a, Ceretti, E., Giardini, C., 2006. Optimization of tool path in two points incremental forming. *Journal of Materials Processing Technology* 177, 409–412. doi:10.1016/j.jmatprotec.2006.04.047
- Attanasio, a, Ceretti, E., Giardini, C., Mazzoni, L., 2008. Asymmetric two points incremental forming: Improving surface quality and geometric accuracy by tool path optimization. *Journal of Materials Processing Technology* 197, 59–67. doi:10.1016/j.jmatprotec.2007.05.053
- Bagudanch, I., Centeno, G., Vallellano, C., Garcia-Romeu, M.L., 2017a. Revisiting formability and failure of polymeric sheets deformed by Single Point Incremental Forming. *Polymer Degradation and Stability*.

doi:10.1016/j.polymdegradstab.2017.08.021

- Bagudanch, I., Elías-Zúñiga, A., Garcia-Romeu, M.L., 2013. Evaluating material constitutive equations for the simulation of Incremental Sheet Forming applied to form thermoplastic materials. *Key Engineering Materials* 554-557, 1312–1319. doi:10.4028/www.scientific.net/KEM.554-557.1312
- Bagudanch, I., Garcia-Romeu, M.L., Centeno, G., Elías-Zúñiga, A., Ciurana, J., 2015a. Forming force and temperature effects on single point incremental forming of polyvinylchloride. *Journal of Materials Processing Technology* 219, 221–229. doi:10.1016/j.jmatprotec.2014.12.004
- Bagudanch, I., Garcia-Romeu, M.L., Ferrer, I., 2014a. Manufacturing of thermoplastic cranial prosthesis by incremental sheet forming, in: *Proceedings of the 2nd International Conference on Design and Processes for Medical Devices (PROMED)*. Monterrey, pp. 95–98.
- Bagudanch, I., Garcia-Romeu, M.L., Ferrer, I., Ciurana, J., 2018. Customized cranial implant manufactured by Incremental Sheet Forming using a biocompatible polymer. *Rapid Prototyping Journal* 24. doi:10.1108/RPJ-06-2016-0089
- Bagudanch, I., Garcia-Romeu, M.L., Sabater, M., 2016. Incremental forming of polymers: Process parameters selection from the perspective of electric energy consumption and cost. *Journal of Cleaner Production* 112, 1013–1024. doi:10.1016/j.jclepro.2015.08.087
- Bagudanch, I., Lozano-Sánchez, L.M., Puigpinós, L., Sabater, M., Elizalde, L.E., Elías-Zúñiga, A., Garcia-Romeu, M.L., 2015b. Manufacturing of Polymeric Biocompatible Cranial Geometry by Single Point Incremental Forming. *Procedia Engineering* 132, 267–273. doi:10.1016/j.proeng.2015.12.494
- Bagudanch, I., Martínez-Romero, O., Elías-Zúñiga, A., Garcia-Romeu, M.L., 2014b. Identifying polymeric constitutive equations for incremental sheet forming modeling. *Procedia Engineering* 81, 2292–2297. doi:10.1016/j.proeng.2014.10.323
- Bagudanch, I., Pérez-Santiago, R., García-Romeu, M.L., 2011a. Tool path strategies for Single Point Incremental Forming. *Key Engineering Materials* 473, 905–912. doi:10.4028/www.scientific.net/KEM.473.905
- Bagudanch, I., Pérez-Santiago, R., García-Romeu, M.L., Rodríguez, C., 2011b. Forming Force in SPIF of Variable Wall Angle Components : FEM Modeling and Experimental Results, in: *Proceedings of the 10th International Conference on Technology of Plasticity, ICTP 2011*. Aachen, pp. 541–546.
- Bagudanch, I., Vives-Mestres, M., Sabater, M., Garcia-Romeu, M.L., 2017b. Polymer incremental sheet forming process: Temperature analysis using response surface methodology. *Materials and Manufacturing Processes* 32, 44–53. doi:10.1080/10426914.2016.1176191
- Bambach, M., Hirt, G., Junk, S., 2003. Modelling and experimental evaluation of the incremental CNC sheet metal forming process, in: *Proceedings of the 7th International Conference on Computational Plasticity (COMPLAS)*.
- Bambach, M., Taleb Araghi, B., Hirt, G., 2009. Strategies to improve the geometric accuracy in asymmetric single point incremental forming. *Production Engineering* 3, 145–156. doi:10.1007/s11740-009-0150-8

- Callegari, M., Amodio, D., Ceretti, E., Giardini, C., 2006. Sheet Incremental Forming : Advantages of Robotised Cells vs . CNC Machines. Simulation.
- Castelan, J., Schaeffer, L., Daleffe, A., Fritzen, D., Salvaro, V., Da Silva, F.P., 2014. Manufacture of custom-made cranial implants from DICOM images using 3D printing, CAD/CAM technology and incremental sheet forming. *Revista Brasileira de Engenharia Biomedica* 30, 265–273. doi:10.1590/rbeb.2014.024
- Centeno, G., Bagudanch, I., Martínez-Donaire, A.J., Garcia-Romeu, M.L., Vallellano, C., 2014. Critical analysis of necking and fracture limit strains and forming forces in single-point incremental forming. *Materials and Design* 63, 20–29. doi:10.1016/j.matdes.2014.05.066
- Centeno, G., Martinez-Donaire, A.J., Morales-Palma, D., Vallellano, C., Silva, M.B., Martins, P.A.F., 2015. Novel experimental techniques for the determination of the forming limits at necking and fracture, in: *Materials Forming and Machining: Research and Development*. pp. 1–24. doi:10.1016/B978-0-85709-483-4.00001-6
- Centeno, G., Morales-Palma, D., Gonzalez-Perez-Somarrriba, B., Bagudanch, I., Egea-Guerrero, J.J., Gonzalez-Perez, L.M., García-Romeu, M.L., Vallellano, C., 2017. A functional methodology on the manufacturing of customized polymeric cranial prostheses from CAT using SPIF. *Rapid Prototyping Journal* 23. doi:10.1108/RPJ-02-2016-0031
- Ceretti, E., 2004. Experimental and simulative results in sheet incremental forming on CNC machines. *Journal of Materials Processing Technology* 152, 176–184. doi:10.1016/j.jmatprotec.2004.03.024
- Davarpanah, M.A., Bansal, S., Malhotra, R., 2017. Influence of Single Point Incremental Forming on Mechanical Properties and Chain Orientation in Thermoplastic Polymers. *Journal of Manufacturing Science and Engineering* 139, 21012–21019. doi:10.1115/1.4034036
- Davarpanah, M.A., Mirkouei, A., Yu, X., Malhotra, R., Pilla, S., 2015. Effects of incremental depth and tool rotation on failure modes and microstructural properties in Single Point Incremental Forming of polymers. *Journal of Materials Processing Technology* 222, 287–300. doi:10.1016/j.jmatprotec.2015.03.014
- Deshmukh, R., 2014. World bio-implants market (types and geography) opportunities and forecast, 2013-2020.
- Duflou, J., Callebaut, B., Verbert, J., Debaerdemaeker, H., 2008. Improved SPIF performance through dynamic local heating. *International Journal of Machine Tools and Manufacture* 48, 543–549. doi:10.1016/j.ijmachtools.2007.08.010
- Duflou, J., Lauwers, B., Verbert, J., 2007a. Study on the achievable accuracy in single point incremental forming. *Advanced Methods in Material Forming* 251–262.
- Duflou, J., Tunckol, Y., Szekeres, A., Vanherck, P., 2007b. Experimental study on force measurements for single point incremental forming. *Journal of Materials Processing Technology* 189, 65–72. doi:10.1016/j.jmatprotec.2007.01.005
- Duflou, J.R., Behera, A.K., Vanhove, H., Bertol, L.S., 2013. Manufacture of Accurate Titanium Cranio-Facial Implants with High Forming Angle Using Single Point Incremental Forming. *Key Engineering Materials* 549, 223–230.

doi:10.4028/www.scientific.net/KEM.549.223

- Duflou, J.R., Lauwers, B., Verbert, J., Gelaude, F., Tunckol, Y., 2005. Medical application of single point incremental forming: Cranial plate manufacturing, in: *Virtual Modelling and Rapid Manufacturing - Advanced Research in Virtual and Rapid Prototyping*. pp. 161–166.
- Durante, M., Formisano, A., Langella, A., 2010. Comparison between analytical and experimental roughness values of components created by incremental forming. *Journal of Materials Processing Technology* 210, 1934–1941. doi:10.1016/j.jmatprotec.2010.07.006
- Echraf, S.B.M., Hrairi, M., 2014. Significant Parameters for the Surface Roughness in Incremental Forming Process. *Materials and Manufacturing Processes* 29, 697–703. doi:10.1080/10426914.2014.901519
- Emmens, W.C., Sebastiani, G., van den Boogaard, a. H., 2010. The technology of Incremental Sheet Forming—A brief review of the history. *Journal of Materials Processing Technology* 210, 981–997. doi:10.1016/j.jmatprotec.2010.02.014
- Emmens, W.C., van den Boogaard, a. H., 2009. An overview of stabilizing deformation mechanisms in incremental sheet forming. *Journal of Materials Processing Technology* 209, 3688–3695. doi:10.1016/j.jmatprotec.2008.10.003
- Fan, G., Gao, L., Hussain, G., Wu, Z., 2008. Electric hot incremental forming: A novel technique. *International Journal of Machine Tools and Manufacture* 48, 1688–1692. doi:10.1016/j.ijmactools.2008.07.010
- Fan, G., Sun, F., Meng, X., Gao, L., Tong, G., 2009. Electric hot incremental forming of Ti-6Al-4V titanium sheet. *The International Journal of Advanced Manufacturing Technology* 49, 941–947. doi:10.1007/s00170-009-2472-2
- Filice, L., Ambrogio, G., Micari, F., 2006. On-Line Control of Single Point Incremental Forming Operations through Punch Force Monitoring. *CIRP Annals - Manufacturing Technology* 55, 245–248. doi:10.1016/S0007-8506(07)60408-9
- Fiorentino, a, Marenza, G.P., Marzi, R., Ceretti, E., Kemmoku, D.T., Silva, J.V.L., 2012. Rapid prototyping techniques for individualized medical prosthesis manufacturing. *Innovative Developments in Virtual and Physical Prototyping* 1, 589–594. doi:10.1201/b11341-94
- Fiorentino, A., Ceretti, E., Attanasio, A., Mazzoni, L., Giardini, C., 2009. Analysis of forces, accuracy and formability in positive die sheet incremental forming. *International Journal of Material Forming* 2, 805–808. doi:10.1007/s12289-009-0467-z
- Franzen, V., Kwiatkowski, L., Martins, P., Tekkaya, a, 2009. Single point incremental forming of PVC. *Journal of Materials Processing Technology* 209, 462–469. doi:10.1016/j.jmatprotec.2008.02.013
- Franzen, V., Kwiatkowski, L., Sebastiani, G., Shankar, R., Tekkaya, a. E., Kleiner, M., 2008. Dyna-Die: Towards Full Kinematic Incremental Forming. *International Journal of Material Forming* 1, 1163–1166. doi:10.1007/s12289-008-0187-9
- Fratini, L., Ambrogio, G., Di Lorenzo, R., Filice, L., Micari, F., 2004. Influence of mechanical properties of the sheet material on formability in single point incremental

- forming. *CIRP Annals - Manufacturing Technology* 53, 207–210. doi:10.1016/S0007-8506(07)60680-5
- Garcia-Romeu, M.L., Pérez-Santiago, R., Bagudanch, I., Puigpinós, L., 2012. Fabrication of a Biopsy Micro-Forceps prototype with Incremental Sheet Forming, in: *Proceedings of the 1st International Conference on Design and Processes for Medical Devices (PROMED)*. pp. 103–106.
- Göttmann, A., Korinth, M., Schäfer, V., Araghi, B.T., Bambach, M., Hirt, G., 2013. Manufacturing of Individualized Cranial Implants Using Two Point Incremental Sheet Metal Forming. *Future trends in Production Engineering* 5, 287–295. doi:10.1007/978-3-642-24491-9
- Guerras, L.A., Navas, J.E., 2015. *La dirección estratégica de la empresa. Teoría y aplicaciones*, 5th editio. ed. Thomson Reuters.
- Hagan, E., Jeswiet, J., 2004. Analysis of surface roughness for parts formed by computer numerical controlled incremental forming. *Proceedings of the Institution of Mechanical Engineers, Part B: Journal of Engineering Manufacture* 218, 1307–1312. doi:10.1243/0954405042323559
- Ham, M., Jeswiet, J., 2008. Dimensional Accuracy of Single Point Incremental Forming. *International Journal of Material Forming* 1171 – 1174. doi:10.1007/s12289-008-0
- Hamilton, K., Jeswiet, J., 2010. Single point incremental forming at high feed rates and rotational speeds: Surface and structural consequences. *CIRP Annals - Manufacturing Technology* 59, 311–314. doi:10.1016/j.cirp.2010.03.016
- Han, F., Mo, J.H., Wang, P., Deng, Y.Z., 2010. A Digital Manufacture Technology for Skull Prosthesis Using Incremental Sheet Forming Method. *Advanced Materials Research* 102-104, 348–352. doi:10.4028/www.scientific.net/AMR.102-104.348
- Hino, R., Kawabata, K., Yoshida, F., 2014. Incremental Forming with Local Heating by Laser Irradiation for Magnesium Alloy Sheet. *Procedia Engineering* 81, 2330–2335. doi:10.1016/j.proeng.2014.10.329
- Hirt, G., Ames, J., Bambach, M., Kopp, R., 2004. Forming strategies and Process Modelling for CNC Incremental Sheet Forming. *CIRP Annals - Manufacturing Technology* 53, 203–206. doi:10.1016/S0007-8506(07)60679-9
- Honarpisheh, M., Abdolhoseini, M.J., Amini, S., 2015. Experimental and numerical investigation of the hot incremental forming of Ti-6Al-4V sheet using electrical current. *The International Journal of Advanced Manufacturing Technology* 83, 2027–2037. doi:10.1007/s00170-015-7717-7
- Husmann, T., Magnus, C.S., 2016. Thermography in incremental forming processes at elevated temperatures. *Measurement* 77, 16–28. doi:10.1016/j.measurement.2015.09.004
- Hussain, G., Gao, L., Dar, N., 2007. An experimental study on some formability evaluation methods in negative incremental forming. *Journal of Materials Processing Technology* 186, 45–53. doi:10.1016/j.jmatprotec.2006.12.005
- Hussain, G., Gao, L., Hayat, N., Cui, Z., Pang, Y., Dar, N., 2008a. Tool and lubrication for negative incremental forming of a commercially pure titanium sheet. *Journal of*

- Materials Processing Technology 203, 193–201. doi:10.1016/j.jmatprotec.2007.10.043
- Hussain, G., Gao, L., Hayat, N., Dar, N.U., 2009. The formability of annealed and pre-aged AA-2024 sheets in single-point incremental forming. *The International Journal of Advanced Manufacturing Technology* 46, 543–549. doi:10.1007/s00170-009-2120-x
- Hussain, G., Gao, L., Zhang, Z.Y., 2008b. Formability evaluation of a pure titanium sheet in the cold incremental forming process. *The International Journal of Advanced Manufacturing Technology* 37, 920–926. doi:10.1007/s00170-007-1043-7
- Hussain, G., Mahna, A., Iqbal, A., 2016. Response surface analysis of cold formability of polymers in Incremental Sheet Forming: Effect of parameters and associated thermal softening. *International Journal of Precision Engineering and Manufacturing* 17, 613–621. doi:10.1007/s12541-016-0074-0
- Ingarao, G., Ambrogio, G., Gagliardi, F., Di Lorenzo, R., 2012. A sustainability point of view on sheet metal forming operations: Material wasting and energy consumption in incremental forming and stamping processes. *Journal of Cleaner Production* 29-30, 255–268. doi:10.1016/j.jclepro.2012.01.012
- Ingarao, G., Vanhove, H., Kellens, K., Duflou, J.R., 2014. A comprehensive analysis of electric energy consumption of single point incremental forming processes. *Journal of Cleaner Production* 67, 173–186. doi:10.1016/j.jclepro.2013.12.022
- Iseki, H., 2001. An approximate deformation analysis and FEM analysis for the incremental bulging of sheet metal using a spherical roller. *Journal of Materials Processing Technology* 111, 150–154. doi:10.1016/S0924-0136(01)00500-3
- Isik, K., Silva, M.B., Tekkaya, A.E., Martins, P.A.F., 2014. Formability limits by fracture in sheet metal forming. *Journal of Materials Processing Technology* 214, 1557–1565. doi:10.1016/j.jmatprotec.2014.02.026
- Jackson, K., Allwood, J., 2009. The mechanics of incremental sheet forming. *Journal of Materials Processing Technology* 209, 1158–1174. doi:10.1016/j.jmatprotec.2008.03.025
- Jackson, K., Allwood, J., Landert, M., 2008. Incremental forming of sandwich panels. *Journal of Materials Processing Technology* 204, 290–303. doi:10.1016/j.jmatprotec.2007.11.117
- Jeswiet, J., Adams, D., Doolan, M., McAnulty, T., Gupta, P., 2015. Single point and asymmetric incremental forming. *Advances in Manufacturing* 3, 253–262. doi:10.1007/s40436-015-0126-1
- Jeswiet, J., Duflou, J.R., Szekeres, A., 2005a. Forces in single point and two point incremental Forming, in: *Advanced Materials Research*. Trans Tech Publications, pp. 449–456.
- Jeswiet, J., Micari, F., Hirt, G., Bramley, a, Duflou, J., Allwood, J., 2005b. Asymmetric Single Point Incremental Forming of Sheet Metal. *CIRP Annals - Manufacturing Technology* 54, 88–114. doi:10.1016/S0007-8506(07)60021-3
- Jeswiet, J., Szekeres, A., 2005. Forces in Single Point Incremental Forming, in: *Transactions of the North American Manufacturing Research Institute of SME*. pp. 399–404.
- Ji, Y., Park, J., 2008. Formability of magnesium AZ31 sheet in the incremental forming at

- warm temperature. *Journal of Materials Processing Technology* 201, 354–358. doi:10.1016/j.jmatprotec.2007.11.206
- Kim, Y., Park, J., 2002. Effect of process parameters on formability in incremental forming of sheet metal. *Journal of Materials Processing Technology* 130-131, 42–46. doi:10.1016/S0924-0136(02)00788-4
- Kopac, J., Kampus, Z., 2005. Incremental sheet metal forming on CNC milling machine-tool. *Journal of Materials Processing Technology* 162-163, 622–628. doi:10.1016/j.jmatprotec.2005.02.160
- Le, V.S., Ghiotti, a., Lucchetta, G., 2008. Preliminary Studies on Single Point Incremental Forming for Thermoplastic Materials. *International Journal of Material Forming* 1, 1179–1182. doi:10.1007/s12289-008-0191-0
- Li, Y., Liu, Z., Daniel, W.J.T. (Bill., Meehan, P. a., 2014. Simulation and Experimental Observations of Effect of Different Contact Interfaces on the Incremental Sheet Forming Process. *Materials and Manufacturing Processes* 29, 121–128. doi:10.1080/10426914.2013.822977
- Li, Y., Lu, H., Daniel, W.J.T., Meehan, P.A., 2015. Investigation and optimization of deformation energy and geometric accuracy in the incremental sheet forming process using response surface methodology. *International Journal of Advanced Manufacturing Technology* 79, 2041–2055. doi:10.1007/s00170-015-6986-5
- Liu, Z., Liu, S., Li, Y., Meehan, P.A., 2014. Modeling and Optimization of Surface Roughness in Incremental Sheet Forming using a Multi-objective Function. *Materials and Manufacturing Processes* 29, 808–818. doi:10.1080/10426914.2013.864405
- Lozano-Sánchez, L.M., Sustaita, A.O., Soto, M., Biradar, S., Ge, L., Segura-Cárdenas, E., Diabb, J., Elizalde, L.E., Barrera, E.V., Elías-Zúñiga, A., 2017. Mechanical and structural studies on single point incremental forming of polypropylene-MWCNTs composite sheets. *Journal of Materials Processing Technology* 242, 218–227. doi:10.1016/j.jmatprotec.2016.11.032
- Lu, B., Ou, H., Shi, S.Q., Long, H., Chen, J., 2016. Titanium based cranial reconstruction using incremental sheet forming. *International Journal of Material Forming* 9, 361–370. doi:10.1007/s12289-014-1205-8
- Madeira, T., Silva, C.M. a., Silva, M.B., Martins, P. a. F., 2015. Failure in single point incremental forming. *The International Journal of Advanced Manufacturing Technology* 1471–1479. doi:10.1007/s00170-014-6381-7
- Marques, T. a., Silva, M.B., Martins, P. a. F., 2012. On the potential of single point incremental forming of sheet polymer parts. *The International Journal of Advanced Manufacturing Technology* 60, 75–86.
- Martins, P. a. F., Kwiatkowski, L., Franzen, V., Tekkaya, a. E., Kleiner, M., 2009. Single point incremental forming of polymers. *CIRP Annals - Manufacturing Technology* 58, 229–232. doi:10.1016/j.cirp.2009.03.095
- Martins, P., Bay, N., Skjoedt, M., Silva, M., 2008. Theory of single point incremental forming. *CIRP Annals - Manufacturing Technology* 57, 247–252. doi:10.1016/j.cirp.2008.03.047

- Meier, H., Buff, B., Laurischkat, R., Smukala, V., 2009. Increasing the part accuracy in dieless robot-based incremental sheet metal forming. *CIRP Annals - Manufacturing Technology* 58, 233–238. doi:10.1016/j.cirp.2009.03.056
- Micari, F., Ambrogio, G., Filice, L., 2007. Shape and dimensional accuracy in Single Point Incremental Forming: State of the art and future trends. *Journal of Materials Processing Technology* 191, 390–395. doi:10.1016/j.jmatprotec.2007.03.066
- Milutinovic, M., Lendel, R., Potran, M., Vilotic, D., Skakun, P., Plancak, M., 2014. Application of Single Point Incremental Forming for manufacturing of denture base. *Journal for technology of plasticity* 39, 15–24.
- NanoMarkets, 2013. *Worldwide Medical Polymer Markets 2013-2020*.
- Obikawa, T., Satou, S., Hakutani, T., 2009. Dieless incremental micro-forming of miniature shell objects of aluminum foils. *International Journal of Machine Tools and Manufacture* 49, 906–915. doi:10.1016/j.ijmachtools.2009.07.001
- Oleksik, V., Pascu, A., Deac, C., Fleaca, R., Roman, M., Bologa, O., Barlat, F., Moon, Y.H., Lee, M.G., 2010. The Influence of Geometrical Parameters on the Incremental Forming Process for Knee Implants Analyzed by Numerical Simulation. *Romania* 1208–1215. doi:10.1063/1.3457520
- Park, J., Kim, J., Park, N., Kim, Y., 2009. Study of Forming Limit for Rotational Incremental Sheet Forming of Magnesium Alloy Sheet. *Metallurgical and Materials Transactions A* 41, 97–105. doi:10.1007/s11661-009-0043-7
- Park, J., Kim, Y., 2003. Fundamental studies on the incremental sheet metal forming technique. *Journal of Materials Processing Technology* 140, 447–453. doi:10.1016/S0924-0136(03)00768-4
- Pérez-Santiago, R., 2012. Forming force estimation in single point incremental forming of uniform and variable wall angle components. *Instituto tecnológico y de estudios superiores de Monterrey*.
- Pérez-Santiago, R., Bagudanch, I., García-Romeu, M.L., 2011. Force Modeling in Single Point Incremental Forming of Variable Wall Angle Components, in: *Key Engineering Materials*. pp. 833–840. doi:10.4028/www.scientific.net/KEM.473.833
- Pérez-Santiago, R., Bagudanch, I., García-Romeu, M.L., Hendrichs, N., 2012a. Effect of strain hardening exponent in the incremental sheet forming force, in: *Steel Research International*. Wiley-VCH Verlag, pp. 439–442.
- Pérez-Santiago, R., García-Romeu, M.L., Bagudanch, I., 2012b. Fabrication of a Biopsy Micro-Forceps Prototype with Incremental Sheet Forming, in: *Innovative Developments in Virtual and Physical Prototyping - Proceedings of the 5th International Conference on Advanced Research in Virtual and Rapid Prototyping*. pp. 429–435.
- Petek, A., Kuzman, K., Kopaè, J., 2009. Deformations and forces analysis of single point incremental sheet metal forming. *Archives of Materials Science and Engineering* 35, 107–116.
- Puigpinós, L., Bagudanch, I., Garcia-Romeu, M.L., Perez-Santiago, R., 2012. Incremental Sheet Forming (ISF) technology applied to form thin metal sheets, in: *Steel Research*

International. Wiley-VCH Verlag, pp. 443–446.

- Radu, M.C., Cristea, I., 2013. Processing Metal Sheets by SPIF and Analysis of Parts Quality. *Materials and Manufacturing Processes* 28, 287–293. doi:10.1080/10426914.2012.746702
- Rauch, M., Hascoet, J.-Y., Hamann, J.-C., Plenel, Y., 2009. Tool path programming optimization for incremental sheet forming applications. *Computer-Aided Design* 41, 877–885. doi:10.1016/j.cad.2009.06.006
- Santo, L., Quadrini, F., Trovalusci, F., 2010. A miniaturized machine for micro-sheet forming. *International Journal of Material Forming* 3, 1091–1094. doi:10.1007/s12289-010-0961-3
- Schafer, T., Schraft, R.D., 2005. Incremental sheet metal forming by industrial robots. *Rapid Prototyping Journal* 11, 278–286. doi:10.1108/13552540510623585
- Silva, M., Skjoedt, M., Martins, P., Bay, N., 2008. Revisiting the fundamentals of single point incremental forming by means of membrane analysis. *International Journal of Machine Tools and Manufacture* 48, 73–83. doi:10.1016/j.ijmachtools.2007.07.004
- Silva, M.B., Alves, L.M., Martins, P. a. F., 2010. Single point incremental forming of PVC: Experimental findings and theoretical interpretation. *European Journal of Mechanics - A/Solids* 29, 557–566. doi:10.1016/j.euromechsol.2010.03.008
- Silva, M.B., Martinho, T.M., Martins, P.A.F., 2013. Incremental Forming of Hole-Flanges in Polymer Sheets. *Materials and Manufacturing Processes* 28, 330–335. doi:10.1080/10426914.2012.682488
- Silva, M.B., Martins, P.A.F., 2013. Two-point incremental forming with partial die: Theory and experimentation. *Journal of Materials Engineering and Performance* 22, 1018–1027. doi:10.1007/s11665-012-0400-3
- Silva, M.B., Nielsen, P.S., Bay, N., Martins, P.A.F., 2011. Failure mechanisms in single-point incremental forming of metals. *International Journal of Advanced Manufacturing Technology* 56, 893–903. doi:10.1007/s00170-011-3254-1
- Soeiro, J.M.C., Silva, C.M.A., Silva, M.B., Martins, P.A.F., 2015. Revisiting the formability limits by fracture in sheet metal forming. *Journal of Materials Processing Technology* 217, 184–192. doi:10.1016/j.jmatprotec.2014.11.009
- Sy, L. Van, Nam, N.T., 2015. Effect of strain rate and temperature on formability of warm-incremental forming process with magnesium alloy sheet AZ31. *Journal of manufacturing technology research* 6, 17–31.
- Takano, H., Kitazawa, K., Goto, T., 2008. Incremental forming of nonuniform sheet metal: Possibility of cold recycling process of sheet metal waste. *International Journal of Machine Tools and Manufacture* 48, 477–482. doi:10.1016/j.ijmachtools.2007.10.009
- Tanaka, S., Nakamura, T., Hayakawa, K., Nakamura, H., Motomura, K., 2007. Residual stress in sheet metal parts made by incremental forming process. *AIP Conference Proceedings* 908, 775–780. doi:10.1063/1.2740904
- Tekkaya, a. E., Shankar, R., Sebastiani, G., Homberg, W., Kleiner, M., 2007. Surface reconstruction for incremental forming. *Production Engineering* 1, 71–78.

doi:10.1007/s11740-007-0024-x

- TMR, 2014. Biomaterials Market for Implantable Devices (Material Type - Metals, Polymers, Ceramics and Natural, Applications - Cardiology, Orthopedics, Dental, Ophthalmology and Others) - Global Industry Analysis, Size, Share, Growth, Trends and Forecast, 2013 – 201.
- Tuomi, J., Lamminen, L., 2004. Incremental Sheet Forming as a Method for Sheet Metal Component Prototyping and Manufacturing, in: 10èmes Assises Européennes de Prototypage Rapide.
- Verbert, J., Aerens, R., Vanhove, H., Aertbeliën, E., Duflou, J.R., 2009. Obtainable Accuracies and Compensation Strategies for Robot Supported SPIF. *Key Engineering Materials* 410-411, 679–687. doi:10.4028/www.scientific.net/KEM.410-411.679
- Verbert, J., Belkassam, B., Henrard, C., Habraken, a. M., Gu, J., Sol, H., Lauwers, B., Duflou, J.R., 2008. Multi-Step toolpath approach to overcome forming limitations in single point incremental forming. *International Journal of Material Forming* 1, 1203–1206. doi:10.1007/s12289-008-0157-2
- Zhang, Q., Guo, H., Xiao, F., Gao, L., Bondarev, a. B., Han, W., 2009. Influence of anisotropy of the magnesium alloy AZ31 sheets on warm negative incremental forming. *Journal of Materials Processing Technology* 209, 5514–5520. doi:10.1016/j.jmatprotec.2009.05.012
- Zhang, Q., Xiao, F., Guo, H., Li, C., Gao, L., Guo, X., Han, W., Bondarev, a. B., 2010. Warm negative incremental forming of magnesium alloy AZ31 Sheet: New lubricating method. *Journal of Materials Processing Technology* 210, 323–329. doi:10.1016/j.jmatprotec.2009.09.018
- Ziran, X., Gao, L., Hussain, G., Cui, Z., 2009. The performance of flat end and hemispherical end tools in single-point incremental forming. *The International Journal of Advanced Manufacturing Technology* 46, 1113–1118. doi:10.1007/s00170-009-2179-4